

Green synthesis of silver, selenium and zinc oxide nanoparticles using extracts and isolated secondary metabolites of *Chrysanthemoides monilifera* and *Harpephyllum caffrum* and their biological activity

By

Ntombizodwa Vundla

Submitted in fulfilment of the academic requirements for the degree of Master of Science in the School of Chemistry and Physics at the University of KwaZulu-Natal, Durban

2018

As the candidates supervisor and co-supervisor, I have/ have not approved this dissertation for submission

Signed: _____

Name: _____

Date: _____

Signed: _____

Name: _____

Date: _____

ABSTRACT

The method of using plant extracts for the synthesis of metal-based nanoparticles is a recently developed technique which is not only cost effective but environmentally friendly. It has very low energy requirements, needs no specialised equipment and reactions are completed within minutes. The resultant materials can be applied to catalysts, medicine, electronics and optics. The biological activity of plant extracts and nanoparticles have each been studied and are well known. In addition to being green, nanoparticles produced by the plant-mediated synthesis route are being utilised in biomedical applications with the added advantage of increased activity arising from the synergistic effects of both the biologically active nanoparticles and plant extracts or phytochemicals.

In this project, extracts and phytochemicals from the indigenous, South African, medicinal plant species *Chrysanthemoides monilifera* and *Harpephyllum caffrum* were obtained and used to synthesise and stabilise silver, zinc oxide and selenium nanoparticles. The plant extracts and phytochemicals were characterised using spectroscopic techniques. Quercetin was isolated from the extract of *C. monilifera* and catechin from the extract of *H. caffrum*. The growth of nanoparticles was investigated at various concentrations of phytochemicals. The synthesised nanoparticles were characterised using spectroscopic and microscopic techniques.

Growth seemed to occur by agglomeration and subsequent re-orientation. Changes in concentration had an effect on the yield, shapes and sizes of the synthesised nanoparticles. To investigate the synergistic or antagonistic effect of the capping agents on the biological activity of synthesised nanoparticles, freestanding (uncapped) nanoparticles were synthesised, using sodium borohydride as a reducing agent, for comparison. Results showed biosynthesised nanoparticles to be capped with plant biomolecules. The biosynthesised nanoparticles had a wider size distribution than freestanding nanoparticles. The particles were tested for their antioxidant activity using three different assays (1,1-diphenyl-2-picrylhydrazyl radical (DPPH•) radical scavenging, ferric reducing antioxidant power (FRAP) and H₂O₂ radical scavenging). The results showed plant biomolecules to enhance the antioxidant activity of the biosynthesised nanoparticles. The anti-microbial activities of the nanoparticles were evaluated with the Kirby-Bauer disc diffusion susceptibility test. Capping of selenium and zinc oxide nanoparticles with plant biomolecules did not have any effect on antibacterial activity. *H. caffrum* was found to enhance the activity of the silver nanoparticles whilst quercetin promoted its anti-quorum sensing ability.

DECLARATION – PLAGIARISM

I, _____ Declare that

1. The research reported in this thesis, except where otherwise indicated, is my original research.
2. This thesis has not been submitted for any degree or examination at any other university
3. This thesis does not contain other person/s data, pictures, graphs or other information, unless specifically acknowledged as being sourced from the other person/s.
4. This thesis does not contain other person/s writing, unless specifically acknowledged as being sourced from other researcher/s. Where other written sources have been quoted, then:
 1. Their words have been re-written but the general information attributed to them has been referenced.
 2. Where their exact words have been used, then their writing has been placed in italics and/or inside quotation marks, and referenced.
 3. This thesis does not contain text, graphics or tables copied and pasted from the internet, unless specifically acknowledged, and the source being detailed in the thesis in the Reference section.

Signed: _____

PREFACE

The experimental work described in this thesis was carried out in the School of Chemistry and Physics at the University of KwaZulu-Natal, Durban, from March 2015 to December 2017 under the supervision of Dr Roshila Moodley and Dr Karin Pruessner.

These studies present original work by the author and have not otherwise been submitted in any form for any degree or diploma to any tertiary institution. Where use has been made of the work of others, it is duly acknowledged in the text.

Signed: _____

Name: _____

Date: _____

DEDICATION

To my sister Zanele Vundla and my magical son Jake. Even when I had nothing, I had you.

ACKNOWLEDGEMENTS

As a scientist thus far, I have made many things (just crystals, complexes and complexes nothing much), so more than anyone, I understand that there is a maker. I would like to thank God for making me. Many thanks go to my funders, NRF and Thuthuka, without support from you, this work could never have been written. My supervisor, Dr Moodley, you're a song written by the hands of God. I'm grateful for all the advice, that I followed immediately or much later, it made me a better scientist. Everyone in the Natural Products Research group, I have never met a group of more kind and helpful individuals. You give up your time to offer assistance at no reward, nonetheless. (Dr N. Mahlangeni, Bongisiwe Shelembe, Slungile Mhlongo, Nonhlanhla Joyisa, Judie Magura, Olusola Sunday Bodede and Olumuyiwa Ogunlaja). All the technicians at the chemistry building, (Dillip Jagjivan, Anita Niadoo, Unathi Bongoza, Vasthi Reddy and Brian Ndlovu) and microscopy technicians (Philip Christopher, Vishal Bharuth and Subashen Naidu). Thank you for all your assistance. My family has shaped me as a human being before anything else. Starting with the head of this home, Thuleleni Getrude Vundla, whose genetic make-up I am grateful for not in just appearance but in brain matter. Mother, I can think and work this hard because of you. My Father, Michael Vundla. Thank you for choosing mom. You are the reason why the science is in me. You prepared me for this even before I knew what it was. My magical son Jake, a piece of my soul would have remained dormant and inaccessible if you never came into my life. I want to be alive just to watch you live. In chronological order, my nephew and two nieces, Luyanda Vundla (Bana/Stormrider), Londiwe Vundla (Miss Beans/ Skywalker) and Lisakhanya Vundla (BMO/ Sunshine), of-course without you, this thesis would have been ready two years earlier but I found that in the process of raising you, I grew to a better version of myself (Version 1.0 to 3.0). Fathima Ally and Carice Frank, you are where I learnt the truth and true happiness. Philani Mpungose and Neo Sehloko (Zanele Vundla included), the eating club was great, not only because the food I made was so great (even though you can't have a conversation over bad food) but because the conversations were conversations and before you knew it time passed really well. The doctors Mduduzi Cele and Thandanani Cwele thank for all the protection, I didn't die because of you.

TABLE OF CONTENTS

| | |
|--|-----|
| ABSTRACT | ii |
| DECLARATION – PLAGIARISM | iii |
| PREFACE | iv |
| DEDICATION | v |
| ACKNOWLEDGEMENTS | vi |
| CHAPTER 1 | 1 |
| INTRODUCTION | 1 |
| 1.1 Problem Statement | 5 |
| 1.2 Aim | 6 |
| 1.3 Objectives | 6 |
| CHAPTER 2 | 7 |
| LITERATURE REVIEW | 7 |
| 2.1 Background | 7 |
| 2.2 Synthesis of Nanoparticles | 8 |
| 2.2.1 Physical and chemical synthesis of nanoparticles | 9 |
| 2.2.2 Biosynthesis of nanoparticles | 10 |
| 2.2.2.1 Microorganism-mediated synthesis of nanoparticles | 10 |
| 2.2.2.2 Plant-mediated synthesis of nanoparticles | 11 |
| 2.3 Overview of Traditional Medicine | 13 |
| 2.4 Plants in this Study | 14 |
| 2.4.1 Taxonomy of <i>Chrysanthemodis monilifera</i> | 15 |
| 2.4.2 <i>Chrysanthemodis monilifera</i> | 16 |
| 2.4.3 An ethnomedicinal and phytochemical review of some Asteracea species ... Error! Bookmark not defined. | |
| 2.4.4 Taxonomy of <i>Harpephyllum caffrum</i> | 18 |
| 2.4.5 <i>Harpephyllum caffrum</i> | 19 |
| 2.4.6 An ethnomedicinal and phytochemical review of some Anacardiaceae species | 20 |
| 2.5 Secondary Metabolites | 21 |
| 2.5.1 Phenolic compounds | 22 |
| 2.5.1.1 Flavonoids | 22 |
| 2.5.1.2 Structure - activity relationships of flavonoids | 26 |
| 2.6 Characterisation of Natural Products | 29 |
| 2.6.1 Extraction methods - chromatography | 29 |
| 2.6.1.1 Column chromatography | 29 |
| 2.6.1.2 Thin layer chromatography (TLC) | 31 |
| 2.6.2 Gas chromatography (GC) | 32 |

| | |
|--|----|
| 2.6.3 Nuclear magnetic resonance (NMR) spectroscopy | 34 |
| 2.6.4 Ultraviolet-visible (UV-Vis) spectroscopy | 36 |
| 2.6.5 Infra-red (IR) spectroscopy | 37 |
| 2.7 Characterisation of Nanoparticles | 38 |
| 2.7.1. Spectroscopy (ultraviolet-visible and infrared)..... | 39 |
| 2.7.2 Powder X-ray diffraction (PXRD)..... | 39 |
| 2.7.3. Microscopy | 42 |
| 2.7.3.1 Scanning electron microscopy (SEM) | 42 |
| 2.7.3.2 Transmission electron microscopy (TEM)..... | 44 |
| 2.7.4 Energy-dispersive X-ray spectroscopy (EDS) | 46 |
| 2.7.5 Selected area electron diffraction pattern (SAED)..... | 46 |
| 2.8 Biological Activity and Applications of Nanoparticles | 49 |
| 2.8.1 Silver (Ag) | 49 |
| 2.8.2 Selenium (Se)..... | 51 |
| 2.8.3 Zinc oxide (ZnO) | 54 |
| 2.9 Biological Applications of Phytocompounds and Nanoparticles..... | 56 |
| 2.9.1 Antioxidant assays | 56 |
| 2.9.1.1 The 1,1-diphenyl-2-picrylhydrazyl (DPPH') radical scavenging assay | 56 |
| 2.9.1.2 Ferric reducing antioxidant power (FRAP) assay | 57 |
| 2.9.1.3 Hydrogen peroxide (H ₂ O ₂) radical scavenging activity assay | 58 |
| 2.9.2 Antibacterial assays | 58 |
| 2.9.2.1 Antibacterial testing - Kirby-Bauer disc diffusion susceptibility test | 59 |
| 2.12 Toxicity of Nanoparticles..... | 60 |
| CHAPTER 3 | 62 |
| EXPERIMENTAL TECHNIQUES | 62 |
| 3.1 Sampling and Sample Preparation | 62 |
| 3.2 Reagents..... | 62 |
| 3.3 Characterisation and Quantification Methods..... | 62 |
| 3.4 Preparation of Extracts..... | 63 |
| 3.4.1 Isolation of compounds from <i>Chrysanthemoides monilifera</i> and <i>Harpephyllum caffrum</i> | 64 |
| 3.5 Synthesis of Silver, Selenium and Zinc Oxide Nanoparticles | 64 |
| 3.5.1 Effects of concentration on nanoparticle growth | 65 |
| 3.5.2 Synthesis of freestanding and capped nanoparticles | 65 |
| 3.5.2.1 Synthesis of freestanding (uncapped) nanoparticles | 65 |
| 3.5.2.2 Plant extract-mediated synthesis of nanoparticles | 65 |
| 3.5.2.3 Flavonoid-mediated synthesis of nanoparticles | 66 |
| 3.6 Biological Testing..... | 66 |

| | |
|---|-----|
| 3.6.1 The 1,1-diphenyl-2-picrylhydrazyl (DPPH) radical scavenging assay | 67 |
| 3.6.2 Ferric reducing antioxidant power (FRAP) assay | 67 |
| 3.6.3 Hydrogen peroxide (H ₂ O ₂) radical scavenging assay..... | 67 |
| 3.6.4 Kirby-Bauer disc diffusion susceptibility test..... | 68 |
| 3.7 Statistical analysis..... | 68 |
| CHAPTER 4 | 68 |
| STRUCTURE ELUCIDATION OF PHYTOCOMPOUNDS AND SYNTHESIS AND CHARACTERISATION OF NANOPARTICLES RESULTS AND DISCUSSION | 68 |
| 4.1 Structure Elucidation of Phytocompounds | 69 |
| 4.1.1 Nuclear magnetic resonance (NMR) and mass spectrometry (MS)..... | 69 |
| 4.1.2 Fourier-transform infrared (FTIR) spectroscopy | 72 |
| 4.1.3 Ultraviolet-visible (UV-Vis) spectroscopy | 75 |
| 4.2 Effects of Concentration on Nanoparticle Growth..... | 76 |
| 4.2.1 Ultraviolet-visible (UV-Vis) spectroscopy | 76 |
| 4.2.2 Transmission electron microscopy (TEM)..... | 79 |
| 4.3 Effects of Various Reducing Agents on Nanoparticle Growth..... | 86 |
| 4.3.1 Ultraviolet-visible (UV-Vis) spectroscopy | 86 |
| 4.3.1.1 Silver nanoparticles..... | 86 |
| 4.3.1.2 Selenium nanoparticles | 87 |
| 4.3.1.3 Zinc oxide nanoparticles | 88 |
| 4.3.2 Energy-dispersive X-ray spectroscopy (EDS) | 90 |
| 4.3.2.1 Silver nanoparticles..... | 90 |
| 4.3.2.2 Selenium nanoparticles | 93 |
| 4.3.2.3 Zinc oxide nanoparticles | 95 |
| 4.3.3 Infra-red (IR) spectroscopy | 97 |
| 4.3.4 Scanning electron microscopy (SEM) | 100 |
| 4.3.4.1 Silver nanoparticles..... | 100 |
| 4.3.4.2 Selenium nanoparticles | 102 |
| 4.3.4.3 Zinc oxide nanoparticles | 104 |
| 4.3.5 Transmission electron microscopy (TEM)..... | 106 |
| 4.3.5.1 Silver nanoparticles..... | 106 |
| 4.3.5.2 Selenium nanoparticles | 109 |
| 4.3.5.3 Zinc oxide nanoparticles | 112 |
| 4.3.6 Powder X-ray diffraction (PXRD)..... | 114 |
| 4.3.6.1 Silver nanoparticles..... | 114 |
| 4.3.6.2 Selenium nanoparticles | 117 |
| 4.3.6.3 Zinc oxide nanoparticles | 118 |

| | |
|---|-----|
| 4.3.7 Selected area electron diffraction (SAED)..... | 120 |
| 4.3.7.1 Silver nanoparticles..... | 120 |
| 4.3.7.2 Selenium nanoparticles..... | 122 |
| 4.3.7.3 Zinc oxide nanoparticles..... | 123 |
| CHAPTER 5..... | 125 |
| BIOLOGICAL TESTING..... | 125 |
| 5.1 Results and Discussion..... | 125 |
| 5.1.1 The 1,1-diphenyl-2-picrylhydrazyl (DPPH) radical scavenging activity..... | 125 |
| 5.1.1.1 Plants extracts and isolated flavonoids..... | 125 |
| 5.1.1.2 Silver nanoparticles..... | 127 |
| 5.1.1.3 Selenium nanoparticles..... | 128 |
| 5.1.1.4 Zinc oxide nanoparticles..... | 129 |
| 5.1.2 Ferric reducing antioxidant power (FRAP)..... | 131 |
| 5.1.2.1 Plant extracts and isolated flavonoids..... | 131 |
| 5.1.2.2. Silver nanoparticles..... | 132 |
| 5.1.2.3 Selenium nanoparticles..... | 133 |
| 5.1.2.4 Zinc oxide nanoparticles..... | 134 |
| 5.1.3 H ₂ O ₂ radical scavenging..... | 136 |
| 5.1.3.1 Plant extracts and isolated flavonoids..... | 136 |
| 5.1.3.2 Silver nanoparticles..... | 137 |
| 5.1.3.3 Selenium nanoparticles..... | 138 |
| 5.1.3.4 Zinc oxide nanoparticles..... | 139 |
| 5.2 Kirby-Bauer Disk Diffusion Susceptibility Test..... | 143 |
| CHAPTER 6..... | 149 |
| SUMMARY AND FINDINGS..... | 149 |
| 6.1 Overall Summary..... | 149 |
| 6.2 Conclusion..... | 150 |
| 6.3 Recommendation for further work..... | 151 |
| REFERENCES..... | 152 |

ABBREVIATIONS

| | |
|-----------------------------|--|
| ¹³C-NMR | ¹³ C- nuclear magnetic resonance spectroscopy |
| ¹H-NMR | Proton nuclear magnetic resonance spectroscopy |
| ax | axial |
| <i>C. monilifera</i> | <i>Chrysanthemodis monilifera</i> |
| <i>C. violaceum</i> | <i>Chromobacterium violaceum</i> |
| COSY | Correlation spectroscopy |
| d | Doublet |
| dd | Doublet of doublets |
| DEPT | Distortionless enhancement by polarization transfer |
| DPPH | 2,2-diphenyl-1-picrylhydrazyl |
| <i>E. coli</i> | <i>Escherichia coli</i> |
| EDS | Energy-dispersive X-ray spectroscopy |
| FTIR | Fourier-transform infrared |
| GC-MS | Gas chromatography-mass spectrometry |
| h | hour |
| Hz | Hertz |
| <i>H. cafferum</i> | <i>Harpephyllum cafferum</i> |
| HRTEM | High resolution transmission electron microscopy |
| ICP-OES | Inductively coupled plasma - optical emission spectrometry |
| J | Coupling constant |
| <i>K. pneumonia</i> | <i>Klebsiella pneumonia</i> |
| NPs | Nanoparticles |
| <i>P. aeruginosa</i> | <i>Pseudomonas aeruginosa</i> |
| ppm | parts per million |
| <i>S. aureus</i> | <i>Staphylococcus aureus</i> |
| SD | Standard deviation |
| SEM | Scanning electron microscope |
| SPR | Surface Plasmon Resonance |
| TEM | Transmission electron microscope |
| TLC | Thin-layer chromatography |
| UV-Vis | Ultraviolet visible spectroscopy |

| | |
|---------------|--------------------------|
| XRD | X-ray diffraction |
| AgNPs | Silver nanoparticles |
| SeNPs | Selenium nanoparticles |
| ZnONPs | Zinc oxide nanoparticles |

LIST OF FIGURES

| | |
|--|----|
| Figure 2.1: Schematic showing the categories of (i) bottom-up method and (ii) top-down method for the synthesis of nanoparticles | 9 |
| Figure 2.2: Proposed mechanism for biosynthesis of NPs via reduction and stabilisation of a metal ion using crude plant extracts or isolated phytochemicals | 12 |
| Figure 2.3: Map of the world's countries that use herbal medicine whether or not it has been registered in the country | 14 |
| Figure 2.4: Lineage of the <i>Chrysanthemoides monilifera</i> plant species | 16 |
| Figure 2.5: Plant species in this study, <i>Chrysanthemoides monilifera</i> | 17 |
| Figure 2.6: Lineage of the <i>Harpephyllum caffrum</i> plant species | 19 |
| Figure 2.7: Plant species in this study, <i>Harpephyllum caffrum</i> | 20 |
| Figure 2.8: Classes of flavonoids | 23 |
| Figure 2.9: Chelating site for quercetin | 25 |
| Figure 2.10: The two isomers of catechin are (+)-catechin and (-)-catechin | 26 |
| Figure 2.11: Ring B catechol moiety | 27 |
| Figure 2.12: Formation of quinone from free radical scavenging..... | 27 |
| Figure 2.13: Potential coordination spaces in some structure of flavonoids..... | 28 |
| Figure 2.14: Purification of a complex mixture using column chromatography | 30 |
| Figure 2.15: Thin layer chromatography (TLC) of fractions collected using column chromatography where numbers 1-13 indicate the different fractions..... | 32 |
| Figure 2.16: Components of a gas chromatography instrument | 33 |
| Figure 2.17: Basic operation of a mass spectrometer | 34 |
| Figure 2.18: Schematic representation of the operating principles of nuclear magnetic resonance spectroscopy..... | 35 |
| Figure 2.19: Schematic of an ultraviolet-visible (UV-Vis) double beam instrument | 36 |
| Figure 2.20: Schematic diagram of the operating principles of an infrared spectrophotometer | 38 |
| Figure 2.21: (a) Schematic of the working principle of an X-ray diffraction (XRD) instrument | 41 |
| b) a typical spectrum obtained from the instrument..... | 41 |
| Figure 2.22: Schematic diagram of a scanning electron microscope | 43 |
| Figure 2.23: Schematic diagram of a transmission electron microscope | 45 |
| Figure 2.24: The spot diffraction pattern from a single crystal of aluminium alloy | 47 |
| Figure 2.25: The ring diffraction pattern from a polycrystalline pure gold film with an f.c.c crystal structure. Crystal planes are indexed and inter-planar spacing is shown by Miller indices..... | 48 |
| Figure 2.26: Diffraction pattern of amorphous material | 48 |
| Figure 2.27: Face centred cubic lattice | 50 |
| Figure 2.28: S8 packing of atoms for selenium (Se)..... | 52 |
| Figure 2.29: Hexagonal packing of selenium (Se) atoms | 53 |
| Figure 2.30: Crystal phases of zinc oxide (ZnO) (a) hexagonal phase (wurtzite) crystal lattice of zinc oxide (b) cubic phase (zinc blende) crystal lattice of ZnO | 54 |
| Figure 2.31: Mechanism of action for the reduction of 1,1-diphenyl-2-picrylhydrazyl (DPPH) | 57 |
| Figure 2.33: Possible pathways of human interactions with nanoparticles..... | 61 |
| Figure 4.1: Fourier-transform infrared (FTIR) spectra of the crude methanol extracts of <i>Chrysanthemoides monilifera</i> and <i>Harpephyllum caffrum</i> | 73 |
| Figure 4.2: Fourier-transform infrared (FTIR) spectra of quercetin isolated from <i>Chrysanthemoides monilifera</i> and catechin isolated from <i>Harpephyllum caffrum</i> | 74 |
| Figure 4.3: Ultraviolet-visible (UV-Vis) spectra of the crude methanol extracts of <i>Chrysanthemoides monilifera</i> and <i>Harpephyllum caffrum</i> | 75 |
| Figure 4.4: Ultraviolet-visible (UV-Vis) spectra of quercetin and catechin | 76 |

| | |
|---|-----|
| Figure 4.5: Ultraviolet-visible (UV-Vis) spectra of silver nanoparticles (AgNPs) reduced with 0.1-3 mM quercetin | 77 |
| Figure 4.6: Structure of quercetin with possible chelating sites | 78 |
| Figure 4.7: Silver nanoparticles (AgNPs) synthesised (0.1 mM quercetin)..... | 80 |
| Figure 4.8: Silver nanoparticles (AgNPs) synthesised (0.2 mM quercetin)..... | 80 |
| Figure 4.9: Silver nanoparticles (AgNPs) synthesised (0.4 mM quercetin)..... | 81 |
| Figure 4.10: Silver nanoparticles (AgNPs) synthesised (0.8 mM quercetin)..... | 82 |
| Figure 4.11: Silver nanoparticles (AgNPs) synthesised (1mM quercetin) (A) general population of the synthesised nanoparticles (B) various shapes of the nanoparticles (C) incomplete hexagon (D) capping on the surface of the nanorods | 83 |
| Figure 4.12: Silver nanoparticles (AgNPs) synthesised (2 mM quercetin)..... | 84 |
| Figure 4.13: Silver nanoparticles (AgNPs) synthesised (3 mM quercetin)..... | 85 |
| Figure 4.14: Ultraviolet-visible (UV-Vis) spectra of silver nanoparticles (AgNPs) synthesised with the various reducing agents..... | 86 |
| Figure 4.15: Colour change from reducing silver ions to silver nanoparticles | 87 |
| Figure 4.16: Colour change from reducing selenium ions to selenium nanoparticles | 87 |
| Figure 4.17: Ultraviolet-visible (Uv-Vis) spectra of selenium nanoparticles (SeNPs) synthesised with the various reducing agents..... | 88 |
| Figure 4.18: No colour change from reducing zinc oxide ions to zinc oxide nanoparticles | 88 |
| Figure 4.19: Ultraviolet-visible (Uv-Vis) spectra of zinc oxide nanoparticles (ZnONPs) synthesised with the various reducing agents..... | 89 |
| Figure 4.20: Energy dispersive X-ray spectroscopy (EDS) of freestanding silver nanoparticles (AgNPs) | 90 |
| Figure 4.21: Energy dispersive X-ray spectroscopy (EDS) of silver nanoparticles (AgNPs) (<i>C. monilifera</i>) | 91 |
| Figure 4.22: Energy dispersive X-ray spectroscopy (EDS) of silver nanoparticles (AgNPs) (<i>H. cafferum</i>)..... | 91 |
| Figure 4.23: Energy dispersive X-ray spectroscopy (EDS) of silver nanoparticles (AgNPs) (quercetin) | 92 |
| Figure 4.24: Energy dispersive X-ray spectroscopy (EDS) of silver nanoparticles (AgNPs) (catechin) | 92 |
| Figure 4.25: Energy dispersive X-ray spectroscopy (EDS) of selenium nanoparticles (SeNPs) (freestanding) | 93 |
| Figure 4.26: Energy dispersive X-ray spectroscopy (EDS) of selenium nanoparticles (SeNPs) (<i>C. monilifera</i>) | 94 |
| Figure 4.27: Energy dispersive X-ray spectroscopy (EDS) of zinc oxide nanoparticles (ZnONPs) (freestanding) | 95 |
| Figure 4.28: Energy dispersive X-ray spectroscopy (EDS) of zinc oxide nanoparticles (ZnONPs) (<i>C. monilifera</i>)..... | 96 |
| Figure 4.29: Infrared spectra for freestanding silver, selenium and zinc oxide nanoparticles | 97 |
| Figure 4.30: Infrared spectra for <i>C. monilifera</i> extract and silver, selenium and zinc oxide nanoparticles synthesised from the <i>C. monilifera</i> extract | 98 |
| Figure 4.31: Infrared spectra for quercetin and silver, selenium and zinc oxide nanoparticles synthesised from quercetin | 99 |
| Figure 4.32: Scanning electron micrograph of AgNPs (freestanding)..... | 100 |
| Figure 4.33 :(A) Scanning electron micrograph of AgNPs (<i>C. monilifera</i>) (B) Scanning electron micrograph of AgNPs (<i>H. cafferum</i>) | 100 |
| Figure 4.34 (A) Scanning electron micrograph of AgNPs (quercetin) (B) Scanning electron micrograph of AgNPs (catechin) | 101 |
| Figure 4.35: Scanning electron micrograph of AgNPs (freestanding)..... | 102 |

| | |
|--|-----|
| Figure 4.36: (a) Scanning electron micrograph of SeNPs (<i>C. monilifera</i>) (b) Scanning electron micrograph of SeNPs (<i>H. caffrum</i>) | 102 |
| Figure 4.37: Scanning electron micrograph SeNPs (quercetin)..... | 103 |
| Figure 4.38: Scanning electron micrograph of SeNPs (freestanding)..... | 104 |
| Figure 4.39: (A) Scanning electron micrograph of AgNPs (<i>C. monilifera</i>) (B)SEM micrograph of AgNPs (<i>H.caffrum</i>) | 104 |
| Figure 4.40: (A)Scanning electron micrograph of AgNPs (quercetin) (B) Scanning electron micrograph of AgNPs (catechin) | 105 |
| Figure 4.41: Transmission electron micrograph of AgNPs (freestanding) | 106 |
| Figure 4.42: Transmission electron micrograph of AgNPs (<i>C. monilifera</i>)..... | 107 |
| Figure 4.43: Transmission electron of AgNPs (<i>H. caffrum</i>)..... | 107 |
| Figure 4.44: Transmission electron micrograph of AgNPs (quercetin) | 108 |
| Figure 4.45: Transmission electron micrograph of AgNPs (catechin)..... | 108 |
| Figure 4.46: Transmission electron microscopy (TEM) micrograph of SeNPs (freestanding) | 109 |
| Figure 4.47: Transmission electron micrograph of SeNPs (<i>C. monilifera</i>) | 110 |
| Figure 4.48: Transmission electron micrograph of SeNPs (<i>H. caffrum</i>) | 111 |
| Figure 4.49: Transmission electron of SeNPs (quercetin) | 111 |
| Figure 4.50: Transmission electron microscopy of ZnONPs (freestanding) | 112 |
| Figure 4.51: Transmission electron micrograph of ZnONPs (<i>C. monilifera</i>) | 112 |
| Figure 4.52: Transmission electron micrograph of ZnONPs (<i>H. caffrum</i>) | 113 |
| Figure 4.53: Transmission electron micrograph of ZnONPs (quercetin)..... | 113 |
| Figure 4.54: Transmission electron micrograph of ZnONPs (catechin) | 114 |
| Figure 4.55: Powder X-ray diffraction patterns of AgNPs (freestanding) and AgNPs (quercetin) | 115 |
| Figure 4.56: Powder X-ray diffraction pattern of freestanding selenium nanoparticles | 117 |
| Figure 4.57: Powder X-ray diffraction pattern with inset electron diffraction pattern of hexagonal phase (wurzite structure) of freestanding zinc oxide NPs..... | 119 |
| Figure 4.58: (A) Selected area electron diffraction (SAED) pattern of AgNPs (<i>C. monilifera</i>) (B) SAED pattern of AgNPs (<i>H. caffrum</i>) | 120 |
| Figure 4.59: (A) Selected area electron diffraction (SAED) pattern of AgNPs (quercetin) (B) SAED pattern of AgNPs (catechin)..... | 121 |
| Figure 4.60: (A) Selected area electron diffraction (SAED) pattern of SeNPs (<i>C. monilifera</i>) (B) SAED pattern of SeNPs (<i>H. caffrum</i>) | 122 |
| Figure 4.61: Selected area electron diffraction (SAED) pattern of SeNPs (quercetin)..... | 122 |
| Figure 4.62: (A) Selected area electron diffraction (SAED) pattern of ZnONPs (<i>C. monilifera</i>) (B) SAED pattern of ZnONPs (<i>H. caffrum</i>)..... | 123 |
| Figure 4.63: (A) Selected area electron diffraction (SAED) pattern of ZnONPs (quercetin) (B) SAED pattern of ZnONPs (catechin) | 124 |
| Figure 5.1: DPPH radical scavenging ability of isolated compounds and plant extracts with ascorbic acid as a standard | 126 |
| Figure 5.2: DPPH radical scavenging activity of synthesised silver nanoparticles (AgNPs) with various reducing agents with ascorbic acid as a standard | 127 |
| Figure 5.3: DPPH radical scavenging of synthesised selenium nanoparticles (SeNPs) with various reducing agents with ascorbic acid as a standard..... | 128 |
| Figure 5.4: DPPH radical scavenging of synthesised zinc oxide nanoparticles (ZnONPs) with various reducing agents with ascorbic acid as a standard..... | 129 |
| Figure 5.5: Overall DPPH radical scavenging activity of the plant extracts, isolated compounds and synthesised nanoparticles (NPs) at 100 μ L | 130 |
| Figure 5.6: Ferric reducing antioxidant power (FRAP) of the plants extracts and the isolated compounds | 131 |

| | |
|---|-----|
| Figure 5.7: Ferric reducing antioxidant power (FRAP) of silver nanoparticles (AgNPs) synthesised with the various reducing agents..... | 132 |
| Figure 5.8: Ferric reducing antioxidant power (FRAP) of selenium nanoparticles (SeNPs) synthesised with the various reducing agents..... | 133 |
| Figure 5.9: Ferric reducing antioxidant power (FRAP) of zinc oxide nanoparticles (ZnONPs) synthesised with the various reducing agents | 134 |
| Figure 5.10: Overall ferric reducing antioxidant power (FRAP) of the plant extracts, isolated compounds and synthesised nanoparticles (NPs) at 100 μ L (2.5 absorbance units is taken to be 100%) | 135 |
| Figure 5.11: H ₂ O ₂ radical scavenging ability of the plant extracts and isolated compounds..... | 136 |
| Figure 5.12: H ₂ O ₂ radical scavenging activity of the silver nanoparticles (AgNPs) synthesised with the various reducing agents..... | 137 |
| Figure 5.13: H ₂ O ₂ radical scavenging activity of the selenium nanoparticles (SeNPs) synthesised with the various reducing agents..... | 138 |
| Figure 5.14: H ₂ O ₂ radical scavenging activity of the zinc oxide nanoparticles (ZnONPs) synthesised with the various reducing agents..... | 139 |
| Figure 5.15: Overall H ₂ O ₂ radical scavenging activity of the plant extracts, isolated compounds and synthesised nanoparticles (NPs) at 100 μ L | 140 |

LIST OF TABLES

| | |
|---|-----|
| Table 2.1: Quercetin and catechin and their uses..... | 24 |
| Table 2.2: Properties of the elements (Ag and Se) and metal oxide (ZnO) used in this study | 55 |
| Table 3.1: Mass of metal salts used to prepare 1 mM metal salt stock solutions (1 Mm, 1L)..... | 64 |
| Table 3.2: Concentration of the volumes sampled during biological testing..... | 66 |
| Table 4.1: Nuclear magnetic resonance (NMR) spectroscopic data for quercetin and catechin..... | 71 |
| Table 4.2: Peak locations and peak shifts of quercetin with silver colloid solutions in nanometres (nm)..... | 78 |
| Table 4.3: Diffraction angles (2θ), d-spacings (\AA), Miller indices and Intensity for AgNPs (freestanding) and AgNPs (quercetin) | 116 |
| Table 4.4: The values of diffraction angle (2θ), d-spacing (\AA), Miller indices and Intensity for SeNPs (freestanding)..... | 118 |
| Table 4.5: The values of diffraction angle (2θ), d-spacing (\AA), Miller indices and Intensity for ZnONPs (freestanding) | 119 |
| Table 5.1: Comparison of antioxidant results obtained by the three different assays for plant extracts, isolated compounds and synthesised nanoparticles at 100 μL | 141 |
| Table 5.2: Zones of inhibition (mm) against various Gram-negative bacterial strains..... | 143 |
| Table 5.3. Zones of inhibition (mm) against various gram-positive bacterial strains..... | 145 |

CHAPTER 1

INTRODUCTION

Nanotechnology is a branch of technology that is concerned with the production and application of a wide class of materials whose dimensions are within the nanoscale region i.e. 100 nm and less. Since their introduction in 1959, after the speech by Richard Feynman where he said, “Theres plenty of room at the bottom” (Feynman, 1960), nanomaterials have become increasingly popular amongst researchers. Nanoparticles (NPs) are of particular interest in material science since particles size has a major influence on the physiochemical properties of a given material. By merely altering the size of a material to the nanoscale level, a host of new properties (electrical, magnetic, structural, morphological, and chemical) that are a consequence of the NPs large surface area-to-volume ratio and quantum confinement are produced (Tiwari et al., 2011). With these new properties, the applications of NPs have increased considerably. Current applications include catalysis, water purification, fuel cells, computing, textiles, drug delivery, cosmetics, medicine, automotive industry and food and beverages industry (Storhoff et al., 2000; Omid and Ghaderi, 2009). Novel applications of NPs are rapidly being discovered with the biomedical sciences being one of the most promising applications since NPs have the same size range as biological entities.

To date, majority of the research on nanotechnology have focussed on the synthesis of silver (Ag), gold (Au), platinum (Pt) and zinc oxide (ZnO) NPs. These metals are inert when in bulk form but their reactivity increases when at the nano-size range and they also have the ability to facilitate reactions at this size range (Freyschlag et al., 2011). Metal NPs and their oxides are also prospective candidates for the fabrication of new classes of antibacterial agents and as drug delivery vectors (Dizaj et al., 2014). They exhibit extraordinary antibacterial properties which are of interest to researchers due to growing microbial resistance against conventional antibiotics (Cherrak et al., 2016). From the biomedical application perspective, these metals are popular for their large surface area-to-volume ratio and size that allow them, for example, to pass into cells or through the blood brain barrier which makes them more reactive thereby allowing for more interaction with biological entities (Zhang et al., 2012). Metal oxides, in general, have versatile surface chemistries which impart interesting biological properties. There is huge scope to investigate other metal and metal oxide NPs and their potential interaction with biological systems. However, use of NPs in the biomedical sciences has been limited due to toxicity associated with the hazardous chemicals from which they are

synthesised. These include the precursors, tetramethoxysilane (TMOS) and tetraethoxysilanes (TEOS) which form silica gels, used for the chemical synthesis of NPs.

Metal and metal oxide NPs may be incorporated into modern medicine for their therapeutic effectiveness or as drug carriers. However, side effects such as accumulation in selected organs associated with the nature of the NPs have to be considered though (Khan et al., 2017). When used as drug carriers, the surface of NPs are modified with appropriate receptor units that target specific sites where they provide a local drug supply whilst remaining selective in their pharmacological action (Singh and Lillard, 2009; Lahkar and Das, 2013). To date, various chemical and physical methods are available for the synthesis of NPs that attempt to resolve several challenges surrounding NP design, including size and shape control, scale up and uniformity. Depending on the applications of the NPs, most of the synthesis methods involve the reduction of metal ions from aqueous solutions and the use of a chemical stabiliser to avoid agglomeration (Mallick et al., 2004). Chemical synthesis of NPs involve the use of reducing agents such as sodium citrate, sodium borohydride and hydrazine, to reduce the aqueous metal ions and create a uniform suspension (Sudarshan, 2000). Physical synthesis of NPs predominantly make use of evaporation-condensation and laser ablation to prevent the use of and contamination by solvents (Iravani et al., 2014). The limitations of chemical and physical methods include high cost, use of toxic solvents, high energy consumption and the generation of hazardous by-products. Biosynthetic methods have since been explored as a cost-effective and environmentally friendly alternative to purely chemical and physical methods.

Biosynthesis of NPs involves synthesis of NPs at ambient temperatures with a wide range of biological materials such as plant material, bacteria, fungi and viruses, which engender significant diversity and advantages over chemical and physical methods of synthesis (Pantidos et al., 2018; Kuppusamy et al., 2016). The active component in plants is usually a secondary metabolite, while in fungi different proteins and enzymes can be active. One advantage of biosynthesis is environmental compatibility as it eliminates the use of toxic chemicals which could pose a threat to human life if used in pharmaceutical and biomedical applications (Sudarshan, 2000). Using plants over micro-organisms for NP synthesis is also more favourable, in that, many plants are easy to work with and inexpensive to culture or obtain. Production of NPs using plants is also safer, production times are shorter and production volumes are easy to scale up. Plant mediated synthesis is possible due to the wide variety of primary and secondary metabolites (phenolic compounds, alkaloids, sterols etc.) present in

plants that can effectively reduce metal ions and subsequently stabilise the resulting NPs in a single step (Subhankari and Nayak, 2013). In addition, secondary metabolites are known to possess interesting biological properties which have given them importance in both conventional (allopathic) and traditional (herbal) medicine (Kurek et al., 2011).

Since time immemorial, plants have been a primary source of medicine to the world. The extracts from different parts of plants such as roots, stems, leaves, flowers and fruits are used in traditional medicine to treat a variety of conditions. The medicinal properties of plant extracts (antibacterial, antioxidant, anti-inflammatory, anti-cancer etc.) are not considered to be new as plants have been used over centuries for medicinal purposes. In South Africa, medicinal plants are an important part of the daily lives of many people and are an integral part of the South African heritage (van Wyk, 1997). Southern Africa has a huge plant biodiversity of more than 30 000 species of higher plants with approximately 3000 species of plants being used medicinally (van Wyk, 1997). Toxic effects of plant extracts vary with plant species. Studies have shown that administration of crude extracts of medicinal plants to animals subjects have no toxic effects whilst other studies suggest that their indiscriminate use should be avoided due to toxicities (van Wyk, 1997; Rajalakshmi et al., 2014). This indicates that, although plant extracts are not completely harmless (depending on the class of compounds present), they are significantly less toxic than the chemicals used for chemical synthesis of NPs.

Although studies on the biosynthesis of NPs have been conducted and reported, mechanisms are still not well understood. For most applications, NPs of specific size and shape are needed for consistent results (Suárez-Cerda et al., 2014). The plant extract plays a key role in the synthesis; the nature of the plant extract is critical in determining the kind of NPs synthesised (Daisy and Saipriya, 2012). The plants ability to synthesis NPs stems from the hundreds of compounds that are present in them that can effectively reduce metal precursors. Temperature, pressure, time, pH and concentration are some of the synthesis parameters that can be optimised to achieve the goal of specifically tailored NPs for various applications. Synthesis can easily be conducted without any specialised equipment or technical processes.

Previous studies have reported good results for NP synthesis using plant extracts albeit, the method is not without limitations. Whole plant tissue is unable to tailor make NPs of a specific size and shape. The size and morphology of NPs synthesised from whole plants vary from plant

to plant (Makarov et al., 2014). This may hinder their use in applications where specific sizes and shapes are required. However, better results and control have been reported when isolated compounds were used (Malik et al., 2014). The identification of active compounds and their mechanisms have been under explored. Isolated flavonoids and flavonoid glycosides, in particular, have been shown to induce the formation of metal NPs (Kasthuri et al., 2009). Flavonoids are secondary metabolites produced by plants that are known to have antioxidant properties (Sim et al., 2007). They are also known to play an important role in the treatment of different human diseases such as cancer, cardiovascular and respiratory disorders as well as arthritis.

The surface of NPs make for interesting chemistry as it can be modified and/or functionalised with molecules, polymers, surfactants and metal ions (Shin et al., 2016). Organic molecules that are used to coat inorganic NPs act as stabilisers and/or capping agents to limit further growth and agglomeration. Nanoparticles that do not make use of stabilisers or capping agents are referred to as freestanding NPs. Flavonoids show their antioxidant ability by using their carbonyl groups or π -electrons to scavenge radicals and chelate metal ions (Afanas'Ev, 1996). The chelating activity of the flavonoids vary with some having significantly higher activities than others. This chelating ability may result in the flavonoids adsorbing onto the surface of growing NPs when they are used as reducing agents. This probably means, in addition to the bioreduction, that they may also be involved in the nucleation and aggregation stages of nanoparticle growth. NPs consisting of an inorganic metal core capped with a bioactive molecule brings about a new class of materials that may exhibit enhanced biological activity with low toxicity compared to their freestanding counterparts. It is therefore likely that they will advance the biomedical field. Since flavonoids have therapeutic value, have been a prime source of drugs and have provided leads for the development of drugs for the treatment of many diseases, their combined therapeutic effects with that of NPs makes plant mediated synthesis of NPs desirable for synthesis (Kulkarni and Muddapur, 2014).

1.1 Problem Statement

Bacterial infections are a serious health concern and have drawn much attention worldwide due to their threat to human health. They are one of the main causes of chronic infections and mortality (Dye, 2014). Currently, antibiotics are used to treat bacterial infections. These are usually complex molecules that contain functional groups in their chemical structures (Grenni et al., 2017). Their function is to disrupt the metabolic processes of bacteria to either kill or inhibit their growth. After they are administered, the body can only partially metabolise these complexes, therefore large amounts are excreted either unaltered or as active metabolites via urine and faeces (Grenni et al., 2017). Overuse of antibiotics have resulted in high concentrations of these pharmaceuticals in the environment (Manzetti and Ghisi, 2014). This has consequently led to the development of extreme drug resistant bacteria which pose a serious threat to the lives of humans (Grenni et al., 2017). This is exacerbated by the decline in the development of new anti-biotic drugs and lack of suitable vaccines in underdeveloped countries (Kurek et al., 2011). For example, infections by *Shigella flexneri* cause 1.5 million deaths annually, due to contaminated food and drinks. Thus the development of novel antibacterial agents has become critical. In view of this problem, there has been a growing interest in studies to develop and employ new therapeutic strategies against bacterial pathogens, such as *Escherichia coli*, *Staphylococcus aureus*, *Pseudomonas aeruginosa* and *Enterococcus faecalis* that may replace conventional antibiotics (Awwad et al., 2012). One such strategy involves the plant-mediated synthesis of metal and metal oxide NPs that can be used to treat bacterial infections. Nanoparticles of certain elements e.g. silver and gold are known to have biological activity, and the use of plant derived pharmaceuticals for disease treatment is also well established. The combination of both might lead to synergistic effects and superior efficiency.

1.2 Hypothesis

Possible synergistic effects could be offered by the combination of a biologically active biomolecule from plant material with a biologically active metal or metal oxide nanoparticle. We hypothesise, using a plant-mediated synthesis approach, that biomolecules from plant materials would similarly adsorb onto the surface of the NPs and would enhance their therapeutic value due to their combined medicinal properties.

1.3 Aim

The aim of the study is to phytochemically and analytically investigate two medicinal plant species that are indigenous to South Africa (*Chrysanthemoisis monilifera* and *Harpephyllum caffrum*). Their secondary metabolites will be extracted and isolated and used in the synthesis of silver, selenium and zinc oxide nanoparticles.

1.4 Objectives

The research objectives are:

- To extract, isolate and identify the secondary metabolites from two medicinal plant species using spectroscopic techniques such as 1D and 2D nuclear magnetic resonance (NMR), ultraviolet-visible spectroscopy (UV-Vis), gas chromatography - mass spectrometry (GC-MS), and Fourier-transform infrared spectroscopy (FTIR).
- To synthesise silver, selenium and zinc oxide nanoparticles end capped with biomolecules from the crude methanol extracts and isolated phytocompounds under a variety of concentrations to find optimum conditions for nanoparticle growth, and to characterise them using FTIR, UV-Vis, X-ray powder diffraction (PXRD), scanning electron microscopy (SEM), energy dispersive X-ray spectroscopy (EDX) and transmission electron microscopy (TEM).
- To synthesise freestanding nanoparticles (uncapped) using sodium borohydride i.e. nanoparticles that are synthesised without the use of phytocompounds and have clean surfaces.
- To test the end-capped and freestanding (uncapped) nanoparticles, plant extracts and isolated phytocompounds for biological activity (antioxidant and antibacterial) and to compare their efficiency relative to each other and known standards.

CHAPTER 2

REVIEW OF SYNTHESIS, CHARACTERISATION AND BIOLOGICAL ACTIVITIES OF METAL (AG AND SE) AND METAL OXIDE (ZNO) NPS VIA THE PLANT-MEDIATED SYNTHESIS ROUTE

2.1 Background

Nanotechnology involves the controlled synthesis of materials where at least one dimension of the structure is less than 100 nm. This range is similar in size to naturally occurring proteins and biomolecules in the cell, and is particularly smaller than the typical diameter of many human cells which are approximately 7 μm (Rasmussen et al., 2010). This allows for a unique interaction between nanoparticles with cell biomolecules and enables their physical transport into the interior structures of cells. The size reduction of the bulk material into the nanoscale dimension introduces a range of new properties (electrical, magnetic, structural, morphological and chemical properties) compared to the bulk material that are the consequence of the NPs large surface area-to-volume ratio and quantum confinement (Issa et al., 2013). NPs have a larger percentage of atoms at their surface which leads to high surface reactivity. The introduction of NPs has brought about scientific and technological innovations that would not be possible otherwise. These materials offer enhanced chemical reactivity, energy absorption and biological mobility (Yazeji et al., 2017). They have been found to be useful in the chemical and electrical industries as well as in medicine (Astruc and Daniel, 2004; Bindhu and Umadevi, 2013). Metal based NPs, in particular, offer features such as catalytic and optical activities as well as magnetic and electrical properties (Lazarides et al., 2000; Ponomareva et al. 2007; Key and Leary, 2014). In medicine, they have been applied in optical imaging, magnetic resonance imaging (MRI) and drug and gene delivery due to their efficiency and reduced side effects (Murthy, 2007; Kumari et al., 2017).

Nanoparticles show great potential for a wider range of applications, specifically in the biomedical fields, but their use is limited due to environmental concerns brought about by their toxicity. This challenge results from the current synthesis methods which involve the use of hazardous and toxic chemicals. The chemicals are adsorbed onto the surface of the NPs and their toxicity, inherently, pose a threat to humans for applications in the medical field. In addition, NPs (with or without phytochemicals) are easily inhaled and enter the lungs from where they get into the bloodstream (Yah et al., 2012). They can penetrate the skin as well as

the blood brain barrier and can be transmitted to a fetus. The field of nanotechnology is still relatively young and the final fate of NPs e.g. size dependant accumulation in different organs is not well understood (Saraiva et al., 2016). The leading physical and chemical preparation methods for these powders include sol-gel, hydrothermal, flame combustion, pyrolysis and chemical vapour deposition (Tavakoli et al., 2007). Additionally, some of these preparation methods have high energy requirements for the initiation of the reaction and, in some cases, they utilise specialised equipment and glassware (Krutuyakov et al., 2008). Other methods further call for specialised inert atmosphere protection (Perez-Tijerina et al., 2008). Consequently, the development of alternative, greener synthesis routes for the production of NPs is critical.

Green synthesis methods are more cost effective, provide the added benefit of environmental compatibility and do not require high temperatures and pressures. The green synthesis routes make use of biological materials such as plants, fungi, bacteria, viruses and yeast for the synthesis of NPs (MubarakAli et al., 2011; Awwad et al., 2012; Lahkar and Das, 2013; Husen and Siddiqi, 2014). Plant materials are inexpensive to culture compared to microorganisms which makes them ideal for the green synthesis of NPs.

Presently, the majority of literature on metal-based NPs focuses mainly on silver, gold, zinc oxide and platinum. These metals are inert in themselves and their larger surface area-to-volume ratios of their nanoparticles allow them to facilitate neighbouring chemical reactions well. They have excellent catalytic abilities which are used in a number of industrial processes and other important electronic and physical applications. This chapter will review the synthesis, characterisation and biological activities of metal (Ag and Se) and metal oxide (ZnO) NPs via the plant-mediated synthesis route.

2.2 Synthesis of Nanoparticles

The synthesis of NPs (Figure 2.1) falls broadly into two categories: (i) top-down methods and (ii) the bottom-up methods. The top down methods involves the physical breaking down of a bulk material into small particles. These methods are not cheap and they require sophisticated equipment to reach uniform and scale up is difficult. The bottom-up methods starts with atoms or molecules that self-assemble and that grow into nanostructures. The control of size and shape

of the NPs is difficult but scale-up is easier. Compared to the top-down approach, fabrication (bottom-up) of NPs is less expensive.

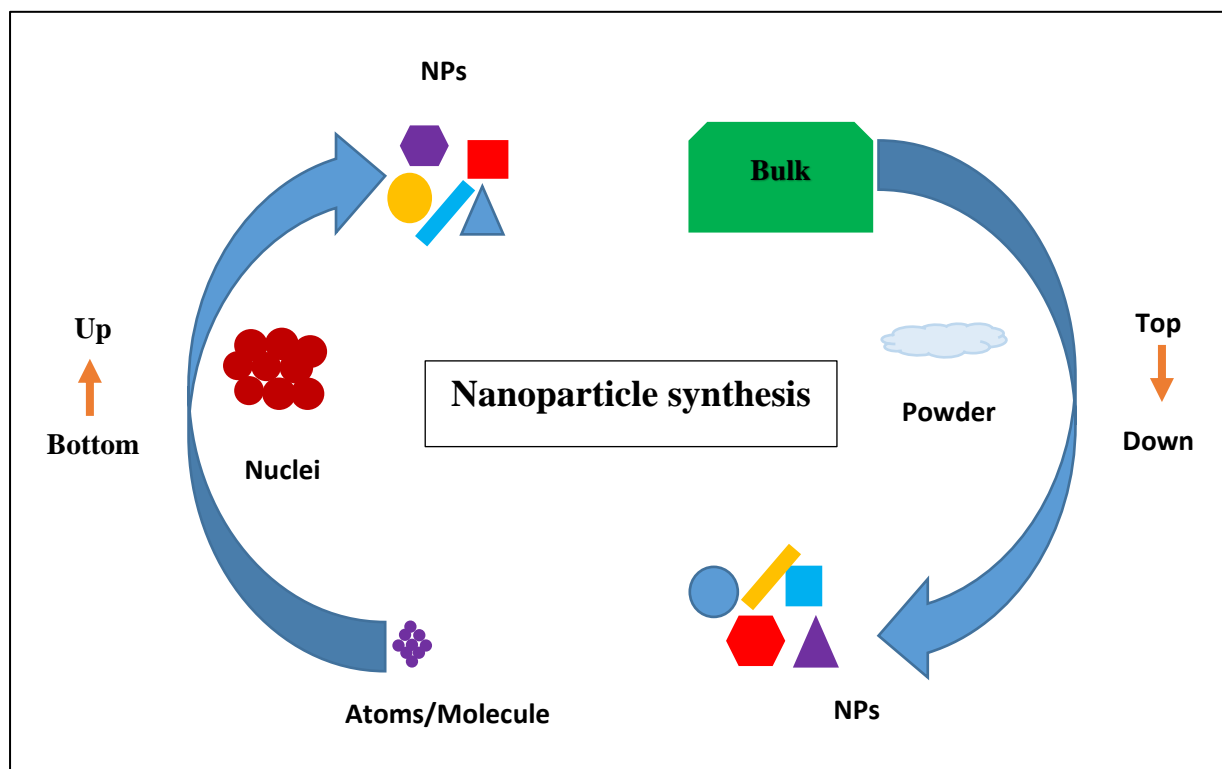


Figure 2.1: Schematic showing the categories of (i) bottom-up method and (ii) top-down method for the synthesis of nanoparticles

2.2.1 Physical and chemical synthesis of nanoparticles

This is a mechanical process where nanosizes are achieved through a milling/attrition process. Its main disadvantage is the broad size distribution which can vary from 10-100 nm. The particles also vary in shape and geometry. Nanoparticles synthesised with this method are often used for nanocomposites and nano-grained bulk materials. Literature reports inert-gas condensation, chemical vapour deposition (CVD), solvothermal reaction as well as sol-gel fabrication as the leading methods of choice when chemically synthesising NPs (Rajput, 2015). With CVD for instance, the major drawbacks arise from the precursor which are not only volatile but toxic - ($\text{Ni}(\text{CO})_4$), explosive (B_2H_6) and/or corrosive (SiCl_4) (Park, 2001). The by-products of CVD reactions can also be hazardous (CO , H_2 or HF). Some of the metal-organic precursors used in this process are very costly. The other major disadvantage is operation at elevated temperatures. This limits the nature of substrates coated on the NPs. Considering the

sol-gel method, the typical precursors used are metal alkalooids or metal chlorides. The most widely used are tetramethoxysilane (TMOS) and tetraethoxysilanes (TEOS) which form silica gels. These precursors are usually hazardous and toxic and therefore the NPs cannot be used for biomedical applications. It is important that NPs for biomedical applications be prepared only with biocompatible chemicals. This serves to minimize their toxic effect and increase the safe usage of NPs (Petrucci et al., 2014).

2.2.2 Biosynthesis of nanoparticles

The biological synthesis of NPs is a “bottom up” approach and it occurs with the assistance of microorganisms (bacteria, fungi, yeast and viruses) or plant extracts. The major advantages that biosynthesis of NPs have over chemical synthesis are economic feasibility and compatibility with the environment which favour pharmaceutical applications.

2.2.2.1 Microorganism-mediated synthesis of nanoparticles

The synthesis of NPs using microorganisms is based on oxidation/reduction reactions in solution and the NPs can be synthesised intracellularly (inside the cell) or extracellularly (outside the cell) (Das et al., 2014; Otari et al., 2015). The process involves use of microbial enzymes or proteins. The biomolecules or enzymes act as reducing agents on the metal ions to form the desired NPs. The NPs synthesised at the intracellular locations are much smaller than those synthesised extracellularly. This allows for the ability to tailor make NPs for specific applications as major physiochemical properties will become more prominent at smaller sizes. The downside of intracellularly synthesised NPs is the low yields since the synthesised NPs are difficult to extract. On the other hand, NPs synthesised at extracellular locations are easier to isolate and produce higher yields. Both intra/extracellular synthesis of NPs have been reported to be mainly due to the specific alteration in the reaction parameters (Ahmad et al., 2005). Bacterial synthesis relies heavily on temperature and pH operational parameters. Some studies show size of NPs to be affected by incubation period of bacterial cultures. Bacterial-mediated synthesis of NPs works best for nitrate-based metal salts. This is because the mechanism of synthesis of NPs is based on the nitrate reductase enzyme which converts nitrate

into nitrite and the electron is transferred to the metal ion (M^+ to M^0). The most sought after bacterial species include *Pseudomonas lactobacillus* and *Escherichia coli*.

Fungi make NPs by trapping the M^+ ions at the surface of the fungal cells. The M^+ ion is then reduced by enzymes that are present on the fungal system. Fungal-mediated synthesis of NPs offers greater yields than bacterial-mediated synthesis. This is because fungal species grow very fast. This enables the release, in sufficiently large amounts, of the required enzymes that allow for easier bio-reduction of metal salts to form biochemically reduced metallic ions as zero-valent NPs. The amount of enzymes released, directly translates to a yield of NPs which is high (Xie et al., 2007). Moreover, culturing of fungi can easily be scaled up compared to bacterial-based extracts. *Fusarium oxysporum* (Zielonka and Klimek-Ochab, 2017), *Trichothecium* (Ahmad et al., 2005) and *Aspergillus fumigatus* (Bhainsa and D'Souza, 2006) are a few fungal species that have been reported to synthesise silver and gold NPs.

2.2.2.2 Plant-mediated synthesis of nanoparticles

Plant-mediated synthesis of NPs is a much faster process in comparison to the use of microbes and fungi (Ahmed et al., 2016). Plants are more readily available and don't need to be cultured, consequently, making plants more cost-effective to work with than microorganisms. They also have an expansive variety of metabolites that aid in the reduction of metal ions to form NPs. The exact mechanism of synthesis varies for each plant as the phytochemicals vary but the major mechanism involved is the reduction of metal ions in solution. Terpenoids, flavonoids, alkaloids and polyphenols are just a few major classes of phytochemicals present in plants that can aid in the synthesis of NPs (Verma and Mehata, 2016). The reduction and stabilisation of NPs occurs in one single step by plant-mediated synthesis routes (Njagi et al., 2011). The resulting NPs are end-capped by the metabolites from the plant and this enhances their stability. Whole plant tissue, crude plant extracts or compounds can be isolated and used for synthesis. Studies using isolated compounds, as opposed to crude plant extracts, have been reported to allow much better control during synthesis and significantly improve biological activity (Mittal et al. 2014, Kuppusamy et al., 2016). Different plant extracts affect the morphology and size of NPs synthesised due to their different structures and chemical properties (Nagarajan and Kuppusamy, 2013).

Secondary metabolites of therapeutic value have been a prime source of drugs and have provided leads for the development of drugs for the treatment of many diseases (Kulkarni and Muddapur, 2014). Their combined therapeutic effects with that of the NPs make them sought after for the synthesis of NPs. The laboratory synthesis of NPs using plant extracts and phytochemicals is easily performed at ambient conditions and is robust to scale up. It enables the products to be exploited for multiple applications and, more specifically, applications in the biomedical field. The synthesis procedure is simple (Figure 2.2) and the reaction can be completed within minutes depending on the combination of metal and secondary metabolite. The aqueous plant extract is mixed with the metal solution at room temperature and pressure. Nitrates, chlorides, sulphates etc. are amongst the commonly used precursors for the metal. At the molecular level, the metal ion is reduced from their mono or divalent oxidation states to their zero states and this results in the formation of NPs.

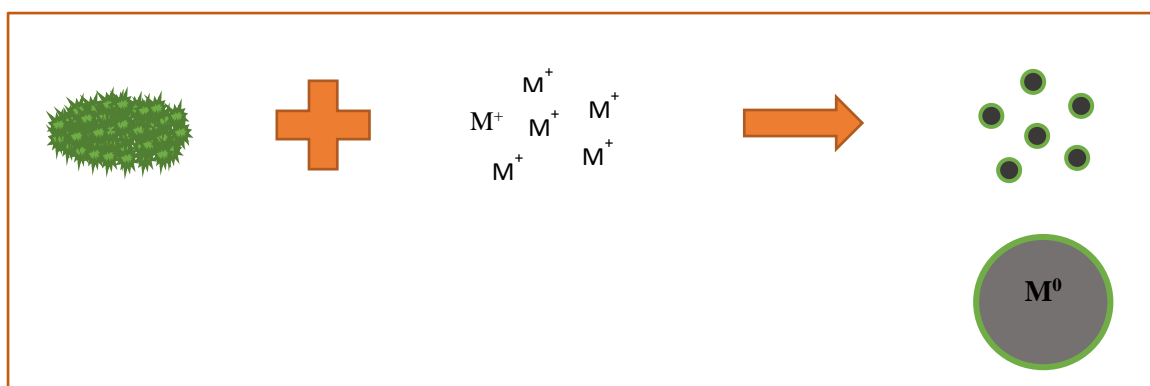


Figure 2.2: Proposed reaction scheme for biosynthesis of NPs via reduction and stabilisation of a metal ion using crude plant extracts or isolated phytochemicals

The reaction is monitored by observing the colour change of the solution when the NPs are formed which can be monitored by UV-Vis. The reactions are reliable and versatile and well known plants such as *Aloe vera* (Tippayawat et al., 2016), *Camellia sinensis* (Sun et al., 2014), *Pelargonium roseum* (Akhtar et al., 2013), *Nelumbo nucifera* (Santhoshkumar et al., 2011), *Calotropis gigantea* (Raman, 2014) and *Magnolia kobus* (Song et al., 2009) have already been reported to produce NPs. The extracts were found to contain flavonoids and terpenoids which were reported to be responsible for stabilising the synthesised silver NPs.

Plants have been used for thousands of years to treat health conditions and to prevent diseases including epidemics. Secondary metabolites are usually responsible for the biological activity of plant species (Cowan, 1999). Biological properties of plants include, inter alia, antibacterial, antioxidant, anti-fungal and anti-cancer activity (Silva and Fernandes Júnior, 2010; Majouli et al., 2017). Products derived from plants may potentially control microbial growth in diverse situations. In the specific case of disease treatment, numerous studies have focused on the chemical composition of plant antimicrobials and the mechanisms of action for microbial growth inhibition, either individually or associated with conventional antimicrobials. The use of plants with biologically active compounds for the synthesis of active NPs could introduce a major breakthrough in medicine. Since the NPs and the plant extract or isolated compound have therapeutic value, it is possible that their combination will provide superior activity than the individual components. The antimicrobial action of plant extracts, the synergism between conventional antimicrobial drugs and products obtained from medicinal plants have also been reported (Haroun and Al-Kayali, 2016; Kuok et al., 2017). Possible interactions among medications are frequently observed, which has motivated researchers to test such possibilities for NPs as well.

2.3 Overview of Traditional Medicine

The World Health Organization (WHO) defines traditional medicine as "the sum total of the knowledge, skills, and practices based on the theories, beliefs, and experiences indigenous to different cultures, whether explicable or not, used in the maintenance of health as well as in the prevention, diagnosis, improvement or treatment of physical and mental illness". Traditional medicine makes use of naturally occurring plant-derived materials with minimal, if any, industrial preparation to cure diseases and illnesses. There are great variations in the practice of traditional medicine from country to country, as it is influenced by factors such as culture, history, personal attitudes and philosophy. Their theory and applications, in most cases, are different from those of conventional medicine. This knowledge, is passed on from generation to generation. Efficiency and safety have been demonstrated by tradition but scientific research has to be used to provide the mechanism of the effect and identity of the compounds responsible for the healing properties. The use of traditional medicine dates back centuries and is still very popular in many countries but, it is often not recognised by conventional medicine. There isn't enough good quality data on the safety and efficiency of traditional medicine in order for it to

be supported worldwide (Cheng and Phillips, 2014). It is reported that over 80% of the African continent makes use of traditional herbal medicine with its worldwide annual market approaching \$60 Billion. Figure 2.3 shows the countries that use herbal medicine.

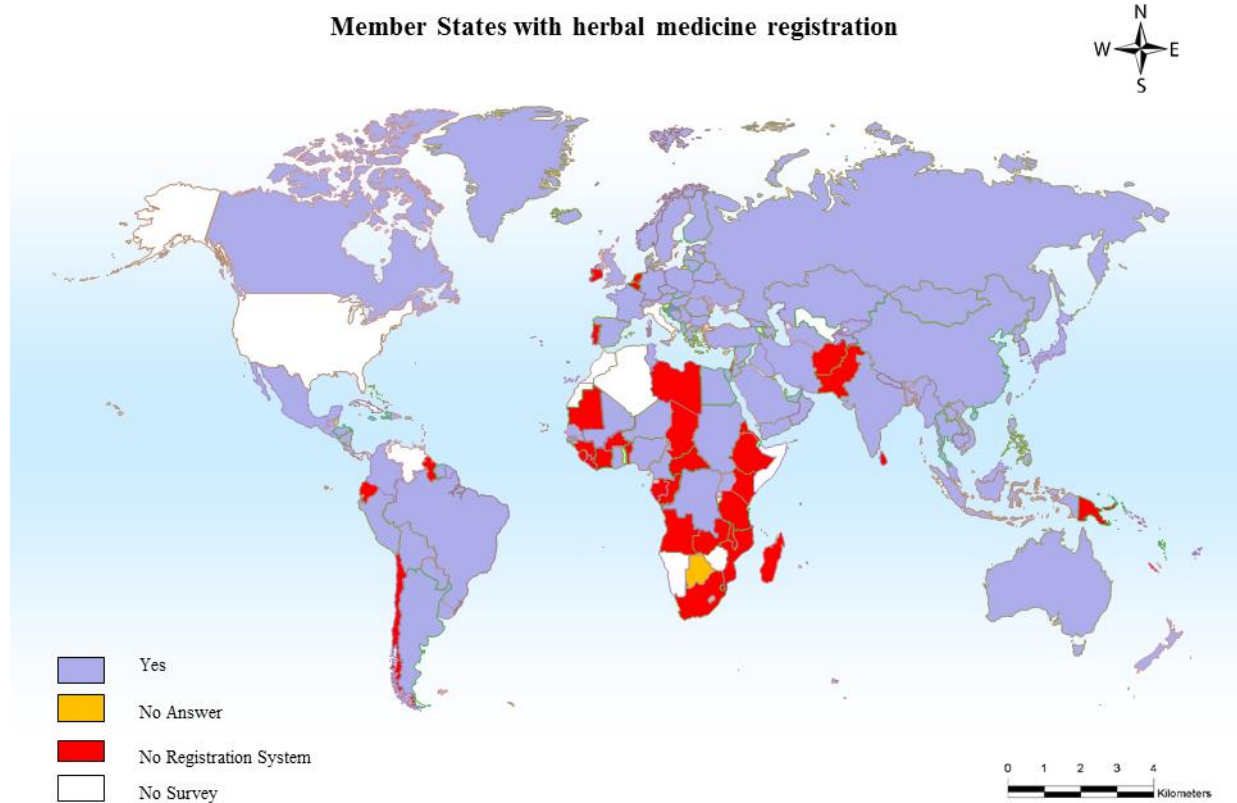


Figure 2.3: Map of the worlds countries showing extent of herbal medicine registration

South Africa has a rich plant diversity with as many as over 20 000 different plant species being of great interest to the scientific community (van Wyk, 1997). Many of these plant species have been screened for their biological activity but a large proportion still remains unstudied and their health benefits and mechanisms of action in the body are unknown (Solowey et al., 2014).

2.4 Plants in this Study

Two medicinal plants, *Chrysanthemodis monilifera* and *Harpephyllum caffrum*, both found in KwaZulu-Natal and with reported medicinal use (Pujol, 1990; Scott, 1996) were chosen for

this study. These plants also bear fruits that are easily collected and consumed thereby imparting nutritional and medicinal benefits.

2.4.1 Taxonomy of *Chrysanthemodis monilifera*

The Asteracea plant family, commonly termed the daisy or sunflower family, is documented as the largest family of flowering plants worldwide. It includes mainly herbaceous plants. There are over 25 thousand species growing at high mountain peaks as well as at sea level across the world. The species are grouped into 1700 genera and 12 subfamilies (Zavada and de Villiers, 2000). There is great variation in their morphology and growth since they are found in many different parts of the world such as Central America, eastern Brazil, the Andes, the Mediterranean, Levant parts of Middle East, central Asia, South Africa and southwestern China (Bohm and Stuessy, 2001). *Chrysanthemodis monilifera* belongs to the Asteroideae subfamily and is one of two members of the *Chrysanthemodis* genus along with *Chrysanthemodis incana*. Many of the species found in this family have economic value (Ivan, 1994). Sunflower oil and kernels are the leading food products provided to man by this plant family. French artichokes, lettuce and herbal teas like cammomile are also included. Various plant species are available to animals since they grow in many habitats. Animals use *Chrysanthemoides monilifera*, *Felicia muricata* and *Phymaspermum parvifolium* for grazing. These plants are easily obtained and some are used medicinally. Most of the medicinal plants belong to the Anthemideae tribe (of the subfamily Asteroideae) whose plants are usually recognised by their aroma. The African Wormwood or the wilde-als (*Artemisia afra*) (Rabe and van Staden, 1997), kapkokbos or wild rosemary (*Eriocephalus africanus*) (Catarino et al., 2015) and the wild camphor bush (*Tarchonanthus littoralis*) (Ali et al., 2013) are just a few plants from this subfamily which have been used by the people medicinally. These plants have been studied and found to contain high phenolic and flavonoid content which results in their biological activities (antioxidant, anti-fungal, anti-inflammatory, antibacterial, anti-cancer etc.).

The lineage of *Chrysanthemodis monilifera* is illustrated in Figure 2.4 and is as follows:

Family: Asteracea

Subfamily: Asteroideae

Tribe: Calenduleae

Genus and species: *Chrysanthemodis monilifera*

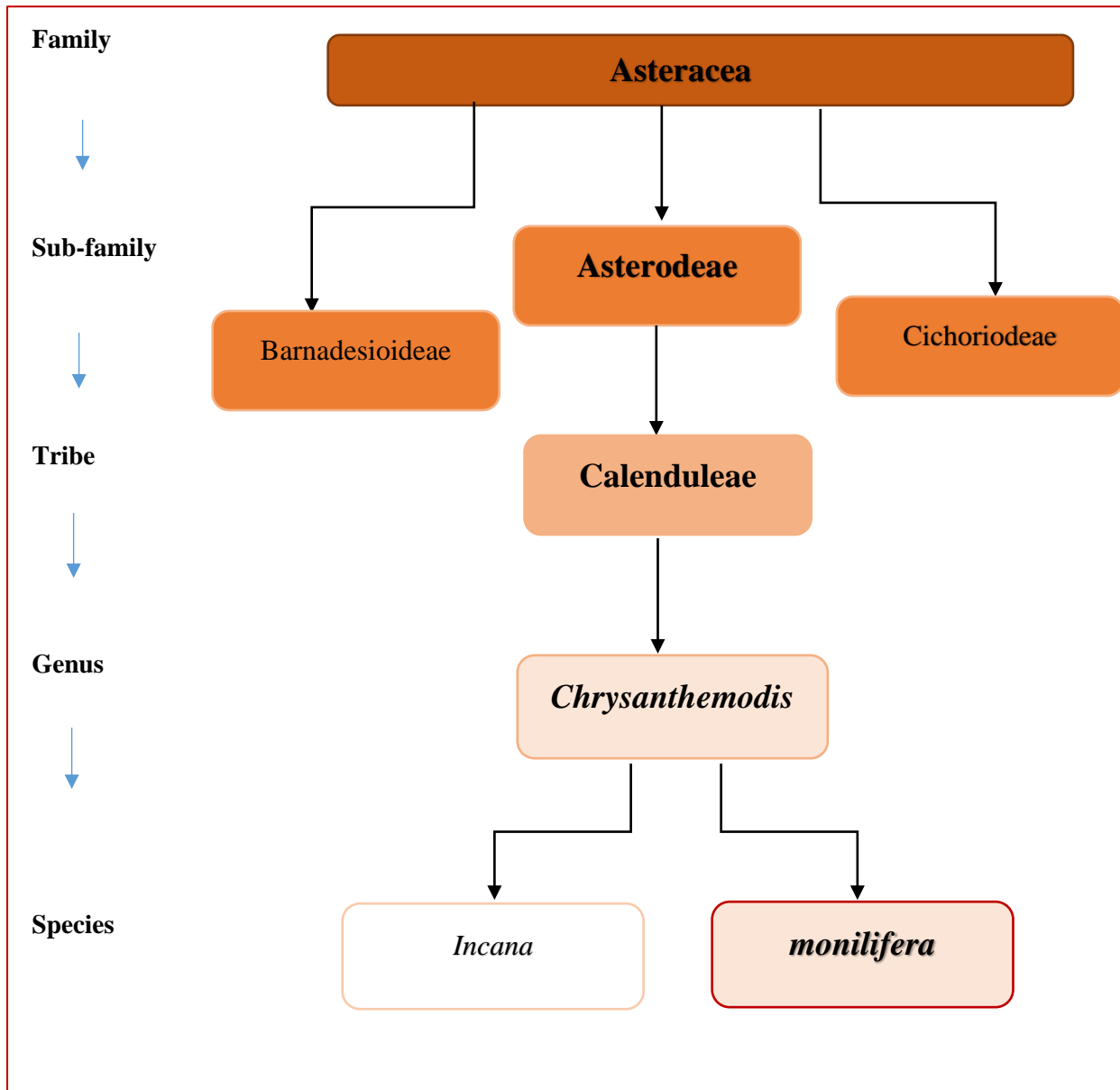


Figure 2.4: Lineage of the *Chrysanthemodis monilifera* plant species

2.4.2 *Chrysanthemodis monilifera*

Chrysanthemodis monilifera (Figure 2.5) is known as boneseed and bitou bush in Australia and bietou, tick berry, bosluisbessie, wekusbietou and iTholanja (isiZulu) in South Africa. It is a

drought resistant, fast growing ever-green, semi-succulent shrub or small tree. The leaves are oval and green in colour. The young leaves are covered densely with web-like hairs giving them a slightly green-to-grey colour. *Chrysanthemodis monilifera* often grows as shrubs and can reach a height of three metres when upright. It is identified by its yellow daisy sunflower-like flowers. The young stems of the plant are succulent and become woody with age. The green oval fruits which are edible and sweet, ripen to a blackish-purple colour and are enjoyed by birds.



Figure 2.5: Plant species in this study, *Chrysanthemodis monilifera*

The plant is well distributed in the Northern, Western and Eastern Cape Provinces of South Africa. It is also found along the Drakensberg escarpment in KwaZulu-Natal, Swaziland and Mpumalanga. It can also be found further into the Chimanimani Mountains of eastern Zimbabwe and to the north eastern part of Africa. It is found in fynbos, strandvels, grasslands, subtropical coasts and margins of forests. Although native to South Africa, this shrub is a major environmental weed and has been overly successful at invading bushlands in Australia and New-Zealand (Scott, 1996). It can do so because it grows very easily even on nutrient-poor soils and areas exposed to salts such as along the coastlines. Its seeds have the ability to

germinate readily and can persist in the soil seed bank for more than 10 years. Fires can assist *C. monilifera* to spread and because of the soil seed bank, the species can quickly recolonise a previously burnt area (Scott, 1996). The plant grows rapidly and vigorously and is capable of flowering and setting seed within 12-18 months.

The Khoi and the San people used the fruits of the tree as a source for food. Along with Sotho, Zulu and Xhosa, the Khoi also believe the fruit to contain blood strengthening and purifying qualities. Ripe berries are added to porridge and the juice is taken in water or tea. The fruits are believed to clear adolescent acne and skin problems. The leaves are made into an infusion and used as an anema to treat fevers, stomach ailments or gastritis (Herman and Condy, 2017).

2.4.3 Taxonomy of *Harpephyllum caffrum*

The plant family Anacardiaceae Lindl. (cashew family) encompasses two subfamilies namely Anacardioideae and Spondioideae. Within the subfamilies are five tribes (Rhoaeae, Anacardieae, Semecarpeae, Dobineeae and Spondiadeae) with 82 genera and more than 700 species (Pell et al., 2011). The Anacardiaceae comprises trees, shrubs, and lianas with resin canals that contain a clear to milky sap. *Harpephyllum caffrum* of the subfamily Spondiadeae, is indigenous to South Africa and is the only species in the genus. This family is renowned for its cultivated edibles, indehiscent, one-seeded fruits, seeds, and lacquer plants.

The lineage of *Harpephyllum caffrum* (Figure 2.6) is as follows:

Family: Anacardiaceae

Subfamily: Spondiadeae

Tribe: Spondiadeae

Genus and species: *Harpephyllum caffrum*

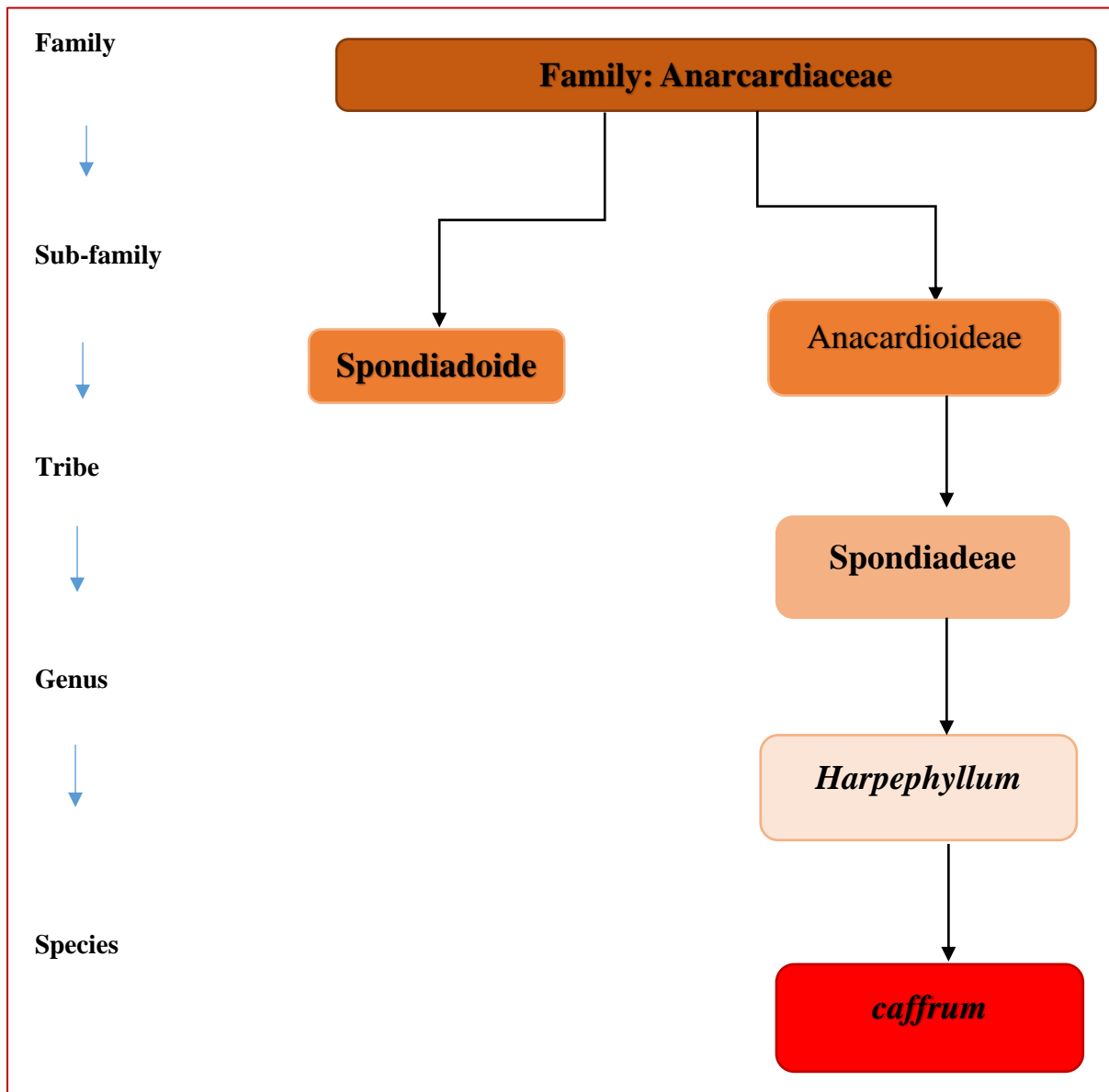


Figure 2.6: Lineage of the *Harpephyllum caffrum* plant species

2.4.4 *Harpephyllum caffrum*

In South Africa, *H. caffrum* (Figure 2.7) is known as wild plum in English, umgwenya in isiZulu, and mothêkêlê in Sesotho. The tree can be found all through the Eastern part of Southern Africa with distribution in South Africa ranging from the Eastern Cape to KwaZulu-Natal and the Limpopo Province. It is seen on the sides of the road in cities and townships as it is a common street tree.



Figure 2.7: Plant species in this study, *Harpephyllum caffrum*

The tree is large, single-stemmed, perennial, erect, evergreen, deciduous tree that reaches a height of about 15 m. The tree has shiny dark green leaves which are divided into several leaflets and its flowers are whitish-green and are borne near the ends of the branches with male and female flowers on separate trees (van Wyk, 1997). The plum-like fruit contains one seed and can be produced off-season if conditions are favourable but the fruit usually ripen in autumn. They are enjoyed by birds, animals, insects, and native humans unlike members of the family that are cultivated worldwide for their edible fruits and seeds, namely mango (*Mangifera indica* L.), pistachio (*Pistacia vera* L.), and cashew (*Anacardium occidentale* L.).

2.4.5 An ethnomedicinal and phytochemical review of some Anacardiaceae species

According to an ethnomedicinal survey, *H. caffrum* is commonly used in South African traditional medicine to treat, manage and control a variety of human illnesses. These include

uses as blood purifiers to treat skin conditions such as acne and eczema, for pain relief, and to manage and control childhood seizures and epilepsy (van Wyk, 1997; Pujol, 1996). Reports show that the aqueous extract of the stem bark possesses hypoglycaemic, hypotensive, anticonvulsant, and analgesic properties (Ojewole, 2006). Other species belonging to the Anacardiaceae are also used in traditional systems of medicine in different parts of the world. Different morphological parts of *Anacardium occidentale* L. are used in African Traditional Medicine. South Asian Traditional Medicine uses different morphological parts of *Mangifera indica* L. and of *Ozoroa insignis* Del. The ethanolic extracts of *H. Caffrum* from the leaves were reported to contain protocatechuic acid, gallic acid, methyl gallate, quercetin, and kaempferol (El Sherbeiny and El Ansari, 1976). Compounds isolated from other trees belonging to the same family include anacardic acid, anacardic acid methyl esters, cardols, cardanols, flavonoids, and triterpenoids. More recently the fruit extract of *H. caffrum* were reported to contain triterpenoids (β -sitosterol and lupeol) and (+)-catechin. A mixture of cardanols (1-hydroxy-3-((Z)-12'-nonadecenyl) benzene, 1-hydroxy-3-((Z)-12'-heptadecenyl) benzene, 1-hydroxy-3-heptadecanyl benzene and 1-hydroxy-3-pentadecanyl benzene), the alkyl *p*-coumaric acid ester (eicosanyl-*trans-p*-coumarate), and 129 (+)-catechin were isolated from the stem bark (Moodley, et al. 2014).

2.5 Secondary Metabolites

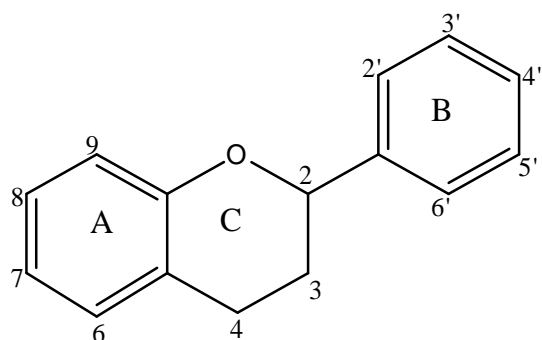
Secondary metabolites are organic compounds found in living organisms. They assist in the normal growth and development of an organism and play a defensive or protective role in plants. Some of the secondary metabolites are toxic so they can act as repellents to herbivores and pathogens. Humans have made use of secondary metabolites for medicinal purposes, flavouring as well as recreational drugs. The different plant families, genus and species produce specific and characteristic blends of these phytochemicals. In some cases, they have been used as taxonomic markers for identifying and classifying plants. A simple classification of secondary metabolites includes three main groups: terpenes (such as plant volatiles, cardiac glycosides, carotenoids and sterols), phenolics (such as phenolic acids, coumarins, lignans, stilbenes, flavonoids and tannins) and nitrogen containing compounds (such as alkaloids and glucosinolates). Chemical structures are used as a basis of classifying secondary metabolites and structures may or may not contain rings. The classes discussed herein are based on the phytocompounds isolated in this project.

2.5.1 Phenolic compounds

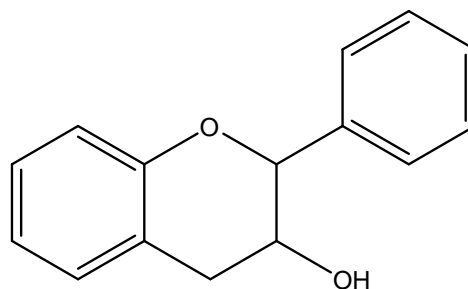
To date, there have been over ten thousand natural plant phenols that have been identified with half of them being of the flavonoid type and therefore remain a major topic to investigate when dealing with natural products. Flavonoids are widely distributed in nature and are found in most fruits and vegetables. Their chemical structures vary greatly, including simple phenols (C₆), such as hydrobenzoic acid derivatives and catechols, as well as long chain polymers with high molecular weight, such as catechol melanins (C₆)₆, lignins (C₆-C₃)_n and condensed tannins (C₆-C₃-C₆)_n. Phenolics contribute to the organoleptic (property associated with taste, colour and appearance of substances) and the nutritional qualities of fruits and vegetables. Stilbenes (C₆-C₂-C₆) and flavonoids (C₆-C₃-C₆) are phenolic compounds with intermediate molecular weight that present many pharmacological and biological activities. Flavonoids, including anthocyanins, flavonols (such as quercetin and myricetin), isoflavones (such as daidzein and genistein) and others are formed by multiple biosynthetic branches that originate from chalcone.

2.5.1.1 Flavonoids

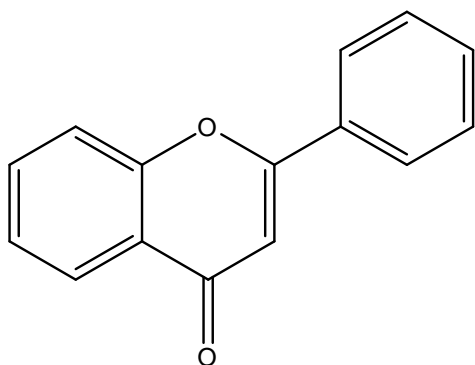
Flavonoids are polyphenolic compounds made up of 15 carbons, two aromatic rings (A- and B-rings) (Figure 2.8) interconnected by a heterocyclic ring (C-ring) (Park et al., 2008). Flavonoids can be subdivided into different subgroups depending on the carbon of the C ring on which the B ring is attached and the degree of unsaturation and oxidation of the C ring. The most widespread flavonoids contain a double bond between C-2 and C-3 and a keto function at C-4 of the C-ring (Figure 2.8). The subgroups of flavonoids include, amongst others, flavonols, flavones and flavanols.



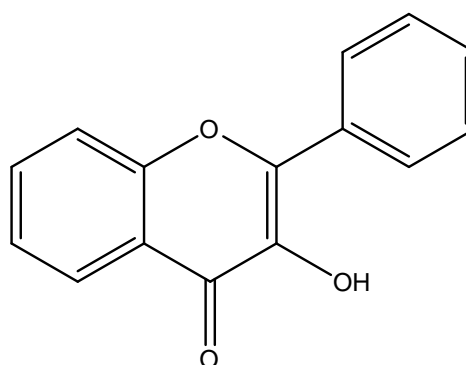
A) Flavonoids



B) Flavanols



C) Flavones

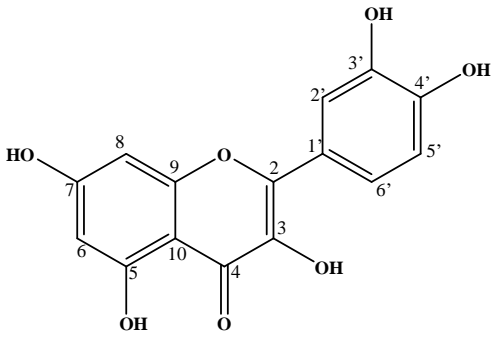
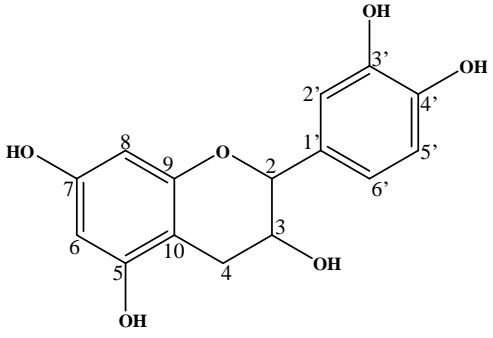


D) Flavonols

Figure 2.8: Classes of flavonoids

Flavonoids act as pigments in plants and are present in most tissues of fruits, flowers and vegetables with the coloured flavonoids seen best in flower and fruit epidermal tissue. An adult human will consume at least 10 g of flavonoids daily through fruits and vegetables. The biological activities of flavonoids, inter alia, include antioxidant, anti-inflammatory, anti-viral, anti-microbial, anti-ulcer, anti-osteoporotic, anti-allergic and anti-hepatotoxic (Einbond et al., 2004). Flavonoids have also been associated with prevention of cancer, cardiovascular diseases, premature aging and neurodegenerative diseases but their mechanism of action is still not known. Their biological effects are due mainly to their ability to interact easily with proteins and their extremely powerful antioxidant ability which arises from their phenolic substituents in their rings that have also demonstrated an ability to form chelate complexes (Rahman, 2007; Korkina and Afanas'Ev, 1996). Table 2.1 summarises the medicinal uses of the flavonoids (quercetin and catechin).

Table 2.1: Quercetin and catechin and their uses

| Structure, name and formula | Plants | Biological activity | References |
|---|---|--|--|
|  <p>Quercetin- $C_{15}H_{10}O_7$</p> | High concentrations in apples, onions and <i>Moringa oleifera</i> | Antioxidant activity, anti-cancer properties, cures certain allergies and reduces blood pressure | Wanget al., 2014 Horbowicz, 2002 Dmitrienko et al., 2012 |
|  <p>Catechin - $C_{15}H_{14}O_6$</p> | High concentrations in <i>Camellia sinensis</i> (tea plant), <i>Senegalia catechu</i> and <i>H. caffrum</i> | antioxidant activity and improves blood pressure | Vuong et al., 2010 Hye et al., 2009 Moodley et al., 2014 |

Quercetin belongs to the subgroup flavonols (Figure 2.8 D) and is the main flavonoid among the flavonols. Studies have shown quercetin exhibit powerful antioxidant, anticancer, anti-inflammatory and antiviral activity (Panche et al., 2016). Quercetin is also used to treat cardiovascular diseases. The other health benefits of quercetin include diarrhoea, allergies, asthma, hay fever, heart disease, hypertension, diabetes and rheumatoid arthritis (Joy, et al. 2016).

Hydroxyl groups present in the structure of quercetin are capable of forming complexes with various ion of metals. Quercetin, in particular, has a very strong chelating activity (Makarov et al., 2014). It can chelate at three positions, the carbonyl with hydroxyls at C3 (Ring C) and C5 (Ring A) and the catechol group at C3 and C4 (Ring B) (Bukhari et al., 2009; Wang et al.,

2014) (Figure 2.9). The chelating mechanism could explain the flavonoids ability to be adsorbed onto the surface of a growing nanoparticle. This also suggests that apart from bioreduction, flavonoids are also involved in the initiation stages of NP formation (nucleation) and further aggregation, in addition to the bioreduction stage.

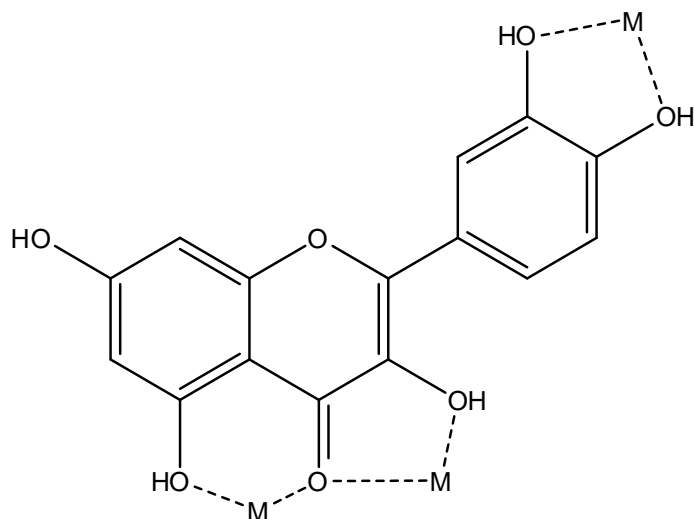


Figure 2.9: Chelating sites for quercetin (Symonowicz and Kolanek, 2012)

Catechin belongs to the subgroup flavanols (Figure 2.8 B) unlike quercetin which belongs to the flavonols. The C2-C3 double bond conjugated with a 4-keto group is a feature present for quercetin but not for catechin. The catechins are receiving significant consideration for their potential benefits to human health. Epidemiology and *in vivo* studies have associated the green tea catechins with the prevention of skin and liver cancers (Khan and Mukhtar, 2010; Isomura et al., 2016). Other studies have shown catechins to reduce the development of lung, gastric, and breast cancers (Yuan et al., 2011; Yuan, 2013). Other health benefits of catechins include the reduction of cardiovascular disease, dental decay, obesity, diabetes, and an improvement in the immune system (Weerawatanakorn et al., 2015; Velayutham et al., 2008; Chacko et al., 2010). There are two isomers of catechin (Figure 2.10) which are (-)-catechin and (+)-catechin, with the latter known as one of the most powerful free radical inhibitors. Moodley et al. (2014) isolated (+)-catechin from *H. caffrum* and it was found to have the highest antioxidant activity compared to other isolated compounds in the plant (Moodley et al., 2014).

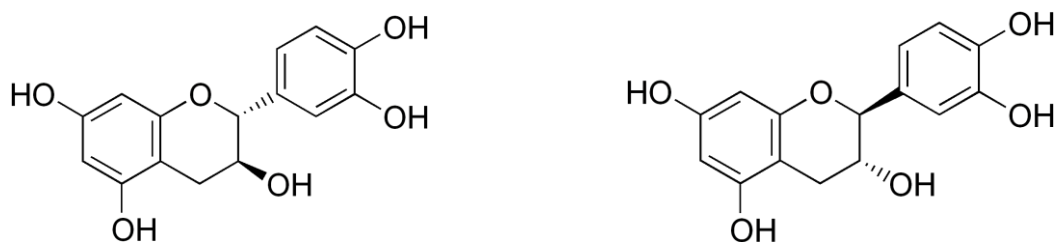


Figure 2.10: The two isomers of catechin are (+)-catechin and (-)-catechin

The structural characteristics of catechins allow them to donate hydrogens from the hydroxyl groups in their structure. They have been found to have excellent antioxidant activities, expressed through their free radical scavenging ability, being more powerful than vitamin C, vitamin E, or β -carotene (Murkovic, 2003; Flora, 2009; Intra and Kuo, 2007). Studies have also shown that due to the presence of the catechol group in catechin, the compound has chelating ability with transition metal ions (Cherrak et al., 2016).

2.5.1.2 Structure - activity relationships of flavonoids

Almost every group of flavonoids has a capacity to act as antioxidants for protecting the body against reactive oxygen species. Studies have shown their antioxidant capacities to be much stronger than those of vitamins C and E. The anti-oxidative property can be attributed to the phenolic hydroxyl groups attached to the flavonoid structure. The structural difference in each flavonoid subgroup results from the variation in the number and substitution position/pattern of the hydroxyl groups (Francisco, 1995). Flavonoids can prevent injury caused by free radicals in various ways and one way is the direct scavenging of free radicals. Flavonoids are oxidised by radicals, resulting in a more stable, less-reactive radical. Radicals are made inactive due to the high reactivity of the hydroxyl group of the flavonoids. The radical scavenging ability of the flavonoids depends largely on the availability of phenolic hydrogens and on the possibility of stabilisation of the resulting phenoxyl radicals via hydrogen bonding or by expanded electron delocalisation. The presence of a 3',4'-dihydroxy (o-dihydroxy) group (catechol structure in Figure 2.11) in the B ring is considered to be an essential structural requirement for effective radical scavenging (Seyoum et al., 2006).

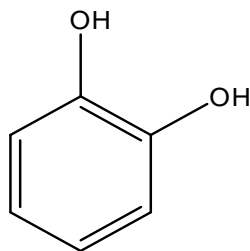


Figure 2.11: Ring B catechol moiety

The catechol structure has been shown to possess electron donating properties and being a radical target. Depending on a number and position of OH groups they may proceed as multiple sequential $1\text{H}^+ / 1\text{e}^-$ electron mechanisms. Catecholic (o-diphenolic) compounds are able to scavenge two free radicals via semiquinone formation (Figure 2.12), in two successive $1\text{H}^+ / 1\text{e}^-$ electron processes which results in quinone formation (Amic et al. 2013).

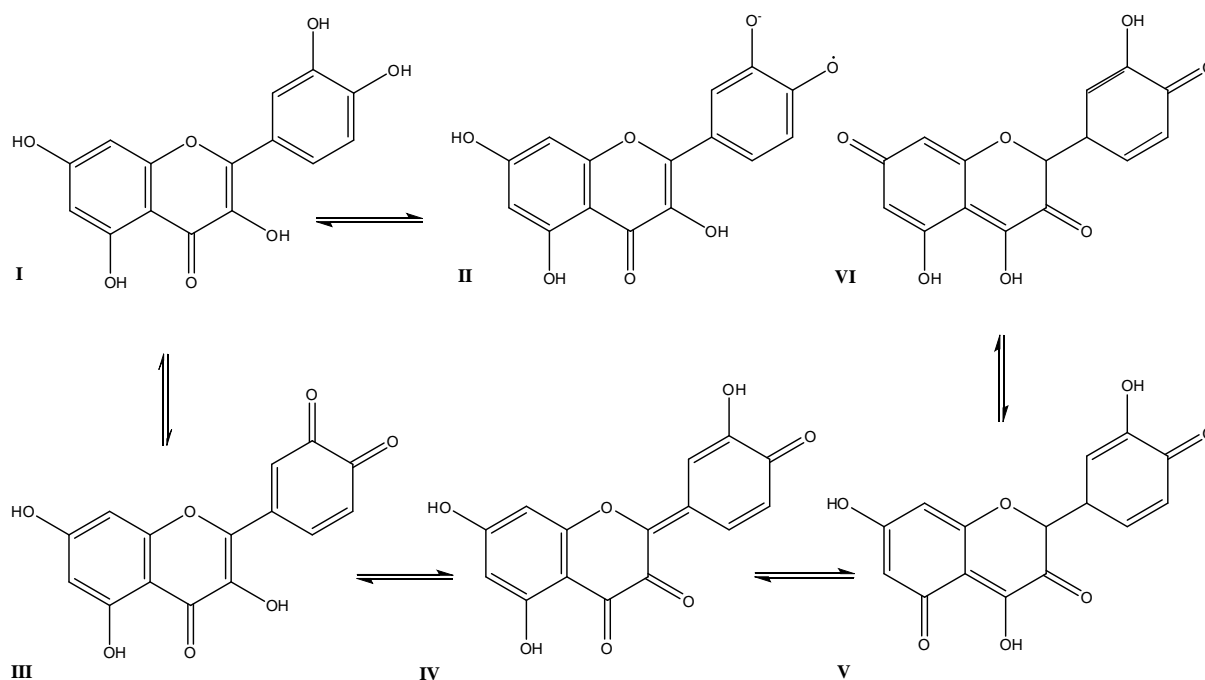


Figure 2.12: Formation of quinone from free radical scavenging

The 3-OH moiety of the C ring has also been shown to be beneficial for the antioxidant activity of flavonoids (Sim et al., 2007). The presence of the C2-C3 double bond conjugated with a 4-keto group that is responsible for electron delocalization from the B ring, further enhances the radical-scavenging capacity (Bors et al., 1990; Droy-Lefaix, 1997) and saturation of this C2-C3 double bond is believed to cause a loss of anti-oxidant activity potential (Rice-Evans et al.,

1996). The combined presence of 3-OH and 5-OH groups with a 4-carbonyl function and C2-C3 double bond can also increase the radical scavenging activity (Heijnen et al., 2001). These structural features contribute to the increase of the phenoxyl radical stability, i.e., the radical scavenging activity of the parent flavonoid. The mechanisms of action can generally be grouped into two types of processes: H-atom abstraction and subsequent radical adduct formation (Seyoum et al., 2006). The H-atom abstraction process may occur via at least three different mechanisms: hydrogen atom transfer, electron transfer followed by proton transfer and sequential proton loss electron transfer. Other possible mechanisms such as proton-coupled electron transfer and sequential proton-loss hydrogen-atom have also been observed (Chang et al., 2004).

Flavonoids interact with metal ions to form chelates (Symonowicz and Kolanek, 2012). In the structure of several flavonoids are three potential coordination sites (Figure 2.13):

- a) Between 5-hydroxy and 4-carbonyl group,
- b) Between 3-hydroxy and 4-carbonyl group,
- c) Between 3', 4'-hydroxy group in B ring

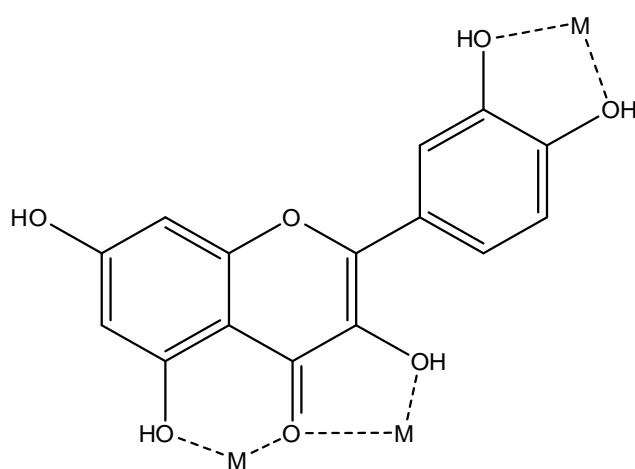


Figure 2.13: Chelating sites for quercetin (Symonowicz and Kolanek, 2012)

Many studies have confirmed that flavonoids can behave as antioxidants because of their chelating properties (Symonowicz and Kolanek, 2012). Flavonoids contain various functional groups capable of NP formation. It is believed that the tautomeric transformations of flavonoids from the enol-form to the keto-form may release a reactive hydrogen atom that is needed to reduce metal ions to form NPs. A study conducted by Ahmad et al. (2010) showed that during the synthesis of silver NPs using *Ocimum basilicum* (sweet basil) extracts, the transformation

of flavonoids (luteolin and rosmarinic acid) from the enol to the keto form played a key role in the formation of silver NPs from silver ions.

2.6 Extraction and Characterisation of Natural Products

Natural products from medicinal plants, either isolated as pure compounds or used as crude extracts, have provided limitless opportunities for new drug leads because of chemical diversity coupled with their availability. The extraction, isolation and characterisation of natural products is discussed in this section. The strengths and weaknesses of different extraction techniques are discussed since extraction is the most significant step in the analysis of components present in plant extracts. The analysis of bioactive compounds in plant extracts involve the applications of common chromatographic techniques such as column chromatography and, thin layer chromatography (TLC) as well as spectroscopic techniques.

2.6.1 Separation methods - chromatography

Chromatography is an analytical technique that is used in the separation of components in complex mixtures. It has been applied to a variety of systems in which all make use of a stationary phase and a mobile phase. The mixture passes through a stationary phase by the flow of either a gaseous or liquid mobile phase. Separation of the mixture is based on the interaction of the components with the stationary phase. The component with stronger interactions with the stationery phase takes longer to elute from the column than those with weaker interactions. This technique can be used to separate anything from secondary metabolites in plants extracts to the purification of mixtures in synthetic reactions. Examples of chromatographic techniques include liquid chromatography, column chromatography (CC), ion selective chromatography, size exclusion chromatography, thin layer chromatography (TLC) as well as gas chromatography. The chromatographic techniques used in this project will be explained in detail (Coskun, 2016).

2.6.1.1 Column chromatography

A stationary phase which is typically silica gel (SiO_2) or alumina (Al_2O_3) is packed into a vertical glass column. The stationary phase for this work was silica gel (Coskun, 2016).

Solvents ranging in polarity from non-polar (hexane) to polar methanol (MeOH) are used as the mobile phase. The mixture, or in this case the extract, being separated is placed in the column above the stationary phase. The working principles are illustrated in Figure 2.14.

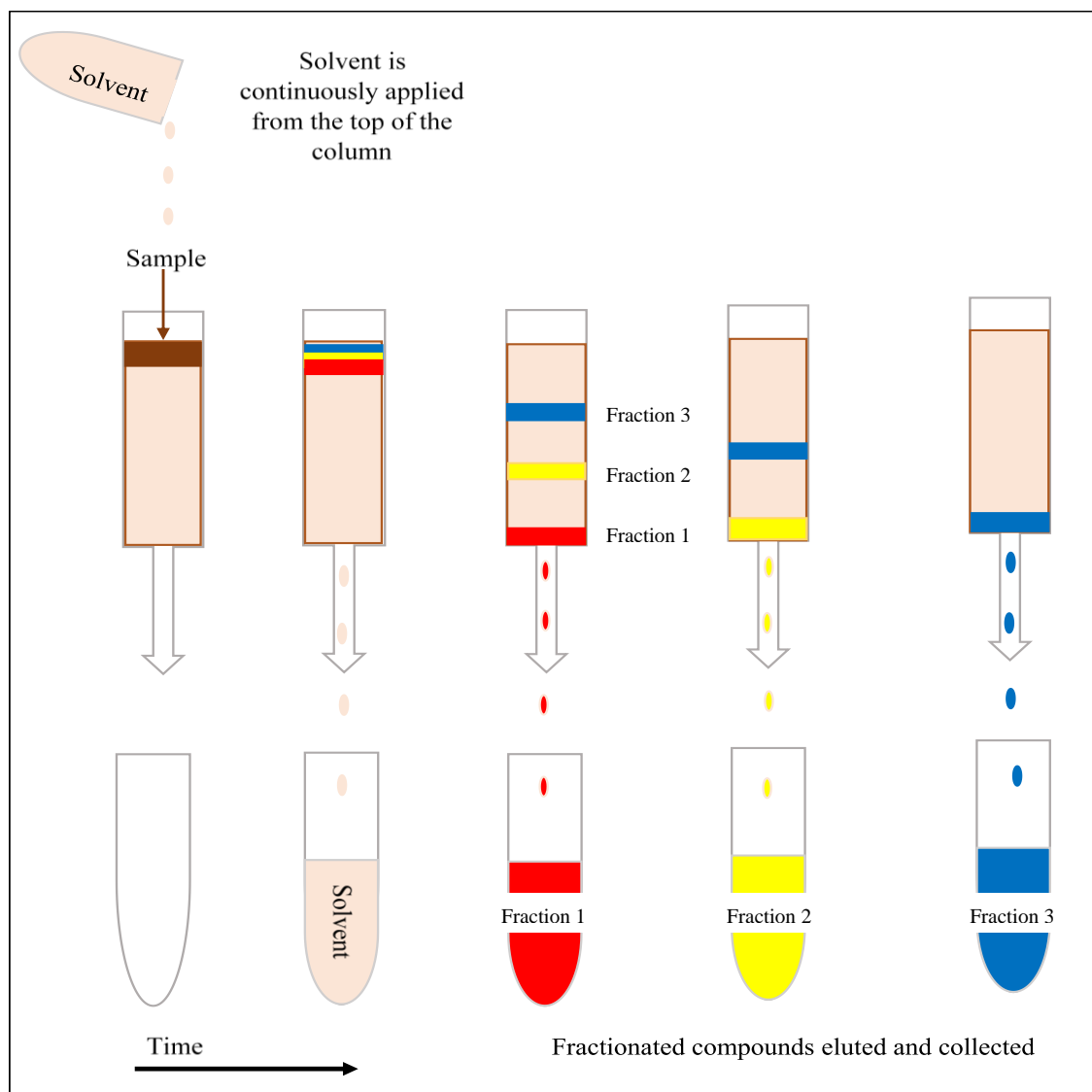


Figure 2.14: Purification of a complex mixture using column chromatography

Solvents, ranging from non-polar to polar are poured from the top of the column. As the solvents flow down the column, they also elute the sample through the column. The components of the plant extract are separated as they elute with the mobile phase that matches their polarity, with the least polar components being eluted first. This technique is most effective with relatively long columns and a low solvent flow rate. The major drawback and environmental concern surrounding the technique is the large consumption of solvents but the technique still remains widely used as an effective separation technique. This shortcoming is

addressed by collecting the solvents frequently via rotary vacuum evaporator leaving the purified material behind.

For elution, a mobile phase consisting of solvents ranging in polarity is used starting with 100% hexane and stepped to 100% ethyl acetate (EtOAc). Fractions are collected in each eluent step. This is known as fractionation and this process divides the mixture into smaller fractions of varying composition. Extracts of similar retention factor (Rf) on thin layer chromatography (TLC) are combined. Single spots on the TLC plate usually indicate a pure compound. Spectroscopic techniques and data published in literature are used to identify the compound.

2.6.1.2 Thin layer chromatography (TLC)

Thin layer chromatography is an inexpensive and simple method of determining the purity of isolated or synthesised compounds. It can also be used to monitor the progress of a chemical reaction (Coskun, 2016). This technique involves the use of an aluminium sheet coated with silica which acts as a stationary phase and is placed in a chamber containing organic solvents of different polarities as illustrated on Figure 2.15. The solvent migrates up the plate carrying with it compounds. Different compounds travel up the TLC plate at different rates. The ratio of the distance that a molecule travelled to the distance that the solvent travelled is called the retention factor (Rf) which is calculated as follows:

$$R_f = \frac{\text{Distance moved by solute}}{\text{Distance moved by solvent}}$$

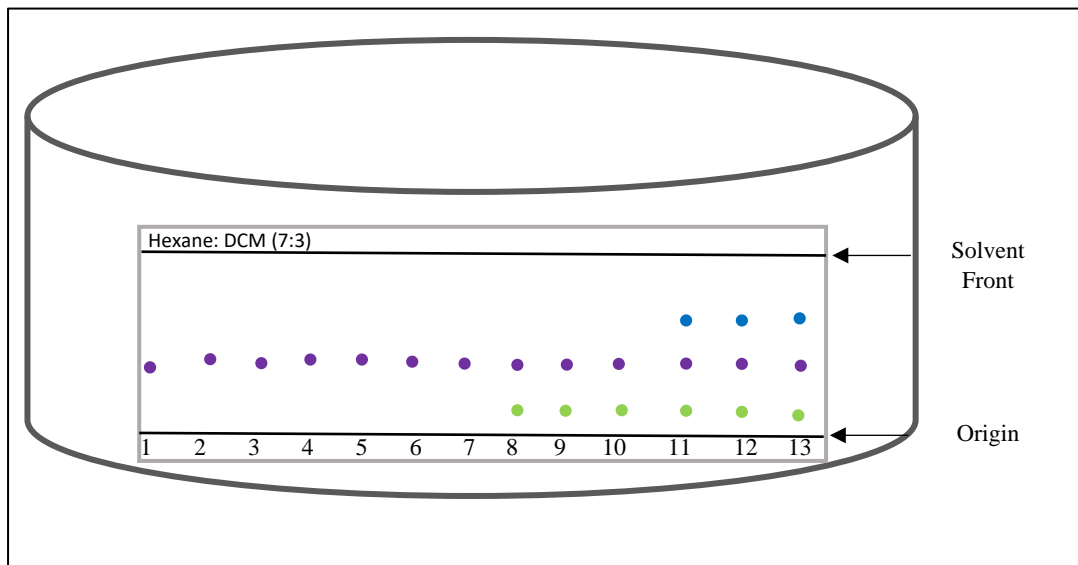


Figure 2.15: Thin layer chromatography (TLC) of fractions collected using column chromatography where numbers 1-13 indicate the different fractions

The eluted fractions from column chromatography are monitored or “spotted” on a TLC plate. Compounds with equal R_f values (spots 1-7 Figure 2.15) are considered the same with regards to purity where as a single spot is an indication of a clean compound and multiple spots are an indication of a mixture that may still undergo purification. Spots 1-7 are not only considered to be the same, but they are also considered to be pure and this is confirmed using other techniques. Spots 8-10 are different from 11-13 but both sets of fractions would need to be fractionated on another column until an individual compound can be isolated. The spots on a TLC can be seen with a naked eye if the compounds are coloured, otherwise a portable UV lamp at 254 nm and 366 nm can be used. This technique is used concurrently with column chromatography.

2.6.2 Gas chromatography (GC)

The separation in gas chromatography (GC) is based on the relative boiling points of compounds and the components relative affinity for the stationary phase (Coskun, 2016). Only volatile compounds can be analysed with this technique. For analysis, a gas is used as a mobile phase. The gas is often an inert gas such as argon which is referred to as the carrier gas. Figure 2.16 shows a schematic diagram of the components of a typical GC instrument.

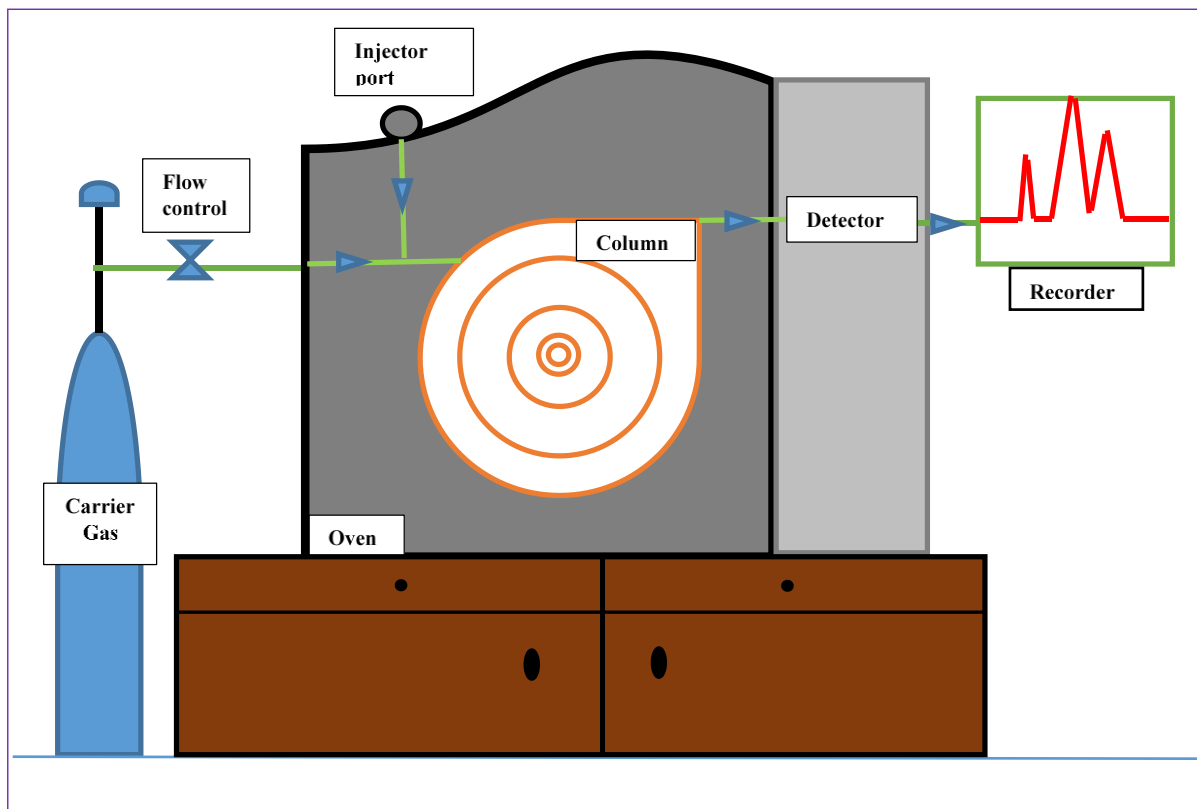


Figure 2.16: Components of a gas chromatography instrument

After being injected through the injector port, which is set at 50 °C lower than the boiling point of the least volatile component of the mixture, the sample is taken by the carrier gas to the column where it is volatilized. The column contains the stationary phase that the components of the mixture can interact with. When the separated components elute the column, they are sent to the detector and are represented as peaks on the chromatogram. GC instruments are compatible with many detectors but in this project the detector was a mass spectrometer. A mass spectrometer is used to identify various components from their distinctive fragmentation patterns. Each compound has a unique or near unique mass spectrum that can be compared with mass spectral databases and thus the compound can be identified. Figure 2.17 shows the basic operations of a mass spectrometer.

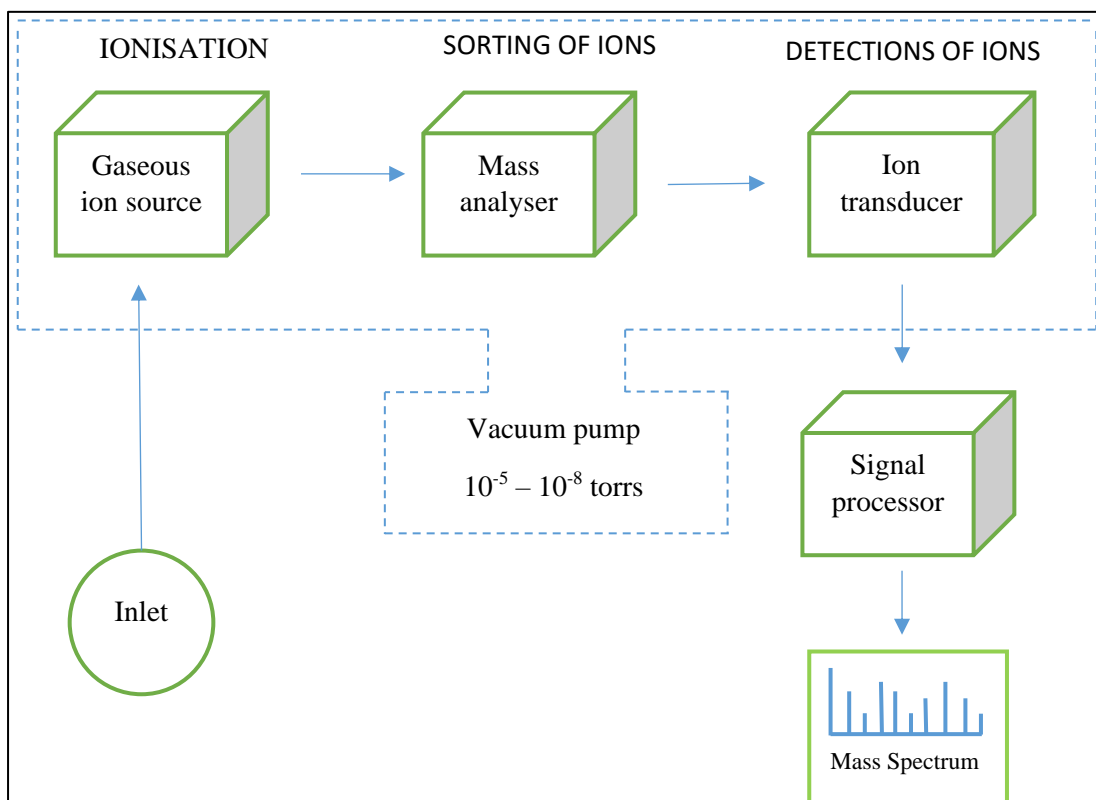


Figure 2.17: Basic operation of a mass spectrometer

A mass spectrometer operates by first creating gas-phase ions of a given sample. The sample can be ionised using a range of ionisation sources such as chemical ionisation (CI), atmospheric pressure CI (APCI), electron impact (EI), electrospray ionization (ESI), fast atom bombardment (FAB), field desorption/field ionisation (FD/FI), matrix assisted laser desorption ionisation (MALDI) and thermospray ionisation (TI). Secondly, the ions are separated in space or time based on their mass-to-charge ratio. Mass spectrometers use the difference in mass-to-charge ratio (m/z) of ionized atoms or molecules to separate them. Finally, the quantity of ions of each mass-to-charge ratio is measured and used to generate a mass spectrum.

2.6.3 Nuclear magnetic resonance (NMR) spectroscopy

Nuclear magnetic resonance (NMR) spectroscopy is a spectroscopic technique that is used to analyse the nuclei of a sample. This technique is only useful at detecting atoms with $\frac{1}{2}$ spin. Examples of atoms with $\frac{1}{2}$ spin include H, C, O, N, F and P (Wong, 2014). This technique is particularly useful for the analysis of the organic phytochemicals isolated from column chromatography. The phytochemicals consist of C and H atoms that could be analysed using this technique. Nuclei with $\frac{1}{2}$ spin have a magnetic moment. Figure 2.18 below illustrates that

at rest, spins are orientated randomly but when a constant external magnetic field (B_0) is applied, the nuclear magnetic field of the nuclei can either align with the external magnetic field or oppose the external magnetic field.

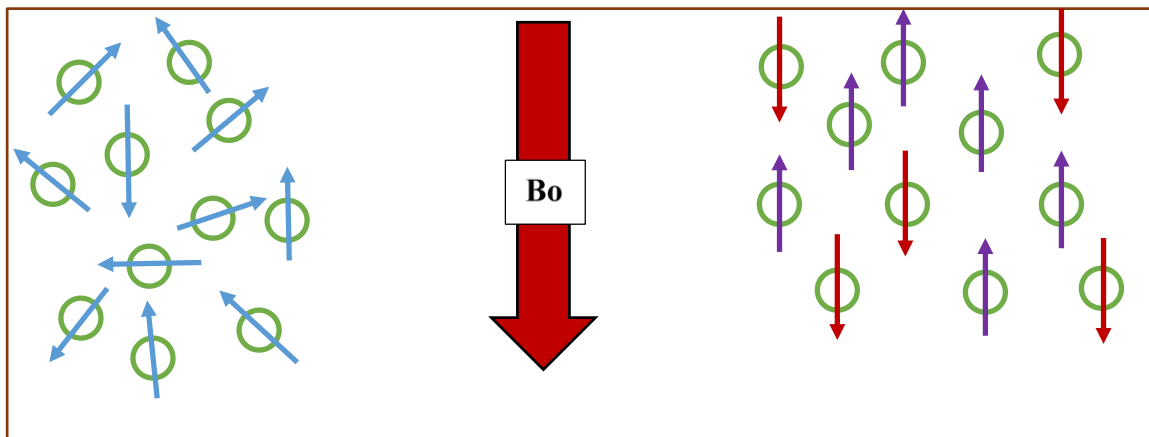


Figure 2.18: Schematic representation of the operating principles of nuclear magnetic resonance spectroscopy

The signals from the nuclei are measured in parts per million (ppm) of static field strength. Therefore, the more concentrated your sample, the greater the intensity of the signal. The instrument operates by pulsing a radio frequency (RF) to make the nuclei resonate. This pulse is a magnetic field (B_1) that is placed perpendicular to the constant magnetic field B_0 . After the pulse, the nuclei return to their ground energy state. This produces a current that can be detected by a coil in the NMR spectrometer. Different nuclei absorb electromagnetic RF at different wavelengths. Nuclei of a given type will resonate at different energies depending on their chemical and electronic environment. The position (chemical shift) and pattern (splitting or multiplicity) of the NMR signals gives important information about the chemical environment of the nuclei. A chemical shift is the exact field strength (in ppm) of a nucleus that resonates relative to the reference standard tetramethylsilane (TMS) which resonates at 0 ppm for ^1H NMR. Electron clouds “shield” nuclei from the external magnetic field causing them to absorb at slightly higher energy. Shielding is the influence of neighbouring functional groups on the electronic structure around a nucleus and consequently the chemical shift of their resonance. Chemically and magnetically equivalent nuclei resonate at the same energy and give a single signal or pattern. The vertical scale measures intensity while the horizontal scale is the chemical shift which is dependent upon the field strength of the external magnetic field. For

^1H NMR, chemical shifts are usually from 1-10 ppm and for ^{13}C NMR, typical chemical shifts are recorded from 1-200 ppm.

2.6.4 Ultraviolet-visible (UV-Vis) spectroscopy

Ultraviolet-visible (UV-Vis) spectroscopy techniques analyse samples based on their ability to absorb light. It is widely used because of its versatility, speed, accuracy and cost effectiveness. UV-Vis spectroscopy requires a light source, in the visible and ultraviolet region, to pass through a sample. The light that emerges from the sample is also measured and the difference is the light absorbed. The schematic in Figure 2.19 shows the basic components of a double spectrophotometer.

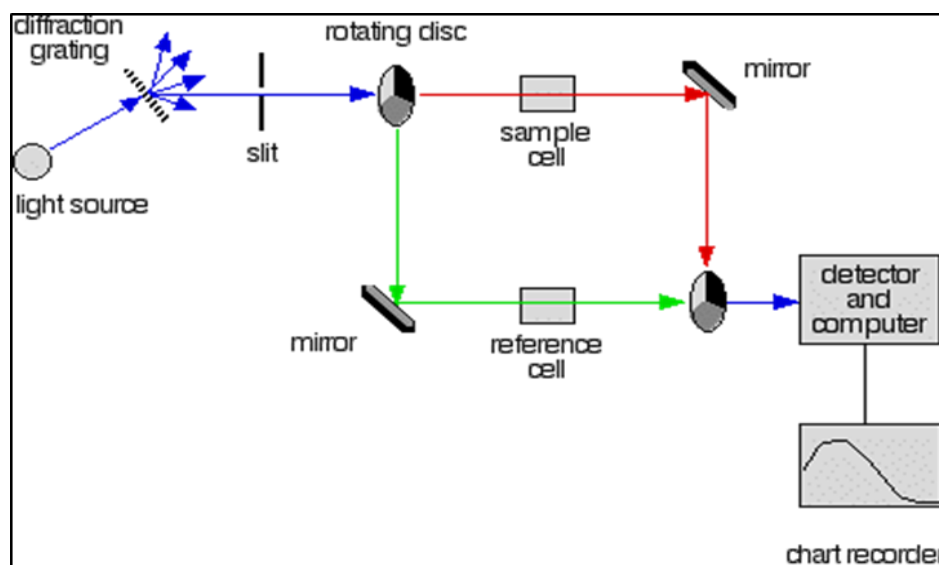


Figure 2.19: Schematic of an ultraviolet-visible (UV-Vis) double beam instrument

The light source in a UV-Vis spectrophotometer is in the ultraviolet and visible region of the electromagnetic spectrum. The visible region (380-750 nm) of the spectrum comprises photon energies of 150.6 to 3012 kJ mol^{-1} , and the near ultraviolet region (190-380 nm), extends this energy range to 598 kJ mol^{-1} (Yu et al., 2018). The colour of a substance is related to its electronic structure. The molecule will only absorb light in the UV-Vis region when the radiation from the light source has resulted in an electronic transition within the structure. The energies mentioned here are sufficient to promote or excite a molecular electron to a higher energy orbital. When sample molecules are exposed to light having an energy that matches a possible electronic transition within the molecule, some of the light energy will be absorbed as

the electron is promoted to a higher energy orbital. Organic compounds with a high degree of conjugation, similar to those used in this work, can absorb light in the UV or visible regions of the electromagnetic spectrum. The absorbance of the sample is measured against a reference material which is typically the solvent in which the sample is dissolved. This ensures that the spectrum obtained is only for the sample of interest and not of the solvent as solvents too can absorb electromagnetic radiation.

2.6.5 Infra-red (IR) spectroscopy

Fourier-transform infrared (FTIR) spectroscopy is a very useful tool for identifying the types of chemical bonds (functional groups) present in compounds or adsorbed on the surface of materials. The wavelength of light absorbed is characteristic of the chemical bond. By interpreting the infrared (IR) absorption spectrum, the chemical bonds in a molecule can be determined. The absorption of IR radiation is commonly expressed in wave numbers (cm^{-1}). The absorption of IR radiation is only possible by those bonds in a molecule that show a change in dipole moment by the absorption of radiation. For example, the vibrational transitions of C=O, O-H, N-H etc. bands are accompanied by a change in dipole moment, hence absorb strongly in the IR region. Fourier-transform infrared can be employed in conjunction with NMR and UV-Vis to establish the identity of a compound or to determine the structure of a new compound.

Photon energies associated with the infrared region of the electromagnetic spectrum (from 4.2 to 62 kJ mol^{-1}) is not large enough to excite electrons, but they can induce vibrational excitation of covalently bonded atoms and groups (McDonald, 1986). Atoms in molecules have a slight rotation about their single bonds and they experience a wide variety of vibrational motions that are characteristic of their component atoms. Essentially all organic compounds will absorb IR radiation that corresponds in energy to these vibrations. Covalent bonds in molecules are not rigid, they behave more like stiff springs that can be stretched and bent. Vibrational modes are often given descriptive names such as stretching, bending, scissoring, rocking and twisting. The exact frequency at which a given vibration occurs is determined by the strengths of the bonds involved and the mass of the component atoms. Infrared spectrophotometers are similar in principle to the UV-Vis spectrophotometers. Absorption spectra of compounds that are a unique reflection of their molecular structure can be obtained. The components of an IR

spectrometer are illustrated in Figure 2.20. Infrared instruments require a light source (IR source) to interact with a sample to induce vibrations. The beam enters an interferometer which measures all the frequencies of the IR beam simultaneously. The beam splitter divides the light beam into two and reflects these beams off mirrors and the beam again later at the beam splitter. The interaction of the two beams creates a signal that is known as an interferogram. The beam is then passed through the sample which will absorb some of the frequencies. The absorbed frequencies are uniquely dependent on the sample that is being analysed. The beam emerging from the sample is then passed to the detector where the signal is measured and sent to a process computer. Fourier-transformation takes place in the computer and the individual frequencies are interpreted to produce a spectrum. The spectrum consists of peaks which correspond to the frequencies at which the bonds of the atoms in the specific molecule will stretch, bend or vibrate. These peaks are unique and can then be matched to different functional groups based on the frequencies at which they appear.

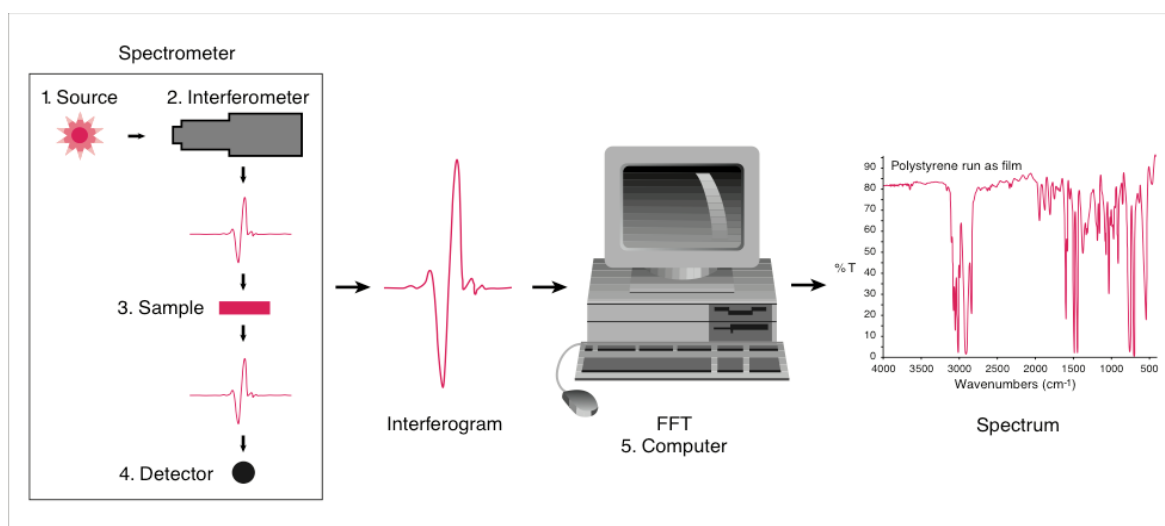


Figure 2.20: Schematic diagram of the operating principals of an infrared spectrophotometer

Since most organic compounds have C-H bonds, absorption in the 2850 to 3000 cm^{-1} is generally due to sp^3 C-H stretching, absorption above 3000 cm^{-1} is from sp^2 C-H stretching and sp C-H stretching near 3300 cm^{-1} .

2.7 Characterisation of nanoparticles

Centrifugation is an important, cost-effective and highly efficient procedure that is employed for the harvesting of NPs. Thereafter, NPs can be characterised with spectroscopic and

microscopic techniques to obtain information such as size, shape, phase and chemical composition of the NPs. Morphology and particle size distribution are amongst the most important parameters for characterising NPs and these factors can be measured by microscopic techniques.

2.7.1. Spectroscopy (ultraviolet-visible and infrared)

Ultraviolet-Visible (UV-Vis) spectroscopy is important for monitoring colloidal solutions to determine the formation of NPs and their stability. Colloidal solutions of NPs usually have intense colours. This property stems from the surface plasmon resonance (SPR) exhibited by these solutions. When free electrons interact with electromagnetic radiation it causes the electrons to oscillate and this gives rise to the intense colour which can be measured using UV-Vis spectroscopy. The surface plasmon absorption in the metal oxide NPs is due to the collective oscillation of the free conduction band electrons which are excited by the incident electromagnetic radiation (Noguez, 2007). Each metal and metal oxide has a characteristic SPR by which it can be identified. Information about the size distribution of the synthesised NPs can be also be observed by peak broadening for a wide size distribution and sharp peaks for a narrow size distribution.

Fourier-transform infrared (FTIR) spectroscopy is conducted to identify the functional groups present on the biosynthesised NPs. The spectrum represents a fingerprint of the NPs consisting of absorption peaks that correspond to the frequencies of vibrations between the bonds of atoms in the NPs. Since each type of NP contains a unique combination of atoms, the identity of the functional groups present on the surface of the NPs can be determined based on the FTIR spectra.

2.7.2 Powder X-ray diffraction (PXRD)

X-ray diffraction (XRD) is a rapid and non-destructive technique that is used to obtain structural information about crystalline solids such as ceramics, metals minerals and inorganic compounds. All crystalline material gives a pattern and the same substances always produce the same pattern. In instances of a mixture of substances, each substance produces its own pattern independently of the other components in the mixture. Using specialised software, the

different substances in the mixture can be distinguished. A powder may be composed of many small and finely ground crystals, known as crystallites which are assumed to be randomly orientated to one another. The arrangement of the atoms thus gives the diffraction pattern by which materials can be identified. The pattern produced gives information about the arrangement of the atoms in a crystal, the degree of crystallinity and particles/crystallite size.

Powder XRD (PXRD) can measure the spacings between rows of atoms. When monochromatic X-rays produced from a cathode array interact with the sample under Bragg conditions (when the wavelength of incident X-rays is the same as the d-spacings) then constructive interference occurs. Electrons in an atom can scatter light. Each atom is then considered a scatter point. The atoms strength to which it scatters light is proportional to the number of electrons around the atom. Since the atoms are arranged in a periodic array, they can therefore diffract light. Diffractions occurs when a wave encounters a slit or an obstacle and a series of bright and dark bands from which illustrate constructive and destructive interferences when the light waves meet in phase and out of phase. Braggs Law dictates that for two incident X-rays in phase and with the same wavelength, have a path difference of

$$\lambda = 2d\sin \theta$$

where d = interplanar distance, θ is the diffraction angle and λ is the wavelength of the incident X-ray beam.

The constructive and destructive interference that occur, result in a pattern of peaks. If the powder is placed in the path of a monochromatic X-ray beam, diffraction will occur from the planes in those crystallites that are oriented at the correct angle to fulfill the Bragg condition. Characteristic diffraction patterns of materials are scanned through a range of 2θ angles where all possible diffraction directions can be accounted for. In order to determine which planes are responsible for each reflection, the reflections would need to be indexed (assigned the correct

hkl). The position of the peaks can then be compared to those of known materials for phase identification (Figure 2.21a and b).

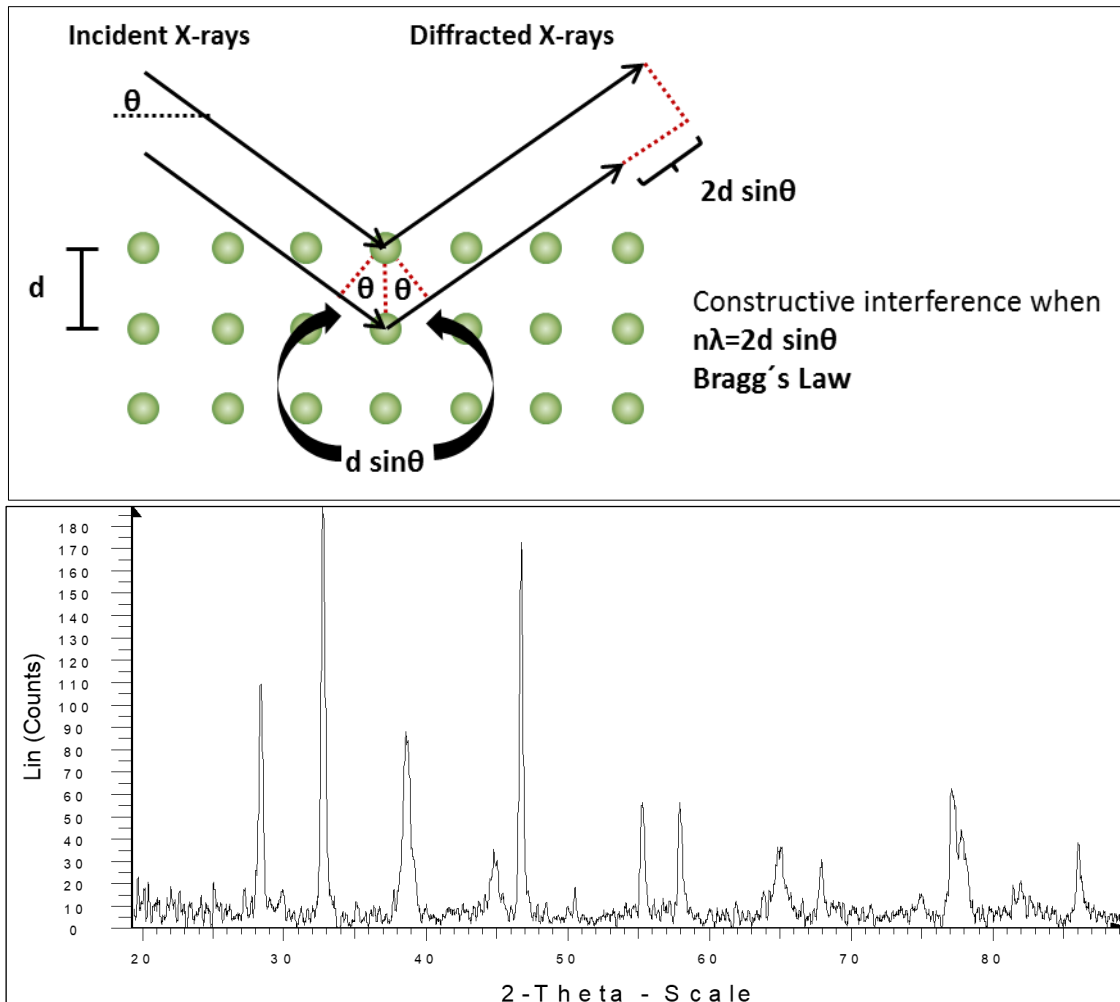


Figure 2.21: (a) Schematic of the working principle of an X-ray diffraction (XRD) instrument
 b) a typical spectrum obtained from the instrument. (Touloukian,1977)

The X-rays that are collected by the detector result when the incident electrons have substantial energy to displace the inner most core electrons of the crystalline material. The resultant spectral lines produced from this atomic transition are named using the Siegbahn notation with the $K\alpha$ and the $K\beta$ being the most commonly observed lines. The wavelengths are specific to the X-ray source material. Copper is the most common with a $K\alpha$ radiation value of 1.5406 Angstroms(\AA) but other sources such as Co can also be used. The wavelength of the X-rays is related to the distance between the atoms in the crystal.

The major drawback associated with most instruments is the capability of only detecting phases around two wt%. To add, large amounts of sample that need to be loaded onto the sample holder although. This, however, is cured by the use of fillers. These are materials that will contribute to the bulk of the material but remain undetected. Discretion still needs to be exercised with regards to the ratio of sample to filler used during analysis.

2.7.3. Microscopy

Microscopy is a field of analysis that uses microscopes to view objects and areas of objects that are not within the resolution range of the normal eye. The three major branches that make up this field are optical, electron and scanning probe microscopy. Optical and electron microscopy rely on the diffraction, reflection, refraction and electron magnetic radiation interacting with a sample for a useful analysis. The scattered radiations along with other signals are collected and an image is produced. The process is carried out by either scanning a fine beam over a sample (scanning electron microscopy (SEM)) or by a wide-field irradiation of the sample (transmission electron microscopy SEM)).

2.7.3.1 Scanning electron microscopy (SEM)

Scanning electron Microscopy (SEM) produce images the surface of a specimen (sample) using a focused beam of electrons which is scanned over the surface. The electron beams interaction with the atoms of the sample produces various signals that give information about the samples topography and composition. For analysis, the nanoparticle solution is dried into a powder, mounted on a sample holder, and coated with a conductive metal such as gold, gold/palladium alloy, platinum, osmium, iridium, tungsten, chromium, or graphite using a sputter coater. The beam of electrons is produced by the thermionic electron gun with the aid of emitters, as seen on Figure 2.22, such as a tungsten filament or LaB₆ crystal. The emitter is electrically heated to produce electrons. The electrons are then passed through lenses that control the beam and focus it onto the sample. When the electron beam passes through the sample; diffraction, scattering and energy loss occur. These signals are then identified by different detectors and a 3D image is recorded. The beam scans the sample in a longitudinal raster and the information on the various intensities due to morphology, composition and orientation are recorded in the

computer's memory. Since SEM is a surface technique it follows that the thickness of the sample is of little consequence since electron beam penetration is not required.

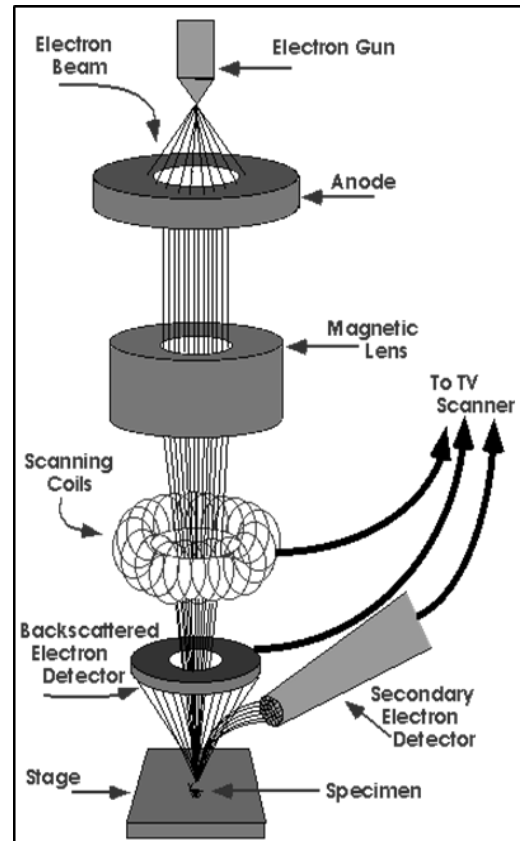


Figure 2.22: Schematic diagram of a scanning electron microscope

Interactions of the electron beam with the sample at different depths results in various signals. These include secondary electrons (SE), reflected or back-scattered electrons (BSE), and characteristic X-rays (Goldstein, 2003). It is rare that a single instrument would have detectors for all possible signals but SE detectors come standard with all SEM equipment. Scanning electron microscopy can produce very high-resolution images of a sample surface, revealing details less than 1 nm in size by using secondary electron imaging, or SEI. This is because in SEI electrons are emitted from very close to the surface of the specimen. Back-scattered electrons (BSE) result from elastic scattering of electrons from the sample (Reimer, 1998). The resolution of BSE images is less than SE images since BSE emerge from deeper locations within the specimen. BSE, however, are very useful in analytical SEM. The intensity of the BSE signal is strongly related to the atomic number (Z) of the specimen therefore elemental

distribution information in the sample can be deduced from BSE images. Bigger atoms (with a greater Z) have a better chance of generating an elastic collision they have bigger cross-sectional area. Therefore, the number of BSE reaching a BSE detector is proportional to the mean atomic number of the sample. A "brighter" BSE intensity correlates with a greater average Z in the sample, and "dark" areas have lower average Z (Krinsley, 1998). This method is based on electron microscopy and offers several advantages for morphological and size analysis; however, it is also associated with several disadvantages, such as the ability to provide only limited information about the size distribution and true population average. This technique is also costly and often requires complementary information about the size distribution.

2.7.3.2 Transmission electron microscopy (TEM)

Transmission electron microscopy (TEM) is one of the most commonly used methods for determination of the shape, size, and morphology of NPs. The inorganic sample is a suspension prepared on carbon-coated copper grids by dropping a very small amount of the sample, suspended typically in ethanol or acetone, onto the grid and then removing the extra solution with blotting paper. The particles are subsequently allowed to dry under a lamp (mercury or UV) and then are exposed to a monochromatic beam of electrons that penetrates the sample and is projected onto a viewing screen to generate an image. Transmission electron microscopy generates images when a beam of electrons interacts and passes through a sample. During the interaction, electrons are scattered and diffracted. The final image is formed from the interaction patterns of the incident and diffracted beams. The skeletal set-up of a TEM instrument in Figure 2.23 resembles that of a light microscope where instead of a light, the TEM uses an electron beam. Due to the smaller de Broglie wavelength of electrons, TEM instruments can image significantly higher magnification images, with very fine detail, that are otherwise impossible with conventional light microscopes (Egerton, 2005). Particles as small as 1–10 nm in size, which is near the atomic level, can be viewed using TEM. Higher resolution images are obtained using high resolution transmission electron microscopy (HRTEM). The crystallographic structure of a sample can be imaged at an atomic scale. Arrangement of the atoms and their local microstructures such as lattice fringe, glide plane, lattice vacancies, defects, and the surface atomic arrangement of crystalline NPs can be analysed using HRTEM.

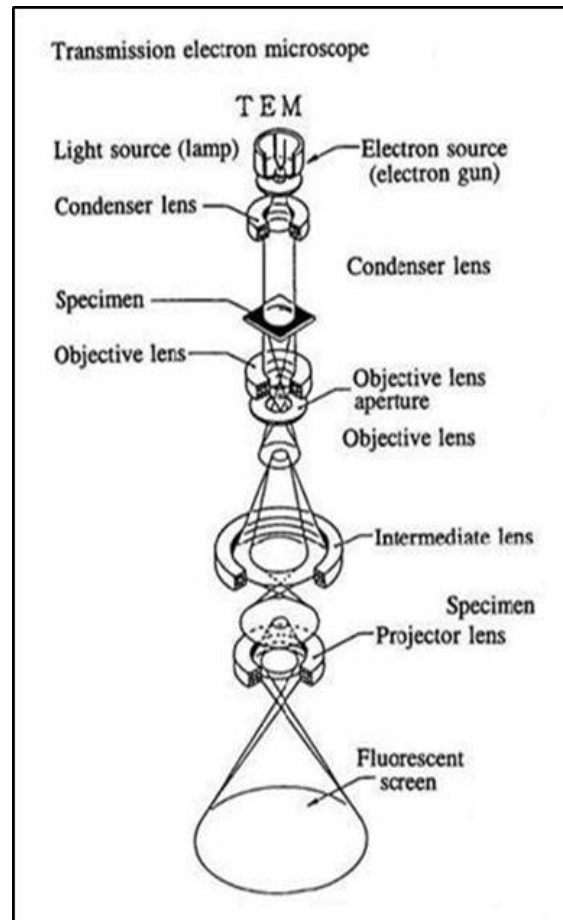


Figure 2.23: Schematic diagram of a transmission electron microscope

In the instrument, the combination of the electron source and the two condenser lenses is referred to as the illumination system. This system is responsible for transferring the electrons to the sample in a parallel or convergent beam. The image which is a shadowgraph is magnified using projection lenses and focused onto an imaging device, typically a fluorescent screen. The final image can be recorded by a sensor such as a charge coupled device (CCD) camera. The instruments can operate in different modes which differ in how they contrast images. An image taken in bright field mode will have the regions with high atomic number appearing darker than those regions with no sample appear bright (hence the term bright field). The reversed is observed for dark field imaging.

2.7.4 Energy-dispersive X-ray spectroscopy (EDS)

Energy-dispersive X-ray spectroscopy (EDS or EDX) is used for the elemental analysis or chemical characterisation of a sample. The analysis uses the X-ray spectrum emitted by a solid sample after bombardment with a focused beam of electrons. Qualitative analysis involves identifying the lines in the spectrum and is fairly straightforward due to the simplicity of X-ray spectra. The fundamental principles of spectroscopy apply in that each element has a unique atomic structure allowing a unique set of peaks on its electromagnetic emission spectrum.

Energy-dispersive X-ray spectroscopy analysis can be coupled with TEM and SEM since they both use electron beams for excitation. A detector is used to convert X-ray energy into signals; this information is sent to a pulse processor, which measures the signals and passes them onto an analyser for data display and analysis. At rest, an atom within the sample contains ground state (or unexcited) electrons in discrete energy levels or electron shells bound to the nucleus. The incident beam may excite an electron in an inner shell, ejecting it from the shell while creating an electron hole where the electron was. An electron from an outer, higher-energy shell then fills the hole, and the difference in energy between the higher-energy shell and the lower energy shell may be released in the form of an X-ray. The number and energy of the X-rays emitted from a specimen can be measured by an energy-dispersive spectrometer. Since the energies of the X-rays are characteristic of the difference in energy between the two shells and of the atomic structure of the emitting element, EDS allows the elemental composition of the specimen to be measured.

2.7.5 Selected area electron diffraction pattern (SAED)

Selected area electron diffraction is a crystallography technique that can be performed inside a HRTEM. It is similar to XRD in that selected area electron diffraction pattern (SAED) is also a diffraction technique that can be used to determine phases of materials. Its uniqueness comes from its ability to examine areas as small as several hundreds of nanometres. The technique obeys the laws of diffraction (treats light as a wave) and makes use of a parallel high energy electron beam that is directed to the sample. Selected area electron diffraction pattern uses to its advantage that the spacing between atoms is at least 100 times larger than the wavelength of high energy electrons that is a few thousandths of a nanometre. The atoms then act as a diffraction grating that diffracts the electrons.

A fraction of the electrons passes through without deflection and the crystal structure of the sample determines the angles to which the electrons will be scattered. The result from this is a series of bright spots. Electron diffraction determines different types of materials which can be single crystalline, polycrystalline or amorphous. The three different types of material will give rise to different patterns which are can also be governed by the thickness of the specimen as well as the crystal structure. Single crystalline materials (Figure 2.24) show a spot pattern which can be indexed for reflection planes. The spots appear in symmetry around the centre of the pattern. By using standard vector rules and the basic parallelogram, the spot pattern can be indexed.

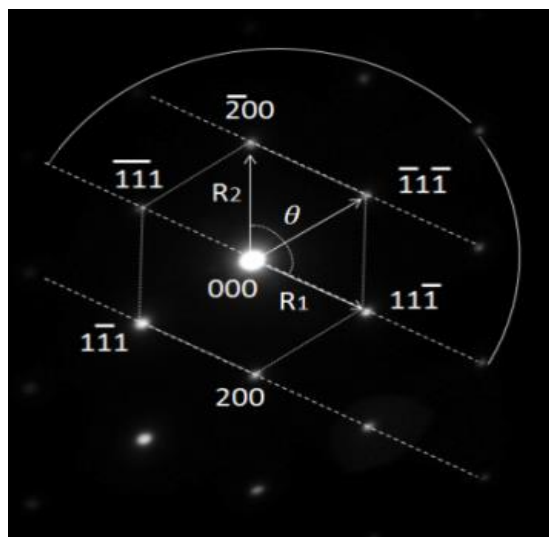


Figure 2.24: The spot diffraction pattern from a single crystal of aluminium alloy

Polycrystalline material (Figure 2.25) exhibit a ring concentric ring pattern that are created by the ultra-fine grains the material is made of. The phase of the material is determined by interpreting the ring patterns by specifying the inter-planar spacing and Miller indices. Using the radius of each ring, the distance between the planes or inter-planar spacing can be specified. Reference specimens are also used to index the diffraction patterns of various materials where the camera length needs to be specified. The pattern of a pure gold sample is known as the standard sample that is used for the identification of crystalline materials.

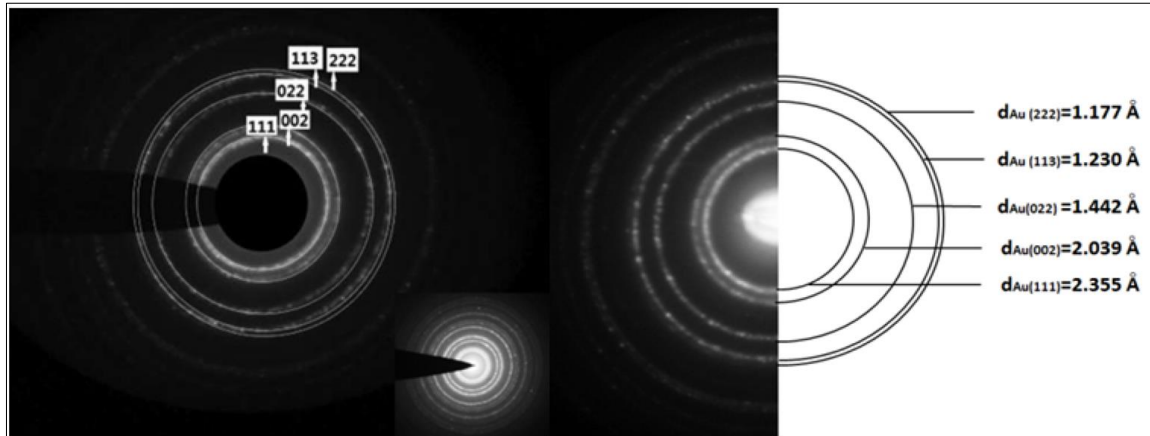


Figure 2.25: The ring diffraction pattern from a polycrystalline pure gold film with an f.c.c crystal structure. Crystal planes are indexed and inter-planar spacing is shown by Miller indices.

For amorphous materials (Figure 2.26), the feature of concentric rings in the pattern disappears and the result is a halo left around the centre spot (Figure 2.26). This shows that the electrons are scattered randomly by the material. This occurs in instances where the grain size of the specimen is extremely fine or the material is completely amorphous.

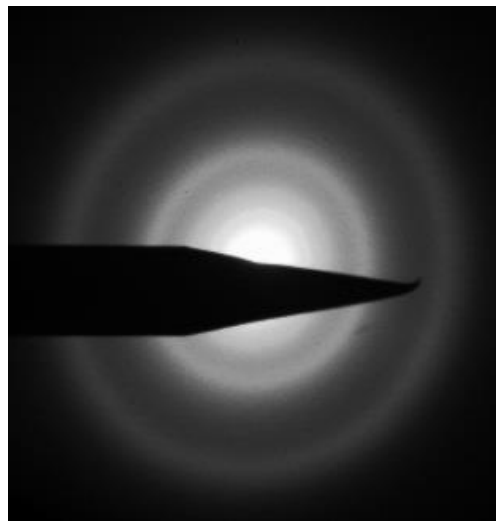


Figure 2.26: Diffraction pattern of amorphous material

2.8 Biological Activity and Applications of Nanoparticles

An assortment of metal and metal oxide NPs are being developed and incorporated into products. They have been widely applied in diagnostics, therapeutics, drug-delivery systems, electronics, cosmetics, personal care products and food additives, due to their magnetic, catalytic, semiconducting, antimicrobial and ultraviolet-protective properties. Recently, much effort has been dedicated to develop NPs for medical applications. While significant advances in the application of metal NPs in medicine for the purposes of diagnosis, imaging, and drug delivery have been made, fewer therapeutic applications of NPs have been reported. Discussed in the following text are the properties and applications of the elements used in this project.

2.8.1 Silver (Ag)

Silver is a metal used industrially in electrical contacts and conductors, in specialised mirrors, window coatings, and in catalysis of chemical reactions. Silver does not react with air, even at red heat, and thus was considered as a noble metal along with gold. Its reactivity is intermediate between that of Cu and Au. Silver and Au have fairly low chemical affinities for oxygen, lower than Cu. The common oxidation states of Ag are (in order of commonness): +1 (the most stable state; for example, silver nitrate, AgNO_3); +2 (highly oxidising; for example, silver(II) fluoride, AgF_2); and even very rarely +3 (extreme oxidising; for example, potassium tetrafluoroargentate(III), KAgF_4). The +1 state is by far the most common.

In group 11, Ag has the lowest first ionization energy due to the instability of the 5s orbital, but has higher second and third ionization energies compared to Cu and Au due to the stability of the 4d orbitals. This explains the chemistry of Ag predominantly exhibiting +1 oxidation state and reflects the limited range of oxidation states along the transition series as the d-orbitals fill and stabilise. Silver is a soft, ductile and malleable transition metal and crystallizes in a face-centred cubic lattice (Figure 2.27) with bulk coordination number 12 (Greenwood, 1997). Unlike metals with incomplete d-shells, metallic bonds in Ag are lacking a covalent character and are relatively weak. This observation explains the low hardness and high ductility of single crystals of Ag.

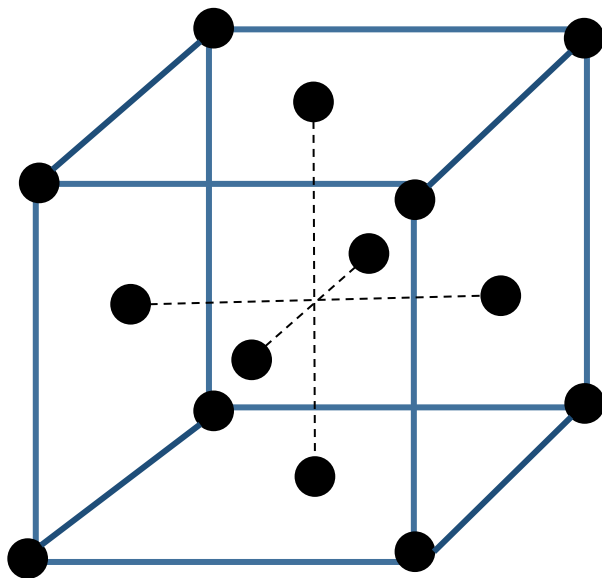


Figure 2.27: Face centred cubic lattice

Silver compounds are taken up by the body like mercury compounds, but lack the toxicity of the latter. They have low toxicity compared to those of most other heavy metals, as they are poorly absorbed by the human body when digested, and that which does get absorbed is rapidly converted to insoluble silver compounds or complexed by metallothionein. Silver nitrate, AgNO_3 , is the most versatile precursor and is the least expensive salt of Ag compared to many other Ag compounds, especially the halides. It is non-hygroscopic, in contrast to silver fluoroborate and silver perchlorate. It dissolves in numerous solvents, including water. Presently Ag is considered a non-essential accumulative element even though it is widely distributed in human body fluid and tissues including heart, lungs, blood, plasma, bones, brain, breast, kidney, urinary bladder, urine, liver, pancreas, muscles, nails, skin, spleen and teeth (dentine and enamel). The widespread distribution in the human body may indicate that this metal could have some specific functions which are not clear at present (Nadeem et al., 1999). Metallic Ag, like Cu, is an antibacterial agent (Maillard and Hartemann, 2013). Silver compounds are used in photographic film and X-rays. Dilute silver nitrate solutions and other Ag compounds are used as disinfectants and microbiocides (oligodynamic effect), added to bandages and wound-dressings, catheters, and other medical instruments (Tran et al., 2013; AshaRani et al., 2009).

In medicine, Ag is incorporated into wound dressings and used as an antibiotic coating in medical devices. Wound dressings containing Ag sulfadiazine or silver nanomaterials are used to treat external infections. Silver ions damage the metabolism of bacteria even at low concentrations such as 0.01–0.1 mg L⁻¹; metallic Ag has a similar effect due to the formation of silver oxide (Agnihotri et al., 2014). This effect is lost in the presence of sulfur due to the extreme insolubility of silver sulfide (Subhankari and Nayak, 2013). Silver is also used in some medical applications, such as urinary catheters (where tentative evidence indicates it reduces catheter-related urinary tract infections) and in endotracheal breathing tubes (Calderón et al., 2017; Beattie and Taylor, 2011).

Silver NPs are one of the most attractive nanomaterials for commercialisation. They have been widely used for antimicrobial, electronic and biomedical products. They are also used medicinally as antibacterial and antifungal agents in much the same way as larger Ag particles (Maillard and Hartemann, 2013). Microbes are unlikely to develop resistance against Ag, as they do against conventional antibiotics. This is because Ag attacks a broad range of targets in the organisms. This would mean that pathogens would have to develop a multitude of mutations, simultaneously, to protect themselves hence Ag. Silver NPs are used as antimicrobials in a variety of industrial, healthcare, and domestic applications (Dallas et al., 2011; García-Barrasa et al., 2011).

2.8.2 Selenium (Se)

Selenium is a non-metal element which has properties that are intermediate between the elements above (sulfur) and below (tellurium) in the periodic table. Minerals that are pure selenide or selenate compounds are known but rare. Today, the primary commercial uses for pure Se are pigments (Craig and Maher, 2003; Lampis et al., 2014). Since the element is also a semiconductor, it has also been used in photocells (Kodeš, 1971). The stable organic Se compounds (selenomethionine and selenocysteine) that have been synthesised are used as antioxidants, enzyme inhibitors, anti-tumour and anti-infective agents, cytokine inducers and immuno-modulators.

Trace amounts of Se salts are crucial for cellular function in many organisms but toxic in large amounts. Selenium is contained in many multivitamins, dietary supplements and infant formula. It has reducing properties and is a component of the antioxidant enzymes such as

glutathione peroxidase, thioredoxin reductase and iodothyronine deiodinases which reduces oxidised molecules in animals and some plants (Rayman, 2000). The amount of Se required in plants and mammals varies by species, with some requiring fairly large quantities and others seemingly requiring none.

The allotropes that exist for Se interconvert with temperature changes and depend largely on the rate of temperature change. The symmetries of the crystals contain nearly identical puckered Se_8 rings (Figure 2.28), as in sulfur, with different arrangements and the packing is markedly most dense in the α form. In the Se_8 rings, the Se-Se distance is 233.5 pm and Se-Se-Se angle is 105.7° . Other Se allotropes may contain Se_6 or Se_7 rings (Greenwood, 1997). The amorphous form of Se is a characteristically brick-red powder. Red α , β , and γ forms of Se are monoclinic phase crystals. The most stable and dense form of the allotropes is Se grey and has hexagonal crystal lattice (Figure 2.29) consisting of helical polymeric Se-Se chains (Greenwood, 1997). Red crystalline form of Se steadily undergoes conversion into the metallic form of Se at temperatures just over 120°C .

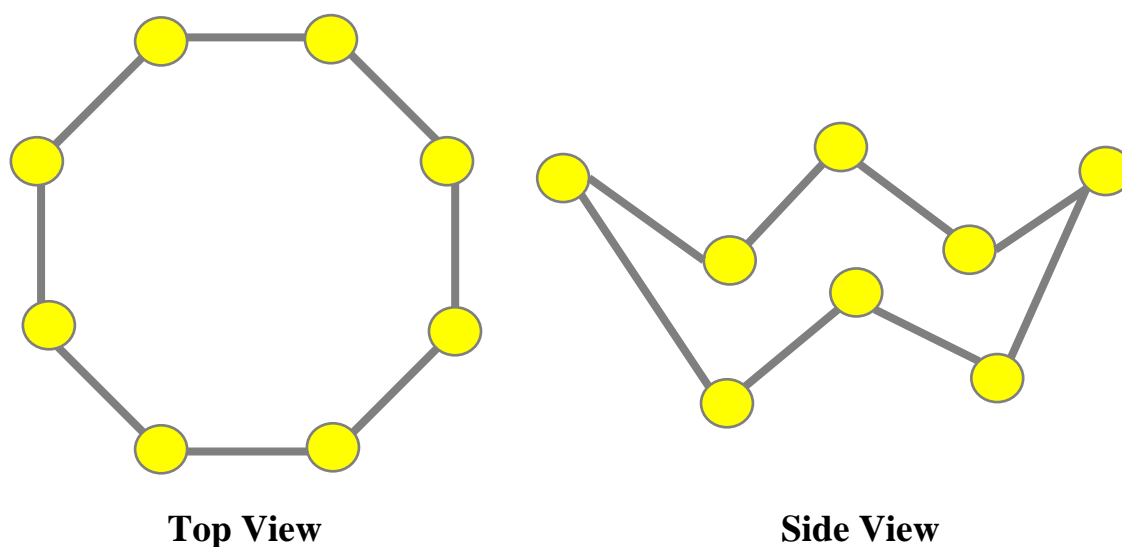


Figure 2.28: S_8 packing of atoms for selenium (Se)

The growing attention received by selenium NPs is due to their excellent biological activities and low toxicity (Burk, 1983). Selenium NPs act as potential chemo-preventive agents with reduced toxicity. Many studies have shown that selenium NPs exhibit novel *in vitro* and *in vivo* antioxidant activities through the activation of selenoenzymes (Seng et al, 2012). Biosynthesis of selenium NPs is often achieved by reduction of selenite (+4)/ selenate (+6) in the presence

of plant extracts containing phenols, flavonoids amines, alcohols, proteins and aldehydes (Husen and Siddiqi, 2014).

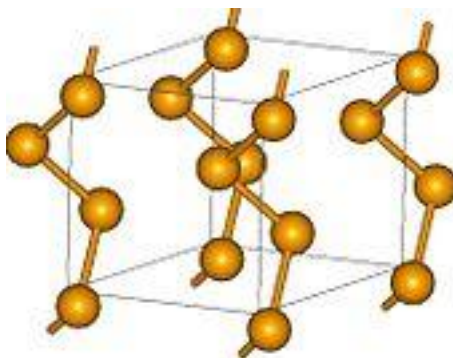
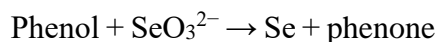
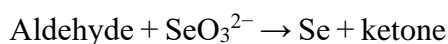
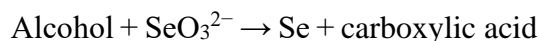
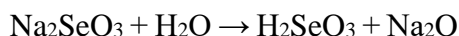


Figure 2.29: Hexagonal packing of selenium (Se) atoms



Nanoparticles of Se have been reported to induce MCF7 cell death through apoptosis but the mechanism of action is not yet known (Ramamurthy, 2013). Selenium nanobelts have been synthesised on large scale with an approximate diameter of 80 nm and length up to 5 μm . The shape, size and structure of the NPs depend on the concentration, temperature, nature of biomolecules and pH of the reaction mixture. The properties of selenium NPs vary with size and shape. For instance, Se nanospheres exhibit high biological activity and low toxicity while Se nanowires of t-Se (trigonal selenium) have high photoconductivity (Husen and Siddiqi, 2014). The growth of selenium NPs has been studied using fenugreek seeds and the NPs were found to inhibit the growth of *Staphylococcus aureus* within 3–4 h with a low concentration of 7–15 $\mu\text{g/mL}$. The results indicated that selenium NPs may be used in nanomedicine against *S. aureus* infections.

2.8.3 Zinc oxide (ZnO)

Zinc oxide is an inorganic white powder that is insoluble in water. It occurs naturally as the mineral zincite, but most ZnO is synthetic (Liedekerke, 2006). Zinc oxide is a wide-bandgap semiconductor of the II-VI semiconductor group with high electron mobility. The primary use of ZnO (zinc white) is in paints and as an additive to ointments. It is the preferred treatment for a variety of skin conditions and is an ingredient in products such as baby powder, creams used for diaper rashes, sun screen, calamine lotion, anti-dandruff shampoos, and antiseptic ointments (Ågren, 1990). When used as an ingredient in sunscreens, ZnO blocks both UVA (320–400 nm) and UVB (280–320 nm) rays of ultraviolet light. Zinc oxide and titanium dioxide are commonly used in sunscreens and are considered to be non-irritating, nonallergenic and non-comedogenic (Mitchnick et al., 1999).

Zinc oxide crystallises in two main forms (Figure 2.30), hexagonal (wurtzite) and cubic (zinc blende). The most common structure is the wurtzite structure as it is most stable at ambient conditions. The zinc blende form, however, can be stabilised by growing ZnO on substrates with a cubic lattice structure. In both cases, the zinc and oxide centres are tetrahedral, the most characteristic geometry for Zn(II) (Claus et al., 2010).

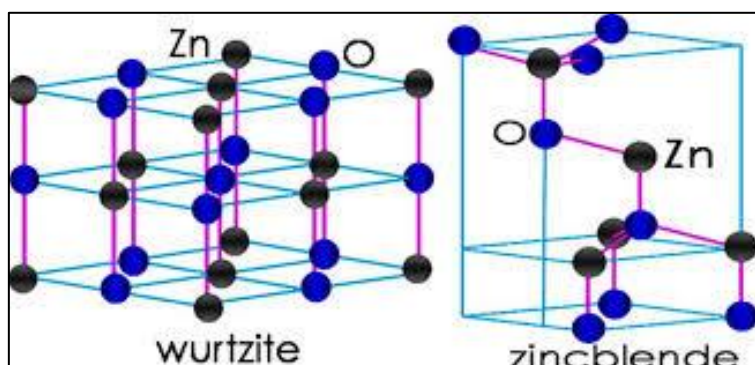


Figure 2.30: Crystal phases of zinc oxide (ZnO) (a) hexagonal phase (wurtzite) crystal lattice of zinc oxide (b) cubic phase (zinc blende) crystal lattice of ZnO (Ashrafia and Jagadish, 2007)

As in most group II-VI materials, the bonding in ZnO is largely ionic ($\text{Zn}^{2+}\text{O}^{2-}$) with the corresponding radii of 0.074 nm for Zn^{2+} and 0.140 nm for O^{2-} . This property accounts for the preferential formation of wurtzite rather than zinc blende structure, as well as the strong piezoelectricity of ZnO. Because of the polar Zn-O bonds, Zn and O planes are electrically charged (Claus et al., 2010).

Zinc oxide NPs have deodorizing and antibacterial properties (Seil and Webster, 2012) and are therefore added to materials including cotton fabric, rubber, oral care products, and food packaging (Klingshirn, 2007; Gokarneshan, et al., 2012). Zinc oxide has been investigated for its antibacterial properties both on the microscale and the nanoscale and exhibit significant antimicrobial activity when particle size is reduced to the nanoscale. Zinc oxide NPs can interact with the bacterial surface and/or with the bacterial core where it can subsequently exhibit distinct bactericidal mechanisms inside the cell.

Several studies have reported zinc oxide NPs to be biocompatible with human cells while still remaining non-toxic to them (Sirelkhatim, et al., 2015). In a study conducted by Akhtar et al. (2012), zinc oxide NPs have shown distinct effects on mammalian cell viability via killing cancer cells (HepG2, A549, and BEAS-2B) while posing no effect on normal cells (ratastrocytes and hepatocytes) (Sirelkhatim et al., 2015). Plants such as *Calotropis gigantea* (Vidya et al., 2013) and leaf extracts of *Parthenium hysterophorus* (Rajiv et al., 2013) were used to synthesise zinc oxide NPs. The studies conducted on the anti-microbial activity of zinc oxide NPs against human pathogens such as *P. aeruginosa*, *E. coli*, *S. aureus*, and *E. faecalis* showed zinc oxide NPs to have strong antibacterial activity toward these human pathogens. The antimicrobial activity of zinc oxide NPs has been studied toward *P. aeruginosa* and *E. coli* which were synthesised using mint leaf extracts (Chitra, 2013). The anti-bactericidal activity of zinc oxide NPs (8–10 nm) tested against *E. coli* and *S. aureus* was found to be effective at 80 and 100 g mL⁻¹.

Table 2.2: Properties of the elements (Ag and Se) and metal oxide (ZnO) used in this study

| | Silver | Selenium | Zinc oxide |
|---------------------------------------|---------------------|------------------------|---------------------|
| Formula | Ag | Se | ZnO |
| Metal/non-metal | Metal | Metalloid | Metal oxide |
| Oxidation states | +1, +2, +3 | -2, 0, +2, +4, and +6. | 2+ |
| Stable allotropes | Face cantered cubic | Hexagonal | Hexagonal (wurzite) |
| Hard and soft acid base (HSAB) | Soft Lewis acid | Soft Lewis base | Intermediate |
| Biological properties | Antibacterial | Antioxidant | Antibacterial |

2.9 Biological Applications of Phytochemicals and Nanoparticles

The green synthesis of nanomaterials in biotechnology merges the fields of material science and biology. Nanoparticles have demonstrated unique properties with a potential for wide-ranging therapeutic applications. In this work, we have not exhaustively covered the field, therefore the following text provides a brief overview of the antioxidant and antibacterial studies of plant extracts, isolated flavonoids and NPs with metals, metal oxides, and non-metals.

2.9.1 Antioxidant assays

Oxidation is a chemical reaction that can produce free radicals of reactive oxygen species. The radicals are useful to the body for redox signalling which is a process that assists the body with anti-aging, rejuvenation and cellular repair. Over-production of free radicals, however, have the potential of causing oxidative cell damage to components such as DNA and proteins. Antioxidants are a good way of maintaining a balance of these radical species. These are substances that when present at low concentrations (compared to those of an oxidisable substrate) significantly delays or inhibits oxidation of that substrate. This means that the radicals will react with the cells at the expense of the antioxidants. Therefore, antioxidants do not remove the radical oxidants, they merely prevent them from reaching optimum levels that can cause damage. Studies have shown that extracts with high phenolic contents exhibit superior antioxidant activities. Results exhibited by phenolics positively correlated with the number of hydroxyl groups bonded to the aromatic ring. To date, various methods have been employed to measure a substance's ability to either scavenge radicals or to reduce them. The text below describes three antioxidant assays used in this work.

2.9.1.1 The 1,1-diphenyl-2-picrylhydrazyl (DPPH[•]) radical scavenging assay

The 1,1-diphenyl-2-picrylhydrazyl (DPPH) radical scavenging assay is based on the capability of an antioxidant to donate free hydrogen radicals or an electron to the DPPH radical, which is stable with a deep violet colour. When the odd electron in the DPPH radical becomes paired in the presence of a radical scavenger (antioxidant agent), DPPH gets reduced to the

corresponding hydrazine. The solution changes colour from its initial deep violet to pale yellow (Figure 2.31).

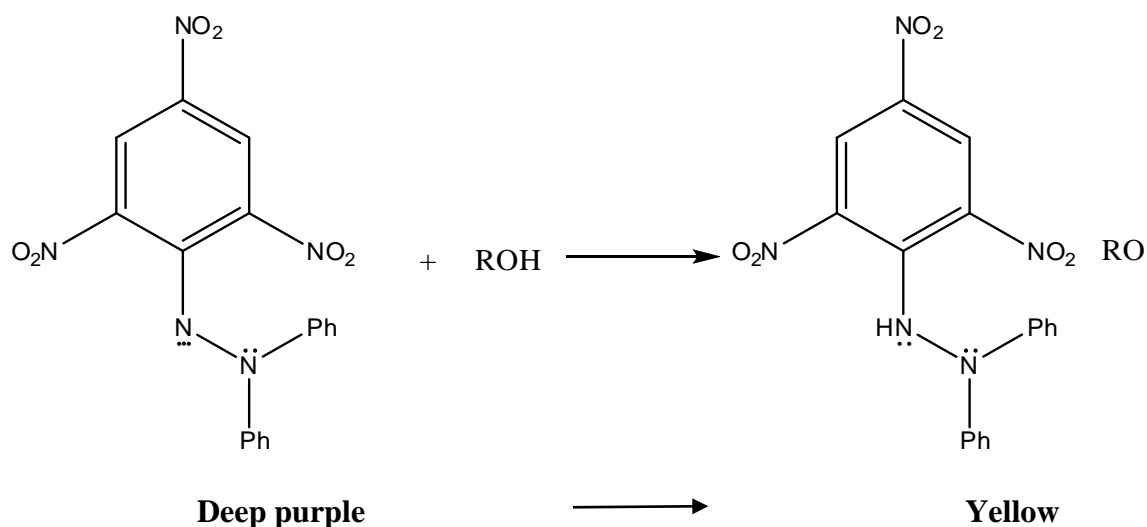


Figure 2.31: Mechanism of action for the reduction of 1,1-diphenyl-2-picrylhydrazyl (DPPH)

The change in absorbance is measured by a spectrophotometer and it is proportional to the concentration of the antioxidant. The absorbance values are used to calculate the radical scavenging activity (percentage scavenging) of DPPH radicals by the antioxidant using the following equation. As is the absorbance of the sample solution and Ac is the absorbance of the control.

$$\% \text{ Scavenging} = \left[\frac{(Ac - As)}{Ac} \right] \times 100$$

2.9.1.2 Ferric reducing antioxidant power (FRAP) assay

This method measures the ferric reducing power (Fe^{3+} to Fe^{2+}) of a substance at a low pH. A phosphate buffer solution (0.2 M, pH = 6.6), 1% potassium ferricyanide ($\text{K}_3\text{Fe}(\text{CN})_6$), 10% trichloroacetic acid (TCA) and 0.1% FeCl_3 are mixed to give a green coloured complex with iron in the +3 oxidation state. In the presence of an antioxidant, which acts as a reducing agent, the complex is reduced to the +2 oxidation state with a deep blue colour. The absorbance of the mixture is then measured at 700 nm using a UV-Vis spectrophotometer. The absorbance is related to the reducing power of the electron donating antioxidant or material present in the test compound or material. The higher the absorbance of the reaction mixture the greater the reducing power. The changes in absorbance are linear over a wide concentration range with

antioxidant mixtures (Benzie and Strain, 1996). Ascorbic acid is commonly used as a positive control for this assay.

2.9.1.3 Hydrogen peroxide (H₂O₂) radical scavenging activity assay

Molecules capable of generating free radicals are termed reactive oxygen species. Amongst these species is the superoxide anion (O₂⁻), the hydroxyl radical (·OH) as well as hydrogen peroxide (H₂O₂). These radicals are produced during normal aerobic metabolic processes and are increased during stress conditions and infections. Hydrogen peroxide in itself is not very reactive, but it is potentially toxic to cells because it decomposes to produce hydroxyl radicals in the cells. The antioxidant can donate a proton converting the hydroxyl radical to water. This gives importance to the removal of H₂O₂ for antioxidant defence in cells. Different oxidants have different scavenging abilities towards the radicals mentioned above. Hydroxyl radical scavenging capacity of an extract is directly related to its antioxidant activity. Techniques available for the scavenging of H₂O₂ employ direct UV measurements of H₂O₂ mixed with a phosphate buffer at 230 nm. As with the DPPH radical scavenging assay, the absorbance values are used to calculate the percentage radical scavenging ability of the sample.

$$\% \text{ Scavenging} = \left[\frac{(Ac - As)}{Ac} \right] \times 100$$

2.9.2 Antibacterial assays

Bacteria generally have the genetic ability to acquire resistance to drugs used as therapeutic agents. This is a cause for concern since some patients are known to have suppressed immunity due to new multi-resistant bacterial strains. Consequently, new infections can occur resulting in high mortality. The use of plant extracts and phytochemicals with known antimicrobial properties have been of great significance in therapeutic treatments. Most of the antibiotic resistance mechanisms are irrelevant for NPs. This is because the anti-microbial action of NPs is direct and there is interaction/contact with the bacterial cell wall without the need to penetrate the cell. This indicates that NPs would be less inclined to promote bacterial resistance unlike antibiotics. This calls for greater attention to be paid to antimicrobial activity screening and

evaluating methods. Bioassays such as disc-diffusion, well diffusion and broth or agar dilution are well known and are commonly used because they do not require specialised equipment or further evaluation for reproducibility and standardisation. The following text discusses the disc-diffusion assay that was used for anti-microbial screening in this study.

2.9.2.1 Antibacterial testing - Kirby-Bauer disc diffusion susceptibility test

The agar disc diffusion method is a rapid test for the sensitivity of bacteria to antibiotics. This method has been standardised and is a viable substitute to broth dilution methods for laboratories without the resources to employ the newer automated methods for broth micro dilution testing. In this test (Figure 2.32), the pathogenic organism is grown on Mueller-Hinton agar in the presence of various antimicrobial impregnated filter paper discs and the discs are allowed to incubate. The estimated time of a bacterial suspension to reach critical mass is 4 to 10 hours for most commonly recovered pathogens, but is characteristic of each species, and influenced by the media and incubation temperature. If the antibiotic inhibits growth or kills the bacteria, there will be a visible area around the filter paper disc where bacterial growth has not occurred. This area is known as the zone of inhibition and the diameters are usually measured in mm. A stronger antibiotic will create a larger zone, because at lower concentrations, the antibiotic is enough to stop growth.

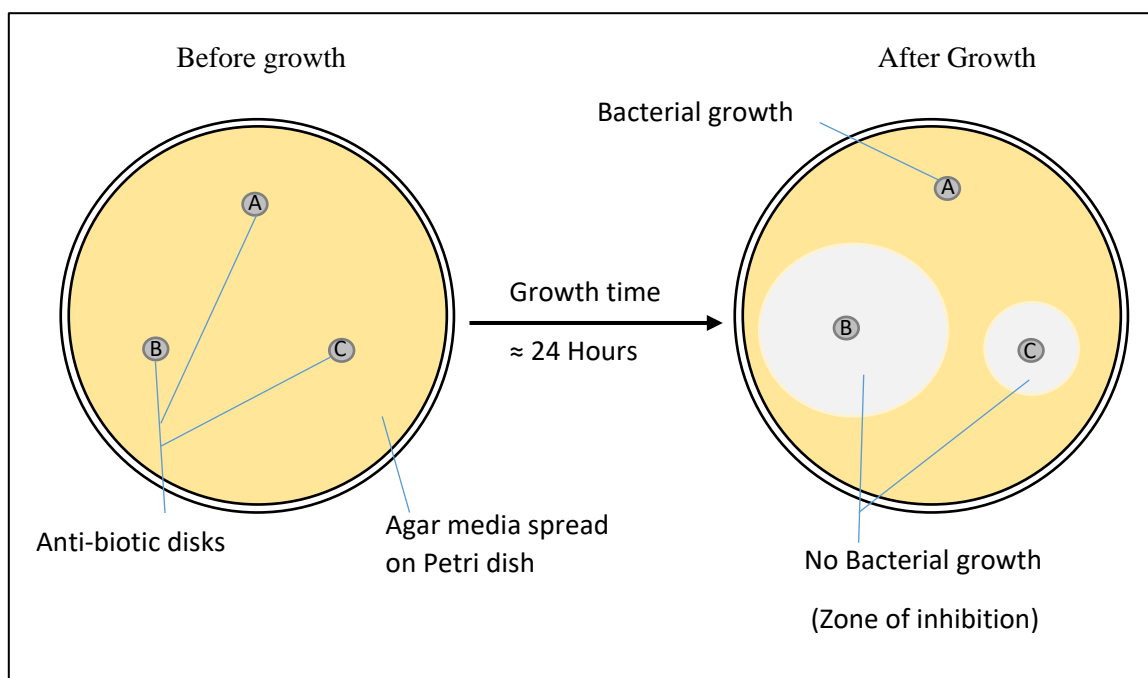


Figure 2.32: Agar disc diffusion assay

The size of the zone of inhibition is also influenced by the depth of the agar, since the antimicrobial agent diffuses in three dimensions; thus a shallow layer of agar will produce a larger zone of inhibition than a deeper layer. The size of the zone of inhibition depends on the effectiveness of the antibiotic at killing or inhibiting bacterial growth. The concentration of antimicrobial compound at this margin is called the critical concentration and is approximately equal to the minimum inhibitory concentration obtained in broth dilution susceptibility tests.

2.12 Toxicity of Nanoparticles

Nanoparticles occur in the environment naturally as minerals, clays, and products of bacteria and have been intentionally used for centuries (Heiligttag and Niederberger, 2013). Their recent wide-spread production and wide range of applications, however, increase their potential to be released into the environment (Bundschuh et al., 2018). This increases the living organism's possibility of being directly or indirectly exposed to NPs, which could induce numerous deleterious effects on human health and the environment. The unique size-dependent physicochemical properties of NPs are often the reason for their increased use in products, but the same unique properties have raised concerns that unique physiological responses will be evoked in living systems by interaction with these materials (Bundschuh et al., 2018). Exposure of the human body to NPs can occur through different routes such as inhalation, ingestion, injection or physical contact with cuts or wounds (Figure 2.33). Therefore, caution is necessary because some *in vitro* data suggests that, even at low concentrations, for example, silver NPs can be toxic. So, while the majority of studies, to date, have focused on human health implications of NPs, other efforts consider their ecological implications, including their fate, transport, and toxicity (Elsaesser and Howard, 2012). This is in order to promote the sustainable use of these novel materials. Although not covered in this work, biokinetic studies on NPs are necessary to provide basic information about their absorption characteristics, bioavailability, residence times, clearance rates, and organs targeted. These studies are essential in terms of predicting potential toxicological effects and for identifying correlations with acute or subacute toxicity.

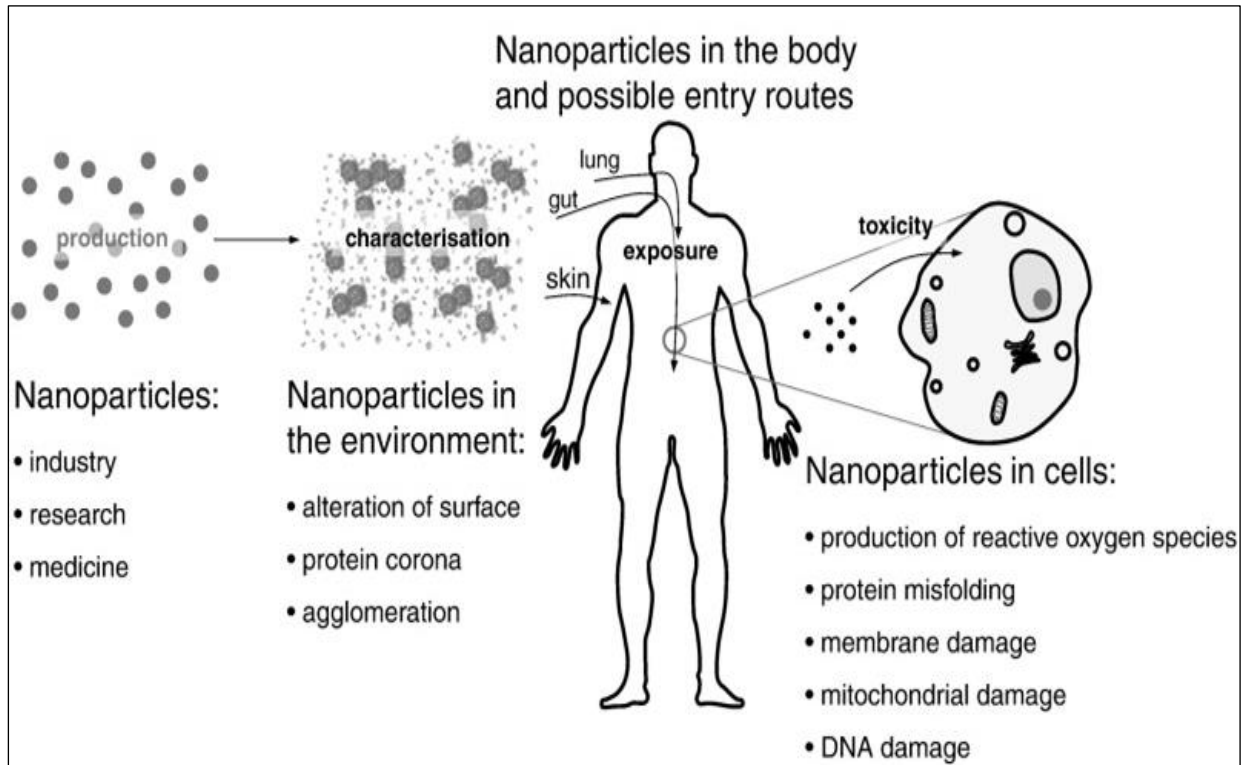


Figure 2.33: Possible pathways of human interactions with nanoparticles (Elsaesser and Howard, 2012)

CHAPTER 3

EXPERIMENTAL TECHNIQUES

This chapter describes the experimental techniques that were employed in the isolation and structural elucidation of the plant metabolites as well as the techniques used to synthesise and characterise of the NPs.

3.1 Sampling and Sample Preparation

Chrysanthemoides monilifera and *Harpephyllum caffrum* leaves were collected by hand picking in summer afternoon (between 2 and 4 pm - 15 January 2015) and identified by taxonomist, Prof. A. Nicholas, from the School of Life Sciences, University of KwaZulu-Natal, Westville. Samples were collected in the from the University of KwaZulu-Natal, Westville grounds. The leaves were taken to the lab where they were washed thoroughly with double distilled water and allowed to dry in air to constant mass. Dried leaf samples were pulverized using a grinding mill and then stored in plastic containers.

3.2 Reagents

All reagents and chemicals used were supplied by Sigma-Aldrich (Germany) and Fluka Analytical, Sigma, Switzerland and were of analytical grade. All dilutions were done using double distilled water. Plastic and glassware were cleaned by soaking in 10% HNO₃ and thoroughly rinsed with double distilled water before use.

3.3 Plant extract and isolated compound Characterisation and Quantification Methods

Nuclear magnetic resonance (NMR) spectra (1D and 2D) were recorded in deuterated chloroform (Merck, Darmstadt, Germany) at room temperature using a 400 MHz spectrometer (AVANCE III, Bruker, Rheinstetten, Germany). Ultraviolet–visible (UV-Vis) spectra were measured by a UV-Vis-NIR spectrophotometer (UV-3600, Shimadzu, Kyoto, Japan). Mass spectra were recorded using a time-of-flight mass spectrometer (LCT Premier TOF-MS, Waters Micro-mass, Milford, MA, USA). Column chromatography was performed using silica

gel (Kieselgel 60, 0.063-0.200 mm, Merck, Darmstadt, Germany). Thin layer chromatography (TLC) (Merck silica gel 60, 20× 20 cm F254 aluminium sheets) was used to monitor the purity of the obtained fractions by viewing TLC plates under an ultraviolet lamp (254 nm) which were developed in 10% H₂SO₄ in methanol (MeOH).

3.4 Nanoparticle Characterisation and Quantification Methods

X-ray diffraction (XRD) was performed using a Bruker D8 Advance diffractometer operated at a current of 30 mA with Cu K α ($\lambda = 1.54056 \text{ \AA}$) radiation in a θ -2 θ configuration ranging from 15 - 90° at a scan step size of 0.014°, at a voltage of 40 kV. For transmission electron microscopy (TEM), a JEOL JEM 1010 microscope was used and for high resolution TEM, a JEOL JEM 2100 microscope was used. The NPs were dispersed in EtOH and sonicated for 10 minutes. A drop of the dispersed sample was placed on lacey copper grid (sitting on absorbent paper) using a pasture pipette. The excess EtOH was allowed to dry under a UV lamp. For phase analysis of the NPs, selected area electron diffraction (SAED) patterns were obtained on the HRTEM instrument. The SEM micrographs were taken using a FEG SEM microscope. For analysis, the nanoparticle solution is dried into a powder, mounted on a sample holder, and coated with a conductive metal (gold) using a sputter coater. Energy dispersive spectroscopy (EDS) and elemental analysis of the samples was obtained using a Bruker detector and Esprit 1.8 software.

3.5 Preparation of Extracts

About 1.1 kg of ground leaves from *C. monilifera* and *H. caffrum* were extracted with MeOH (3 × 2000 mL) on an orbital shaker at room temperature for three days. For filtration of the extracts, Whatman No. 1 filter paper was used. Fractions collected from the crude MeOH extract were concentrated using a rotary evaporator. Methanol was used because of its polarity index (5.1) which gives it the ability to extract more polar compounds, it is relatively inexpensive compared to other solvents (such as chloroform), it presents fewer environmental concerns and it has a low boiling point (65 °C) but it is still toxic.

3.5.1 Isolation of compounds from *Chrysanthemoides monilifera* and *Harpephyllum caffrum*

The crude MeOH extracts of *Chrysanthemoides monilifera* was subjected to column chromatography (column size - 45 mm diameter, 210 mm length) using 100% hexane that was increased in polarity stepwise by adding 10% to 100% vol %ethyl acetate (EtOAc) at a flow rate of 50 mL/min. Ten 100 mL fractions were collected for each eluent step. The *C. monilifera* extract yielded quercetin (215 mg) after elution with 60% hexane: 40% EtOAc obtained from fractions 38-42.

The crude MeOH extract of *Harpephyllum caffrum* was subjected to column chromatography (column size - 45 mm diameter, 210 mm length) using 100% hexane that was increased in polarity stepwise by adding 10% to 100% vol %EtOAc at a flow rate of 50 mL/min. Ten 100 mL fractions were collected for each eluent step. The *H. caffrum* crude extract yielded catechin (92 mg) after elution with 100% EtOAc obtained from fractions 47-51.

3.6 Synthesis of Silver, Selenium and Zinc Oxide Nanoparticles

A 1.0 mM stock solution of the metal salts (Table 3.1) were prepared and stored in a volumetric flasks (1L) covered with foil. Nitrate salts were used for the synthesis of silver nanoparticles (AgNPs) and zinc oxide nanoparticles (ZnONPs) and sodium selenite was used for the synthesis of selenium nanoparticles (SeNPs).

Table 3.1: Mass of metal salts used to prepare 1 mM metal salt stock solutions (1 mM, 1L).

| Metal | Salt | Molar mass (g mol ⁻¹) | Mass (mg) |
|-------|--|-----------------------------------|-----------|
| Ag | AgNO ₃ | 169.87 | 169.87 |
| Se | Na ₂ SeO ₃ | 172.94 | 172.94 |
| ZnO | Zn(NO ₃) ₂ .6H ₂ O | 189.36 | 189.36 |

3.6.1 Effects of concentration on nanoparticle growth

To study the effects of quercetin concentration on the growth of NPs, different concentrations in mM (0.1, 0.2, 0.4, 0.8, 1, 2 and 3) of quercetin in MeOH were prepared in volumetric flasks (100 mL) and reacted with 1 mM AgNO₃. A 3 mM quercetin solution was prepared by dissolving 90.66 mg of quercetin and made to the mark with MeOH. A 2 mM quercetin solution was prepared by dissolving 60.44 mg of quercetin and made to the mark with MeOH. Two 1 mM quercetin solutions were prepared by dissolving 30.22 mg of quercetin and made to the mark with MeOH. The 0.1, 0.2, 0.4 and 0.8 mM concentration solutions were prepared by diluting 5, 10, 15 and 20 mL volumes from the 1 mM quercetin stock solution into 50 mL volumetric flasks and made to the mark with MeOH. The quercetin solutions were then reacted with equal volumes of metal salt solutions by adding the metal salt solutions to the quercetin solutions (50 mL of quercetin at the different concentrations and 50 mL of metal precursor) and allowed to sit for 24 h. The colloidal suspensions were then centrifuged for 30-45 min at 420 rpm in order to harvest the AgNPs. The quercetin-capped AgNPs were re-dispersed in distilled MeOH to wash off the excess quercetin. This process was repeated three times and the resulting colloids were analysed using UV-Vis spectroscopy and TEM.

3.6.2 Synthesis of freestanding and capped nanoparticles

Sodium borohydride (NaBH₄), *C. monilifera* plant extract, *H. caffrum* plant extract, quercetin and catechin were used as reducing agents for the synthesis of AgNPs, SeNPs and ZnNPs.

3.6.2.1 Synthesis of freestanding (uncapped) nanoparticles

Freestanding NPs were synthesised by reacting equal volumes (50 mL) of NaBH₄ (1 mM) with each of the prepared metal salt solutions (1mM).

3.6.2.2 Plant extract-mediated synthesis of nanoparticles

Crude plant extracts (1 g) were dissolved in MeOH and placed in a volumetric flask (100 mL), diluted to the mark with MeOH. This solution was reacted with an equal volume of metal salt stock solution (Table 3.1).

3.6.2.3 Flavonoid-mediated synthesis of nanoparticles

Flavonoid (quercetin and catechin) solutions (2 mM, 50 mL) were reacted with equal volumes of metal salt stock solutions (Table 3.1). The 2 mM quercetin solution was prepared by dissolving 60.44 mg of quercetin in a volumetric flask (100 mL) and made to the mark with MeOH. A 2 mM catechin solution was prepared by dissolving 58.05 mg of catechin in a volumetric flask (100 mL) and made to the mark with MeOH.

The synthesised (freestanding and bio-reduced NPS) colloidal suspensions were then centrifuged for 30-45 min at 420 rpm in order to harvest the AgNPs, SeNPs and ZnONPs. This process was repeated three times and the resulting mixtures were analysed using UV-Vis spectroscopy and TEM.

3.7 Biological Testing

The plant extracts, isolated compounds and synthesised AgNPs, SeNPs and ZnONPs were evaluated for the anti-oxidant and antibacterial activity. Three antioxidant assays were employed, namely, the 1,1-diphenyl-2-picrylhydrazyl (DPPH•) radical scavenging assay, ferric reducing antioxidant power (FRAP) assay and the H₂O₂ radical scavenging assay. The Kirby-Bauer disc diffusion susceptibility test was used for the evaluation of antibacterial activity of plant extracts, flavonoids and synthesised NPs. Table 3.2 shows the concentrations of the volumes sampled for biological testing

Table 3.2: Concentration of the volumes sampled during biological testing

| Volume (µL) | Concentration equivalent | |
|-------------|---|-------------------------------------|
| | Plant extracts and flavonoids (mg L ⁻¹) | Nanoparticles (mg L ⁻¹) |
| 10 | 0.166 | 0.0666 |
| 20 | 0.333 | 0.1333 |
| 40 | 0.666 | 0.2666 |
| 80 | 1.333 | 0.5333 |

| | | |
|-----|-------|--------|
| 100 | 1.666 | 0.6333 |
|-----|-------|--------|

3.7.1 The 1,1-diphenyl-2-picrylhydrazyl (DPPH) radical scavenging assay

A solution of 0.1 mM DPPH was prepared by dissolving 3.9 mg of DPPH in 100 mL of MeOH and stirred to give a purple solution. Equal amounts of MeOH and DPPH solution without sample served as a control. Volumes of test samples of varying concentrations (Table 3.2) were added to 2.5 mL DPPH solution and shaken on an orbital shaker at 123 rpm then kept in the dark for 30 min at room temperature. The absorbance was measured at 517 nm against a blank solution consisting of MeOH (Brand-Williams et al., 1995).

3.7.2 Ferric reducing antioxidant power (FRAP) assay

The ferric reducing antioxidant power (FRAP) assay was carried out as described by Murthy et al. (2012) with some modifications. The plant extracts, isolated flavonoids and synthesised NPs were mixed with 2.5 mL phosphate buffer solution (0.2 M, pH = 6.6) and 2.5 mL of 1% potassium ferricyanide ($K_3Fe(CN)_6$) in test tubes. The mixture was placed in a water bath at 50 °C, for 20 min. A volume of 2.5 mL of 10% trichloroacetic acid (TCA) was added to the mixture and mixed thoroughly. A volume of 2.5 mL of this mixture was then mixed with 2.5 mL distilled water and 0.5 mL $FeCl_3$ solution (0.1 %) and allowed to stand for 30 min. The absorbance of the mixture was measured at 700 nm using a UV-Vis spectrophotometer.

3.7.3 Hydrogen peroxide (H_2O_2) radical scavenging assay

The ability of the plant extracts and NPs to scavenge hydrogen peroxide was determined according to the method of Ruch et al. (1989). A solution of H_2O_2 (40 mM) was prepared in phosphate buffer (pH 7.4). Extracts, flavonoids and NPs were added to the H_2O_2 solution. Absorbance of H_2O_2 at 230 nm was determined 30 min later against a blank solution containing the phosphate buffer without hydrogen peroxide.

3.7.4 Kirby-Bauer disc diffusion susceptibility test

Mueller-Hinton agar was poured onto petri dishes and allowed to cool to form a solid. A pure bacterial culture was suspended in buffer solution and standardised to turbidity using a McFarland standard. Using a swab, the bacterial culture was swabbed uniformly across the solid agar to form a bacterial lawn. To obtain uniform growth, the plate was streaked with the swab in one direction, the plate was rotated 90° and streaked again. The rotation was repeated three times. A filter-paper disc, impregnated with the test compound, was then placed on the surface of the agar. The plate was covered, allowed to cool for 10 min then incubated at 37 °C for 24 h. The diameter of the clear region around the saturated disc was taken as the zone of inhibition (Jorgensen and Turnidge, 2007).

3.8 Statistical analysis

The significant differences between means for antioxidant activity of the different samples was obtained by ANOVA and Tukey's post hoc test at $p < 0.05$ using IBM SPSS Statistics 24.

CHAPTER 4

RESULTS AND DISCUSSION

STRUCTURE ELUCIDATION OF PHYTOCOMPOUNDS AND SYNTHESIS AND CHARACTERISATION OF NANOPARTICLES

This Chapter focusses on the results obtained from the phytochemical investigation of the two medicinal plants species (*Chrysanthemoides monilifera* and *Harpephyllum caffrum*) and the

synthesis and characterisation of the nanoparticles (NPs). For the phytochemical investigation, the spectroscopic techniques used were UV-Vis, FTIR and NMR (1D and 2D). For characterisation of NPs the techniques used were UV-Vis, FTIR, PXRD, SAED, SEM, TEM, HRTEM and EDS.

4.1 Structure Elucidation of Phytochemicals

In the following section the techniques used to identify the isolated compounds will be discussed.

4.1.1 Nuclear magnetic resonance (NMR) and mass spectrometry (MS)

Quercetin was isolated from the crude MeOH extract of *C. monilifera* and catechin was isolated from the crude MeOH extract of *H. caffrum*. $^1\text{H-NMR}$, $^{13}\text{C-NMR}$, DEPT 135 and DEPT 90 were used to elucidate the structure of these isolated compounds. GC-MS was used to further confirm these results.

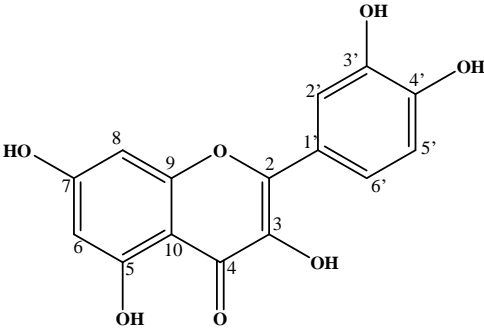
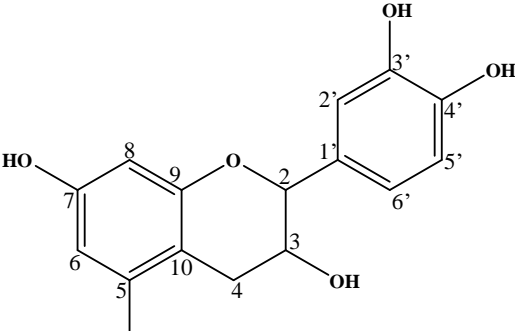
The compound isolated from *C. monilifera* (quercetin), was isolated as a yellow solid with a mass of 210 mg. The $^1\text{H-NMR}$ spectrum (Appendix A) exhibited characteristic resonances for a flavonol (Figure 2.8D). The ^1H and ^{13}C spectral data are shown in Table 4.1. The aromatic region exhibited the ABX system with protons resonating at δ_{H} 7.76 (H-2'), δ_{H} 7.66 (H-6') and δ_{H} 6.91 (H-5') due to di-substitution of ring B and a meta-coupled pattern with protons resonating at δ_{H} 6.41 (H-8) and δ_{H} 6.21 (H-6) due to di-substitution of ring A. The $^{13}\text{C-NMR}$ spectrum (Appendix A) indicated the presence of 15 carbon signals.

The compound isolated from *H. caffrum* (catechin) was isolated as a clear solid with a mass of 92 mg. The $^1\text{H-NMR}$ spectrum (Appendix A) for this compound showed characteristic resonances for flavanols (Figure 2.8D) at δ_{H} 6.74 (H-2'), δ_{H} 6.66 (H-5') and δ_{H} 6.61 (H-6') from the B-ring catechol moiety as well as at δ_{H} 5.83 (H-6) and δ_{H} 5.77 (H-8) from the meta-coupled protons of the A-ring resorcinol moiety. The $^{13}\text{C-NMR}$ spectrum (Appendix A) indicated the presence of 15 carbon signals.

The ^1H and $^{13}\text{C-NMR}$ spectroscopic data obtained match those in the literature for quercetin (Sanghavi et al., 2014) and catechin (Vuong et al., 2010).

The M^+ ion at m/z 302 agrees with the molecular formula $C_{15}H_{10}O_7$ for quercetin (Appendix A). The M^+ ion at m/z 290 is in agreement with the molecular formula of $C_{15}H_{14}O_6$ for catechin (Appendix A). The results obtained for quercetin and catechin correspond with those in the literature (Acharya et al., 2013; Vuong et al., 2010) thereby confirming the compounds to be quercetin and catechin.

Table 4.1: Nuclear magnetic resonance (NMR) spectroscopic data for quercetin and catechin

| ¹ H-NMR and ¹³ C-NMR spectroscopic data | | | | |
|---|---|-----------------------|--|-----------------------|
| | Quercetin | | Catechin | |
| |  | |  | |
| Position | ¹ H (ppm) | ¹³ C (ppm) | ¹ H (ppm) | ¹³ C (ppm) |
| 2 | 7.76 (d, <i>J</i> = 1.50 Hz) | 144.8 | 4.47 (d, <i>J</i> (H2ax-H3ax) = 7.48 Hz) | 156.93 |
| 3 | | 135.8 | 3.88 (dd, <i>J</i> = 5.60 Hz, 7.8 Hz) | 68.83 |
| 4 | | 175.95 | 2.47 (ax, dd, <i>J</i> = 7.80, 16.1 Hz) and 2.48 (eq, dd, <i>J</i> = 5.60 Hz, 16.1 Hz) | 28.53 |
| 5 | | 160.08 | | 157.59 |
| 6 | 6.21 (d, <i>J</i> = 1.4 Hz) | 97.91 | 5.83 (H-6, d, <i>J</i> = 2.24 Hz) | |
| 7 | | 164.22 | | 157.84 |
| 8 | 6.41 (d, <i>J</i> = 1.4 Hz) | 93.08 | 5.77 (H-8, <i>J</i> = 2.24 Hz) | 82.87 |
| 9 | | 156.86 | | 146.27 |
| 10 | | 103.13 | | 95.54 |
| 1' | | 120.32 | | 116.12 |
| 2' | | 114.64 | 6.74 (H-2, d, <i>J</i> = 1.60 Hz) | 100.86 |
| 3' | | 146.38 | | 132.23 |
| 4' | | 146.67 | | 146.24 |
| 5' | 6.91 (d, <i>J</i> = 8.5 Hz) | 114.87 | 6.66 (d, <i>J</i> = 8.2 Hz) | 96.33 |
| 6' | 7.66 (dd, <i>J</i> = 1.5, 8.5 Hz) | 122.76 | 6.61 (dd, <i>J</i> = 1.60 Hz, 8.2 Hz) | 115.28 |

4.1.2 Fourier-transform infrared (FTIR) spectroscopy

The functional groups present in the crude MeOH extract of *C. monilifera* and *H. caffrum* were determined using Fourier-transform infrared (FTIR) spectroscopy. Both extracts (Figure 4.1) exhibited characteristic absorption bands at 3342.50 and 3241.14 cm^{-1} for hydroxyl groups (O-H stretching), at 2929 and 2924 cm^{-1} for C-H groups (C-H stretching), 1456 and 1442 cm^{-1} for C-H groups (C-H bending), 1636 and 1605 cm^{-1} for C=C groups, and 1161 and 1202 cm^{-1} for C-O groups. The results showed both crude extracts to have similar profiles. This implies that both plant extracts have similar classes of compounds present in them.

The FTIR spectra (Figure 4.2) show characteristic bands for the O-H group (3268 and 3206 cm^{-1}), C=C group (1661 and 1621 cm^{-1}) and C-O group (1014 and 1049 cm^{-1}) for both isolated compounds. The spectra are similar to that of flavonoids confirming that the compounds to be quercetin and catechin.

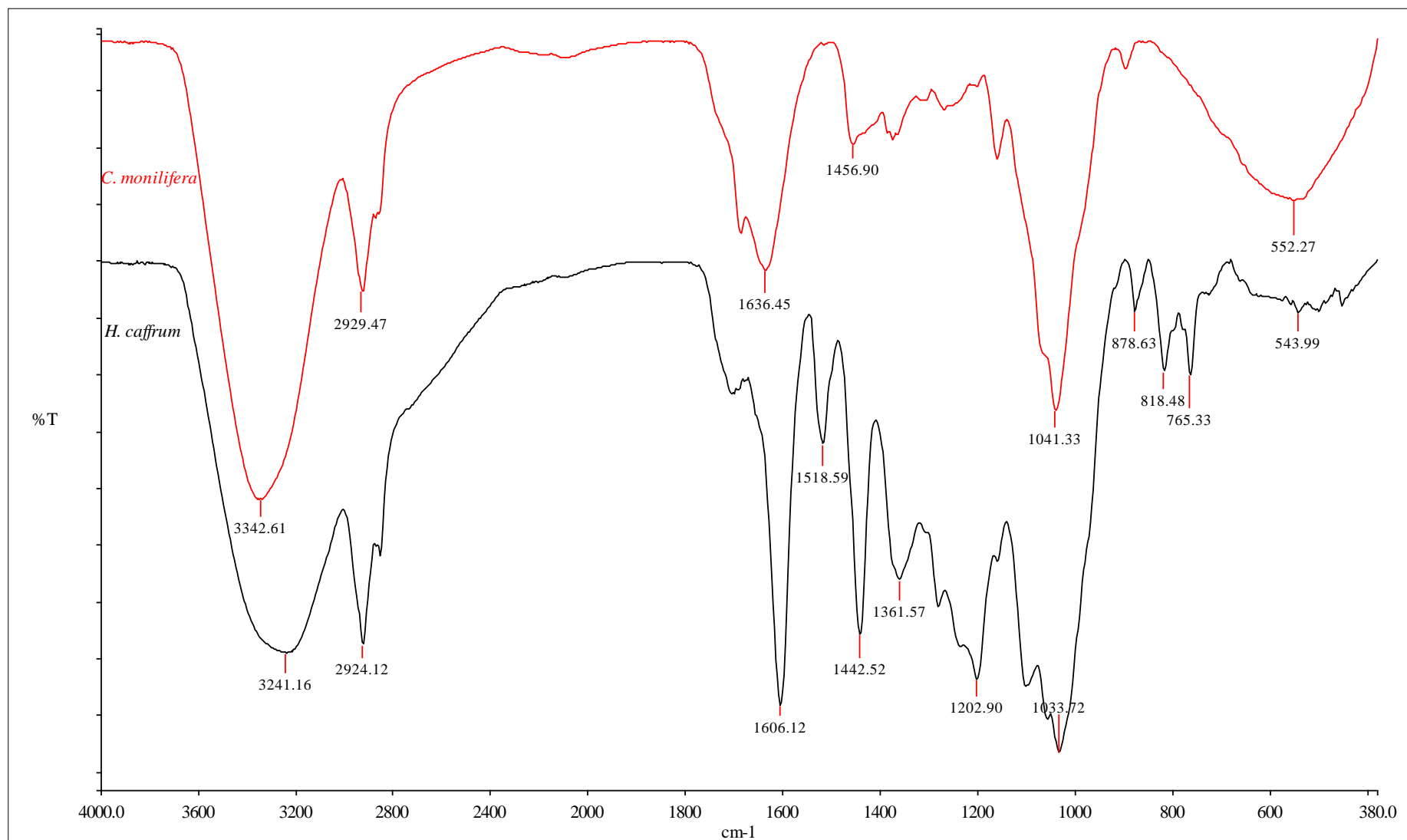


Figure 4.1: Fourier-transform infrared (FTIR) spectra of the crude methanol extracts of *Chrysanthemoides monilifera* and *Harpephyllum caffrum*

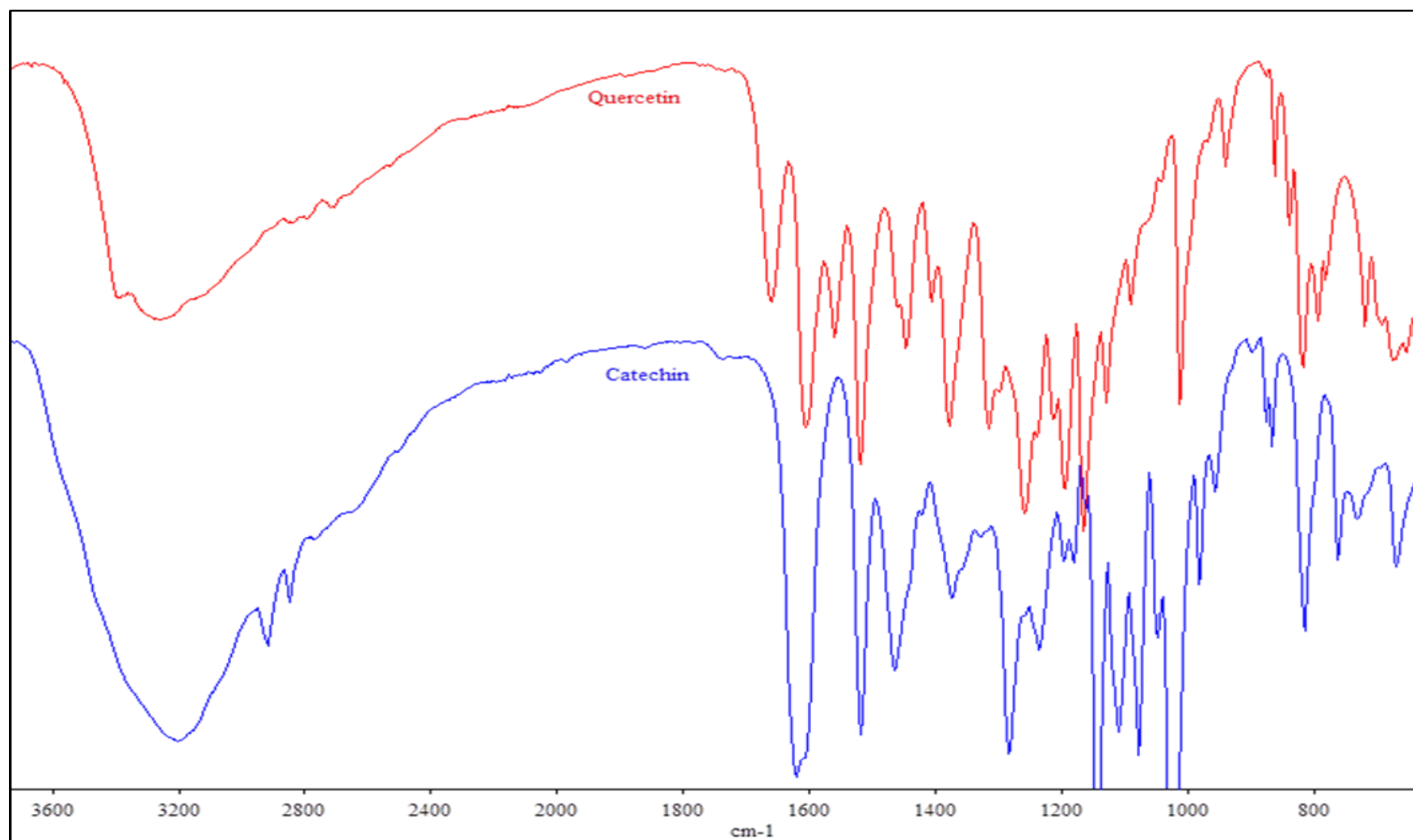


Figure 4.2: Fourier-transform infrared (FTIR) spectra of quercetin isolated from *Chrysanthemoides monilifera* and catechin isolated from *Harpephyllum caffrum*

4.1.3 Ultraviolet-visible (UV-Vis) spectroscopy

The Ultraviolet-visible (UV-Vis) spectra for the plant extracts are shown in Figure 4.3. Both extracts have a small shoulder between 679 nm and 647 nm due to the presence of chlorophylls with a gradual increase in absorbance from 500 nm and less.

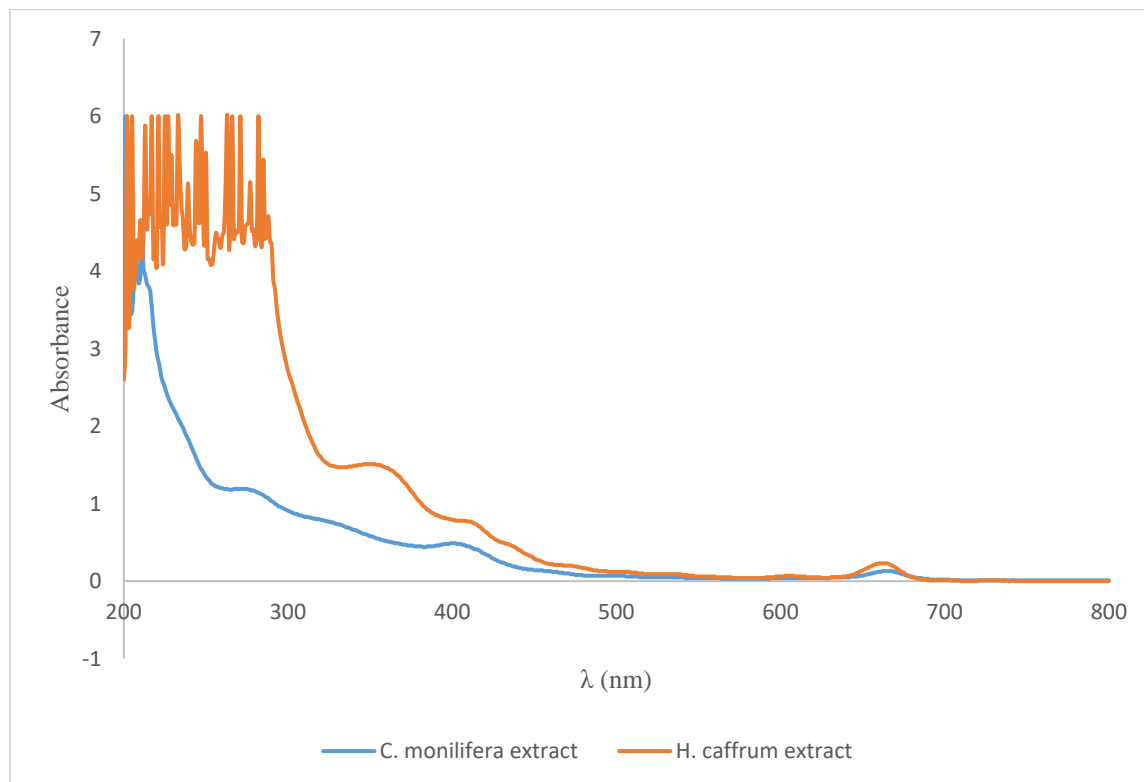


Figure 4.3: Ultraviolet-visible (UV-Vis) spectra of the crude methanol extracts of *Chrysanthemoides monilifera* and *Harpephyllum caffrum*

The UV-Vis results showed *C. monilifera* and *H. caffrum* crude extracts to have similar absorbance profiles which confirm that the plant extracts have similar classes of compounds in them. The UV-Vis spectra of the isolated compounds (Figure 4.4) show two bands which can be attributed to different parts of the conjugated aromatic rings present in flavonoids. The bands originate from the A and B rings of flavonoids (Maoela et al., 2009). For quercetin, the first band was at 255 nm and the second band at 370.5 nm. A strong absorption band was observed at 222 nm and a weaker band at 281 nm for catechin. This confirms the compounds to be quercetin and catechin.

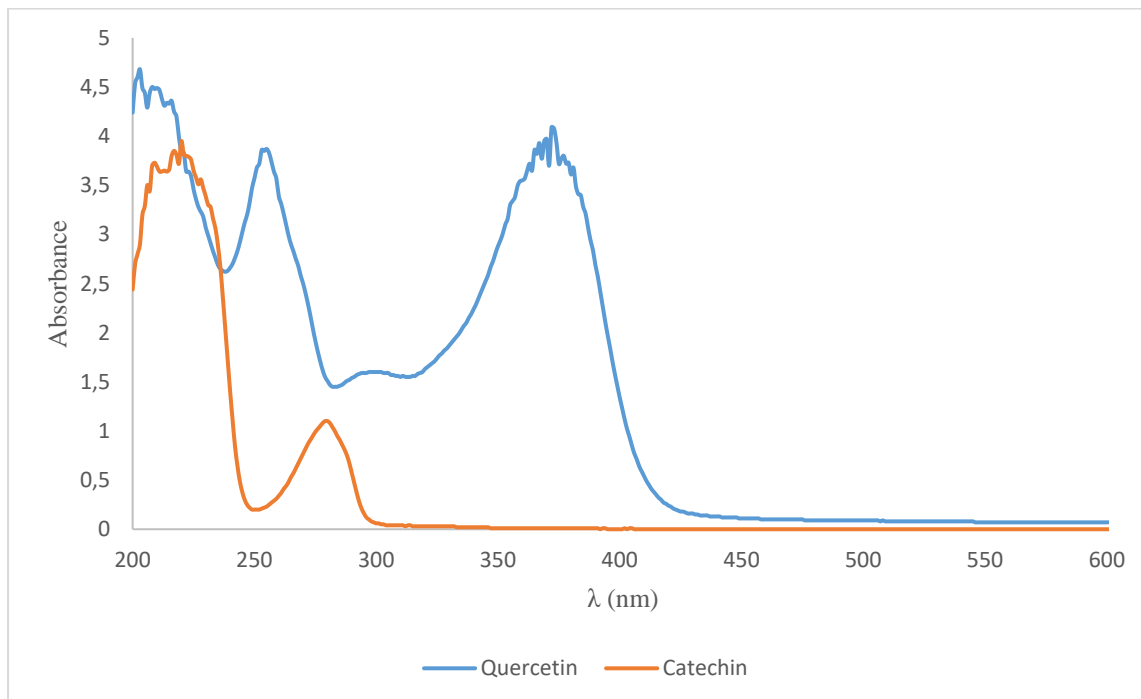


Figure 4.4: Ultraviolet-visible (UV-Vis) spectra of quercetin and catechin

4.2 Effects of Concentration on Nanoparticle Growth

The synthesis of the AgNPs in aqueous solution was monitored by recording the absorption spectra at a wavelength range of 200 to 600 nm. The analysis was performed to monitor the development of NPs. The solution of silver nitrate turned orange brown on addition of quercetin which indicated the formation of AgNPs.

4.2.1 Ultraviolet-visible (UV-Vis) spectroscopy

Colloidal solutions of metal NPs usually have intense colours due to the Surface Plasmon Resonance (SPR) that results from electromagnetic radiation interacting with free electrons causing them to oscillate (Noguez, 2007). Figure 4.5 shows the SPR of AgNP colloids in quercetin (isolated from *C. monilifera* extract) at concentrations ranging from 0.1 mM to 3 mM.

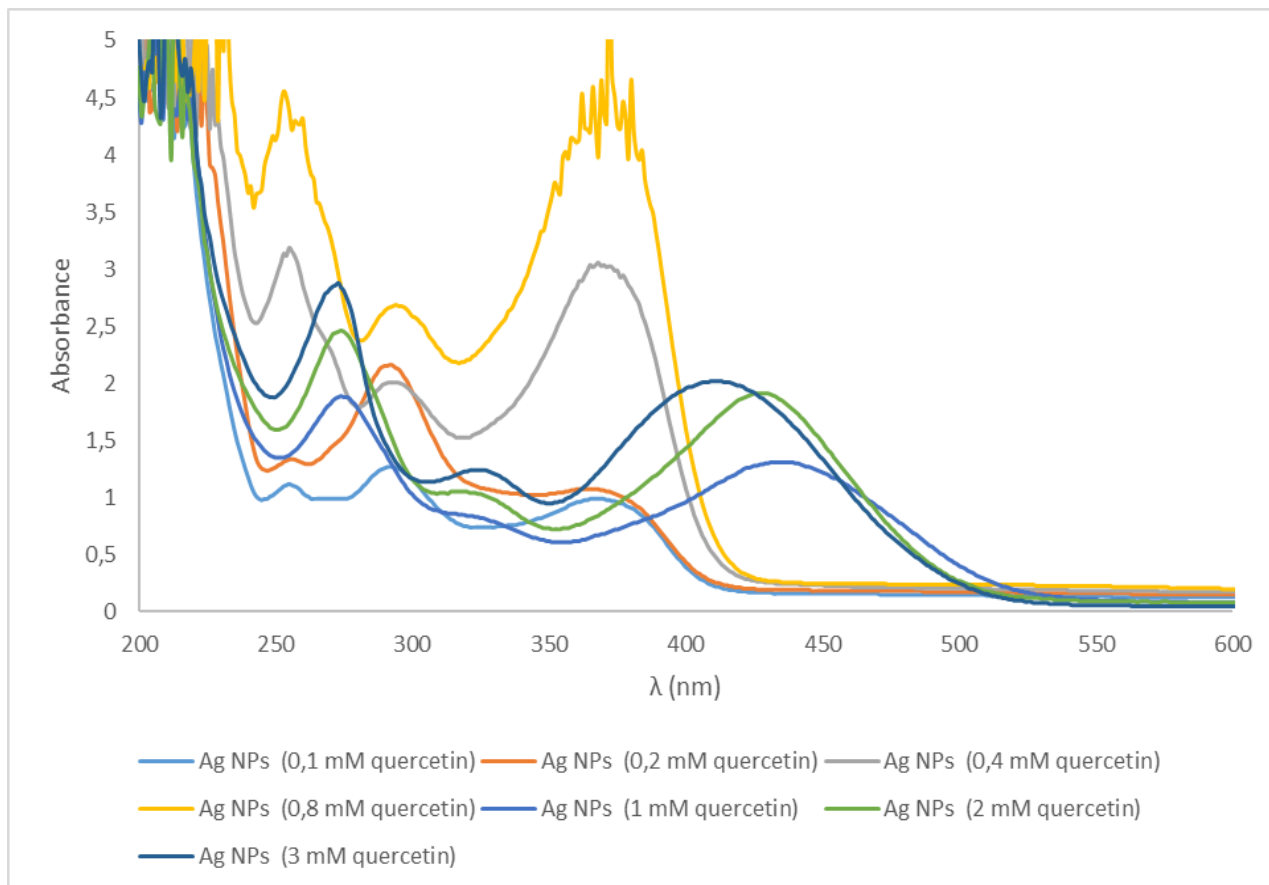


Figure 4.5: Ultraviolet-visible (UV-Vis) spectra of silver nanoparticles (AgNPs) reduced with 0.1-3 mM quercetin

Nanoparticles formed rapidly (within seconds) upon mixing the AgNO_3 solution and quercetin solutions. A strong SPR centred around 367-434 nm was observed which confirms the presence of stable AgNPs. The SPR observed for Ag also corroborates with previous studies (Sun et al., 2014; Verma and Mehata, 2016). All SPR profiles are similar. The first two peaks observed in the UV-Vis profiles are due to the AB ring moiety of quercetin that were observed previously (Figure 4.4). The third peak is due to Ag. However, it is also observed that absorbance peaks due to quercetin have shifted. The original locations and shifts of the absorption peaks due to quercetin along with the AgNPs that were reduced with quercetin are recorded in Table 4.2.

Table 4.2: Peak locations and peak shifts of quercetin with silver colloid solutions in nanometres (nm).

| | Peak 1 (Ring A) | Peak 2 (Ring B) | Peak 3 (Silver) |
|--------------------------|------------------|--------------------|--------------------|
| Pure quercetin | 255 ^a | 370.5 ^a | - |
| AgNPs (0.1 mM quercetin) | 257 ^b | 292 ^a | 367.5 ^b |
| AgNPs (0.2 mM quercetin) | 256 ^b | 292 ^a | 364 ^b |
| AgNPs (0.4 mM quercetin) | 255 ^a | 293 ^b | 368 ^a |
| AgNPs (0.8 mM quercetin) | 253 ^a | 294 ^b | 369 ^a |
| AgNPs (1 mM quercetin) | 274 ^a | No peak | 435 ^b |
| AgNPs (2 mM quercetin) | 247 ^a | 317 ^c | 427.5 ^b |
| AgNPs (3 mM quercetin) | 273 ^a | 324 ^c | 411 ^b |

*superscript (a-c) denotes the relative intensities of the peaks going across the table with (a) denoting the highest intensity and (c) the lowest

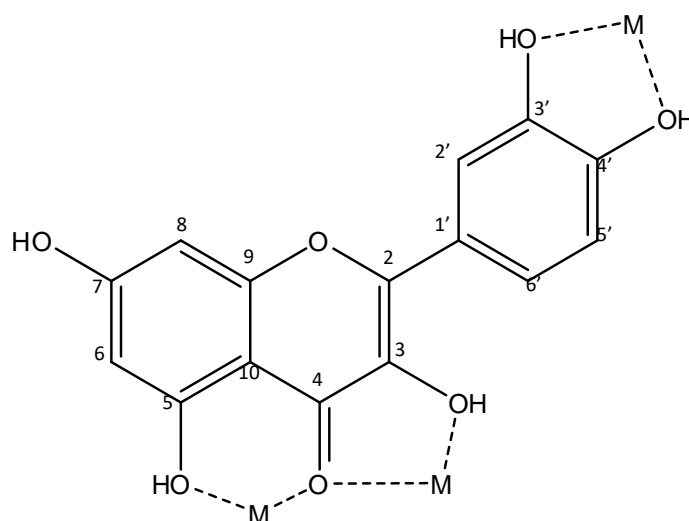


Figure 4.6: Structure of quercetin with possible chelating sites

Interactions between metal ions and flavonoids can lead to chelate formation and subsequent reduction of metal ions which result in the shift of absorption bands. Quercetin is a flavonoid with very strong chelating activity. It has three sites available for chelating involving the carbonyl with hydroxyls at C3 (Ring C) and C5 (Ring A) and the catechol group at C3' and C4' (Ring B) (Kulkarni and Muddapur, 2014). Depending on the chelating position, a corresponding wavelength shift will be observed in the UV-Vis spectrum of quercetin. The absorbance peak for ring A of quercetin was at 255 nm and for ring B was at 370.5 nm and the two peaks are of similar intensities. The absorbance peaks due to ring A remains almost constant at 255 ± 2 nm when quercetin concentrations are below 1 mM.

The absorbance peak, due to ring B, shifts from 370 nm in quercetin to 292 ± 2 nm when quercetin concentrations are below 1 mM in the AgNP solutions. The absorbance of Ag increases resulting in the two peaks having similar intensities at 0.1 mM and 0.2 mM quercetin concentrations but from 0.4 to 3 mM quercetin concentrations, the intensity of the absorbance due to ring B falls as that due to Ag increases. This indicates that the reduction may be occurring at different positions in the quercetin rings as the concentration of quercetin is varied. At quercetin concentrations above 1 mM, the relative intensities of all three peaks are different and all the absorbance peaks due to quercetin shift to longer wavelengths (red shift).

At concentrations between 0.1 and 0.8 mM quercetin, the absorbance for Ag SPR is at 367 ± 2 nm. The SPR absorption peaks shift and broaden between 1 and 3 mM quercetin concentrations. The observed SPR shift is often a result of combined influences from size and shape of the NPs. Large size and shape distribution results in a broad and asymmetric SPR band (Mandal et al., 2003). The broader peaks are indicative of a wider size distribution. This suggests that smaller sized NPs with a narrow size distribution are to be expected at concentrations less than 1 mM relative to those synthesised at 1 mM and above. The absorption maxima of AgNPs shifted to longer wavelengths with increase in AgNP size.

4.2.2 Transmission electron microscopy (TEM)

The micrographs of AgNPs (0.1 mM quercetin) (Figure 4.7 A and B) show that the population of NPs are divided into two distinct sizes of smaller and larger NPs. The NPs are roughly spherical in shape. The smaller population size ranged from 5-10 nm and the larger particles ranged from 60-80 nm.

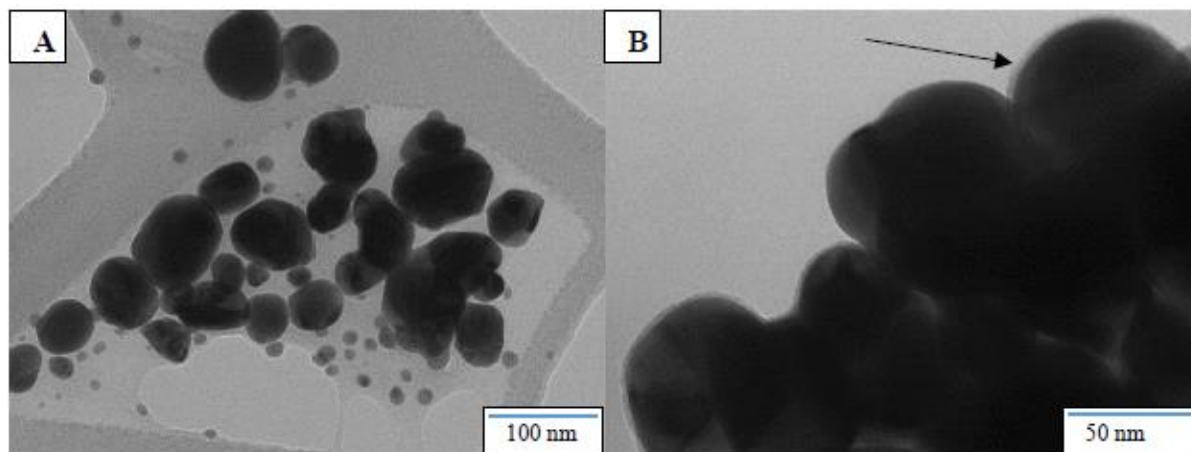


Figure 4.7: Silver nanoparticles (AgNPs) synthesised (0.1 mM quercetin)

At higher magnifications, a quercetin layer can be observed on the surface of the larger particles. The capping was not seen on smaller particles. The chelating ability of quercetin may explain its ability to adsorb onto the surface of growing NPs. This could also mean that quercetin was involved in the initiation of nucleation of NPs, apart from the expected bioreduction.

Increasing the concentration of quercetin from 0.1 to 0.2 mM, produced an increased amount of NPs. Nanoparticles are made of two distinct populations; small and large NPs were observed in experiments with 0.1 mM quercetin. The TEM micrographs for AgNPs (0.2 mM quercetin) are shown in Figure 4.8 A and B. Nanoparticles are still roughly spherical in shape and it appears that small particles attach to the large particles. The small NPs are seen on top of the large particles which is contrary to AgNPs (0.1 mM quercetin) where the two populations existed separately from each another. The capping observed in AgNPs (0.1 mM quercetin) have reduced in size in AgNPs (0.2 mM quercetin).

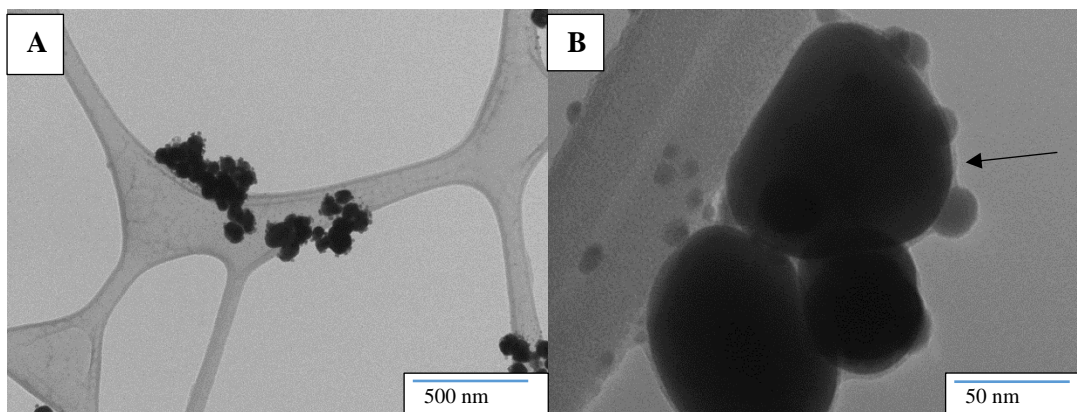


Figure 4.8: Silver nanoparticles (AgNPs) synthesised (0.2 mM quercetin)

The other notable difference between AgNPs (0.1 mM quercetin) and AgNPs (0.2 mM quercetin) was their relative sizes. The smaller sized population of NPs observed for AgNPs (0.2 mM quercetin) ranged between 3 - 5 nm which were smaller than those of AgNPs (0.1 mM quercetin) which ranged from 80 – 95 nm.

Further increasing the concentration of quercetin to 0.4 mM resulted in two populations of large and small particles. The yield increased compared to AgNPs (0.2 mM quercetin). The particles still remained roughly spherical in shape. The sizes of the small particles range from 5 to 25 nm and larger particles range from 40 – 90 nm. The TEM micrographs for AgNPs (0.4 mM quercetin) can be seen on Figure 4.9 A and B. However, as observed in Figure 4.9 B, the particles begin to agglomerate. The capping on the surface of the NPs can no longer be observed. The population of small particles have increased in volume compared to experiments with 0.1 and 0.2 mM quercetin.

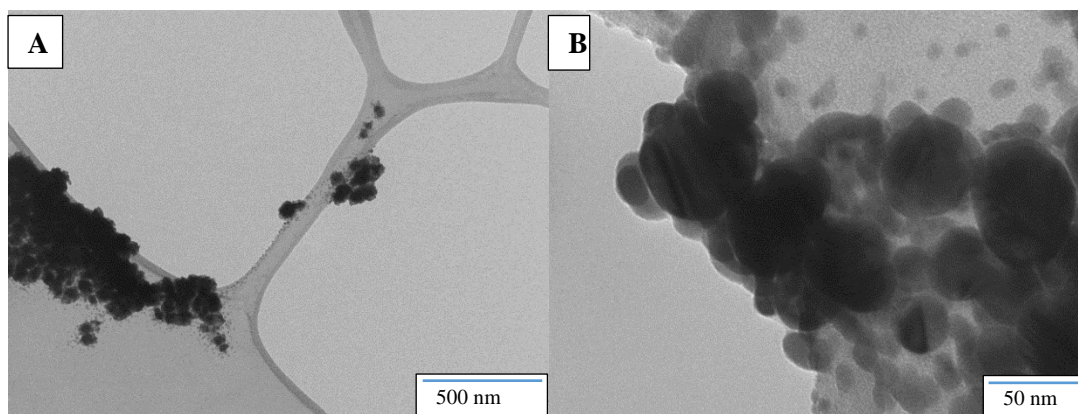


Figure 4.9: Silver nanoparticles (AgNPs) synthesised (0.4 mM quercetin)

Figure 4.10 A and B show AgNPs (0.8 mM quercetin) to increase in yield and agglomeration between particles. There is essentially one observed population size of small, spherical NPs with a size range of 7-10 nm. However, it is apparent that the particles coagulated to form larger oval shaped particles as well as long threads/rods/wires. The capping observed previously for AgNPs (0.1 mM quercetin) and AgNPs (0.2 mM quercetin) cannot be observed.

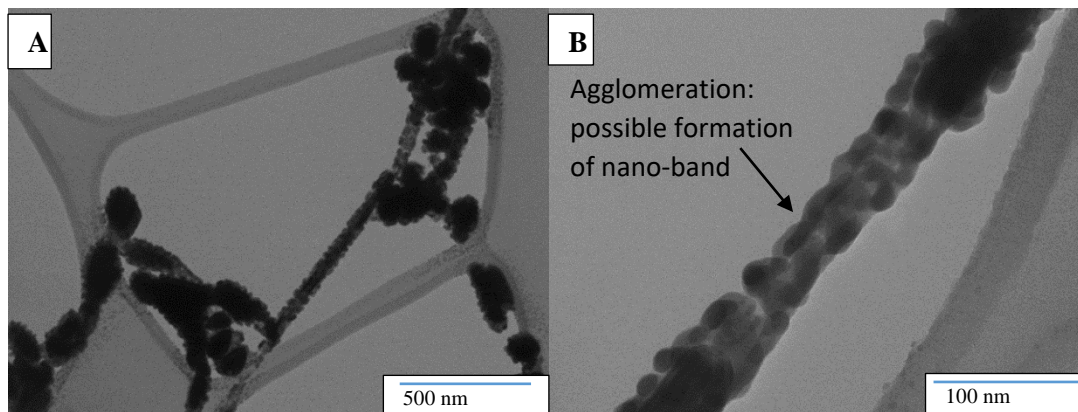


Figure 4.10: Silver nanoparticles (AgNPs) synthesised (0.8 mM quercetin)

The broad SPR of the AgNPs (1mM quercetin) in Figure 4.5 can be accounted for by observing the TEM micrographs in Figure 4.11 A and B which show AgNPs (1 mM quercetin) with a variety of shapes. The TEM micrographs show a mixed population of nano-wires, nano-bands, nano-spheres, nano-triangles and nano-octagons. Their size range is 5 -150 nm with an average size of 89.8 ± 33 nm. The nano-wires are made of two populations. The first being the long and smooth nano-bands and the second being short elongated agglomerations (Figure 4.10 B) which might lead to the formation of nano-bands or nano-rods over time. The length of the long and smooth nanobands reached $5 \mu\text{m}$ with a width of 87 nm. The yield of NPs increased compared to 0.8 mM quercetin experiments.

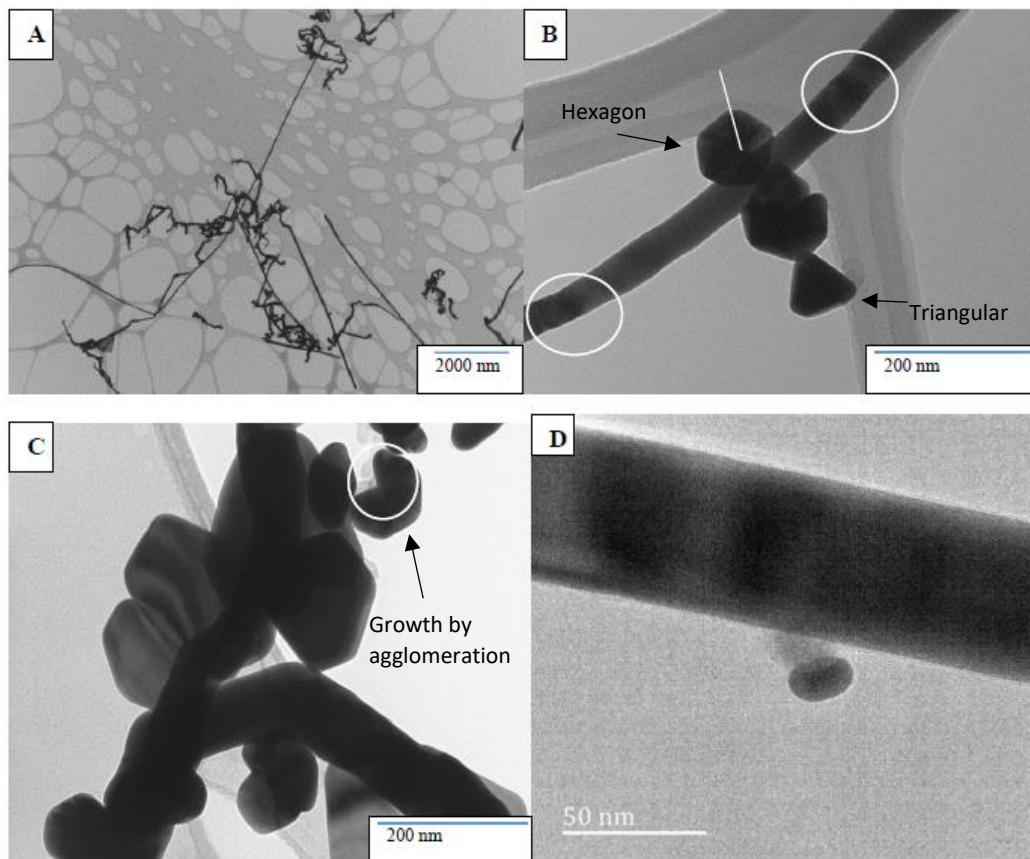


Figure 4.11: Silver nanoparticles (AgNPs) synthesised (1mM quercetin) (A) general population of the synthesised nanoparticles (B) various shapes of the nanoparticles (C) incomplete hexagon (D) capping on the surface of the nanorods

Circled on the nano-bands in Figure 4.11 B are bending contours indicating that they are very thin. Grain boundaries can also be observed on the nano-band and nano-hexagons. The AgNPs (0.8 mM quercetin) suggest that the nanowires observed in Figure 4.11 D may be due to the agglomeration of small particles. The hexagons may also form in a similar fashion where nano-triangles may have agglomerated to form hexagons. This is apparent by Figure 4.11 C where an “incomplete” hexagon (one triangle short of a complete hexagon) is observed. At high magnifications, quercetin capping on the surface of the NPs can again be observed. The capping is only observed on large particles and wires. In Figure 4.11 C and D, no capping is visible on the small particles.

Doubling the concentration of quercetin to 2 mM, significantly increases the yield and affects the shape and size of the NPs. The NPs range from 25-250 nm in size. Figure 4.12 A shows that the population of the NPs no longer comprises of long and smooth nano-band. There are

two populations of shorter and wiggled nano-bands (Figure 4.12 A) and long and smooth (Figure 4.12 B).

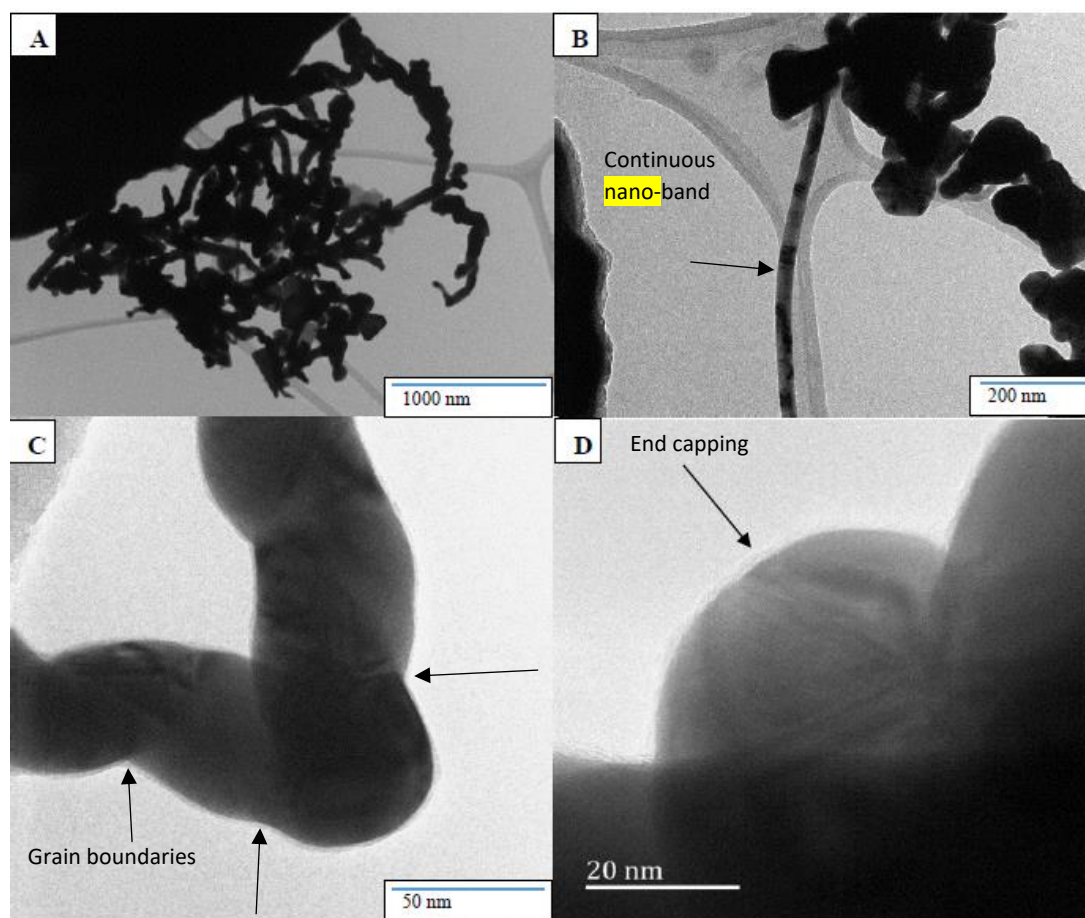


Figure 4.12: Silver nanoparticles (AgNPs) synthesised (2 mM quercetin)

Visible in Figure 4.12 A and B are the wiggled nano-bands, nano-triangles, nano-hexagons and nano-spheres. Grain boundaries of nano-triangles are still visible on the nano-hexagons. At higher magnifications the wiggled nano-wires are observed and consist of a row of agglomerated spherical nanoparticles grain boundaries are visible. Around the surface of the NPs, capping is once again observed.

Increasing the concentration to 3 mM quercetin, larger NPs were formed, however, the amount of particles decreased significantly compared to the AgNPs (2 mM quercetin). Figure 4.13 A shows that the size and shapes of the NPs become more uniform with increase in concentration. Their sizes range from 180 – 250 nm with the average particle size being 213 ± 54 nm. The

shapes observed are nano-spheres, nano-squares and elongated nano-spheres and squares with most of the particles observed to have a quercetin capping on the surface.

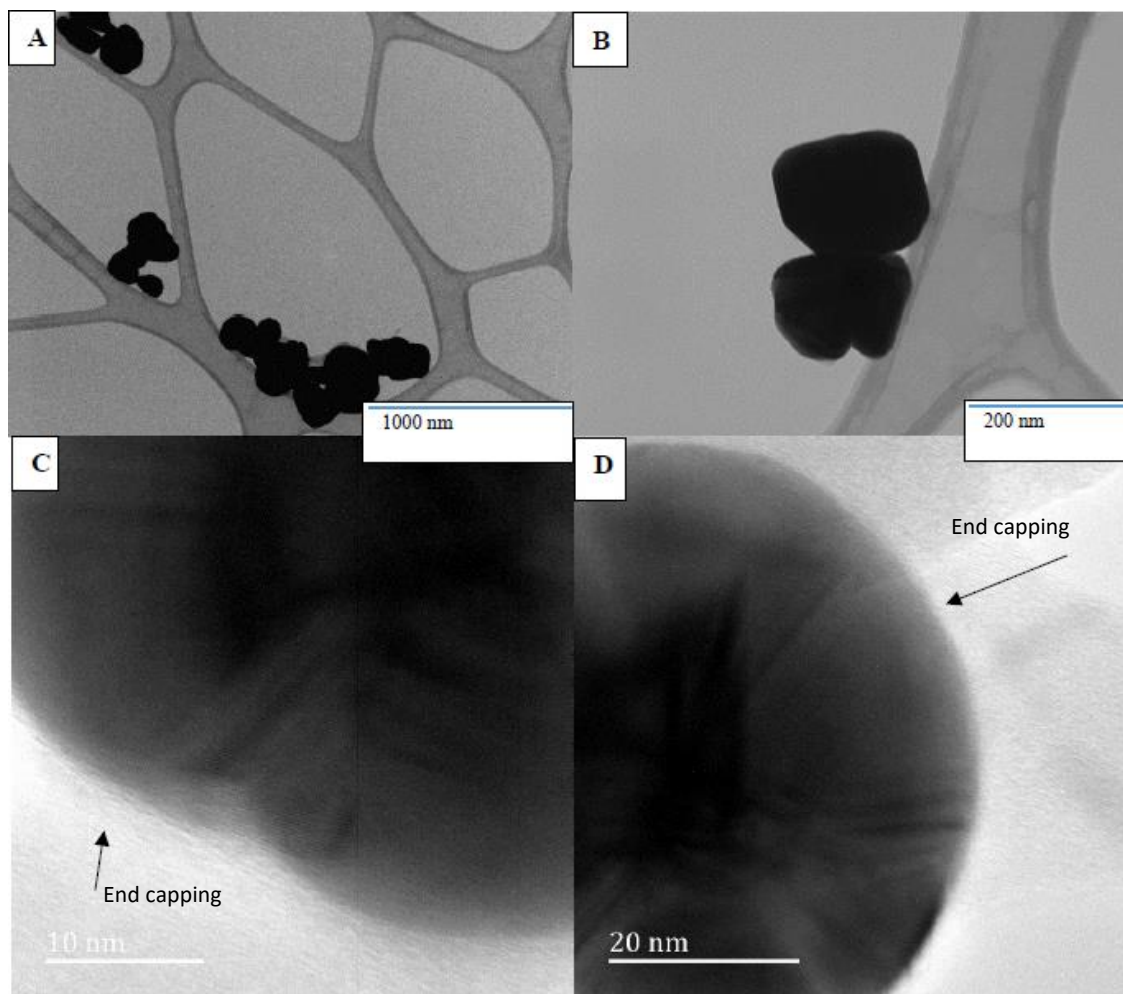


Figure 4.13: Silver nanoparticles (AgNPs) synthesised (3 mM quercetin)

Overall, it is observed that the concentration of quercetin has an effect on the yield, shapes and sizes of the synthesised NPs. Experiments involving 2 mM quercetin produced the highest yield. From the TEM results, it is noted that the NPs reduced significantly in size as the concentration of quercetin was increased from 0.1 to 0.8 mM. The size increased again from 1 to 3 mM quercetin. Growth seem to occur by agglomeration of particles.

Similar studies using ZnO and Se were conducted. However, zinc oxide nanoparticles (ZnONPs) and selenium nanoparticles (SeNPs) were only synthesised using 2 mM quercetin. No SeNPs were formed with catechin at the various concentrations. Characterisation of SeNPs and ZnONPs will be discussed later in this chapter.

4.3 Effects of Various Reducing Agents on Nanoparticle Growth

Reduction with sodium borohydride (NaBH_4) occurred instantaneously and vigorously compared to reduction with *C. monilifera* extract, *H. caffrum* extract or with quercetin and catechin isolated from the extracts which took few seconds. Reduction of the Ag ions occurred faster than the reduction of Se and ZnO. For Ag ions, reduction occurred instantly upon mixing of solutions. For Zn^{2+} ions, reduction times ranged from hours to days while for the Se ions, reduction occurred within days to weeks.

4.3.1 Ultraviolet-visible (UV-Vis) spectroscopy

The synthesis of NPs in aqueous solution was monitored by recording the absorption spectra in the wavelength range of 200 to 800 nm. The analysis was performed to monitor the development of AgNPs, SeNPs and ZnONPs.

4.3.1.1 Silver nanoparticles

The SPR of Ag using NaBH_4 (freestanding NPs), *C. monilifera* extract, *H. caffrum* extract, quercetin and catechin as reducing agents are shown in Figure 4.14.

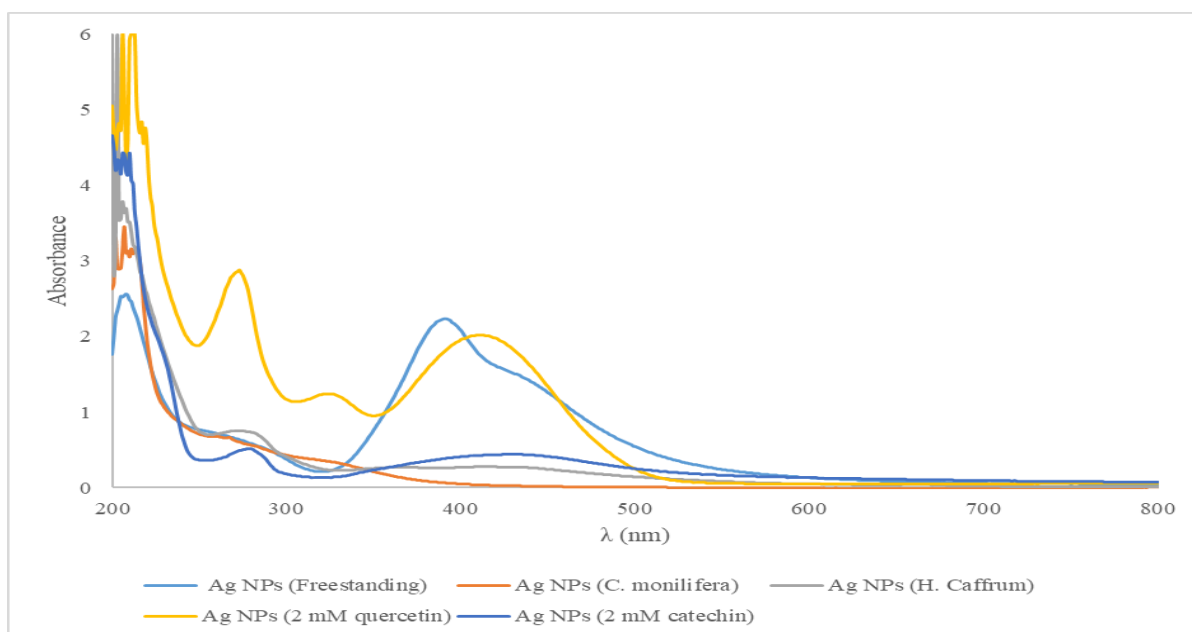


Figure 4.14: Ultraviolet-visible (UV-Vis) spectra of silver nanoparticles (AgNPs) synthesised with the various reducing agents

For freestanding NPs, an orange-brown suspension (Figure 4.15) of Ag⁰ NPs with a sharp SPR band at 399 nm was observed. The sharp peak indicates a narrow dispersity in size of the synthesised AgNPs. The SPR of the AgNPs synthesised using extracts show additive absorbance from the extracts and the characteristic SPR of AgNPs. Silver NPs (quercetin) and AgNPs (catechin) showed the two characteristic absorbances, due to the A and B rings of flavonoids observed in figure 4.4 and a third absorbance due to Ag. This confirms the presence of AgNPs and the compounds (quercetin and catechin) in the product.

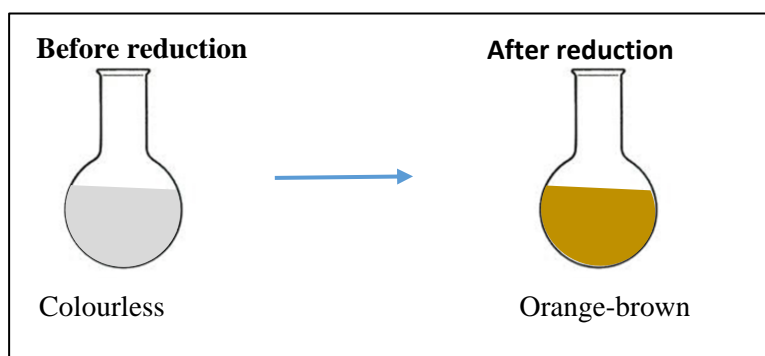


Figure 4.15: Colour change from reducing silver ions to silver nanoparticles

4.3.1.2 Selenium nanoparticles

The formation of SeNPs (freestanding) reduced with NaBH₄ was indicated by a solution colour change to brick red coloured (Figure 4.16) with a gradual increase SPR of 500 nm and below. A similar SPR for the formation of SeNPs can be found in literature (Husen and Siddiqi, 2014).

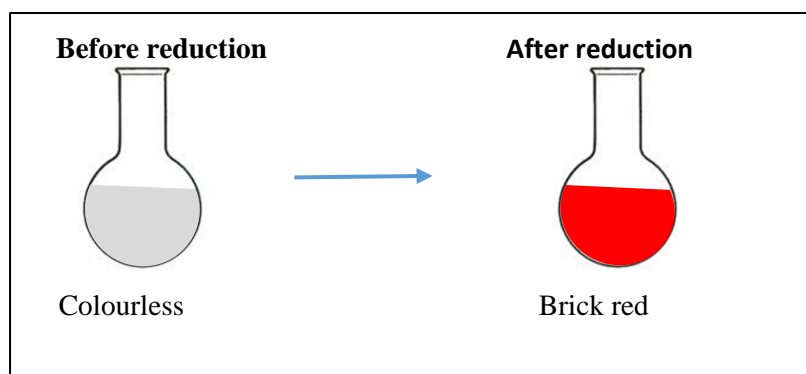


Figure 4.16: Colour change from reducing selenium ions to selenium nanoparticles

Similar to the Ag experiments with plant extracts, the observed profiles seen in Figure 4.17 are due to the additive absorbance of Se colloids (500 nm and below) and the plant extracts in the same regions. Formation of SeNPs with catechin was not observed within the time frame of the experiment.

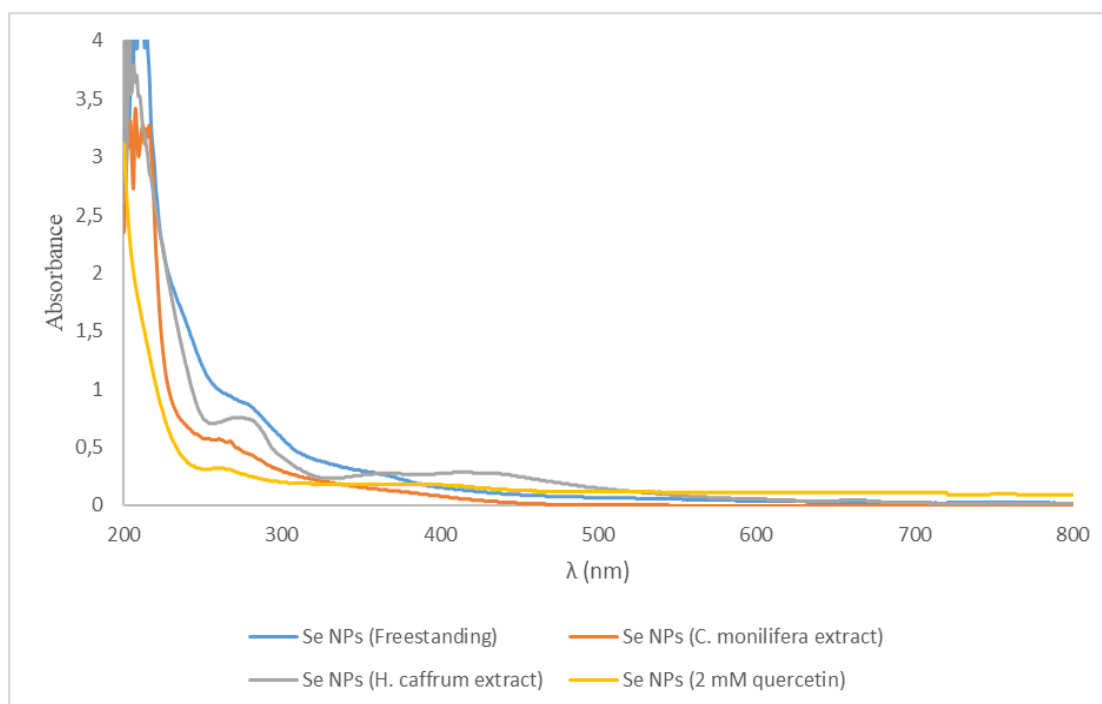


Figure 4.17: Ultraviolet-visible (Uv-Vis) spectra of selenium nanoparticles (SeNPs) synthesised with the various reducing agents

4.3.1.3 Zinc oxide nanoparticles

Zinc oxide NPs are naturally white and solutions containing ZnO colloids formed with NaBH_4 remained colourless (Figure 4.18)

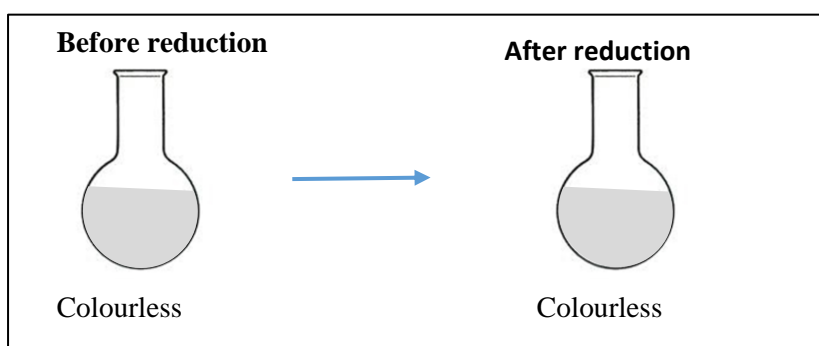


Figure 4.18: No colour change from reducing zinc oxide ions to zinc oxide nanoparticles

Zinc oxide NPs (2 mM quercetin) showed the sharpest SPR peak at 294 nm (Figure 4.19). The sharpness of the peak may be indicative of small sized NPs with a narrow size distribution (Noguez, 2007). Zinc oxide NPs (freestanding) show the broadest SPR peak between 298 and 305 nm. SPR peaks for ZnONPs (catechin) and ZnONPs (*H. caffrum*) are centred around 283 nm. This shows the influence of the structure of the reducing agent on the properties of ZnONPs.

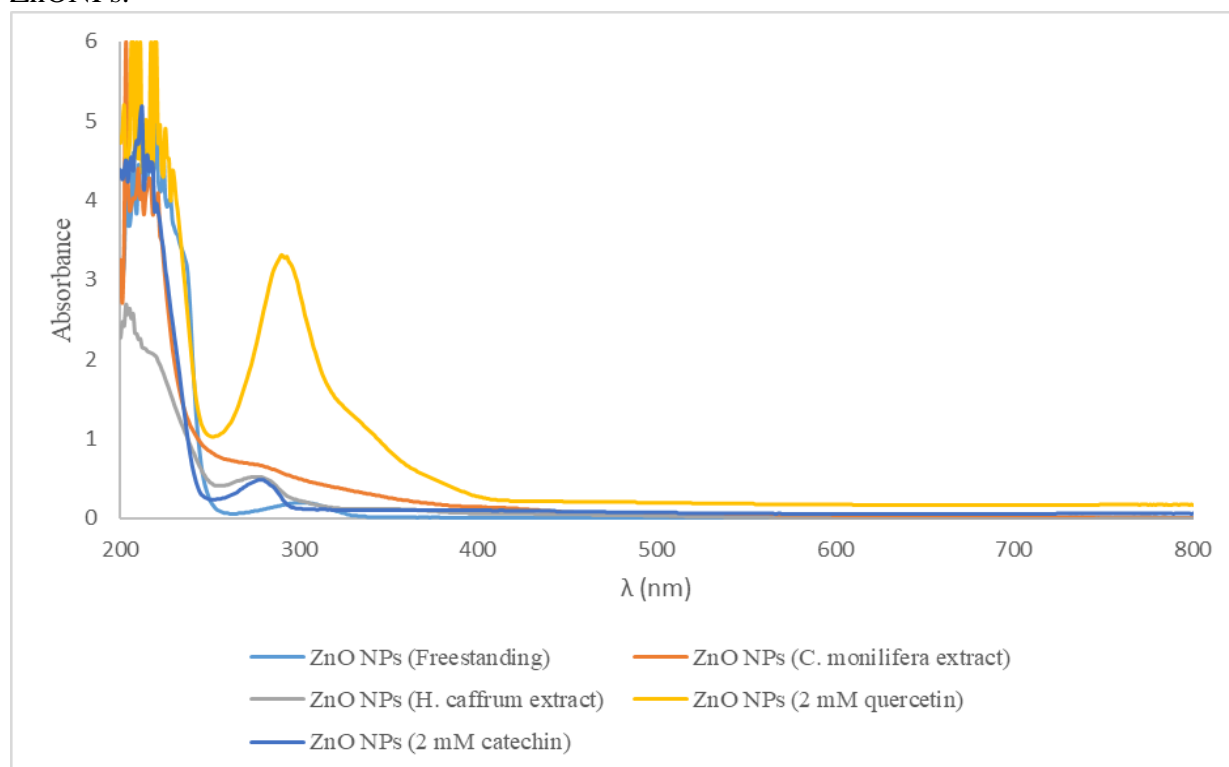


Figure 4.19: Ultraviolet-visible (Uv-Vis) spectra of zinc oxide nanoparticles (ZnONPs) synthesised with the various reducing agents

4.3.2 Energy-dispersive X-ray spectroscopy (EDS)

To confirm the composition of the synthesised NPs, an EDS analysis of the freestanding and end-capped NPs was performed. Prior to reduction to the 0 oxidation state, the oxidation state of silver, selenium and zinc was +1, +4 and +2 respectively.

4.3.2.1 Silver nanoparticles

Energy dispersive X-ray spectroscopy (EDS) was used to analyse AgNPs (freestanding) (Figure 4.20). The spectra indicates low presence of oxygen (O) and sodium (Na). The presence of the strong peak at 3 KeV is characteristic of Ag and corresponds with literature values (Velan et al., 2015). The analysis indicates that the obtained AgNPs are purely Ag. Results from EDS also show the NPs to contain impurities of sodium (nitrate) from the reaction ($\text{AgNO}_3 + \text{NaBH}_4 \rightarrow \text{Ag} + \frac{1}{2} \text{H}_2 + \frac{1}{2} \text{H}_2 + \text{NaNO}_3$).

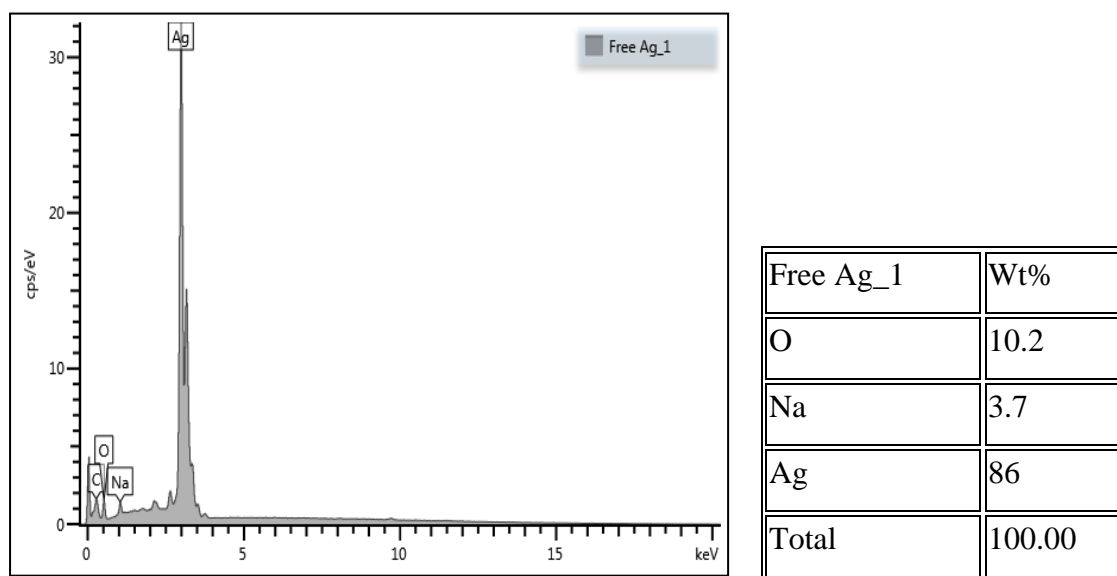


Figure 4.20: Energy dispersive X-ray spectroscopy (EDS) of freestanding silver nanoparticles (AgNPs)

The EDS results for AgNPs (*C. monilifera*) (Figure 4.21) and AgNPs (*H. cafferum*) (Figure 4.22) show a strong peak at 3 KeV which indicates the high Ag content in the synthesised AgNPs. Results from EDS of the biosynthesised NPs show no presence of Na and very high C and O content compared to AgNPs (freestanding). Silver NPs (*C. monilifera*) showed higher C content than O and AgNPs (*H. cafferum*) showed higher O content than C. The C and O originate from the phytochemicals present in the plant extracts used during the synthesis on the AgNPs.

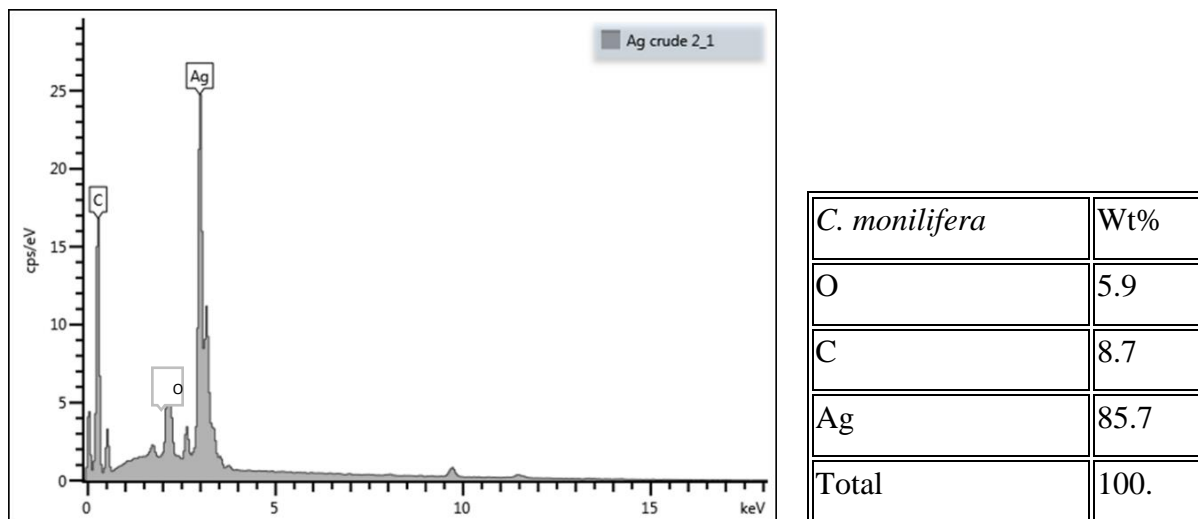


Figure 4.21: Energy dispersive X-ray spectroscopy (EDS) of silver nanoparticles (AgNPs) (*C. monilifera*)

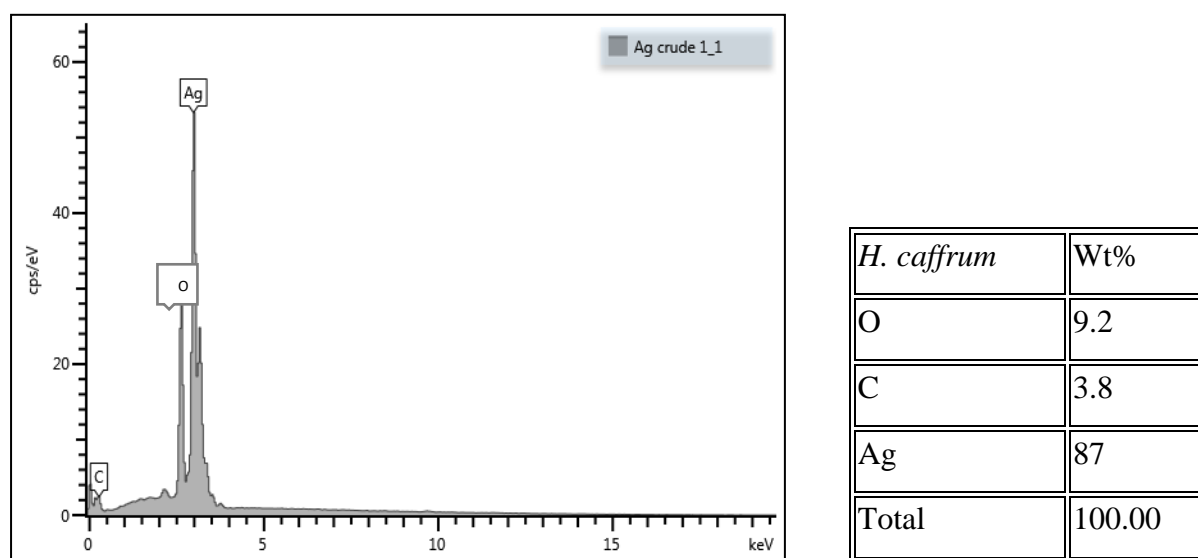
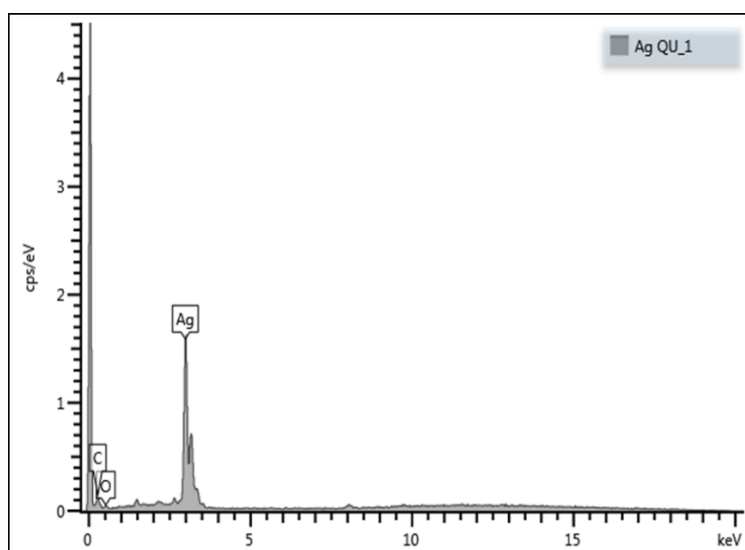


Figure 4.22: Energy dispersive X-ray spectroscopy (EDS) of silver nanoparticles (AgNPs) (*H. caffrum*)

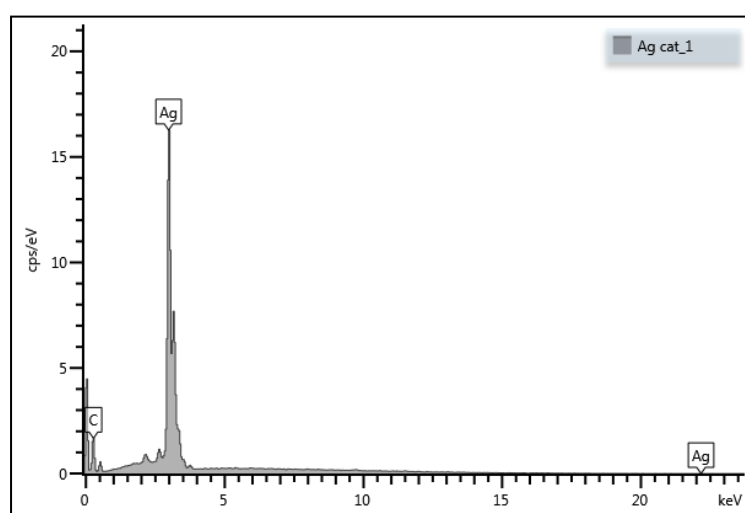
The EDS result for AgNPs (quercetin and catechin) are in Figure 4.23 and 4.24, respectively and the results show a strong peak characteristic for Ag at 3 keV. There are also weak C and O peaks that are stronger than those obtained for AgNPs (freestanding) but weaker than those obtained for AgNPs (*C. monilifera* and *H. caffrum*). AgNPs (quercetin) showed higher O

content than AgNPs (catechin) which is probably due to the fact that the structure of quercetin has more O atoms than catechin.



| Quercetin | Wt% |
|-----------|------|
| O | 4.1 |
| C | 8.5 |
| Ag | 87.4 |
| Total | 100 |

Figure 4.23: Energy dispersive X-ray spectroscopy (EDS) of silver nanoparticles (AgNPs) (quercetin)



| Catechin | Wt% |
|----------|------|
| O | 2.3 |
| C | 9.2 |
| Ag | 88.6 |
| Total | 100 |

Figure 4.24: Energy dispersive X-ray spectroscopy (EDS) of silver nanoparticles (AgNPs) (catechin)

The O content in the synthesised NPs may be due to the OH functionalities in the plant extracts and isolated compounds. The exact molecules responsible for the high C content observed in AgNPs (*C. monilifera* and *H. caffrum* extracts) are not known but plant extracts have a variety of organic (C and O-containing) compounds. The EDS results corroborate UV-Vis results that show AgNPs to be synthesised by the plant extracts or flavonoids.

4.3.2.2 Selenium nanoparticles

Figure 4.25 shows the EDS spectrum of SeNPs (freestanding). The presence of a strong peak at 1.5 is characteristic of Se (Avendaño et al., 2016). Although synthesised with NaBH_4 , the EDS spectra only showed the peaks of Se with a few impurities. In contrast, the spectra of AgNPs showed Na as an impurity.

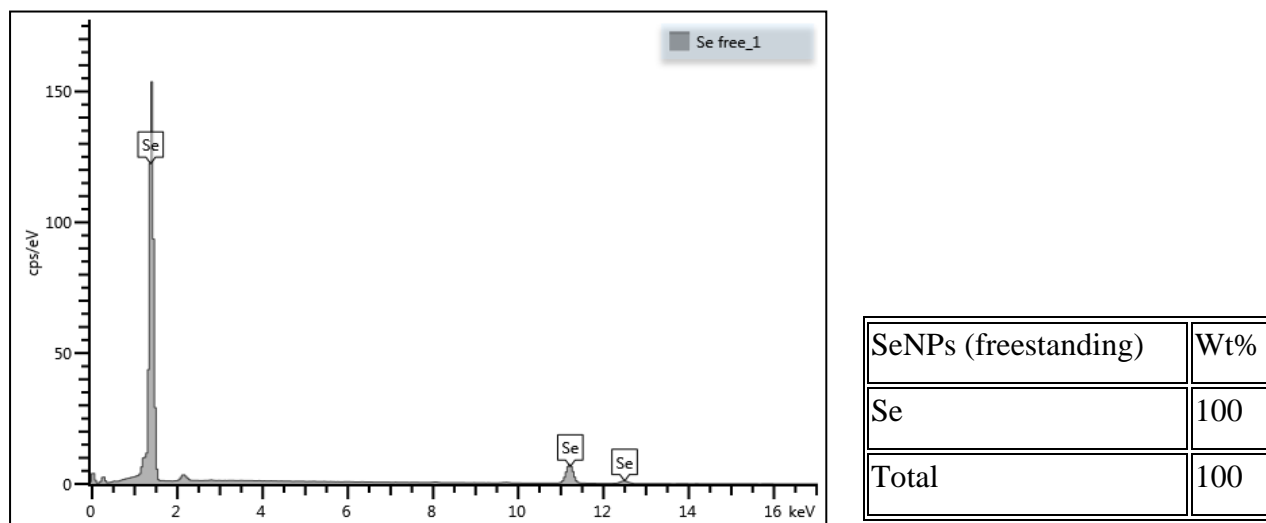
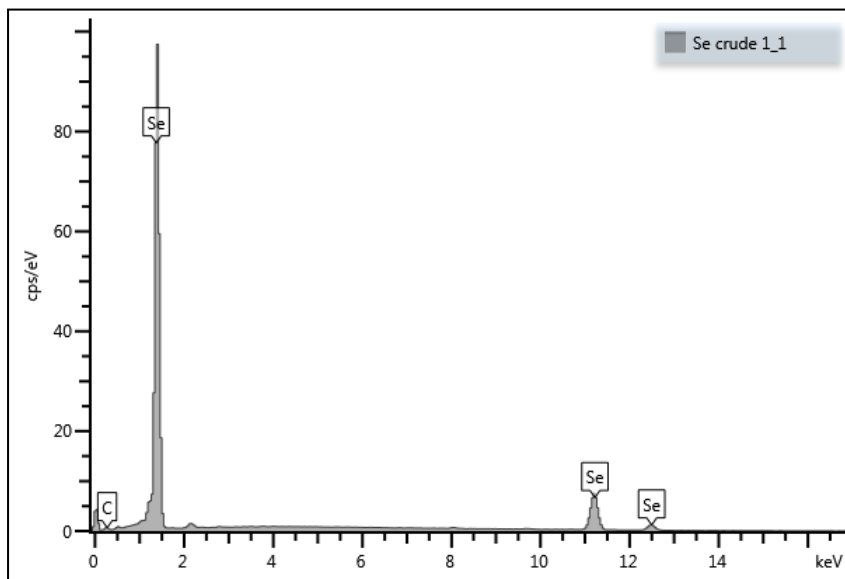


Figure 4.25: Energy dispersive X-ray spectroscopy (EDS) of selenium nanoparticles (SeNPs) (freestanding)

Figure 4.26 shows the EDS spectrum of SeNPs (*C. monilifera*). The presence of a strong peak at 1.5 is characteristic of Se metal as observed with SeNPs (freestanding). The EDS pattern also shows relatively low presence of C. For SeNPs (*C. monilifera*), the weak C peak can possibly be components of the organic extract. For SeNPs (freestanding), the origin of the C peak is not clear. For SeNPs (*C. monilifera*) the C peak is very weak compared to the C peak for AgNPs synthesised with the same reducing agent.



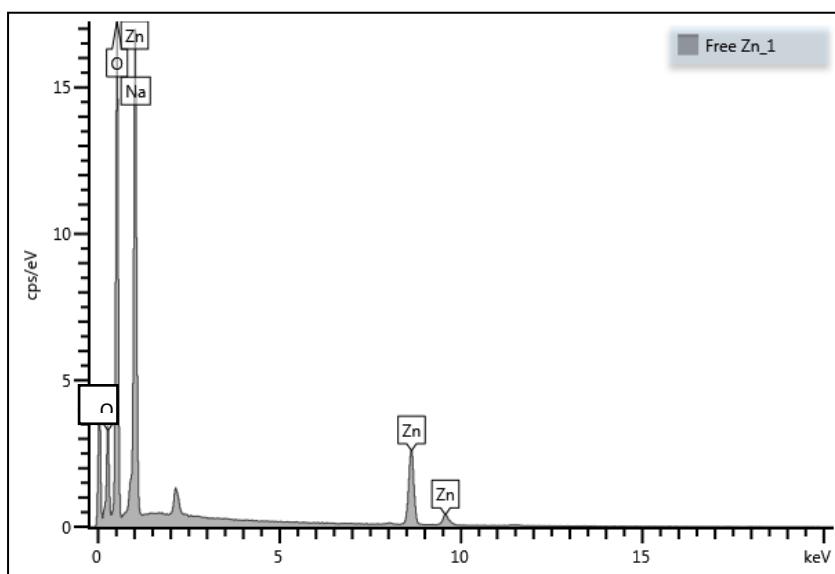
| | |
|--------------|------|
| Se crude 1_1 | Wt% |
| C | 11.7 |
| Se | 88.3 |
| Total | 100 |

Figure 4.26: Energy dispersive X-ray spectroscopy (EDS) of selenium nanoparticles (SeNPs) (*C. monilifera*)

The EDS results of SeNPs (*H. caffrum*) and SeNPs (quercetin) can be found in the appendix B. They are similar to those of SeNPs (*C. monilifera*) in that the spectra show strong a Se peak at 1.5 KeV which confirms that the synthesised NPs are Se. The results also show low levels of C as observed with the SeNPs (*C. monilifera*). The C peak observed might be due to the phytocompounds that are present in the plant extract, that were used to synthesise the NPs.

4.3.2.3 Zinc oxide nanoparticles

Figure 4.27 shows the EDS spectrum of ZnONPs (freestanding). The characteristic peaks for Zn are found at 1, 8.5 and 9.8 keV (Kumar et al., 2013). The O peak is almost as strong as the Zn peak at 1 keV which confirms that the synthesised NPs are ZnO. The results also show low content of Na (nitrate), as observed with AgNPs (freestanding), which are due to the NaBH_4 used to synthesise the ZnONPs (freestanding).



| ZnONPs (Free) | Wt% |
|---------------|--------|
| O | 46.1 |
| Na | 5.4 |
| Zn | 48.5 |
| Total | 100.00 |

Figure 4.27: Energy dispersive X-ray spectroscopy (EDS) of zinc oxide nanoparticles (ZnONPs) (freestanding)

Figure 4.28 shows the EDS spectrum of ZnONPs (*C. monilifera*). The characteristic peaks for Zn are found at 1, 8.5 and 9.8 keV. The O peak is almost as strong as the Zn peak which confirms that the synthesised NPs are ZnO.

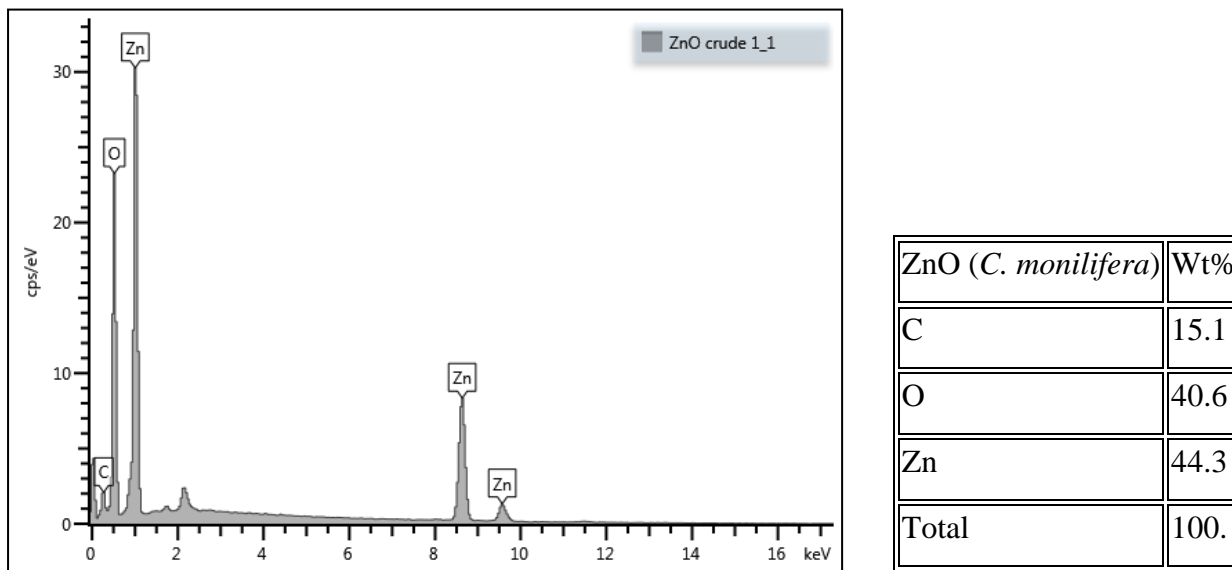


Figure 4.28: Energy dispersive X-ray spectroscopy (EDS) of zinc oxide nanoparticles (ZnONPs) (*C. monilifera*)

Overall, the presence of the characteristic Ag, Se, and Zn and O peaks confirmed that the intended NPs composition were synthesised. All NPs (freestanding) showed weak Na peaks due to NaBH_4 used to as a reducing agent. The C and O signals to be from the biosynthesised NPs are assumed to have originated from the plant extracts and phytochemicals that were used as reducing agents. The EDS and UV-Vis results confirm the formation of AgNPs, SeNPs and ZnONPs. The EDS results for AgNPs, SeNPs and ZnONPs agree with those in the literature (Velan et al., 2015; Avendaño et al., 2016; Kumar et al., 2013).

4.3.3 Infra-red (IR) spectroscopy

The IR studies were conducted to determine the purity and nature of the metal NPs synthesised. Metal and metal oxide NPs generally produce absorption bands in the fingerprint region i.e. below 1000 cm^{-1} arising from inter-atomic vibrations. The peak observed at around 3000 cm^{-1} is present in all the NPs and may be due to O-H stretching and deformation which can be assigned to water adsorption on the metal surface. Figure 4.29 shows the IR spectra of freestanding AgNPs, SeNPs and ZnONPs. The spectra show absence of functional groups on the freestanding NPs.

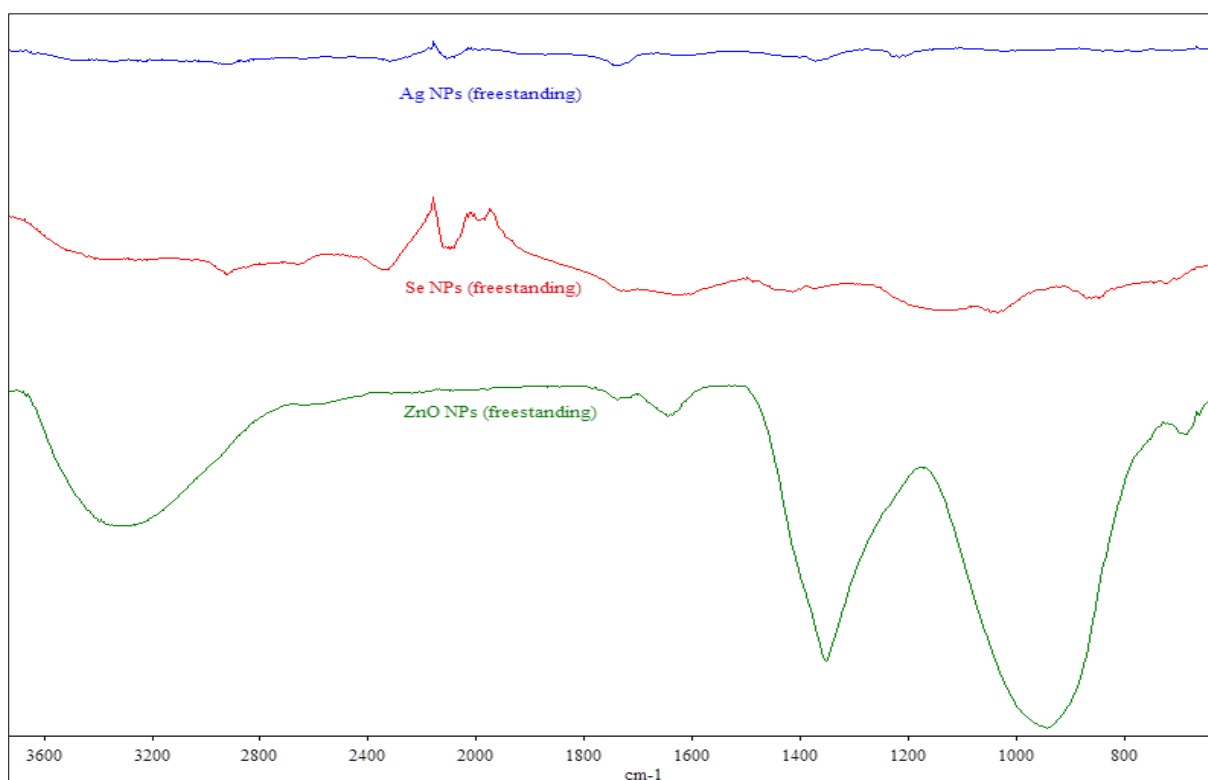


Figure 4.29: Infrared spectra for freestanding silver, selenium and zinc oxide nanoparticles

The IR spectra profiles in Figure 4.30 are for AgNPs, SeNPs and ZnONPs synthesised using *C. monilifera* extract. The profile of the NPs match those of the crude extracts which only showed the presence of functional groups. SeNPs (*C. monilifera*) showed higher IR transmittance intensity than the AgNPs and ZnONPs which had similar intensities. For the IR spectra of the NPs assumed to be capped with the crude extract, there is an additional stretch for the C-H alkyl group (2925 cm^{-1}) and the ketonic group (1750 cm^{-1}). This could be due to compounds in the extract that contain alkyl chains and ketonic groups.

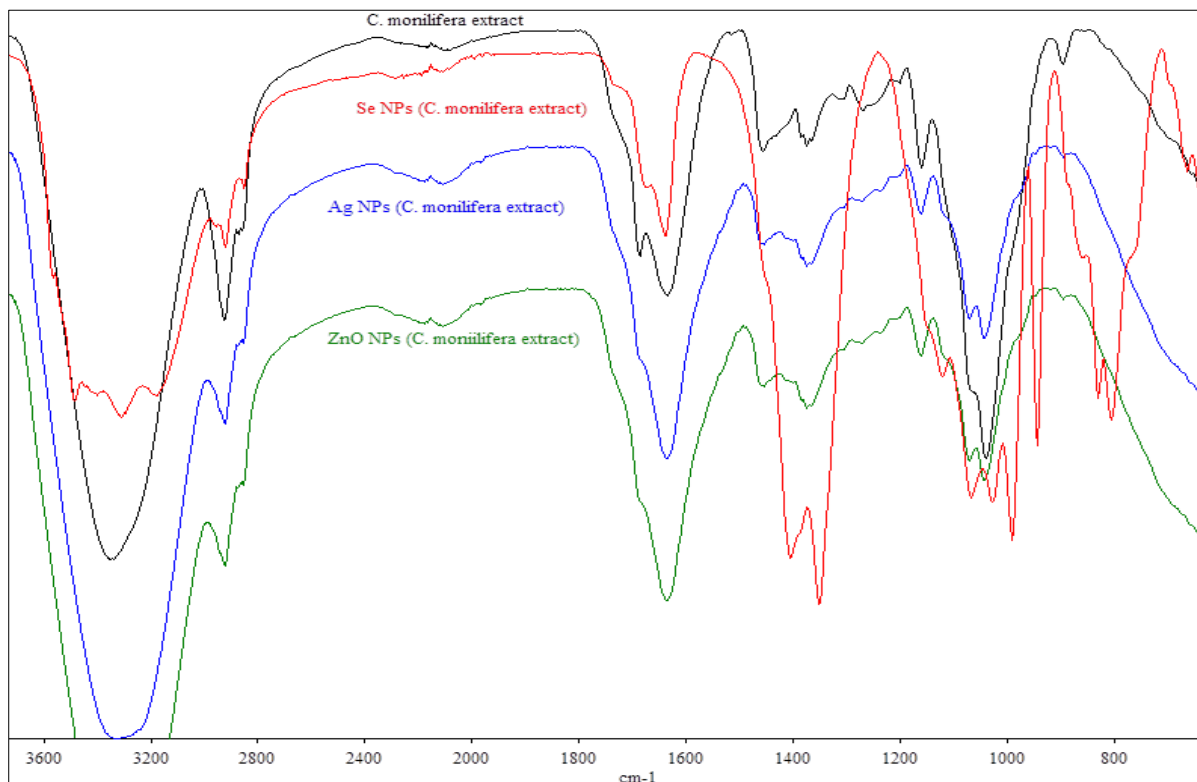


Figure 4.30: Infrared spectra for *C. monilifera* extract and silver, selenium and zinc oxide nanoparticles synthesised from the *C. monilifera* extract

The IR spectra for the AgNPs, SeNPs and ZnONPs synthesised with *H. caffrum* plant extract (Appendix C) are similar those of AgNPs, SeNPs and ZnONPs capped with *C. monilifera*. The profile of the NPs matches that of the crude extract which only showed the presence of functional groups.

The IR spectrum of AgNPs, SeNPs and ZnONPs capped with quercetin (Figure 4.31) showed characteristic absorption bands for the O-H group (3234.18 cm^{-1}), C=C group (1605 cm^{-1}) and C-O group ($1150 - 1010\text{ cm}^{-1}$) which correspond to the absorption peaks of the pure quercetin. Similar to the results of the AgNPs, SeNPs and ZnONPs capped with plant extracts, the profile of the NPs match that of the quercetin.

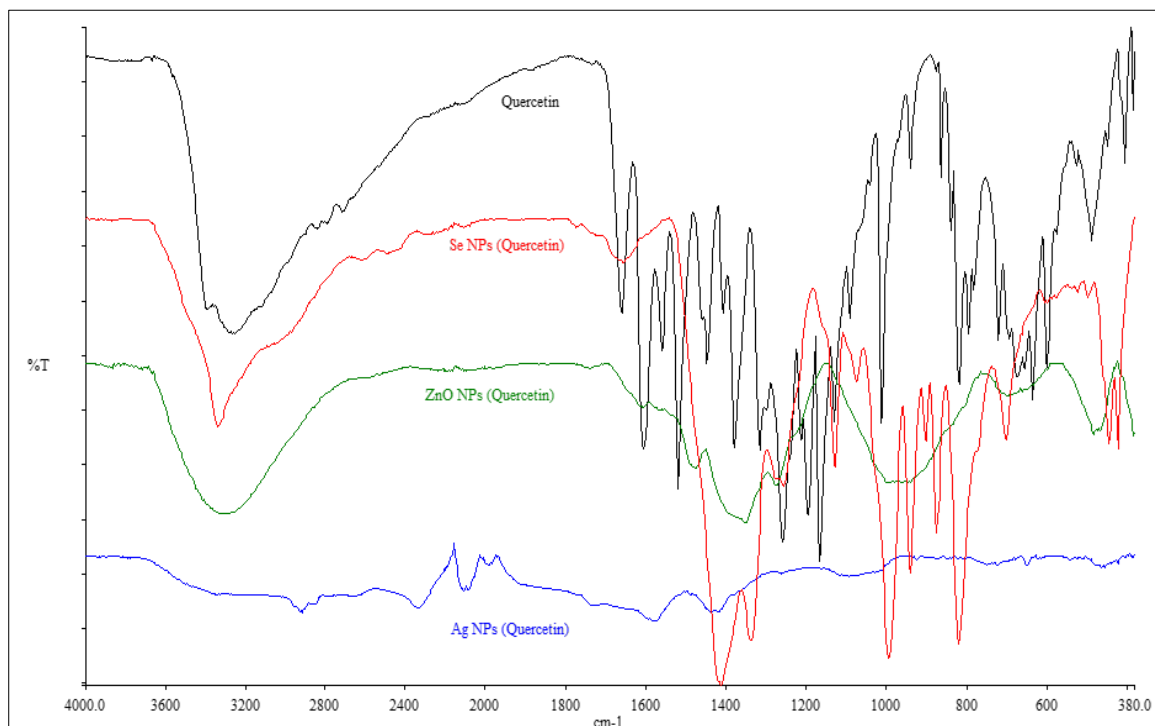


Figure 4.31: Infrared spectra for quercetin and silver, selenium and zinc oxide nanoparticles synthesised from quercetin

The IR results of the AgNPs, SeNPs and ZnONPs capped with catechin, in Appendix C, are similar to results exhibited by AgNPs, SeNPs and ZnONPs capped with quercetin. The profile of the NPs matches that of catechin.

The IR results indicate that the surface of the NPs was strongly adsorbed with the plant material that was used during synthesis. The IR results confirm the UV-Vis results which showed additive absorbance due to the metal NPs and plant extract or phytochemicals used during synthesis. The IR results also account for the carbon and oxygen peaks observed in the EDS patterns.

Similar FTIR findings on NPs were reported by (Kumar et al., 2013). The FTIR spectra show the involvement of plant extracts and flavonoids in biosynthesis of NPs. The plant extracts and flavonoids were responsible for reduction of biosynthesised NPs. The biomolecules present on the surface of NPs act as natural capping agents.

4.3.4 Scanning electron microscopy (SEM)

The morphology of the NPs was characterised using SEM.

4.3.4.1 Silver nanoparticles

The freestanding NPs in Figure 4.32 showed particle size variation and the particles appear to be agglomerated.

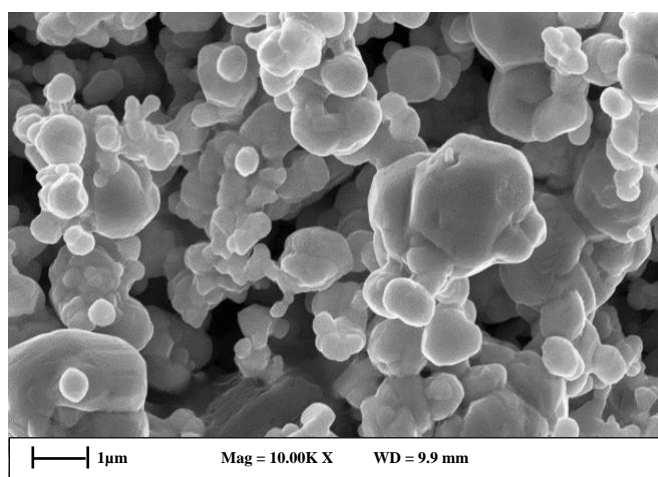


Figure 4.32: Scanning electron micrograph of AgNPs (freestanding)

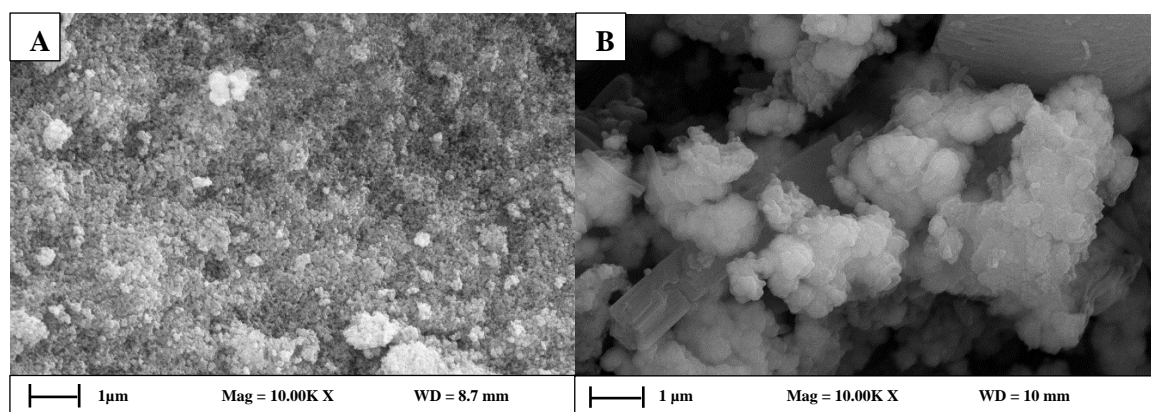


Figure 4.33 :(A) Scanning electron micrograph of AgNPs (*C. monilifera*) (B) Scanning electron micrograph of AgNPs (*H. caffrum*)

Fig 4.33 A and B show the SEM micrographs of the silver NPs synthesised with *C. monilifera* and *H. caffrum* extract, respectively. The NPs synthesised with the plant extracts are smaller

than those synthesised with sodium borohydride. The NPs synthesised with the *C. monilifera* plant extract are strictly spherical in shape and are agglomerated. They are smaller than the NPs synthesised with *H. caffrum* extract. The NPs synthesised with *H. caffrum* extracts are mostly spherical in shape but some rectangular rods can be observed.

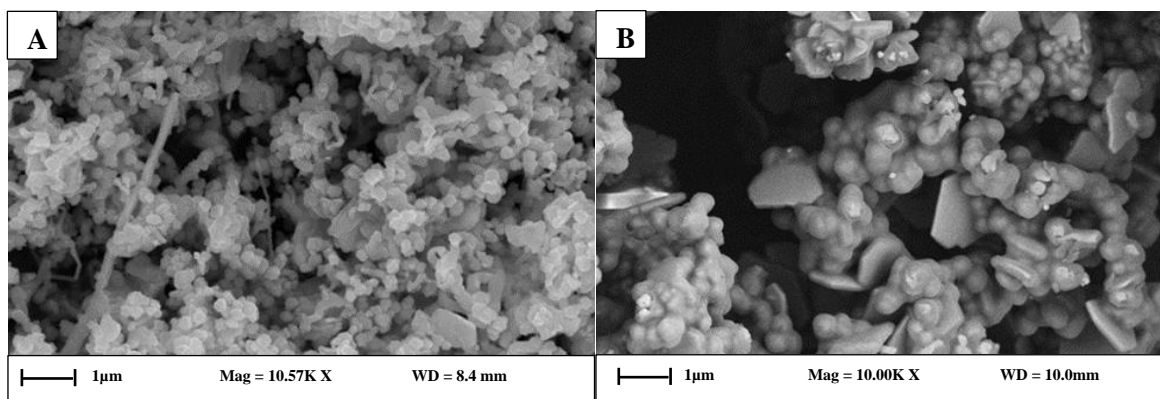


Figure 4.34 (A) Scanning electron micrograph of AgNPs (quercetin) (B) Scanning electron micrograph of AgNPs (catechin)

The AgNPs synthesised with quercetin and catechin in Figure 4.34 A and B, respectively, showed more variation in shapes and sizes compared to the AgNPs (freestanding) and the NPs (*C. monilifera* and *H. caffrum*). Furthermore, AgNPs(quercetin) show more variation in shapes compared to the AgNPs(catechin). Both flavonoids produced a mixture of spherical particles and thin hexagonal sheets but quercetin additionally produced rods and wires.

4.3.4.2 Selenium nanoparticles

The morphology of SeNPs (freestanding) at 3000 X magnification in Figure 4.35 showed the presence of sharp rods and some spherical particles. The average length of the rods is greater than scale of 2 μ m.

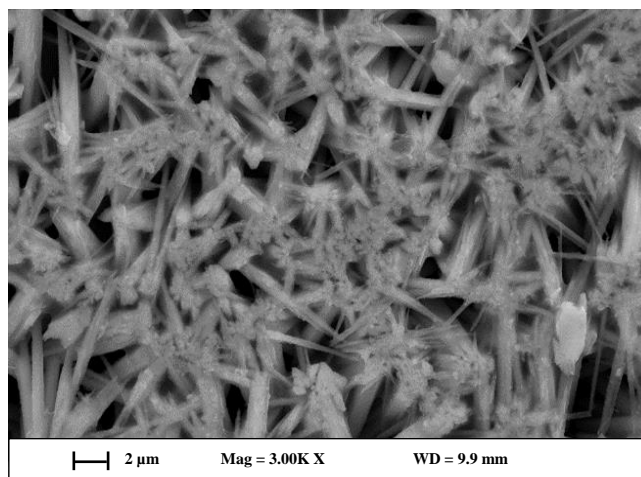


Figure 4.35: Scanning electron micrograph of AgNPs (freestanding)

The SeNPs (*C. monilifera* and *H. caffrum*) in Figure 4.36 A and B, respectively, show a mixture of nanorods and nanosheets. There is a notable difference in size and relative abundance of each shape with the different plant extracts. The *C. monilifera* extracts produced smaller sized Se nano rods and nano sheets in relatively equal amounts whereas the *H. caffrum* extract produced larger particles with more nano sheets of variable size, than nanorods. The Se nanorods synthesised with the *C. monilifera* extract are similar to one another in length.

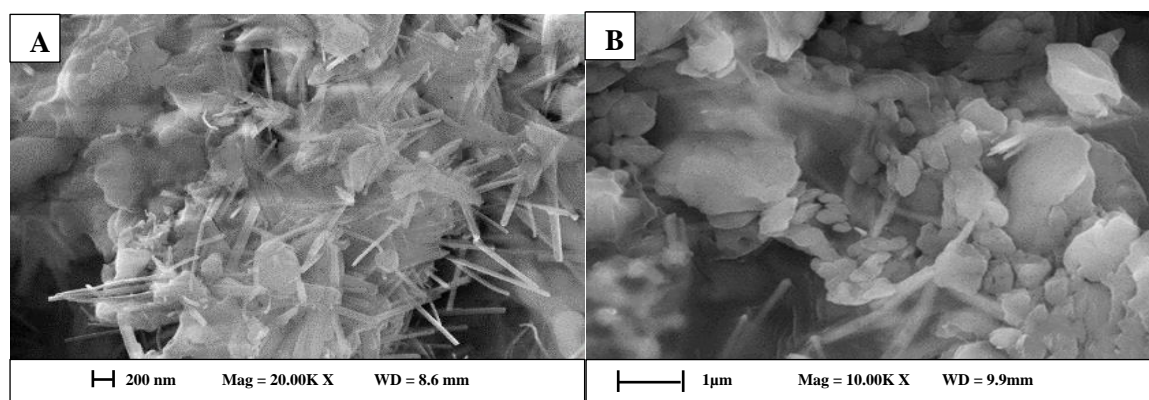


Figure 4.36: (a) Scanning electron micrograph of SeNPs (*C. monilifera*) (b) Scanning electron micrograph of SeNPs (*H. caffrum*)

An SEM micrograph of SeNPs (quercetin) is shown in Figure 4.37. The micrograph reveals large elongated rods that are longer than 1 μm . Small uniform size nano-spheres can be seen on the surface of the large rods.

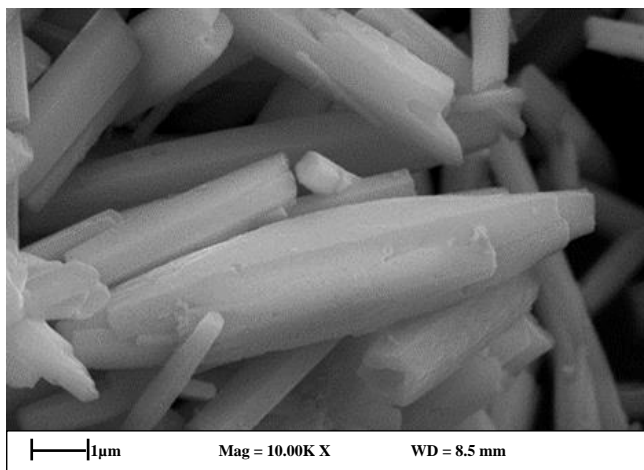


Figure 4.37: Scanning electron micrograph SeNPs (quercetin)

4.3.4.3 Zinc oxide nanoparticles

The SEM micrograph of freestanding ZnONPs (Fig 4.38) reveal small spherical agglomerated NPs with a uniform size distribution.

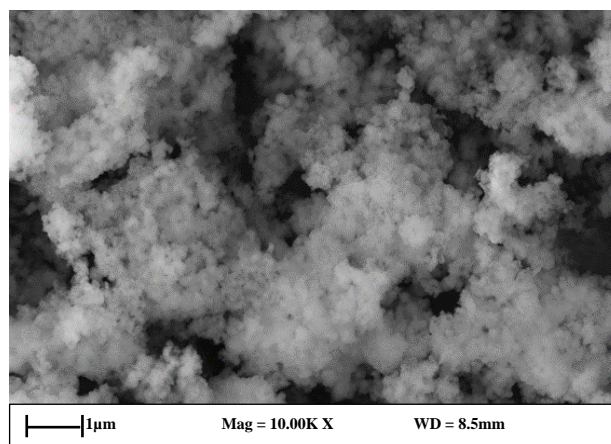


Figure 4.38: Scanning electron micrograph of ZnONPs (freestanding)

The SEM micrographs of the ZnONPs synthesised with *C. monilifera* and *H. caffrum* plant extract are shown on Figure 4.39 A and B, respectively. The micrographs reveal a single population of small and spherical agglomerated NPs in each case.

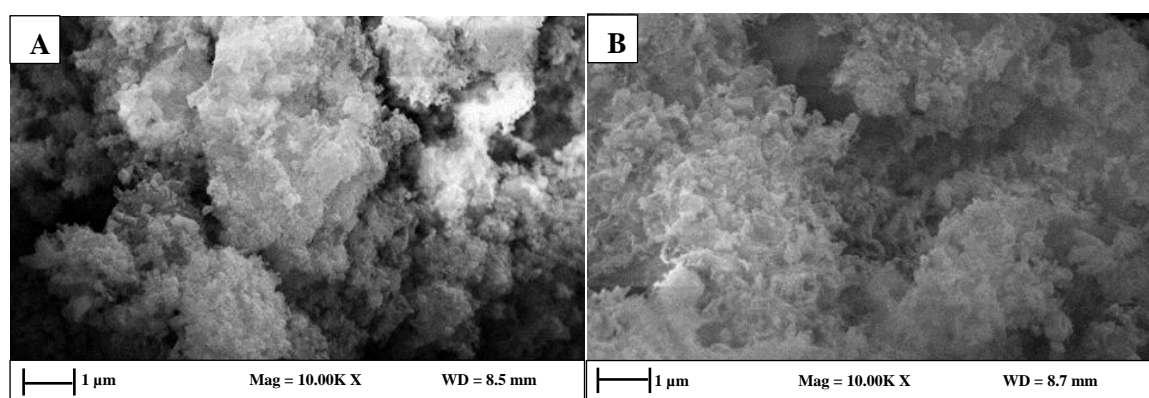


Figure 4.39: (A) Scanning electron micrograph of ZnONPs (*C. monilifera*) (B) SEM micrograph of ZnONPs (*H. caffrum*)

The ZnONPs synthesised with quercetin and catechin are shown in Figure 4.40 A and B respectively. Each flavonoid resulted platelet shaped NPs. The particles synthesised with

catechin are larger than those synthesised with quercetin. The NPs synthesised with quercetin show the size distribution of the NPs to be narrow whereas those synthesised with catechin are of a wider size distribution. The surface of the ZnONPs (catechin) is not smooth but appear to be sponge like. The individual particles have agglomerated and grown together to form larger sheets.

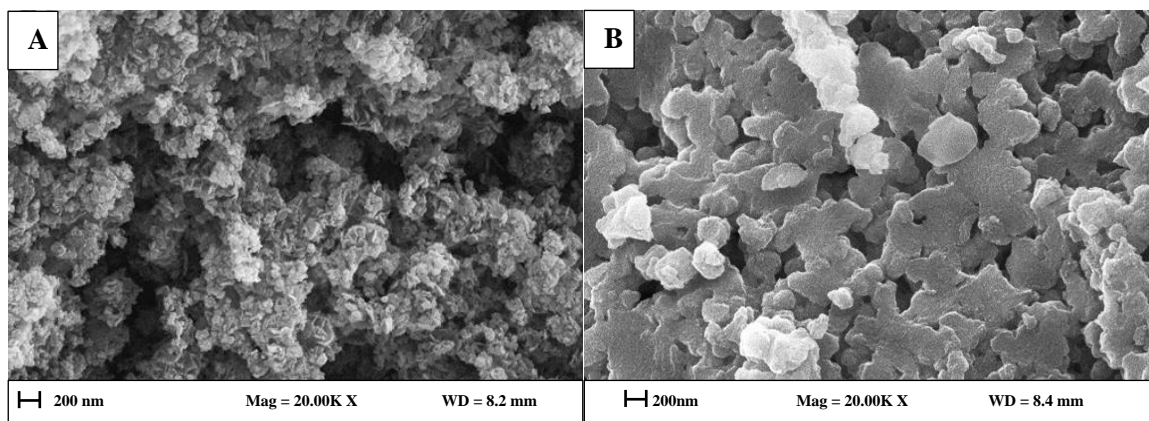


Figure 4.40: (A) Scanning electron micrograph of AgNPs (quercetin) (B) Scanning electron micrograph of AgNPs (catechin)

4.3.5 Transmission electron microscopy (TEM)

The size and morphology of Ag Se and ZnONPs were observed using TEM.

4.3.5.1 Silver nanoparticles

Figures 4.41, 4.42, 4.43, 4.44 and 4.45 below show TEM micrographs for the AgNPs (freestanding) synthesised with NaBH₄, AgNPs (*C. monilifera*), AgNPs (*H. caffrum*), AgNPs (quercetin) and AgNPs (catechin), respectively. Particle diameters were measured from one end of the particle to the other and the elongated particles were measured diagonally. The TEM analysis was done a day after the NPs were synthesised and some of the particles were agglomerated. The diameters of the agglomerated particles could not be measured.

The AgNPs (freestanding) (Figure 4.41) were mostly spherical in shape but also contained elongated spheres and the average diameter of these particles was determined to be 80.55 ± 25.23 nm. Some of the NPs were agglomerated. Therefore, the average diameter was determined using only the well dispersed NPs. Drawbacks associated with sodium borohydride synthesised AgNPs is that they cannot be smaller than 40 nm (Agnihotri et al., 2014).

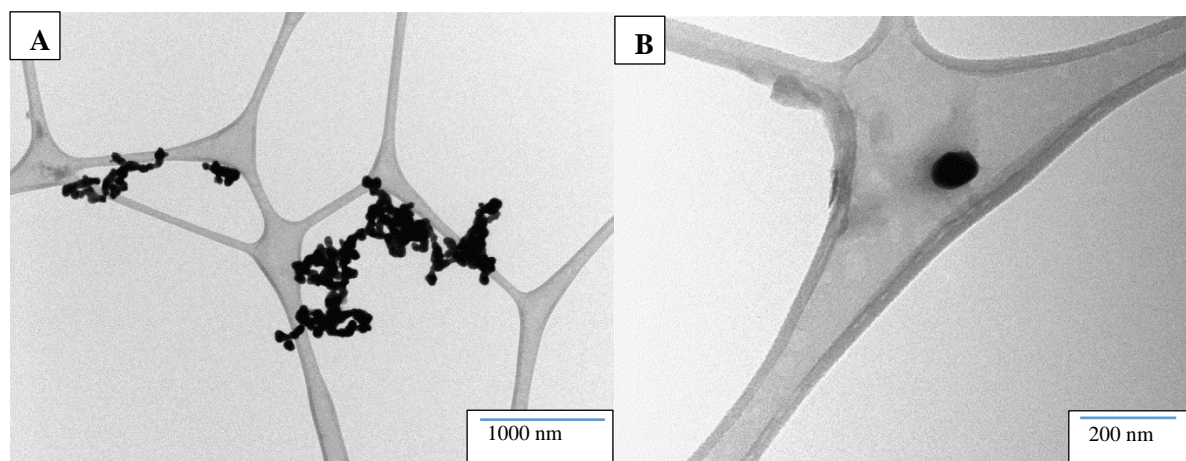


Figure 4.41: Transmission electron micrograph of AgNPs (freestanding)

The major observed differences from the AgNPs synthesised with extracts were their sizes (Figure 4.42 and 4.43). The shapes of the AgNPs synthesised from both extracts are all nearly spherical. The smaller AgNPs were synthesised with the *H. caffrum* extract. The plant extracts of the *C. monilifera* (Figure 4.42) and *H. caffrum* (Figure 4.43) showed populations of NPs with a wide size range. The TEM micrographs in Figure 4.42 B and 4.43 B show that the

AgNPs are capped with plant extract used to synthesise them. The AgNPs (*C. monilifera*) NPs were in the size range of 19-60 nm and were larger than the AgNPs (*H. caffrum*) at the size range of 4-50 nm.

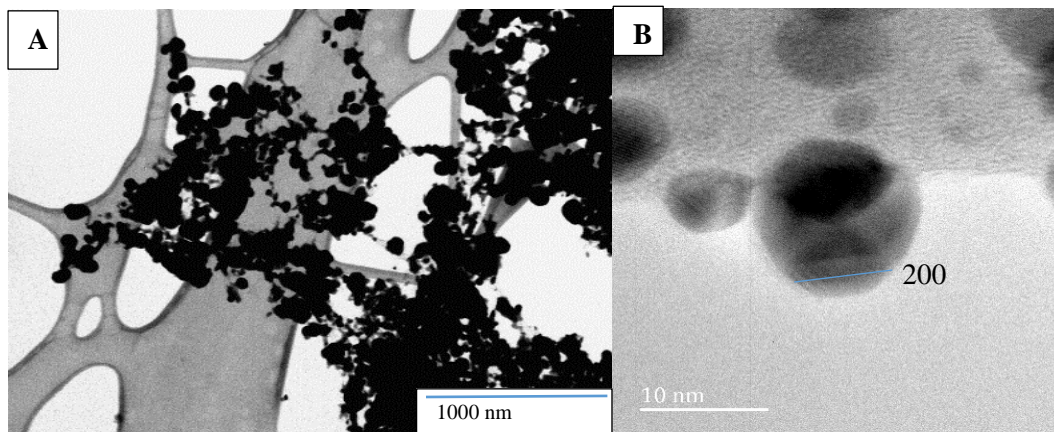


Figure 4.42: Transmission electron micrograph of AgNPs (*C. monilifera*)

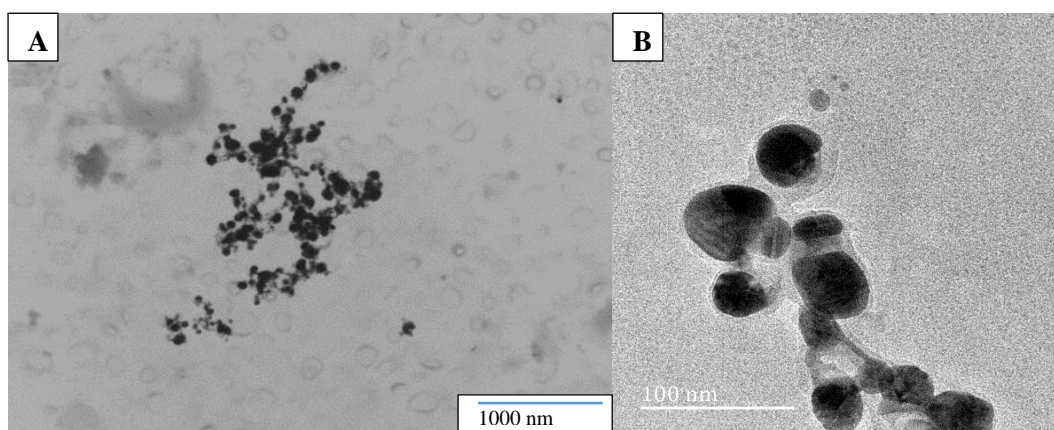


Figure 4.43: Transmission electron of AgNPs (*H. caffrum*)

The isolated quercetin as reducing agents produced a wide variety of shapes of NPs namely nano-rods, nano-wires, nano-spheres, nano-hexagons and nano-triangles (Figure 4.44 A). From Figure 4.44 (B), the quercetin capping can be observed around the NPs. The nano-rods were a mixture of long and smooth rods and wiggled rods. The length of the wiggled could not be determined but the long and smooth rods reached lengths of up to 4 μm . The width of both rod populations was between 60-79 nm. The spherical NPs ranged from 20-30 nm. The nano-hexagons were made of two populations. The small population ranged from 95-100 nm and the large population ranged from 250-300 nm. The nano-triangles ranged from 55-63 nm. Using

TEM, a quercetin capping was observed on the large NPs and on the nano-rods. The thickness of the coating was averaged at 2-3 nm.

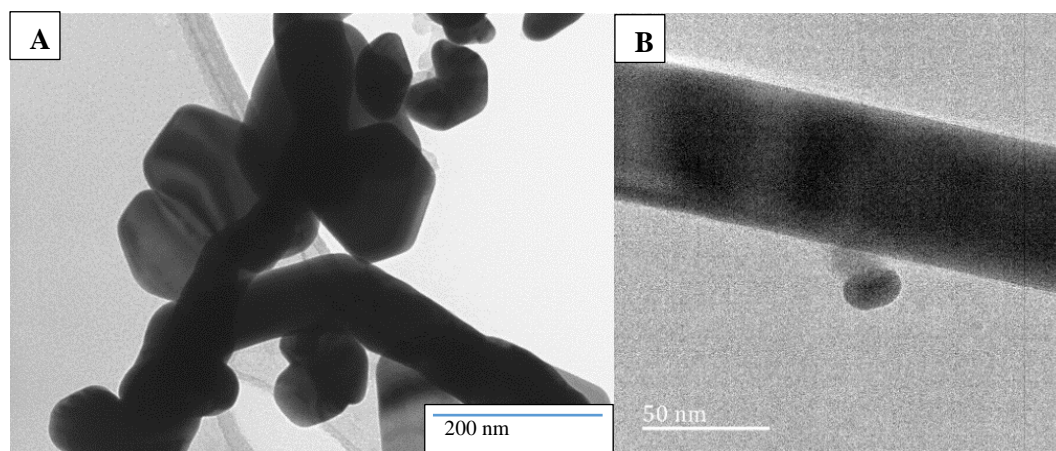


Figure 4.44: Transmission electron micrograph of AgNPs (2mM quercetin)

The AgNPs (catechin) images in Figure 4.45 A and B show spherical and hexagonal particles smaller than those of quercetin. The spherical AgNPs (catechin) were measured to range between 5-11 nm. The nano-hexagons were 200 - 250 nm in size. From the SEM results (Figure 4.34 B) it can be seen that nano-hexagons are thin sheets. A catechin capping (Figure 4.45 B) is observed on the surface of the NPs as with all of the bio-reductants. These TEM results are in agreement with UV and EDS results but most importantly with the IR results (Appendix C) which show that the surface of the AgNPs (catechin) are strongly adsorbed with catechin.

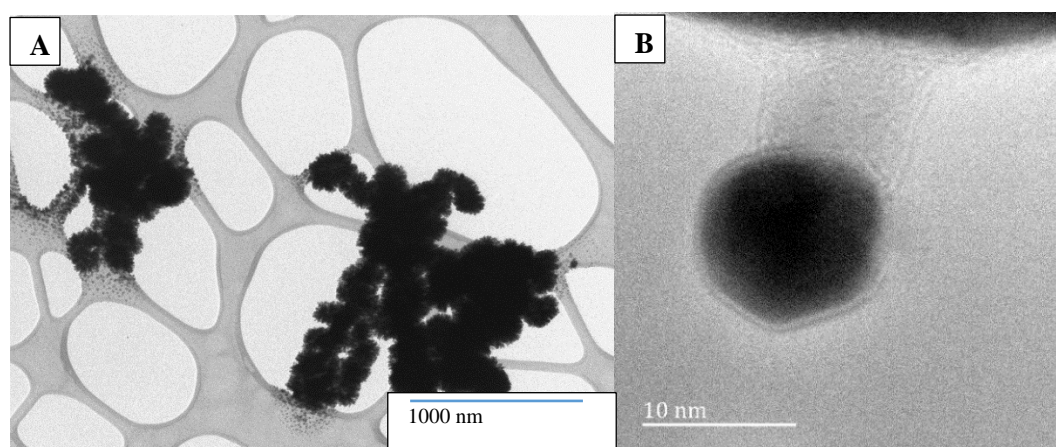


Figure 4.45: Transmission electron micrograph of AgNPs (2 mM catechin)

In order of average size, the following trend is observed for the NPs.

AgNPs: catechin > quercetin > freestanding > *C. monilifera* extract > *H. caffrum* extract

The UV-Vis results for the synthesised AgNPs are consistent with the TEM results. The SPR of the AgNPs (quercetin) and AgNPs (catechin) were the broadest and the SEM and TEM results confirmed that they have the largest size range of NPs. The sharp SPR of the AgNPs (freestanding) was indicative of a narrow size distribution of the AgNPs synthesised with NaBH_4 are confirmed in visualisation of SEM and TEM results. The EDS results suggested a presence of carbon and oxygen with the biosynthesised AgNPs which was confirmed by the IR results which showed that the surface of the NPs were adsorbed with the plant extract or flavonoid used during synthesis.

4.3.5.2 Selenium nanoparticles

The TEM images of the SeNPs (freestanding) in Figure 4.46 are consistent with the SEM results (Figure 4.35) that revealed that the population of synthesised NPs was a mixture of nano-spheres and nano-rods and wires. The nano-spheres ranged from 50-90 nm in size in diameter. The nano-rods ranged from 5 μm to 7.5 μm and their width ranged from 150 nm to 250 nm in length.

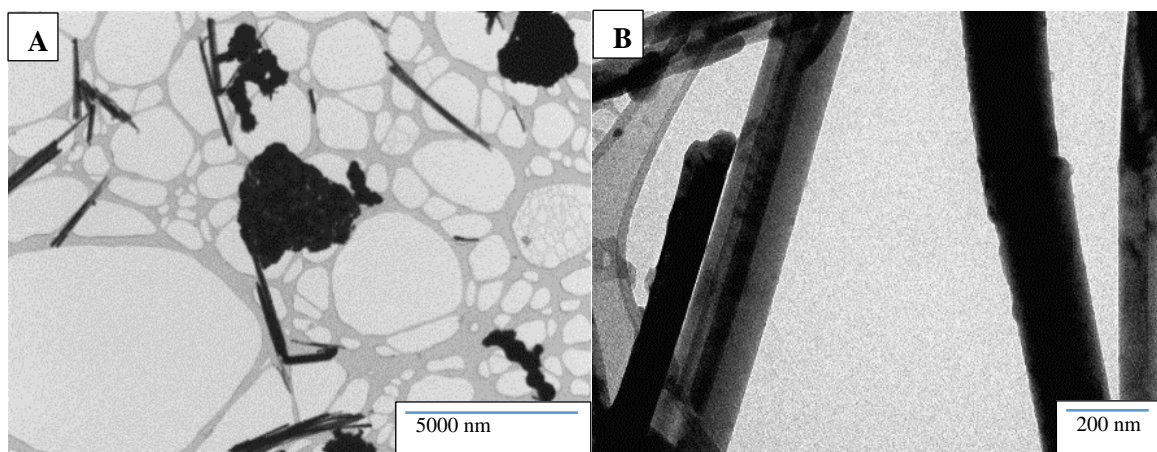


Figure 4.46: Transmission electron microscopy (TEM) micrograph of SeNPs (freestanding)

The TEM micrographs in Figure 4.47 confirm the findings from the SEM studies (Figure 4.36 A) in revealing that the SeNPs (*C. monilifera*) are a mixture of particles and nano-rods. The rods ranged from 0.9 – 4 μm in length. The width of the nano-rods was between 80 and 100 nm. The platelets seen in the SEM images seem to consist of small particles that with

agglomeration and reorientation formed larger particles. The large particles size ranged from 272 nm to 454 nm in diameter. The small particles that agglomerate to form these larger particles ranged from 3 nm to 6 nm in length.

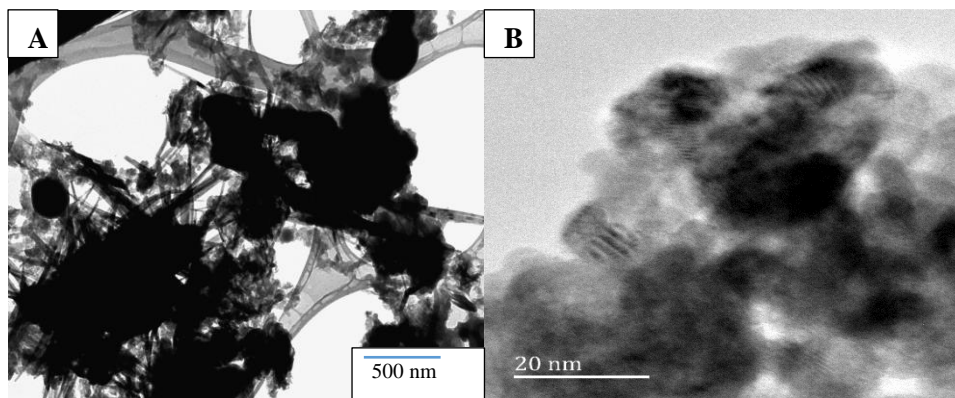


Figure 4.47: Transmission electron micrograph of SeNPs (*C. monilifera*)

The TEM micrographs of SeNPs (*H. caffrum*) in Figure 4.48 confirmed the SEM results (Figure 4.36 B) that showed a mixture of particles and rods. The SEM results also showed the particles dominating the population with few rods and this is also clearly shown in Figure 4.48. A capping on the surface of the surface of the rods and particles can be seen in Figure 4.48 B. The capping was measured to be 5 nm on the rod-shaped particles and up to 14 nm thick on the particles. This is a much thicker coating measurement than any observed on the biosynthesised AgNPs. This explains why the biosynthesised SeNPs showed the higher intensity bands on the FTIR in Figures 4.30, 4.31 and in the appendix C. The particles ranged from 300 nm to 1.5 μm in size. The rod length was measured to range from 1 – 3 μm and the width was in the range of 50-80 nm. The particles, as those synthesised with the *C. monilifera* crude extract, appear to be small particles that agglomerated and formed larger particles over time.

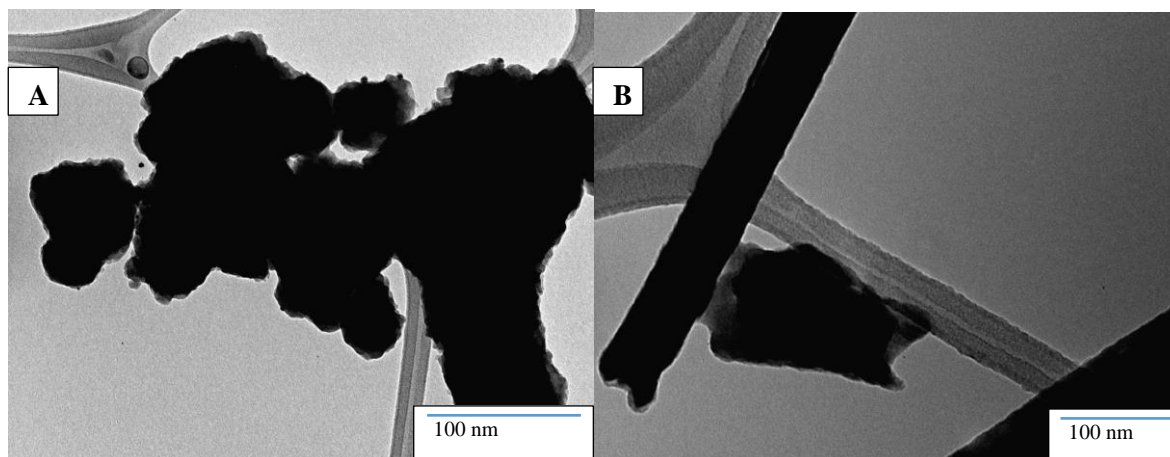


Figure 4.48: Transmission electron micrograph of SeNPs (*H. caffrum*)

The TEM micrographs of SeNPs (quercetin) in Figure 4.49 reveal more detail on the nano-spheres that were difficult to observe on the SEM micrographs due to the magnification scale. The nano-spheres, although agglomerated, appear to be narrow-dispersed with a size range of 4 – 10 nm. The capping observed on the particles ranged from 0.5 – 1 nm in thickness. The rods were in two population sizes. The small rods range between 200 to 400 nm and the longer rods range from 1 μm to 9 μm .

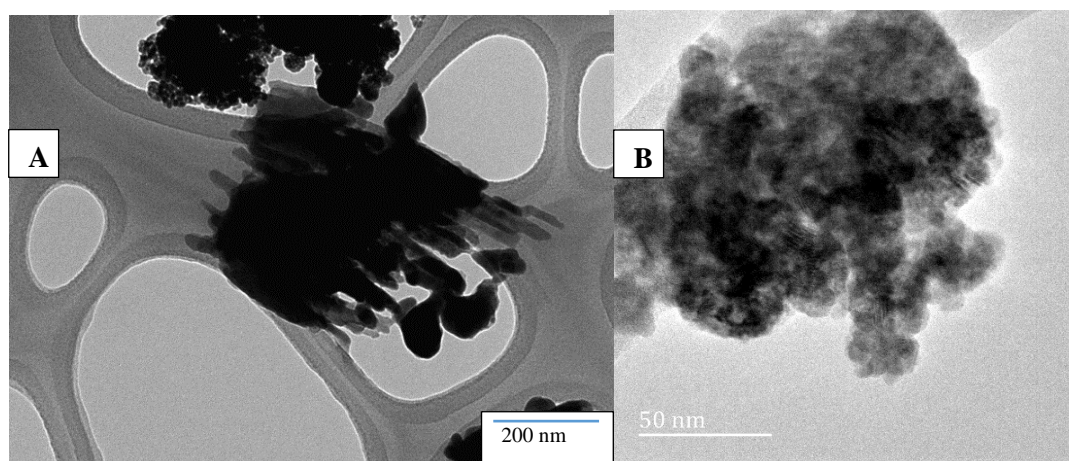


Figure 4.49: Transmission electron of SeNPs (2 mM quercetin)

With regards to size of the particles and length of the rods in order of largest to smallest average size, the following trend was observed:

SeNPs particles: *H. caffrum* extract > *C. monilifera* extract > freestanding > quercetin

SeNPs rods: quercetin > freestanding > *C. monilifera* crude > *H. caffrum* crude

4.3.5.3 Zinc oxide nanoparticles

The micrographs of ZnONPs (freestanding) in Figure 4.50 reveal the particles to be uniform in shape (roughly spherical) with a moderate degree of agglomeration. The largest measured particle was 92 nm, the smallest being 17 nm.

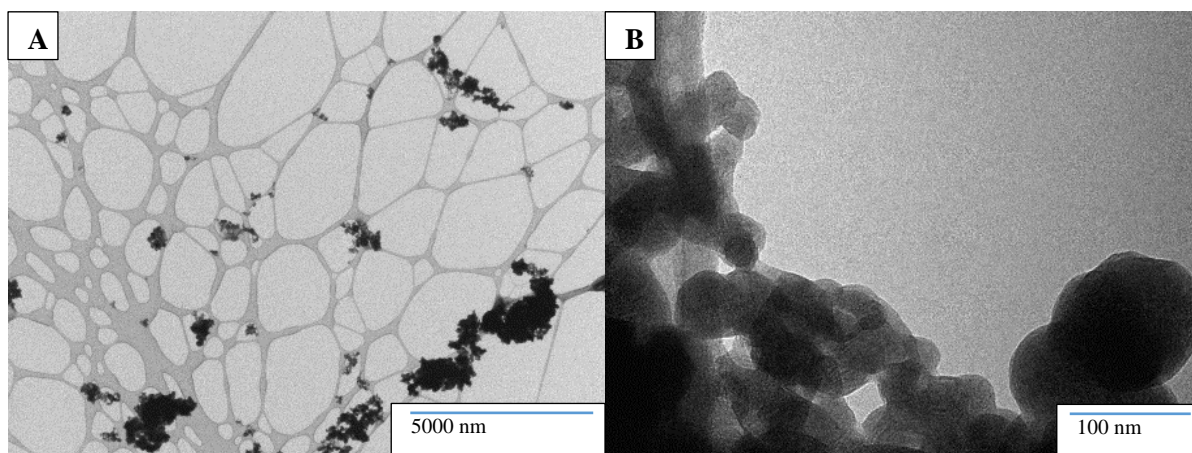


Figure 4.50: Transmission electron microscopy of ZnONPs (freestanding)

Figure 4.51 shows the ZnONPs (*C. monilifera*) to be roughly spherical in shape with a relatively high degree of agglomeration. The particles appear narrow-dispersed as in the SEM micrograph with a size range of 50 - 60 nm. The particles do not appear to be capped with the plant extracts as observed with the AgNPs(*C. monilifera*).

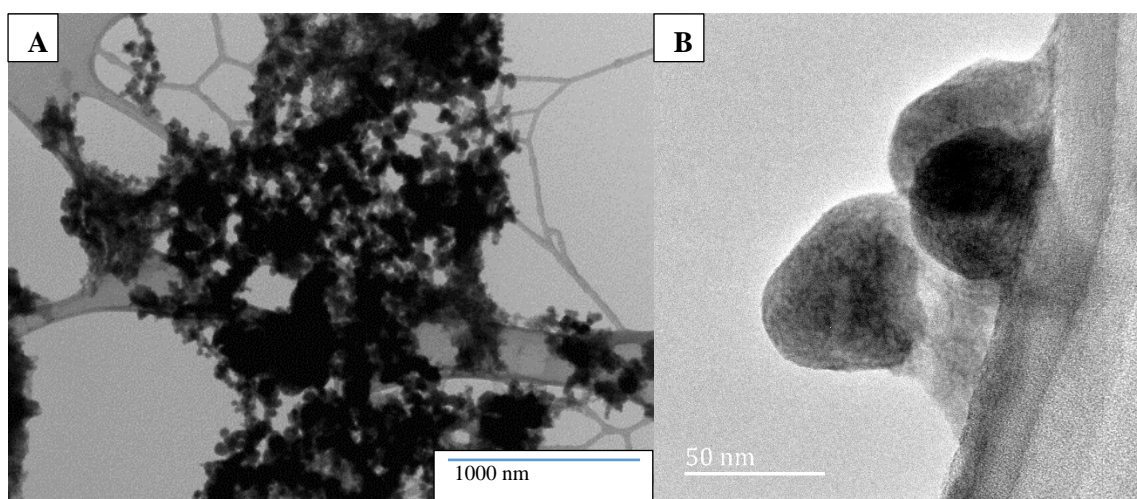


Figure 4.51: Transmission electron micrograph of ZnONPs (*C. monilifera*)

The TEM micrographs of ZnONPs (*H. caffrum*) in Figure 4.52 reveal spherical nano-spheres that are in agreement with the SEM micrographs in Figure 4.39 B. The NPs are also agglomerated as in the ZnONPs (*C. monilifera*). The particles sizes were measured to range between 45 – 55 nm.

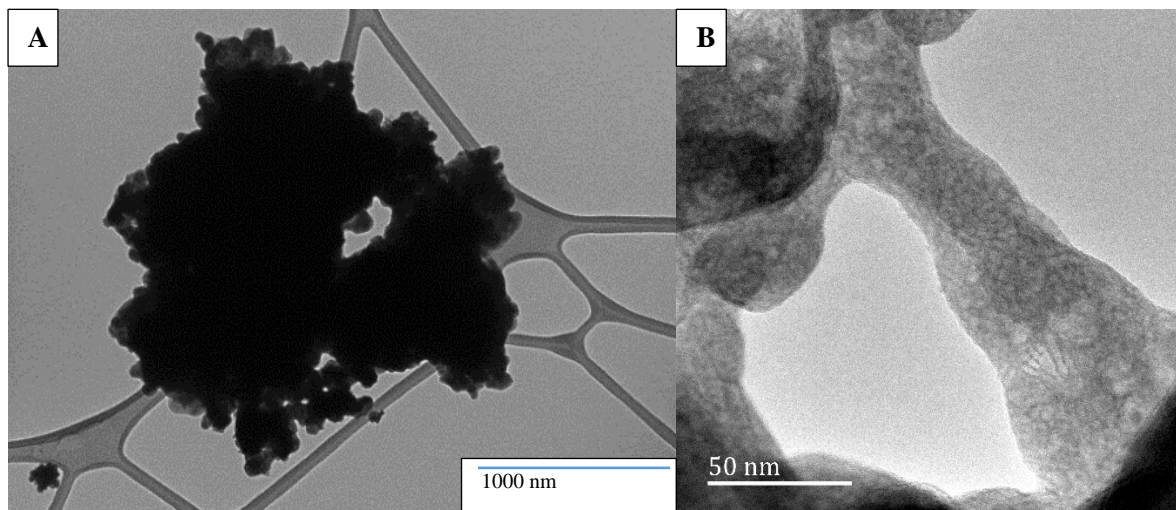


Figure 4.52: Transmission electron micrograph of ZnONPs (*H. caffrum*)

Figure 4.53 shows the TEM micrographs of ZnONPs (quercetin). The TEM micrographs echo the SEM micrographs revealing that the ZnONPs (quercetin) are agglomerated nearly spherical particles with particles sizes less than 200 nm. The particles were revealed in SEM (Figure 4.40 A) to be flat platelets. The actual size range was measured to be between 0.99 nm and 141 nm. The micrographs however reveal two populations of size range 0.99 – 3 nm and 120 - 144 nm.

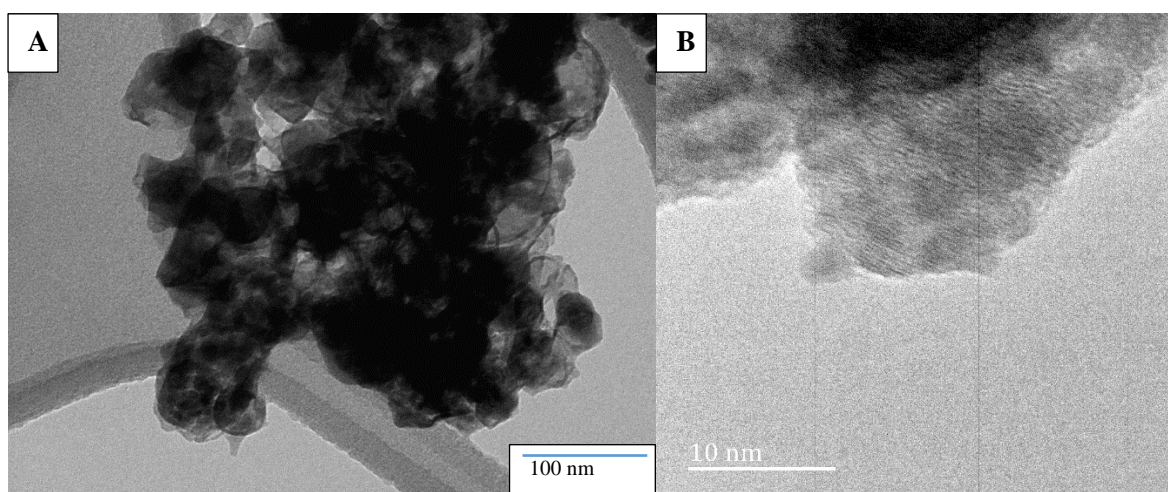


Figure 4.53: Transmission electron micrograph of ZnONPs (2 mM quercetin)

Figure 4.54 show ZnONPs (catechin) to closely resemble the observed results in SEM micrographs (Figure 4.40 b). The particles size range from 116 nm to 433 nm.

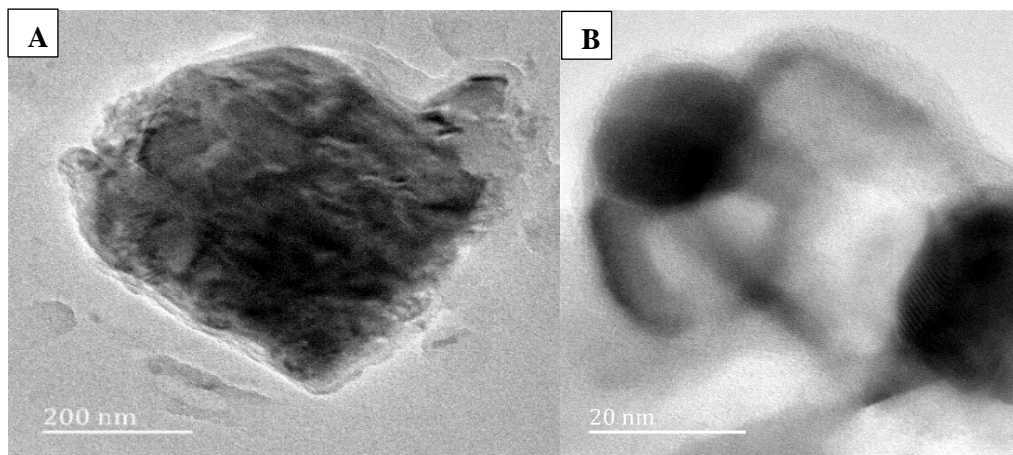


Figure 4.54: Transmission electron micrograph of ZnONPs (2 mM catechin)

With regards to size of the particles in order of largest to smallest average size, the following trend was observed: ZnONPs: catechin > quercetin > freestanding > *C. monilifera* extract > *H. caffrum* extract. Overall the flavonoids capped AgNPs, SeNPs and ZnONPs were largest, followed by the freestanding NPs and lastly the crude extract capped NPs.

4.3.6 Powder X-ray diffraction (PXRD)

The phase and crystallinity of the synthesised NPs synthesized with NaBH_4 was investigated using powder XRD and electron diffraction. The results obtained are compared to the JCPDS file number for silver, selenium and zinc oxide NPs. The d-spacing of the NPs were calculated using Braggs equation;

$$n\lambda = 2.d \sin\theta$$

4.3.6.1 Silver nanoparticles

Silver NPs synthesised at 2 mM quercetin concentration produced appreciable quantities and were therefore analysed using powder PXRD along with all the freestanding NPs. Figure 4.55 shows the PXRD pattern of the synthesised AgNPs (freestanding) and AgNPs (quercetin).

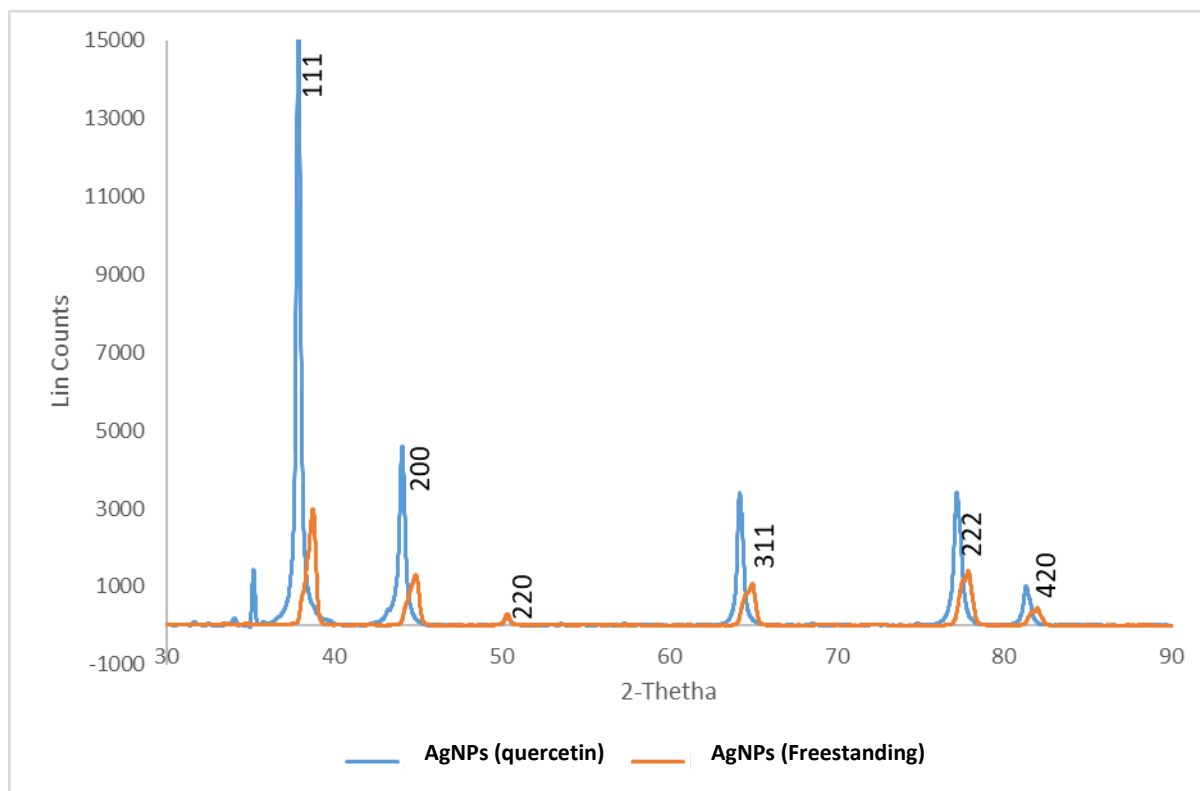


Figure 4.55: Powder X-ray diffraction patterns of AgNPs (freestanding) and AgNPs (quercetin)

For the freestanding NPs, Bragg reflections were detected at 2θ values of 38.77° , 44.88° , 64.99° , 77.87° , and 82.04° and these can be indexed to the (111), (200), (220), (311) and (222) planes. It can be confirmed from the 2θ positions that the structure of the freestanding NPs is face centred cubic (FCC) (Ahmed et al., 2016). The diffractogram of AgNPs (quercetin) is similar to that of the AgNPs (freestanding) but the reflections have shifted and show much higher intensities. These discrepancies could be due to the variations in the particle shapes of the nanoparticles. Other factors including the orientation, stress and strain which all influence the broadening, the intensity and eventually also the position of diffraction peaks. The significant differences in sizes and shapes of the AgNPs (freestanding) and AgNPs (quercetin) observed in the SEM (Figure 4.32 and 4.34A) and TEM (Figure 4.41 and 4.44) images of these particles respectively, could be one of the reasons for the difference in the intensity.

The XRD data of the AgNPs (freestanding) and AgNPs (quercetin) are found in Table 4.3

Table 4.3: Diffraction angles (2θ), d-spacings (\AA), Miller indices and Intensity for AgNPs (freestanding) and AgNPs (quercetin)

| AgNPs (freestanding) | | AgNPs (quercetin) | | <i>hkl</i> | Ag NPs reference | |
|------------------------|----------------------------|------------------------|----------------------------|------------|------------------------|----------------------------|
| 2θ ($^\circ$) | d-spacing (\AA) | 2θ ($^\circ$) | d-spacing (\AA) | | 2θ ($^\circ$) | d-spacing (\AA) |
| 38.77 | 2.32 | 37.88 | 2.31 | 111 | 38.12 | 2.35 |
| 44.88 | 2.01 | 44.08 | 2.01 | 200 | 44.27 | 2.04 |
| 64.99 | 1.43 | 64.23 | 1.43 | 220 | 64.42 | 1.44 |
| 77.87 | 1.23 | 77.18 | 1.23 | 311 | 77.47 | 1.23 |
| 82.04 | 1.17 | 81.32 | 1.16 | 222 | 81.53 | 1.17 |

4.3.6.2 Selenium nanoparticles

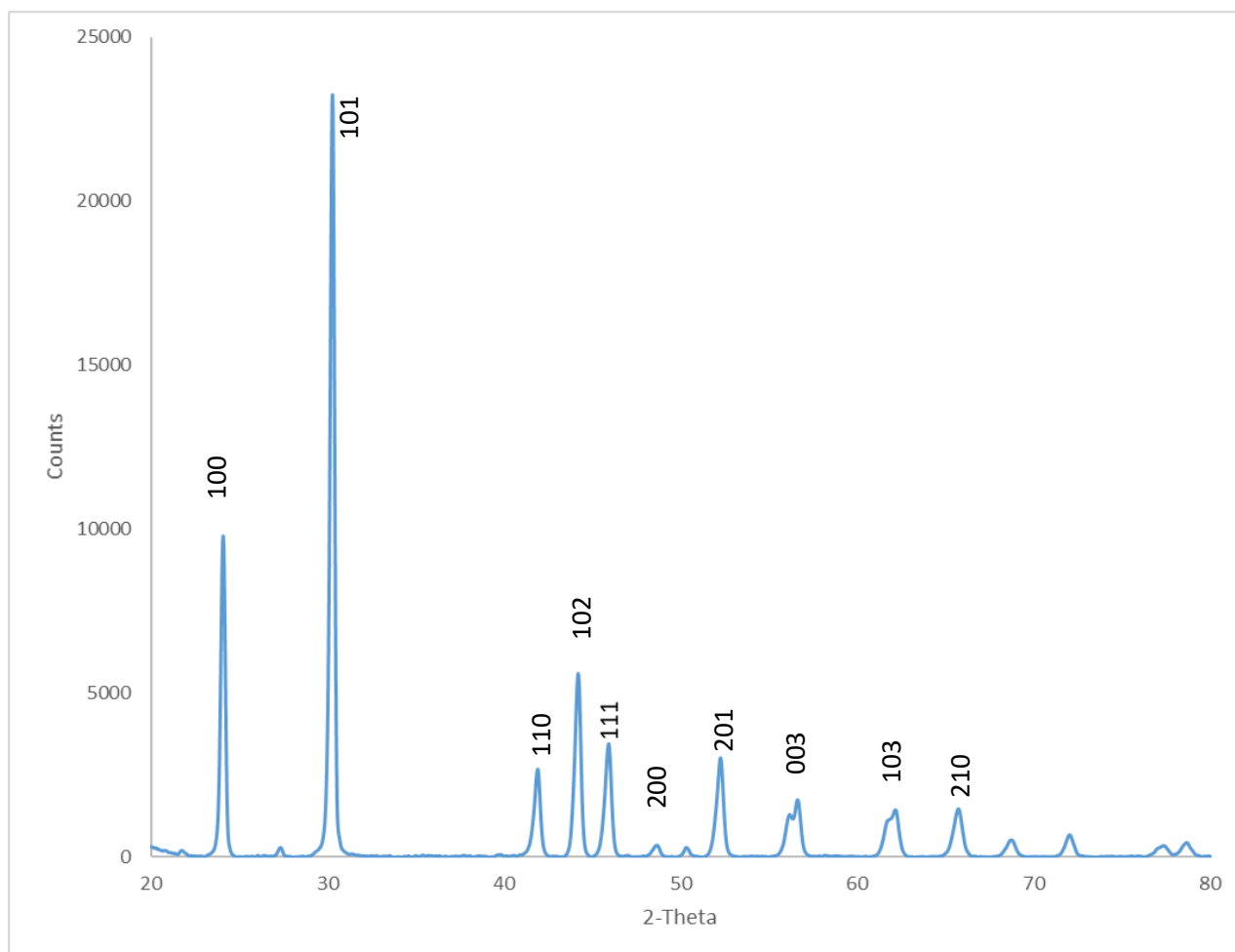


Figure 4.56: Powder X-ray diffraction pattern of freestanding selenium nanoparticles

The observed peaks with 2θ values of 24.12° , 30.30° , 41.95° , 44.24° , 45.99° , 48.84° , 52.29° , 56.70° , 62.28° , and 65.88° correspond to diffraction from (100), (101), (110), (102), (111), (200), (201), (003), (103), and (210) planes respectively (Figure 4.56). The diffraction peaks in the patterns were indexed with the hexagonal phase of selenium with lattice constants $a = 4.357\text{\AA}$ and $c = 4.945\text{\AA}$ and are in good agreement with the standard JCPDS data (JCPDS card No. 06-0362) (Samulski, 2003). The sharpness of the diffraction peaks suggests that the prepared samples are well crystallized. The XRD data for SeNPs (freestanding) are summarised in Table 4.4.

Table 4.4: The values of diffraction angle (2θ), d-spacing (\AA), Miller indices and Intensity for SeNPs (freestanding)

| SeNPs (freestanding) | | h,k,l | SeNPs reference | |
|------------------------|----------------------------|---------|------------------------|----------------------------|
| 2θ ($^\circ$) | d-spacing (\AA) | | 2θ ($^\circ$) | d-spacing (\AA) |
| 24.1 | 3.69 | 100 | 23.57 $^\circ$ | 3.77 |
| 30.3 | 2.95 | 101 | 29.73 $^\circ$ | 3.00 |
| 41.91 | 2.15 | 110 | 41.28 $^\circ$ | 2.18 |
| 44.2 | 2.04 | 102 | 43.68 $^\circ$ | 2.07 |
| 45.92 | 1.97 | 111 | 45.43 $^\circ$ | 1.99 |
| 52.25 | 1.75 | 201 | 51.72 $^\circ$, | 1.77 |
| 56.62 | 1.62 | 003 | 56.07 $^\circ$, | 1.64 |
| 65.73 | 1.42 | 103 | 65.24 $^\circ$ | 1.43 |

4.3.6.3 Zinc oxide nanoparticles

The observed peaks (Figure 4.57) with 2θ values of 30.22 $^\circ$, 31.754 $^\circ$, 33.41 $^\circ$, 38.58 $^\circ$ and 50.28 $^\circ$ correspond to diffraction from (010), (002), (011), (012), and (110) planes, respectively. All characteristic peaks observed for ZnONPs are in closest agreement with those taken from the JCPDS card No. 36-1451 (Thakuria, 2006) that have a wurtzite structure (hexagonal phase). However, there was a strong preferential growth orientation along the (011) plane. The sharpness, strong intensity and narrow width of ZnO diffraction peaks in the XRD pattern indicate that the synthesised ZnO sample is well crystallized.

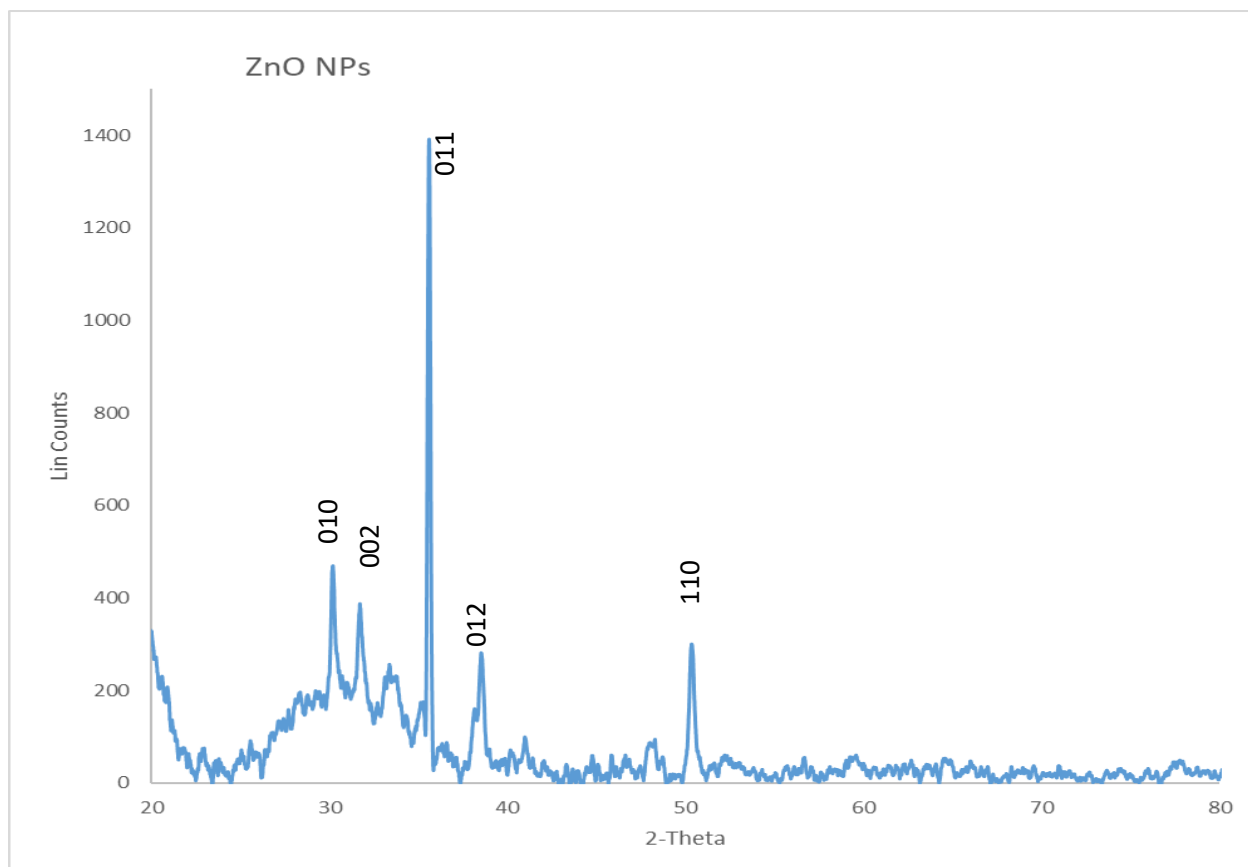


Figure 4.57: Powder X-ray diffraction pattern with inset electron diffraction pattern of hexagonal phase (wurtzite structure) of freestanding zinc oxide NPs

Table 4.5: The values of diffraction angle (2θ), d-spacing (\AA), Miller indices and Intensity for ZnONPs (freestanding)

| ZnONPs (freestanding) | | h,k,l | ZnONPs reference | |
|------------------------|----------------------------|---------|------------------|------|
| 2θ ($^\circ$) | d-spacing (\AA) | | | |
| 30.19 | 2.96 | 010 | 31.84 | 2.81 |
| 31.79 | 2.81 | 002 | 34.52 | 2.60 |
| 35.6 | 2.52 | 011 | 36.33 | 2.47 |
| 38.52 | 2.33 | 012 | 47.63 | 2.00 |
| 50.33 | 1.81 | 110 | 56.71 | 1.62 |

4.3.7 Selected area electron diffraction (SAED)

The selected area electron diffraction patterns of AgNPs, SeNPs and ZnONPs were used to determine the phase of the NPs.

4.3.7.1 Silver nanoparticles

The SAED patterns for AgNPs synthesised with plant extracts (*C. monilifera* and *H. caffrum*) are shown in Figure 4.58 (A and B) and isolated flavonoids are shown in Figure 4.59 (A and B). With the exception of the AgNPs (catechin) diffraction pattern, the patterns demonstrated the concentric diffraction rings as bright spots. This indicates a large number of randomly oriented small grains that cause the spots to merge into rings from sampling all possible diffracting planes. The d spacing of the lattice was calculated using SAED with the formula:

$$rd=L\lambda.$$

The rings correspond to the presence of (200), (111), (220) and (311) planes of the face-centered cubic (fcc) AgNPs which is in agreement with the AgNPs (freestanding) and AgNPs (quercetin) PXRD results (Figure 4.55). AgNPs (catechin) pattern is made of large particles, which produce a pattern for a single crystal material, and some fine grains. Larger crystals => more “spotty” patterns. This confirms that AgNPs (catechin) contains the largest average particle size compared to the AgNPs (crude extracts) and AgNPs (quercetin) as seen in the SEM and TEM results.

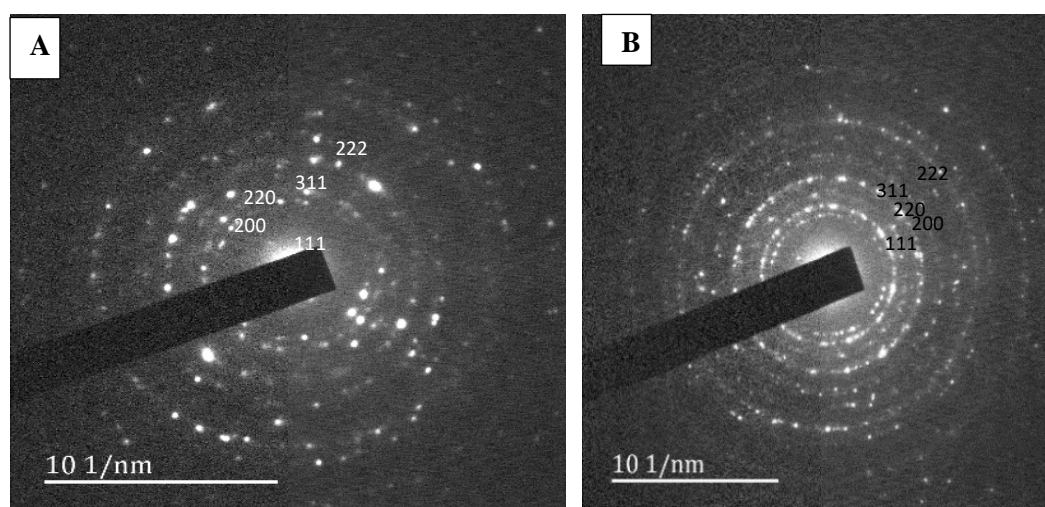


Figure 4.58: (A) Selected area electron diffraction (SAED) pattern of AgNPs (*C. monilifera*) (B) SAED pattern of AgNPs (*H. caffrum*)

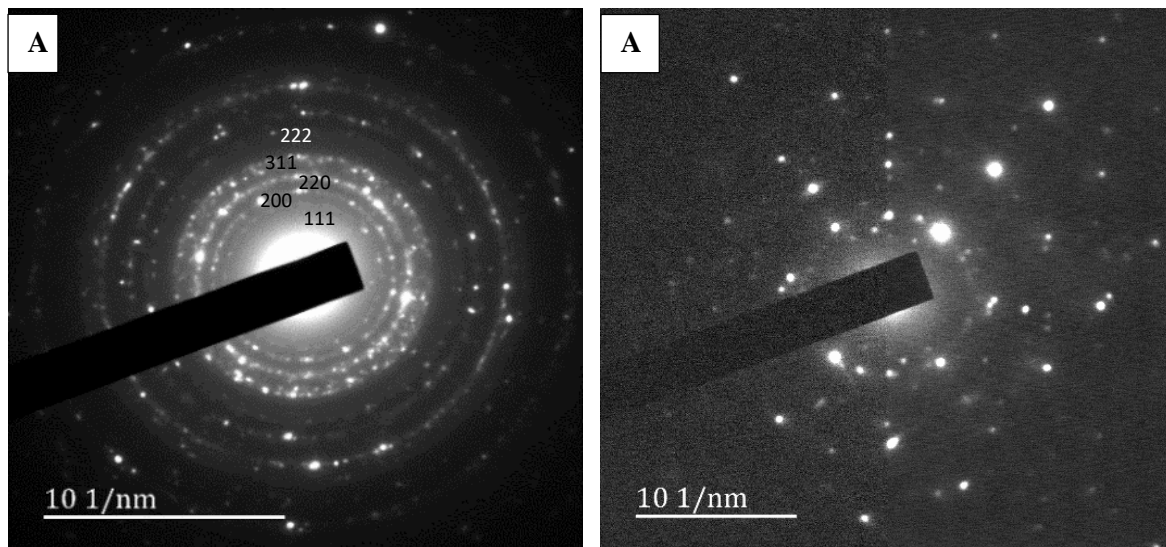


Figure 4.59: (A) Selected area electron diffraction (SAED) pattern of AgNPs (quercetin) (B) SAED pattern of AgNPs (catechin)

The SAED pattern in conjunction with the PXRD results indicated that all the AgNPs particle were crystalline in nature with a FCC crystal lattice. The above results suggested that the size of the AgNPs increased when using flavonoids than when using plant extracts which is also evident in the SEM and TEM results. The SAED for AgNPs is coherent with results obtained by Mohamed, (2015).

4.3.7.2 Selenium nanoparticles

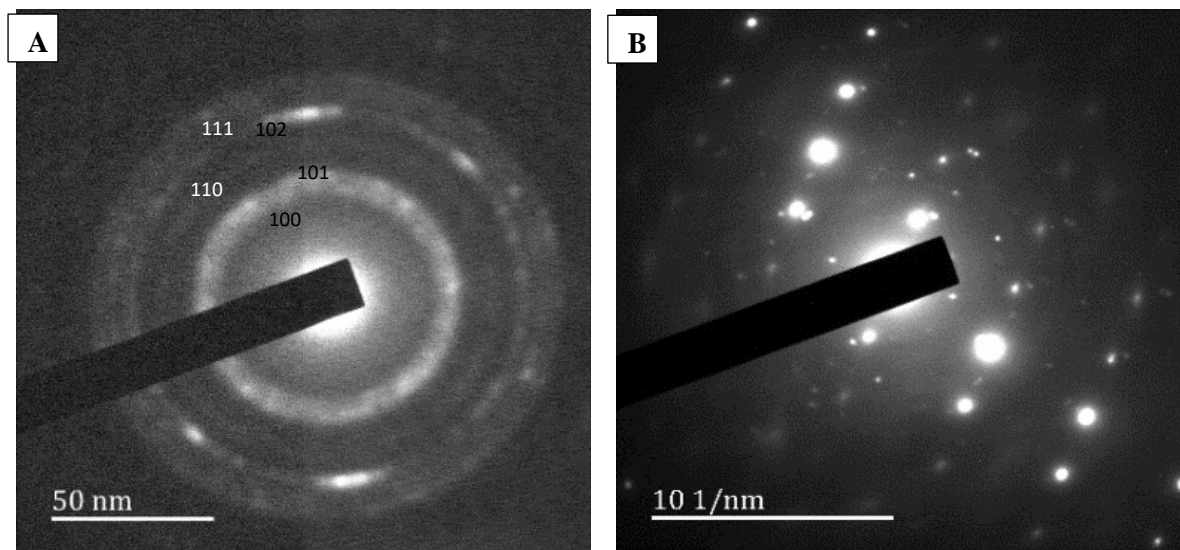


Figure 4.60: (A) Selected area electron diffraction (SAED) pattern of SeNPs (*C. monilifera*) (B) SAED pattern of SeNPs (*H. caffrum*)

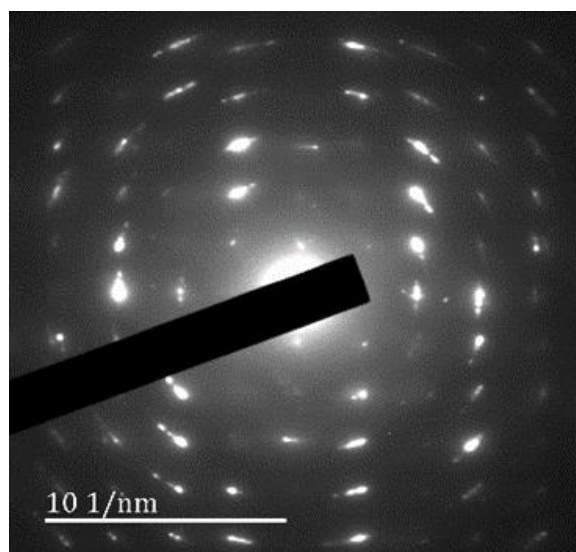


Figure 4.61: Selected area electron diffraction (SAED) pattern of SeNPs (quercetin)

Selected area electron diffraction patterns (Figure 60 A) of SeNPs (*C. monilifera*) exhibit diffraction rings corresponding to the (100), (101), (111), (102), and (110) planes of the hexagonal phase of selenium which is consistent with the PXRD results of SeNPs freestanding.

SAED of SeNPs (*H. caffrum*) is a single-crystal with spots also corresponding to the hexagonal phase of Se.

SAED patterns of SeNPs (quercetin) in Figure 4.61 show a pattern due to a single crystal with “Texture” - i.e. preferential orientation - seen as arcs of greater intensity in the diffraction rings. It can be seen in the SEM results that the SeNPs (quercetin) preferentially stacked almost parallel to one another giving rise to the textured appearance observed in the pattern. Analysing the patterns, it can be confirmed that SeNPs (*H. caffrum*) and SeNPs (quercetin) had larger grain sizes compared to SeNPs (*C. monilifera*) as shown in the SEM and TEM results. The results obtained for SeNPs are in close agreement to those synthesized by Wadhvani (2017).

4.3.7.3 Zinc oxide nanoparticles

The SAED pattern shown in Figure 4.62: (A) ZnONPs (*C. monilifera*), (B) ZnONPs (*H. caffrum*) and Figure 4.63 (A) SAED micrograph of ZnONPs (quercetin) have sharp spots indicative of fine grains of polycrystalline ZnONPs that can be indexed to the hexagonal (wurtzite) structure of ZnONPs. The phase was confirmed by the presence of (010), (002), (011), and (012) planes. The SAED micrograph of ZnONPs (catechin) in Figure 4.63 B is a single crystal with symmetrical orientation of ZnONPs in the hexagonal phase.

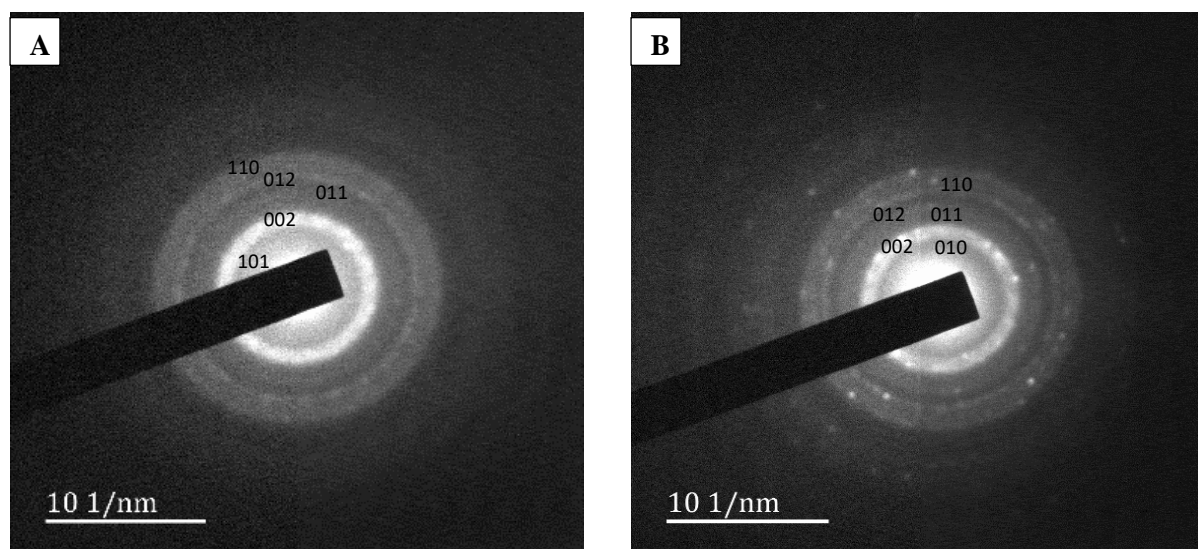


Figure 4.62: (A) Selected area electron diffraction (SAED) pattern of ZnONPs (*C. monilifera*) (B) SAED pattern of ZnONPs (*H. caffrum*)

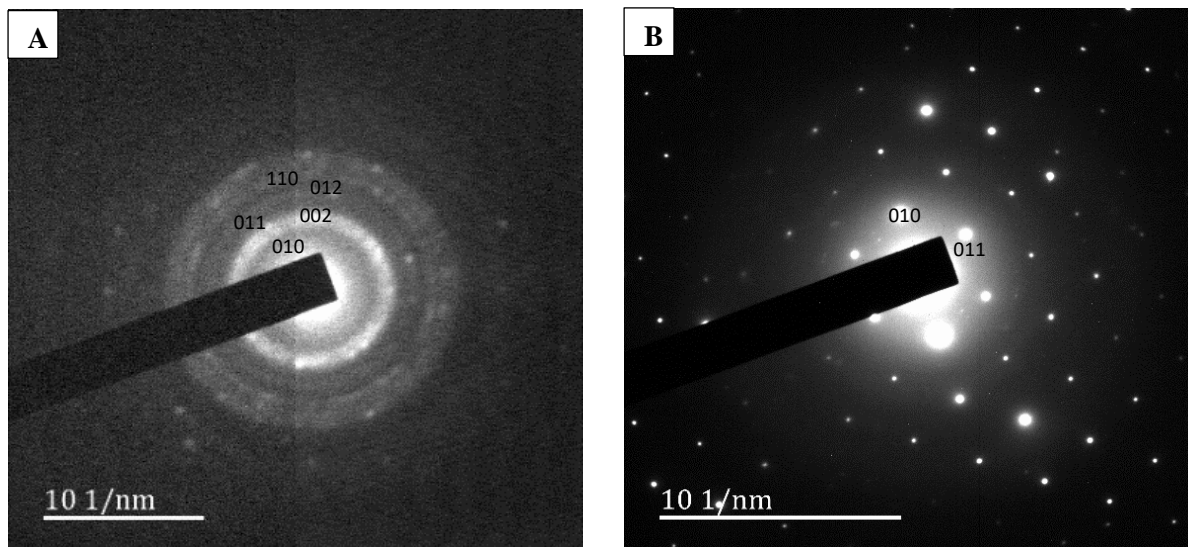


Figure 4.63: (A) Selected area electron diffraction (SAED) pattern of ZnONPs (quercetin) (B) SAED pattern of ZnONPs (catechin)

The Miller indices indexed on the electron diffraction patterns match the respective metal oxide PXRD patterns. This confirms that the freestanding NPs are in the same phase as the NPs synthesised with the biosynthesised NPs. The distance between crystalline planes was consistent with the standard pattern for a wurtzite ZnO crystal structure. The diffraction lines clearly indicate the nanoscale crystallinity of the ZnO particles with randomly oriented polycrystalline. ZnONPs synthesised by Lopez-Romero (2009) exhibited similar SAED results.

CHAPTER 5

BIOLOGICAL TESTING

The crude extracts (*C. monilifera* and *H. caffrum*), isolated flavonoids (quercetin and catechin) and all synthesised NPs were tested for their antioxidant and antibacterial activity. For the antioxidant activity, three assays were used (DPPH free radical scavenging assay, FRAP and H₂O₂ radical scavenging assay). For the antibacterial activity, the disc diffusion method was employed.

5.1 Results and Discussion

In the following sections, the results and discussion for the various assays will be presented.

5.1.1 The 1,1-diphenyl-2-picrylhydrazyl (DPPH) radical scavenging activity

Table 5.1 (Appendix D) shows the DPPH radical scavenging activity of the plant extracts (*C. monilifera* and *H. caffrum*), isolated flavonoids, (quercetin and catechin), freestanding and end-capped NPs.

5.1.1.1 Plants extracts and isolated flavonoids

Figure 5.1 shows the results for the DPPH radical scavenging ability (donation of hydrogen to the DPPH radical) of the plant extracts (*C. monilifera* and *H. caffrum*) and isolated flavonoids (quercetin and catechin) with ascorbic acid as a standard. The scavenging activity of ascorbic acid, quercetin, catechin and *H. caffrum* extract with DPPH was instantaneous showing good antioxidant activity even at low concentrations. From 10 - 100 μ L, ascorbic acid scavenged 95.7 - 97.3 % of the DPPH radicals while quercetin scavenged 87.4 - 92.1 %, catechin 84.1 - 87.1 % and the *H. caffrum* extract scavenged 81.8 - 88.7 %. *C. monilifera* extract showed moderate scavenging of 35.9 % at 10 μ L which increased to 70.6 % at 100 μ L indicating that the radical scavenging ability was concentration dependent. The extract from *H. caffrum* showed higher scavenging ability than that from *C. monilifera*. This could be because catechin,

which is present in *H. caffrum*, has higher antioxidant activity than the quercetin and due to the possible antagonistic effects of other compounds in the extract.

The DPPH radical scavenging ability of the tested samples in decreasing order was found to be: ascorbic acid > catechin > *H. caffrum* extract > quercetin > *C. monilifera* extract.

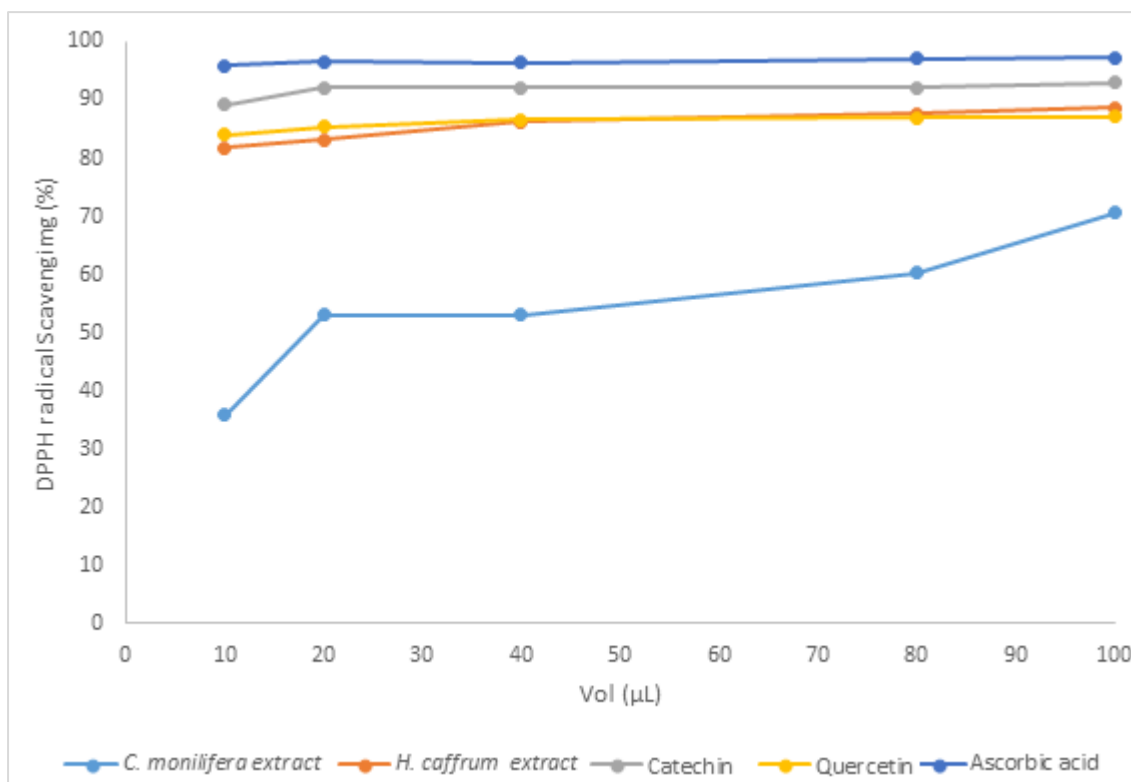


Figure 5.1: DPPH radical scavenging ability of isolated compounds and plant extracts with ascorbic acid as a standard

5.1.1.2 Silver nanoparticles

Figure 5.2 shows the DPPH radical scavenging ability of the synthesised AgNPs with the various reducing agents. Although all NPs showed lower activity than ascorbic acid, their antioxidant activity increased with an increase in concentration. Freestanding NPs showed the lowest activity, followed by AgNPs (*C. monilifera*) whilst AgNPs (*H. caffrum*) showed the highest activity. The order of activity was as follows: ascorbic acid > AgNPs (*H. caffrum*) > AgNPs (catechin) > AgNPs (quercetin) > AgNPs (*C. monilifera*) > AgNPs (freestanding).

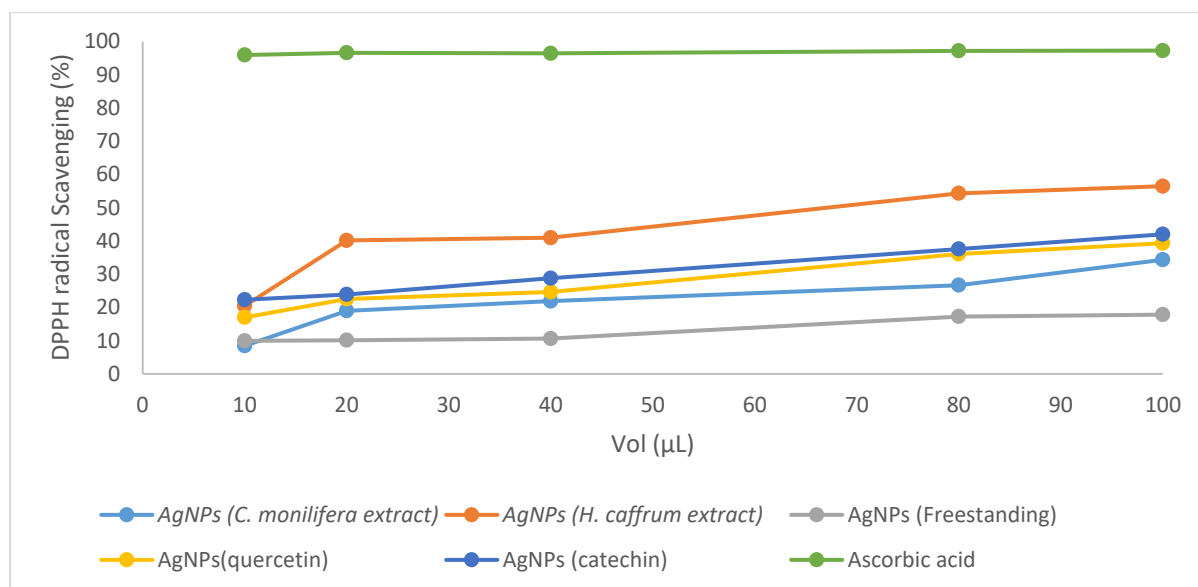


Figure 5.2: DPPH radical scavenging activity of synthesised silver nanoparticles (AgNPs) with various reducing agents with ascorbic acid as a standard

5.1.1.3 Selenium nanoparticles

All of the synthesised SeNPs (Figure 5.3) showed lower activity than ascorbic acid. The trend observed with AgNPs was also observed with the SeNPs. The highest radical scavenging activity was exhibited by SeNPs (*H. caffrum*) whilst no activity was exhibited by SeNPs (catechin). The order of activity was as follows: ascorbic acid > SeNPs (*H. caffrum*) > SeNPs (quercetin) > SeNPs (*C. monilifera*) > SeNPs (freestanding)

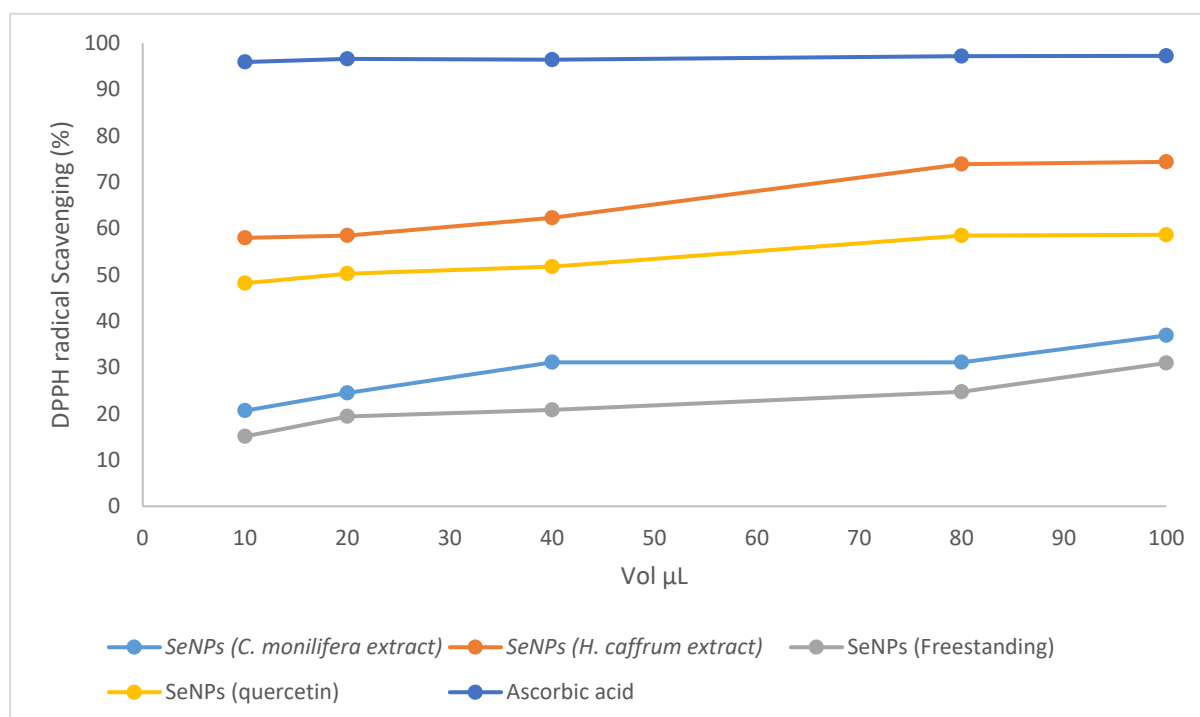


Figure 5.3: DPPH radical scavenging of synthesised selenium nanoparticles (SeNPs) with various reducing agents with ascorbic acid as a standard

5.1.1.4 Zinc oxide nanoparticles

The radical scavenging ability of ZnONPs is shown in Figure 5.4. Once again, the NPs showed lower activity than the standard, ascorbic acid. ZnONPs (*H. caffrum*) showed highest scavenging ability whilst ZnONPs (freestanding) showed the lowest activity. The order of activity was as follows: ascorbic acid > ZnONPs (*H. caffrum*) > ZnO (catechin) > ZnONPs (quercetin) = ZnONPs (*C. monilifera*) > ZnONPs (freestanding).

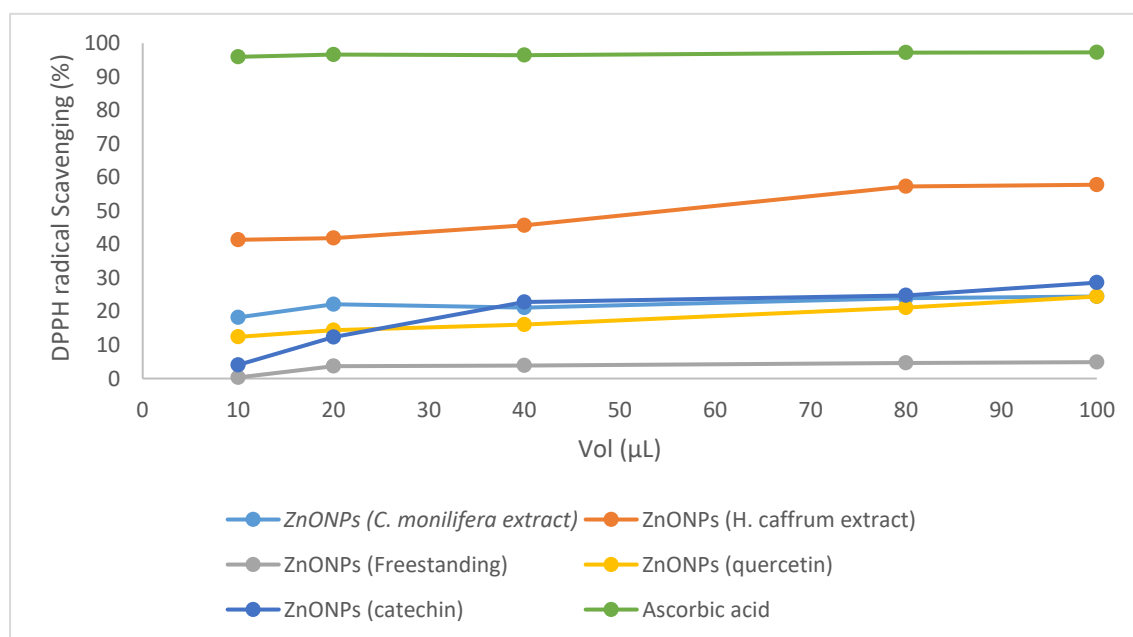


Figure 5.4: DPPH radical scavenging of synthesised zinc oxide nanoparticles (ZnONPs) with various reducing agents with ascorbic acid as a standard

Figure 5.5 compares the DPPH radical scavenging activity of the plant extracts, isolated flavonoids and all synthesised NPs. Since the results in Figure 5.1 - 5.4 were all concentration dependent; the comparison was made at the highest tested concentration which was $100 \mu\text{L}$. The results show plants extracts, isolated compounds and synthesised NPs to have lower activity than the standard, ascorbic acid. The AgNPs, SeNPs and ZnONPs synthesised with *H. caffrum* plant extract showed higher activity than NPs of the same metal synthesised with *C. monilifera*. Freestanding NPs showed lowest activity. This showed that the activity of the synthesised NPs was dependent on the activity of the plant extract or isolated flavonoids. Of the metal NPs synthesised, SeNPs showed higher DPPH radical scavenging ability, followed by Ag then ZnO. The order of activity is illustrated in Figure 5.5.

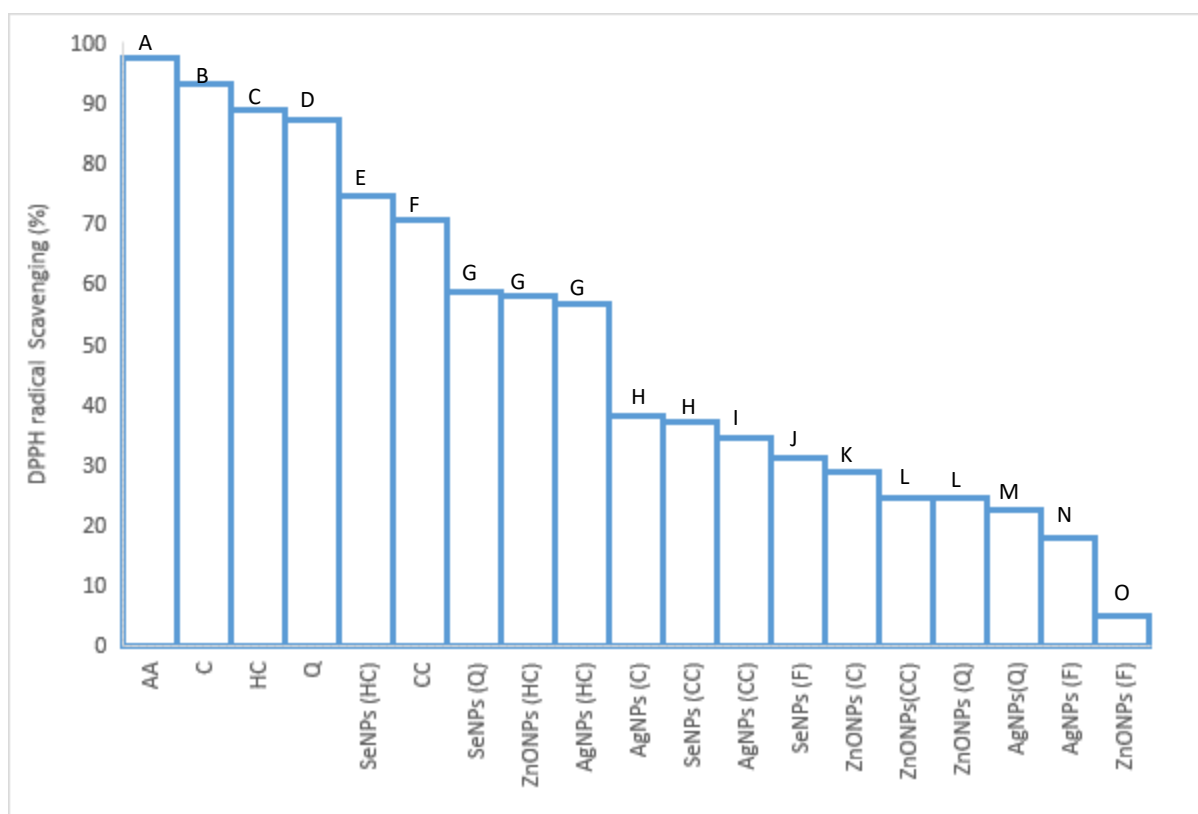


Figure 5.5: Overall DPPH radical scavenging activity of the plant extracts, isolated compounds and synthesised nanoparticles (NPs) at $100 \mu\text{L}$

AA – ascorbic acid, CC - *Chrysanthemodis monilifera* extract, HC - *Harpephyllum caffrum* extract, Q – quercetin, C – catechin, SeNPs – selenium nanoparticles, AgNPs – silver nanoparticles and ZnONPs – zinc oxide nanoparticles. Alphabets A-O are mean separation by Tukey's post-hoc test at 5% level ($n = 3$)

5.1.2 Ferric reducing antioxidant power (FRAP)

Figure 5.6 - 5.9 shows the concentration vs absorbance curves for plant extracts, isolated compounds and synthesised NPs with ascorbic acid as a standard. The individual points represent the mean of three absorbance readings obtained from triplicate runs that were performed.

5.1.2.1 Plant extracts and isolated flavonoids

Figure 5.6 shows the antioxidant activity of the plant extracts and isolated compounds. Quercetin and catechin overlapped and were constant with the highest reducing potential even at very low concentrations. Both flavonoids showed higher reducing potential than the standard (ascorbic acid) and extracts from which they were isolated. The extract of *H. caffrum* showed better reducing potential than that of *C. monilifera*. Similar to results obtained for the DPPH radical scavenging activity, *C. monilifera* plant extract showed the lowest activity. The reducing power of the tested compounds in decreasing order was found to be: quercetin = catechin > ascorbic acid > *H. caffrum* extract > *C. monilifera* extract

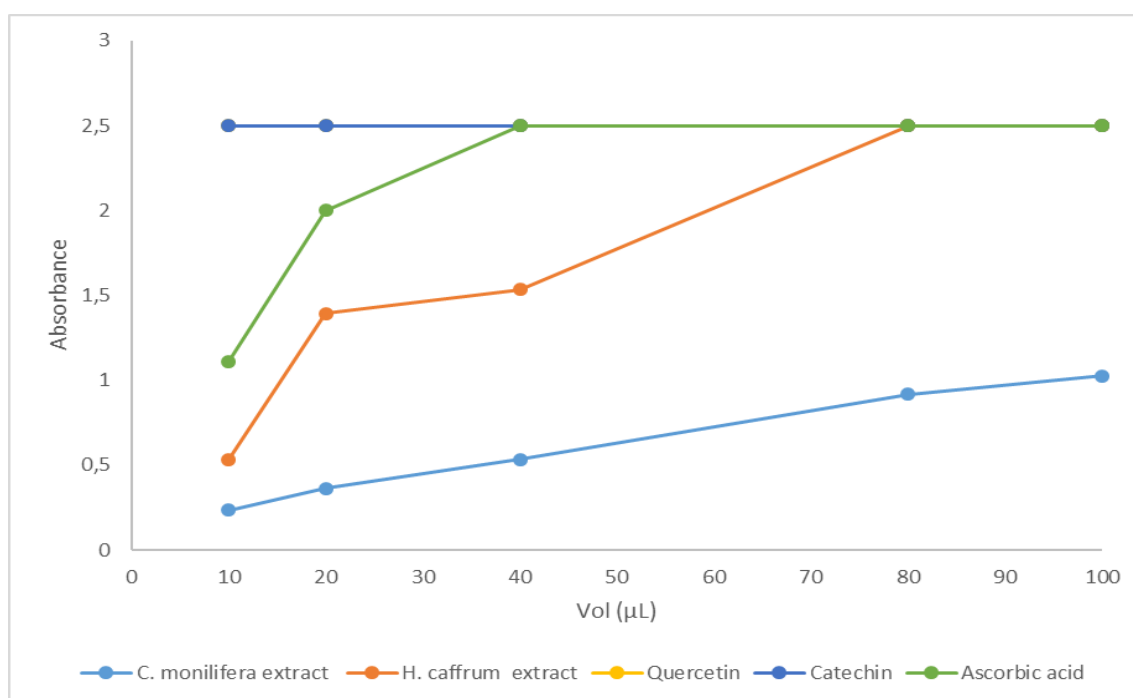


Figure 5.6: Ferric reducing antioxidant power (FRAP) of the plants extracts and the isolated compounds

5.1.2.2. Silver nanoparticles

Figure 5.7 shows the concentration vs absorbance plots using the FRAP assay for AgNPs synthesised with various reducing agents. The results show different activities for the different AgNPs but the reducing power increased with an increase in concentration, suggesting that the results were concentration dependent. The activity of AgNPs is less than that of the standard, ascorbic acid. The highest activity was exhibited by AgNPs synthesised with the flavonoids. However, AgNPs (catechin) showed higher activity than AgNPs (quercetin). AgNPs (free-standing) showed lowest activity, similar to results obtained by the DPPH assay. The reducing power of the tested AgNPs in decreasing order was found to be: ascorbic acid > AgNPs (catechin) > AgNPs (quercetin) > AgNPs (*H. caffrum* extract) > AgNPs (*C. monilifera* extract) > AgNPs (freestanding).

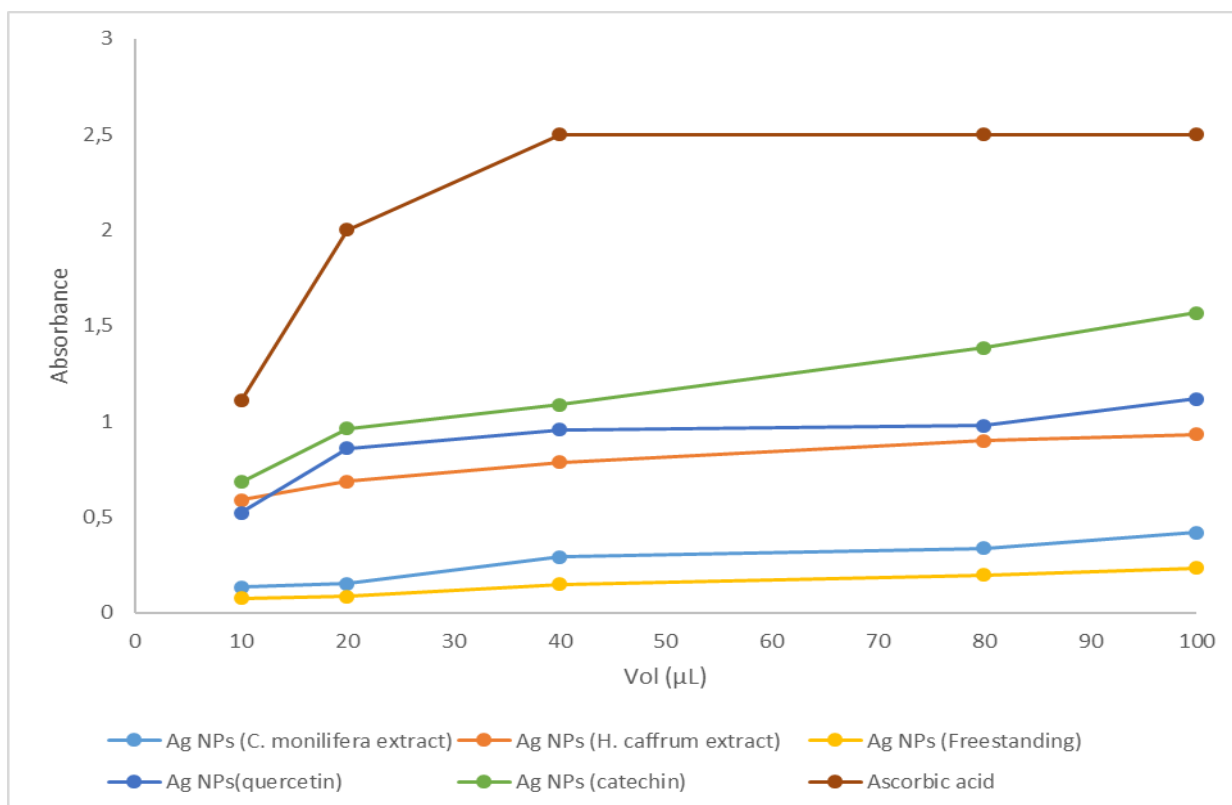


Figure 5.7: Ferric reducing antioxidant power (FRAP) of silver nanoparticles (AgNPs) synthesised with the various reducing agents

5.1.2.3 Selenium nanoparticles

The ferric reducing power of SeNPs in Figure 5.8 shows the activity of SeNPs to be much lower than that of the standard, ascorbic acid. The activity of the NPs however was still concentration dependent. Selenium NPs (quercetin) showed highest activity while SeNPs (freestanding) showed the lowest activity. However, at lower concentrations, the activity of all synthesised NPs were similar. The reducing power of the tested SeNPs in decreasing order was found to be: ascorbic acid > SeNPs (quercetin) > SeNPs (*H. caffrum* extract) > SeNPs (*C. monilifera* extract) > SeNPs (freestanding). Selenium NPs (catechin) were not synthesised. The results produced by the FRAP assay for SeNPs were similar to those of AgNPs with regards to the order of activity. However, for AgNPs, the activities of the synthesised NPs using different capping agents were appreciably different but for SeNPs, they were only marginally different.

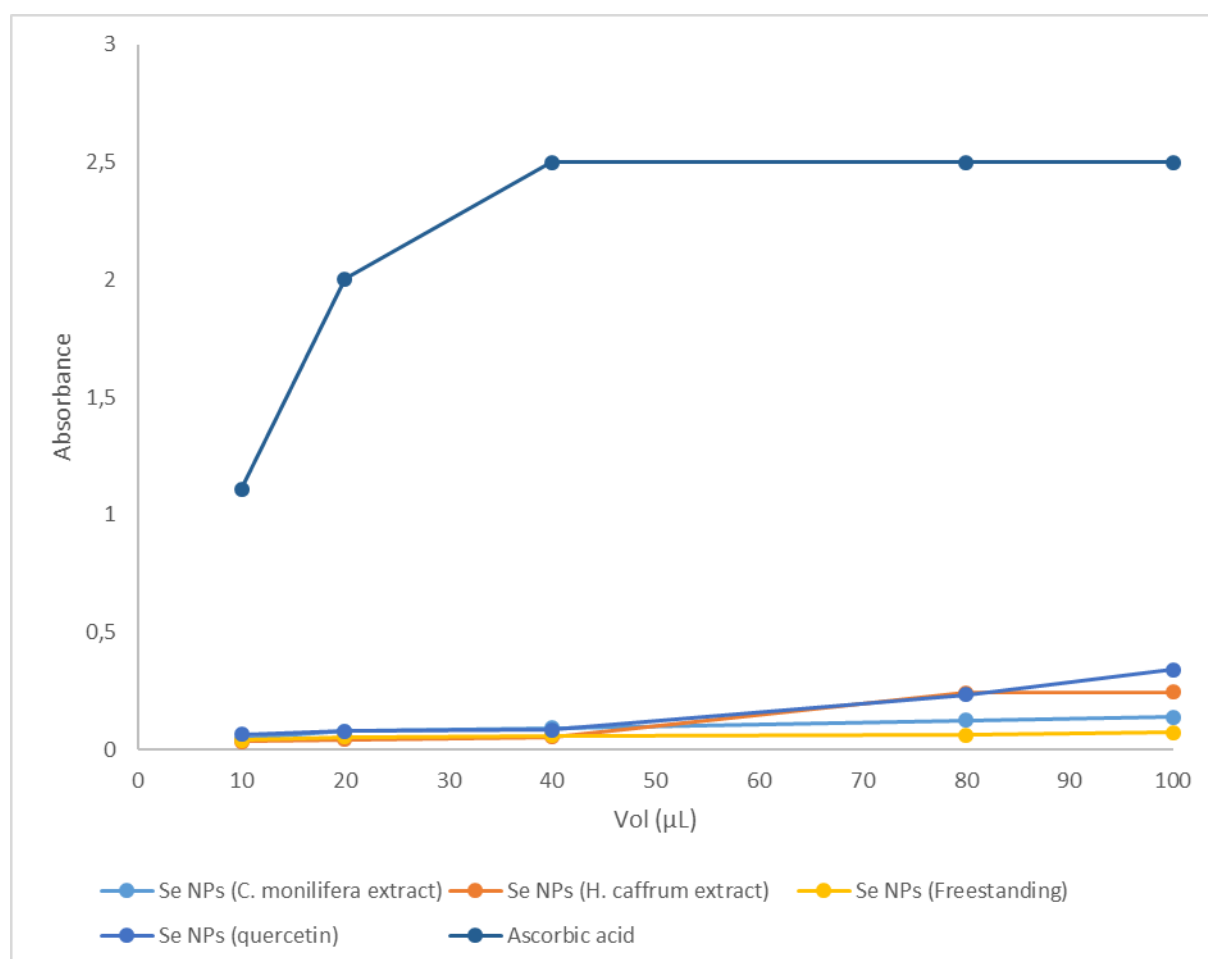


Figure 5.8: Ferric reducing antioxidant power (FRAP) of selenium nanoparticles (SeNPs) synthesised with the various reducing agents

5.1.2.4 Zinc oxide nanoparticles

The FRAP assay for the synthesised ZnONPs using the various reducing agents is shown in Figure 5.9. Zinc oxide NPs (quercetin and catechin) reduced ferric ions instantaneously and showed greater activity compared to ascorbic acid. The ZnONPs synthesised with the plant extracts (*C.monilifera* and *H. caffrum*) and ZnONPs (freestanding) showed lower activity relative to ascorbic acid. The reducing power of the tested ZnONPs in decreasing order was found to be: ZnONPs (catechin) > ZnONPs (quercetin) > ascorbic acid > ZnONPs (*H. caffrum* extract) > ZnONPs (*C. monilifera* extract) > ZnONPs (freestanding).

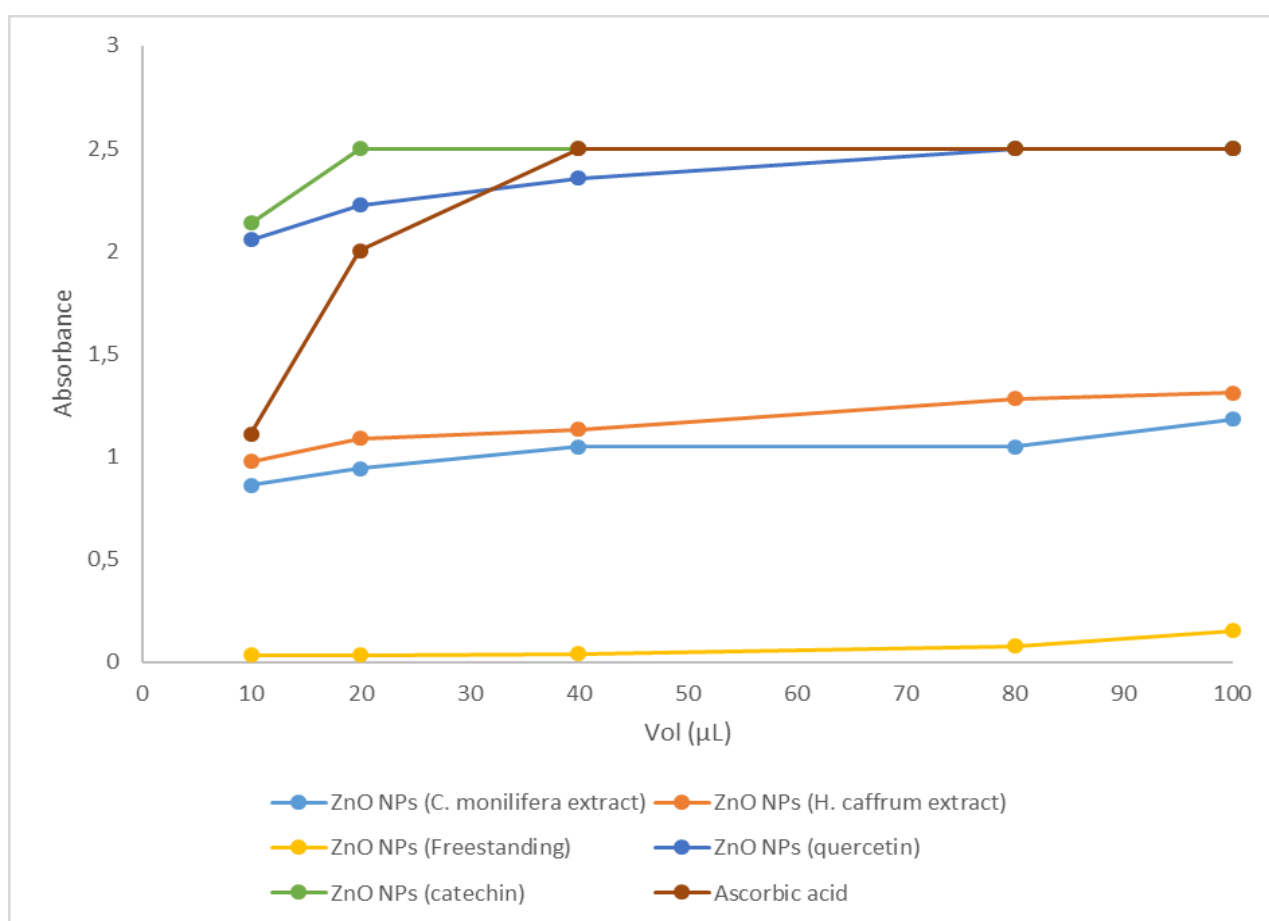


Figure 5.9: Ferric reducing antioxidant power (FRAP) of zinc oxide nanoparticles (ZnONPs) synthesised with the various reducing agents

The overall results once again showed that the activity of the tested extracts, isolated compounds and synthesised NPs was concentration dependent. The maximum absorbance of 2.5 was taken as 100% and the highest tested concentration tested 100 μL was used to plot the histogram (Figure 5.10) to make an over comparison.

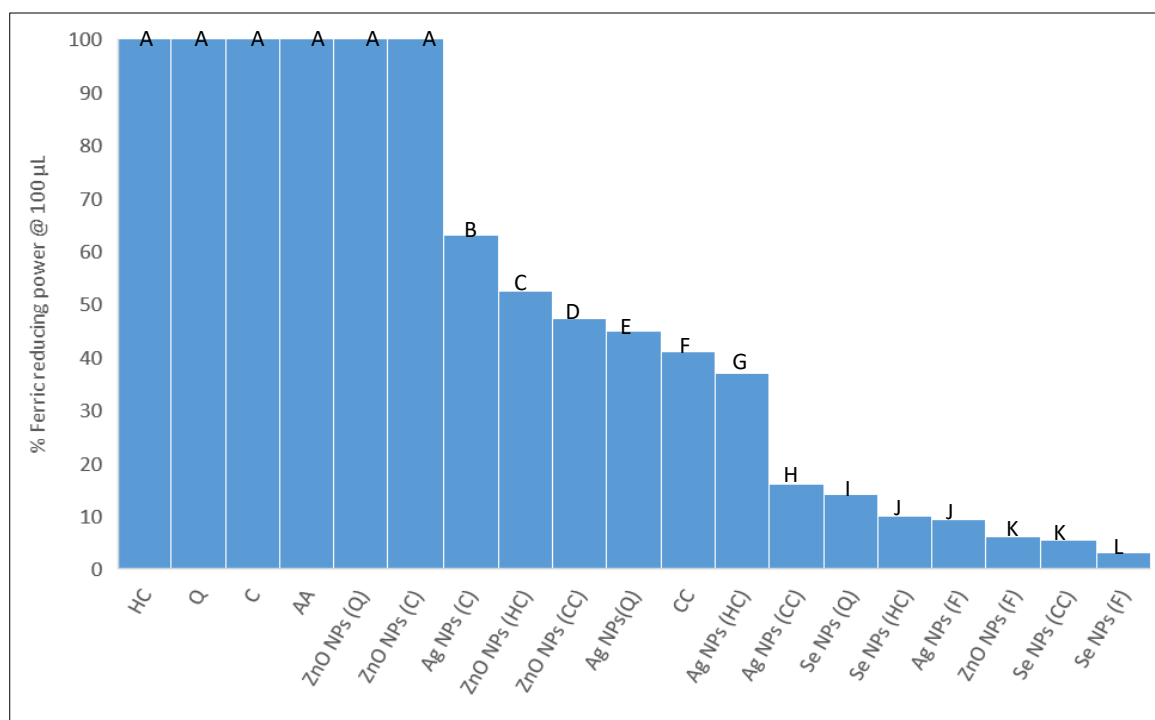


Figure 5.10: Overall ferric reducing antioxidant power (FRAP) of the plant extracts, isolated compounds and synthesised nanoparticles (NPs) at 100 μL (2.5 absorbance units is taken to be 100%)

AA – ascorbic acid, CC - *Chrysanthemodis monilifera* extract, HC - *Harpephyllum caffrum* extract, Q – quercetin, C – catechin, SeNPs – selenium nanoparticles, AgNPs – silver nanoparticles and ZnONPs – zinc oxide nanoparticles. Alphabets A-L are mean separation by Tukey's post-hoc test at 5% level ($n = 3$).

From the results, the standard ascorbic acid, *H. caffrum* extract, both isolated flavonoids (quercetin and catechin) and ZnONPs synthesised with the isolated flavonoids (quercetin and catechin) showed maximum absorbance. Freestanding NPs of metals Ag, Se and ZnO showed lower activity than the biosynthesised NPs of the same metal. The NPs synthesised with the isolated flavonoids showed higher activity compared to the NPs synthesised with plant extracts. The NPs synthesised with *H. caffrum* showed greater activity compared to the NPs synthesised with the *C. monilifera* extract.

5.1.3 H₂O₂ radical scavenging

Table 5.1 (Appendix D) shows the H₂O₂ radical scavenging ability of the plant extracts (*C. monilifera* and *H. caffrum*), isolated flavonoids, (quercetin and catechin), freestanding and end-capped NPs.

5.1.3.1 Plant extracts and isolated flavonoids

Figure 5.11 showing the H₂O₂ radical scavenging results for the plant extracts and isolated compounds. The extracts and isolated compounds scavenged more H₂O₂ radicals than the standard, ascorbic acid. The activity increased with an increase in concentration. At 100 μL, the H₂O₂ radical scavenging activity, in decreasing order, was found to be: quercetin > catechin > *H. caffrum* extract > *C. monilifera* extract > ascorbic acid.

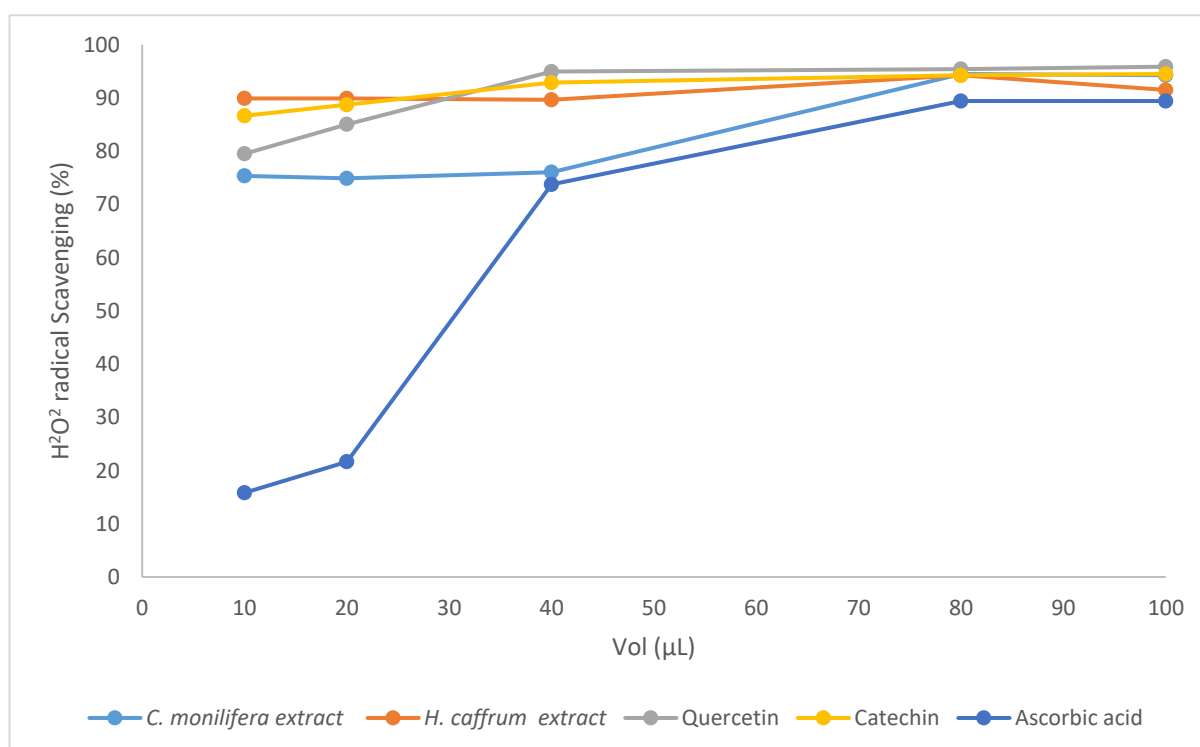


Figure 5.11: H₂O₂ radical scavenging ability of the plant extracts and isolated compounds

5.1.3.2 Silver nanoparticles

All of the synthesised AgNPs showed higher activity than the standard, ascorbic acid (Figure 5.12). Synthesised AgNPs showed high scavenging activity even at very low concentrations. The activity increased slightly with an increase in concentrations from 10 to 20 μL and the activity remained constant throughout the following concentrations. The AgNPs (freestanding) showed lower activity compared to the biosynthesised NPs. At 100 μL , the H_2O_2 radical scavenging activity, in decreasing order, was found to be: AgNPs (quercetin) = AgNPs (catechin) = AgNPs (*H. caffrum* extract) = AgNPs (*C. monilifera* extract) > AgNPs (freestanding) > ascorbic acid.

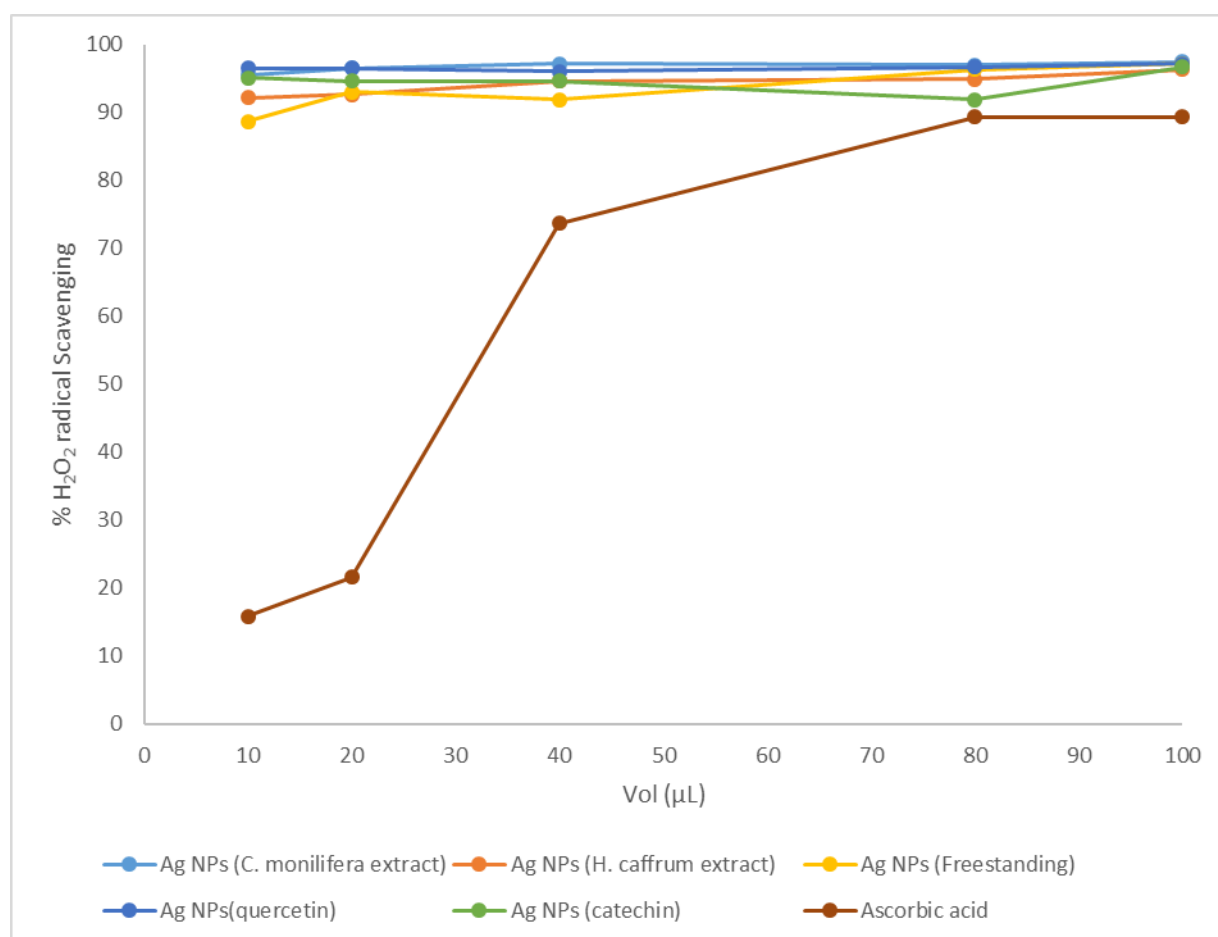


Figure 5.12: H_2O_2 radical scavenging activity of the silver nanoparticles (AgNPs) synthesised with the various reducing agents

5.1.3.3 Selenium nanoparticles

The SeNPs (Figure 5.13) also exhibited higher H_2O_2 radical scavenging activity than the standard, ascorbic acid as was observed with AgNPs in Figure 5.12. The activity of the SeNPs essentially remained constant at all the tested concentrations. At 100 μL , the H_2O_2 radical scavenging activity, in decreasing order, was found to be: SeNPs (quercetin) = AgNPs (*H. caffrum* extract) = SeNPs (*C. monilifera* extract) > SeNPs (freestanding) > ascorbic acid.

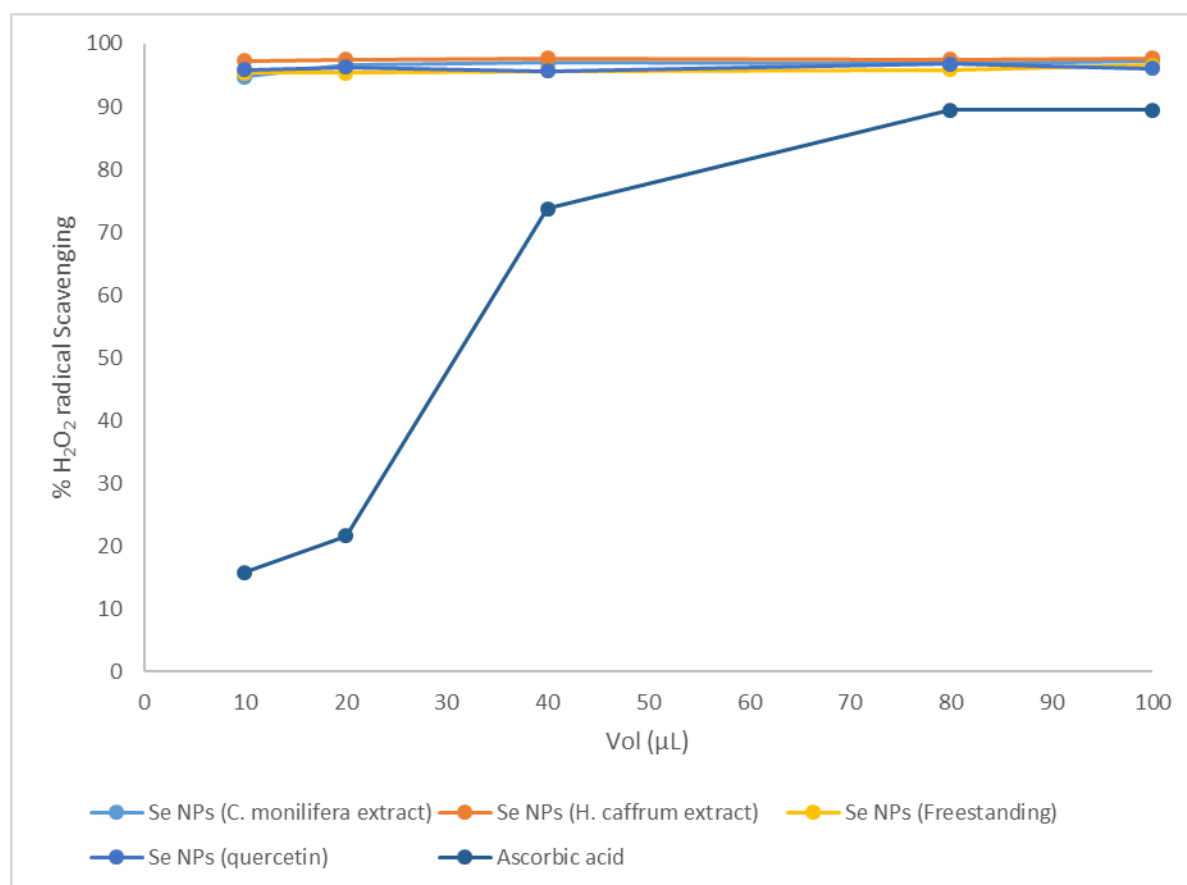


Figure 5.13: H_2O_2 radical scavenging activity of the selenium nanoparticles (SeNPs) synthesised with the various reducing agents

5.1.3.4 Zinc oxide nanoparticles

The H₂O₂ radical scavenging activity of ZnONPs synthesised with various reducing agents are shown in Figure 5.14. The results showed ZnONPs to exhibit higher H₂O₂ radical scavenging activity than ascorbic acid. The scavenging activity of ZnONPs was essentially constant across the tested concentrations with the exception of ZnONPs synthesised with catechin. The slope for ZnONPs (catechin) increased gradually with an increase in concentration. At the highest tested concentration however, ZnONPs (catechin) exhibited similar activity to the other tested ZnONPs. At 100 µL, the H₂O₂ radical scavenging activity, in decreasing order, was found to be: AgNPs (catechin) = AgNPs (*H. caffrum* extract) = AgNPs (*C. monilifera* extract) > AgNPs (freestanding) > AgNPs (quercetin) > ascorbic acid.

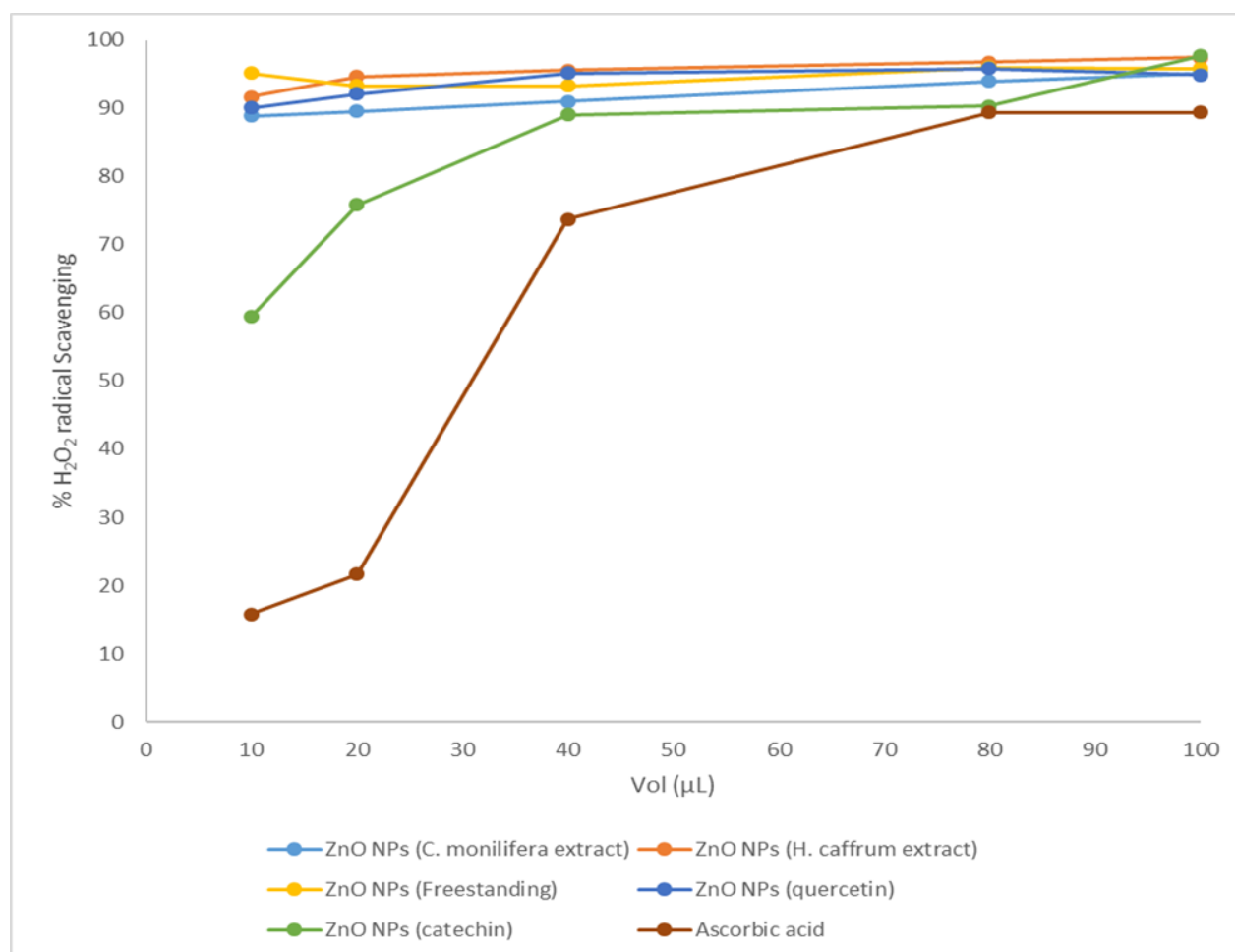


Figure 5.14: H₂O₂ radical scavenging activity of the zinc oxide nanoparticles (ZnONPs) synthesised with the various reducing agents

The H₂O₂ radical scavenging activity of all tested extracts, compounds and synthesised AgNPs, SeNPs and ZnONPs relative to one another is shown in Figure 5.15. It can be seen that all of the synthesised NPs show higher activity than the plant extracts and isolated flavonoids with the exception of ZnONPs (freestanding) and ZnONPs (*C. monilifera*).

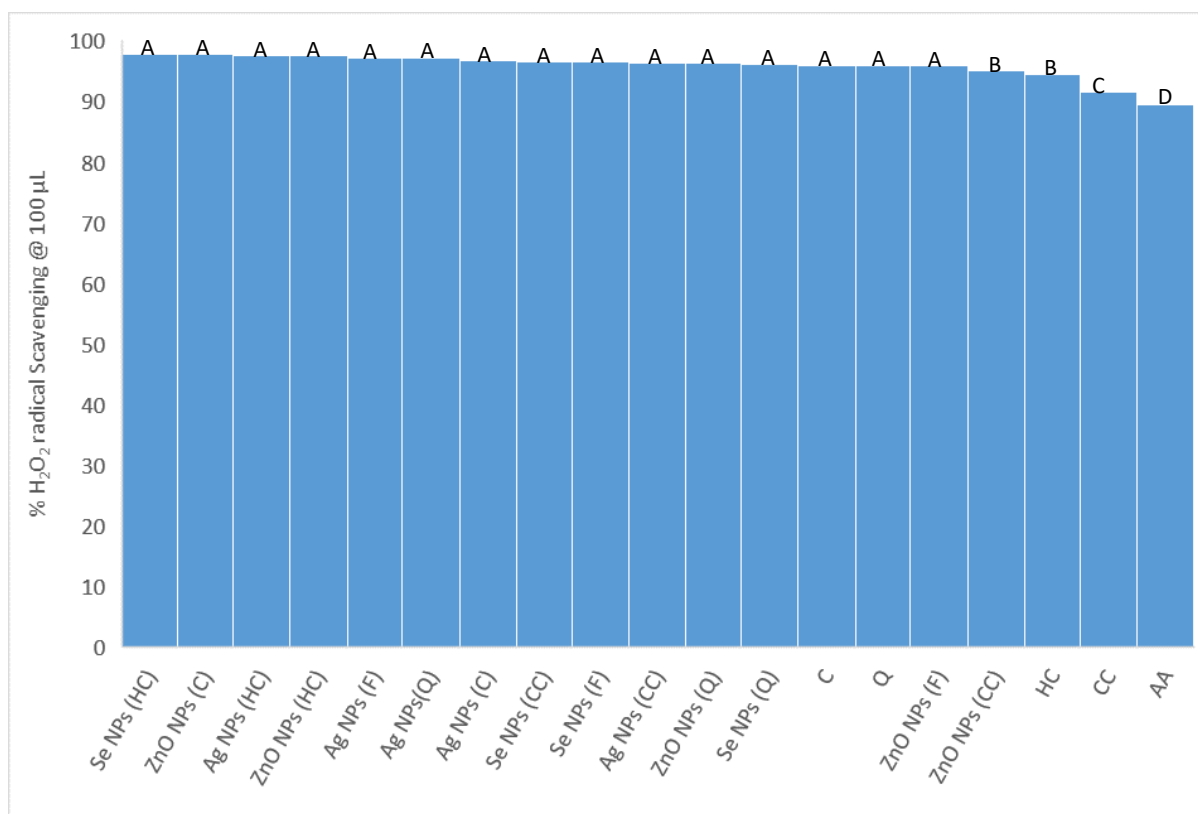


Figure 5.15: Overall H₂O₂ radical scavenging activity of the plant extracts, isolated compounds and synthesised nanoparticles (NPs) at 100 µL

AA – ascorbic acid, CC - *Chrysanthemodis monilifera* extract, HC - *Harpephyllum caffrum* extract, Q – quercetin, C – catechin, SeNPs – selenium nanoparticles, AgNPs – silver nanoparticles and ZnONPs – zinc oxide nanoparticles. Mean separation by Tukey's post-hoc test at 5% level (n = 3).

*Alphabets A-D are mean separation by Duncans Multiple range test at 5% level (n = 3)

Table 5.1: Comparison of antioxidant results obtained by the three different assays for plant extracts, isolated compounds and synthesised nanoparticles at 100 μ L

| ANTIOXIDANT ASSAYS | | | | | | | | | |
|-----------------------------|----------|------|------|----------|-----|------|-----------------------------------|------|-------|
| | DPPH (%) | | | FRAP (%) | | | H ₂ O ₂ (%) | | |
| Ascorbic Acid | 97.25 | | | 100 | | | 89.4 | | |
| <i>C. monilifera</i> | 70.52 | | | 41 | | | 91.47 | | |
| <i>H. Caffrum</i> | 88.72 | | | 100 | | | 94.47 | | |
| Quercetin | 92.9 | | | 100 | | | 95.85 | | |
| Catechin | 87.06 | | | 100 | | | 95.93 | | |
| Nanoparticles | | | | | | | | | |
| | Ag | Se | ZnO | Ag | Se | ZnO | Ag | Se | ZnO |
| Freestanding | 17.8 | 30.9 | 4.9 | 9.4 | 3 | 6.1 | 97.2 | 96.5 | 95.85 |
| <i>C. monilifera</i> | 34.3 | 58.6 | 24.5 | 16 | 5.5 | 47.3 | 96.3 | 96.5 | 95.16 |
| <i>H. Caffrum</i> | 56.5 | 74.4 | 57.8 | 37 | 10 | 52.4 | 97.5 | 97.8 | 97.47 |
| Quercetin | 39.3 | 36.9 | 24.5 | 45 | 14 | 100 | 97.2 | 96.1 | 94.93 |
| Catechin | 37.9 | - | 28.6 | 63 | - | 100 | 96.8 | - | 97.7 |

The isolated flavonoids gave significantly lower values for residual DPPH and H₂O₂ radicals. The high scavenging potential may be explained by the presence of the phenolic moiety in their chemical structure. The antioxidant activity of flavonoids is dependent on the number of hydroxyl groups in the molecule. Both quercetin and catechin have the same number (five) hydroxyl groups in the structure which explains the similarities in antioxidant activity. Quercetin and catechin are also conjugated molecules which would be able to delocalise a negative charge that would arise from donating a proton to the radicals. The major structural characteristics which makes catechin, for instance, a good antioxidant is the cathecol moiety in the B-ring and the hydroxyl group in the C-ring. It can donate two protons from the B-ring hydroxyl groups or, one proton from the B-ring hydroxyl groups and one proton from the C-ring hydroxyl group (Seyoum et al., 2006). The resultant structure from the proton donation would be a stable quinone or 3-chromanone due to the stabilisation of the B-ring that is rich in delocalised pi-electrons (see Figure 2.12).

In each assay, AgNPs, SeNPs and ZnONPs capped with bioactive phytocompounds showed better activity than their freestanding counterparts. The TEM, IR and EDS results showed AgNPs, SeNPs and ZnONPs synthesised with NaBH₄ (freestanding NPs) to be uncapped. This means that the capping or adsorbed bioactive molecules could have assisted in scavenging radicals or reducing ferric ions.

AgNPs (catechin) showed higher reducing power than AgNPs (quercetin) even though the individual flavonoids exhibit similar antioxidant activity. From HRTEM results (Figure 4.44 and 4.45), it was observed that the capping around AgNPs (catechin) was ≈ 1 nm thicker than AgNPs (quercetin). From the EDS (Figure 4.23) and IR (Figure 4.31) results, it was also observed that the active flavonoids adsorbed onto the surface of AgNPs. This may explain the higher activity of AgNPs (catechin) compared to AgNPs (quercetin). This also means that the antioxidant activity also relies on the amount of bioactive compounds on the surface of the synthesised NP. The relatively high activity exhibited by the capped AgNPs compared to uncapped AgNPs suggests a synergistic relationship between the capping agents on the AgNPs.

The activity of the NP depends on the activity of the plant extract for capped NPs. The extract from *H. caffrum* showed higher activity than that from *C. monilifera*; the NPs (Ag, Se and ZnO) synthesised with the *H. caffrum* extract showed higher activity than those synthesised with the *C. monilifera* extract. SeNPs showed the lowest activity of all the NPs at reducing Fe^{3+} but showed good activity against the DPPH and H_2O_2 radicals. The SeNPs synthesised in this work were mostly rods. Sharma (2015) show rod shaped NPs to have better radical scavenging activity than spherical ones. Even though IR and EDS results confirmed SeNPs to be capped with compounds from the plant extract or flavonoid used to reduce them, HRTEM results did not show significant capping as was observed with AgNPs. However, HRTEM results of SeNPs show very large rods and wires which have a smaller surface area compared to the smaller AgNPs with larger surface area. The smaller surface area limits the adsorption of biomolecules on the surface of the SeNPs which could explain the reduced activity of the NPs by the FRAP assay.

ZnONPs (catechin) and ZnONPs (quercetin) showed higher ferric reducing activity than the standard, ascorbic acid. The antioxidant activity of ZnONPs may be due to the transfer of electron density located at oxygen combined with the activity of flavonoids that are adsorbed onto the surface. All the synthesised NPs showed better H_2O_2 scavenging activity than the standard, ascorbic acid and the plant extracts. The overall results with all assays are shown in Table 5.2. The AgNPs, SeNPs and ZnONPs synthesised with compounds exhibiting high antioxidant activity show greater activity than those synthesised with compounds that show moderate antioxidant activity. The *H. caffrum* extract shows good compatibility with the NPs as all NPs synthesised with this extract showed the highest activity.

5.2 Kirby-Bauer Disk Diffusion Susceptibility Test

To determine the effects of capping on the activity of the metal NPs, they were tested against the antibacterial activity of freestanding (uncapped) NPs was tested. Table 5.2 compares the zones of inhibition obtained by the test samples against Gram-negative bacterial strains.

Table 5.2: Zones of inhibition (mm) against various Gram-negative bacterial strains.

| Vol (μL) | <i>E.coli</i> 25992 | | | <i>E.coli</i> 35218 | | | <i>Klebsiella pneumoniae</i> ATCC 70060 | | | <i>Pseudomonas aeruginosa</i> ATCC 27835 | | |
|--|---------------------|----|----|---------------------|----|----|---|----|----|--|----|----|
| | 10 | 20 | 40 | 10 | 20 | 40 | 10 | 20 | 40 | 10 | 20 | 40 |
| Zone of inhibition | | | | | | | | | | | | |
| <i>C. monilifera</i> extract | 0 | 0 | 0 | 0 | 0 | 0 | 0 | 0 | 0 | 0 | 0 | 0 |
| <i>H. caffrum</i> extract | 0 | 0 | 0 | 0 | 0 | 0 | 0 | 0 | 0 | 0 | 0 | 0 |
| Quercetin | 0 | 9 | 10 | 0 | 0 | 0 | 0 | 0 | 0 | 0 | 0 | 0 |
| Catechin | 0 | 0 | 11 | 0 | 8 | 10 | 0 | 0 | 0 | 0 | 0 | 0 |
| 1 mM AgNO ₃ | 10 | 11 | 15 | 11 | 14 | 15 | 0 | 0 | 0 | 10 | 10 | 12 |
| 1 mM NaSeO ₃ | 0 | 0 | 0 | 0 | 0 | 0 | 0 | 0 | 0 | 0 | 0 | 0 |
| 1 mM ZnNO ₃ | 0 | 0 | 0 | 0 | 0 | 0 | 0 | 0 | 0 | 0 | 0 | 0 |
| AgNPs (Freestanding) | 11 | 11 | 12 | 0 | 0 | 0 | 0 | 0 | 0 | 11 | 11 | 12 |
| AgNPs (<i>C. monilifera</i> extract) | 10 | 15 | 20 | 9 | 12 | 12 | 11 | 11 | 13 | 0 | 0 | 10 |
| AgNPs (<i>H. caffrum</i> extract) | 15 | 19 | 19 | 0 | 9 | 10 | 0 | 0 | 0 | 13 | 15 | 16 |
| AgNPs (Quercetin) | 0 | 0 | 12 | 0 | 0 | 12 | 0 | 0 | 0 | 0 | 0 | 0 |
| AgNPs (Catechin) | 0 | 0 | 0 | 0 | 0 | 0 | 0 | 0 | 0 | 0 | 0 | 0 |
| SeNPs (Freestanding) | 0 | 0 | 0 | 0 | 0 | 0 | 0 | 0 | 0 | 0 | 0 | 0 |
| SeNPs (<i>C. monilifera</i> extract) | 0 | 0 | 0 | 0 | 0 | 0 | 0 | 0 | 0 | 0 | 0 | 0 |
| SeNPs (<i>H. caffrum</i> extract) | 12 | 14 | 15 | 0 | 0 | 0 | 0 | 0 | 0 | 0 | 0 | 12 |
| SeNPs (Quercetin) | 0 | 0 | 0 | 0 | 0 | 0 | 0 | 0 | 0 | 0 | 0 | 0 |
| ZnONPs (Freestanding) | 0 | 0 | 0 | 0 | 0 | 0 | 0 | 0 | 0 | 0 | 0 | 0 |
| ZnONPs (<i>C. monilifera</i> extract) | 0 | 0 | 0 | 0 | 0 | 0 | 0 | 0 | 0 | 0 | 0 | 0 |
| ZnONPs (<i>H. caffrum</i> extract) | 0 | 10 | 12 | 0 | 7 | 11 | 0 | 0 | 0 | 0 | 0 | 0 |
| ZnONPs (Quercetin) | 0 | 0 | 0 | 0 | 0 | 0 | 0 | 0 | 0 | 0 | 0 | 0 |
| ZnONPs (Catechin) | 0 | 0 | 0 | 0 | 0 | 0 | 0 | 0 | 0 | 0 | 0 | 0 |

Among the freestanding NPs, the results only show AgNPs to be active against *E.coli* and *P. aeruginosa* at all the tested concentrations. The inhibition diameter increased with increase in concentration. All of the synthesised AgNPs showed varying antibacterial against gram-negative bacteria with the exception of AgNPs (catechin) which showed no promising activity against any of the gram-negative bacteria at the tested concentrations.

To determine whether a synergistic or antagonistic effect results from capping of the freestanding NPs, the plant extracts (*C. monilifera* and *H. caffrum*) and pure compounds (quercetin and catechin) were tested. The crude extracts did not exhibit any antibacterial activity against the four gram-negative strains tested. Catechin exhibited antibacterial activity against both *E. coli* strains tested. Quercetin showed promise against *E.coli* 25992.

The capping of AgNPs with quercetin and catechin appeared to have reduced antibacterial activity compared to freestanding AgNPs. Capping of SeNPs and ZnONPs with quercetin and catechin did not have any effect on the antibacterial activity. The extract from *C. monilifera* enhanced the activity of AgNPs against both strains of *E.coli* and *K. pneumonia* with increased zones of inhibition (Table 5.3) whilst that from *H. caffrum* enhanced the activity of AgNPs against both strains of *E.coli* and *P. aeruginosa*. These were the only NPs that displayed synergy between NPs and capping agent for antibacterial activity. SeNPs and ZnONPs capped with compounds from the *H.caffrum* extract also showed increased activity against *E.coli* relative to the uncapped NPs.

Table 5.3 compares the compares the zone of inhibition obtained by the test samples against gram-positive bacterial strains.

Table 5.3. Zones of inhibition (mm) against various gram-positive bacterial strains.

| Vol μ L | <i>Chromobacterium violaceum</i> ATCC 12472 | | | <i>Staphylococcus aureus</i> ATCC 29213 | | | <i>Staphylococcus aureus</i> ATCC 43300 | | | <i>Enterococcus faecalis</i> ATCC 51299 | | |
|--|---|---------|---------|---|----|----|---|----|----|---|----|----|
| | 10 | 20 | 40 | 10 | 20 | 40 | 10 | 20 | 40 | 10 | 20 | 40 |
| Zone of inhibition | | | | | | | | | | | | |
| <i>C. monilifera</i> extract | 0 | 0 | 0 | 0 | 0 | 0 | 0 | 0 | 0 | 0 | 0 | 0 |
| <i>H. caffrum</i> extract | 0 | 0 | 0 | 0 | 0 | 0 | 0 | 0 | 0 | 0 | 0 | 0 |
| Quercetin | 0 | 0 | 0 | 0 | 0 | 0 | 0 | 0 | 0 | 0 | 0 | 0 |
| Catechin | 0 | 0 | 0 | 0 | 0 | 0 | 0 | 0 | 0 | 0 | 0 | 0 |
| 1 mM AgNO ₃ | 11 | 14 | 15 | 14 | 15 | 15 | 0 | 9 | 12 | 0 | 0 | 11 |
| 1 mM NaSeO ₃ | 0 | 0 | 0 | 0 | 0 | 0 | 0 | 0 | 0 | 0 | 0 | 0 |
| 1 mM ZnNO ₃ | 0 | 0 | 0 | 0 | 0 | 0 | 0 | 0 | 0 | 0 | 0 | 0 |
| AgNPs (Freestanding) | 0 | 11 | 12 | 0 | 0 | 0 | 13 | 15 | 17 | 0 | 0 | 0 |
| AgNPs (<i>C. monilifera</i> extract) | 0 | 0 | 9 | 0 | 12 | 13 | 0 | 0 | 0 | 0 | 0 | 0 |
| AgNPs (<i>H. caffrum</i> extract) | 14 | 16 | 16 | 15 | 16 | 20 | 0 | 9 | 11 | 0 | 0 | 14 |
| AgNPs (Quercetin) | (15/12) | (16/13) | (17/15) | 10 | 12 | 15 | 10 | 12 | 25 | 0 | 0 | 0 |
| AgNPs (Catechin) | 0 | 0 | 0 | 0 | 0 | 0 | 0 | 0 | 0 | 0 | 0 | 0 |
| SeNPs (Freestanding) | 0 | 0 | 0 | 0 | 0 | 0 | 0 | 0 | 0 | 0 | 0 | 0 |
| SeNPs (<i>C. monilifera</i> extract) | 0 | 0 | 0 | 0 | 0 | 0 | 0 | 0 | 0 | 0 | 0 | 0 |
| SeNPs (<i>H. caffrum</i> extract) | 0 | 0 | 0 | 0 | 0 | 0 | 0 | 0 | 0 | 0 | 0 | 0 |
| SeNPs (Quercetin) | 12 | 8 | 10 | 0 | 0 | 0 | 0 | 0 | 0 | 0 | 0 | 12 |
| ZnONPs (Freestanding) | 0 | 0 | 0 | 0 | 0 | 0 | 0 | 0 | 0 | 0 | 0 | 0 |
| ZnONPs (<i>C. monilifera</i> extract) | 0 | 0 | 0 | 0 | 0 | 0 | 0 | 0 | 0 | 0 | 0 | 0 |
| ZnONPs (<i>H. caffrum</i> extract) | 0 | 0 | 0 | 0 | 0 | 0 | 0 | 0 | 0 | 0 | 0 | 0 |
| ZnONPs (Quercetin) | 0 | 0 | 0 | 0 | 0 | 0 | 0 | 0 | 0 | 0 | 0 | 0 |
| ZnONPs (Catechin) | 0 | 0 | 0 | 0 | 0 | 0 | 0 | 0 | 0 | 0 | 0 | 0 |

Amongst the freestanding NPs, the results only show AgNPs to be active against *C. violaceum* and *S. aureus* 43300 at all the tested concentrations. The inhibition diameter increased with increase in concentration. As observed with Gram-negative bacteria (Table 5.2), all of the synthesised AgNPs showed varying antibacterial promise against Gram-positive strains with the exception of AgNPs (catechin).

To determine whether a synergistic or antagonistic effect results from capping the freestanding NPs, the plant extracts (*C. monilifera* and *H. caffrum*) and pure compounds (quercetin and

catechin) were tested. They did not exhibit any antibacterial activity against the four Gram-positive strains tested.

The capping of AgNPs with catechin appeared to have reduced antibacterial activity relative to freestanding AgNPs. Quercetin enhanced the activity of AgNPs against three Gram-negative strains, *C. violaceum* and both *S. aureus* strains. To add, AgNPs capped with quercetin also showed activity towards anti-quorum sensing of *C. violaceum*. Both freestanding and AgNPs capped with quercetin showed no activity against *E. faecalis*. The extract from *C. monilifera* reduced the activity of uncapped AgNPs by showing activity against two bacterial strains only, *C. violaceum* and *S. aureus* 29213 reduced zones of inhibition. *H. caffrum* enhanced the activity of the AgNPs by showing activity against all four tested strains with increased zones on inhibition relative to freestanding AgNPs.

Capping of SeNPs and ZnONPs with the plant extracts or compounds did not have any effect on antibacterial activity. Quercetin enhanced the activity of uncapped SeNPs showing antibacterial activity against *C. violaceum*. Bacteria are generally characterised by a cell membrane, cell wall, and cytoplasm. The resistance of Gram-negative bacteria to anti-bodies is due to the impenetrable cell wall. This cell has two cell membranes, an outer membrane and a plasma membrane with a thin layer of peptidoglycan with a thickness of 7–8 nm (Sirelkhatim et al., 2015). Nanoparticles smaller than 7 nm, as in the case of AgNPs (*H. caffrum*), can easily penetrate the wall causing several pits and eventually damage cell wall leading to cell death (Slawson et al., 1992; Sondi and Salopek-Sondi, 2004). AgNPs (*H. caffrum*) showed better activity than AgNPs (*C. monilifera*) which can attributed to the smaller size range of AgNPs (*H. caffrum*). The smallest measured particle capped with the *H. caffrum* crude extract was 4.31 nm and AgNPs capped with the *C. monilifera* crude extract was 19.26 nm. The high surface area of NPs allows for more active sites to interact with biological entities. The larger surface area of NPs of smaller size range (SEM- Figure 4.33 A and B and TEM- Figure 4.42 and 4.43) capped with compounds from the *H. caffrum* extract made them a better antibacterial agent.

Gram-positive bacteria have one cytoplasmic membrane with a multilayer of peptidoglycan polymer, and a thicker cell wall (20 - 80 nm) which is a larger size range and makes it highly susceptible to damage. To illustrate this, AgNPs (freestanding) killed more Gram-positive bacteria than Gram-negative bacteria which required smaller sized NPs. AgNPs (freestanding) with a size range of 50 - 90 nm were unable to penetrate the Gram-negative bacteria unlike the

smaller sized AgNPs (*H. cafferum*). This also explains why larger zones of inhibition were obtained for Gram-positive bacteria compared to Gram-negative bacteria.

Different types of NPs have different mechanisms for combating microbial resistance. Their toxicity to bacteria can be explained by three types of mechanisms. They can either induce oxidative stress, release metal ions or by non-oxidative mechanisms (Wang et al., 2017). The mechanisms may occur simultaneously. Silver NPs have the ability to anchor onto the bacteria and penetrate its wall (Sondi and Salopek-Sondi, 2004). Also proposed is the release of metal ions from the NPs when in contact with bacteria. This can be seen in Table 5.2 and 5.3 where the 1 mM silver ion solution showed good activity against bacterial growth. In addition, silver metal is a soft acid and will easily interact with bacterial cells since they contain sulfur and phosphorus groups which are soft bases (Masallat et al., 2016). The cells then take in the silver ions and possibly inhibit respiratory enzymes that generate free oxygen species that can also attack the cell causing cell death (Jyoti et al., 2016).

This explains why AgNPs showed better activity compared to the SeNPs and ZnONPs. Worth noting is the inactivity exhibited by the AgNPs (catechin) given that pure catechin inhibited growth of *E. coli* 25922 and *E. coli* 35218. AgNPs (catechin) differed from AgNPs (quercetin) with regards to their shapes, sizes and capping thickness. AgNPs (quercetin) were nano-spheres, nano-rods, nano-plates (triangles and hexagons) (SEM Figure 4.34 and TEM Figure 4.44) with a size range of (5-11 and 150-250 nm) whereas AgNPs (catechin) consisted of more nano-spheres at a size range of 5-11 nm and some nano-hexagons with sizes ranged between 200-250 nm (SEM Figure 4.34 B and TEM Figure 4.45). AgNPs (catechin) also had 1 nm thicker capping of catechin on the surface of the NPs than AgNPs (quercetin). Studies conducted by Pal et al, (2007) report that triangular nanoplates with a (111) lattice plane as the basal plane, which are high in atom density, display the strongest anti-microbial action, compared to spherical and rod-shaped NPs. They added that spherical NPs predominantly have 100 facets along with a small percentage of 111 facets. From XRD analysis in Figure 55, it can be seen that both AgNPs (freestanding) and AgNPs (quercetin) had preferential growth in the (111) plane which explains their good antibacterial activity. It can also be speculated that capping agents could also act as a passivating layer for antibacterial action when it is thick. Further experiments which can include testing NPs with various thicknesses for antibacterial activity and increasing incubating times could help shed more light to these claims.

Results obtained for SeNPs are similar to studies that reported SeNPs to show antibacterial activity against *Staphylococcus aureus* ATCC (Husen and Siddiqi, 2014; Nguyen et al., 2017). The antibacterial mechanism for SeNPs is not known but Stolzoff et al. (2016) postulated that SeNPs deplete glutathione (GSH), an antioxidant that is vital for neutralising reactive oxygen species in bacteria. The major drawback with this mechanism is that the re-introduction of the antioxidant protein can easily reverse the effect. The exact toxicity mechanism of SeNPs is not completely understood and is still controversial. Distinctive mechanisms that have been put forward in the literature are listed as following: direct contact of SeNPs with cell walls, resulting in destroying bacterial cell integrity, liberation of antimicrobial ions, and reactive oxygen species formation (Venkatasubbu et al., 2016).

With regard to the antibacterial action of ZnONPs following the mechanism of releasing Zn^{2+} ions, studies have demonstrated that the released Zn^{2+} ions are insufficient for bacterial toxicity (Sirelkhatim et al., 2015). This can also be seen in Table 5.2 and 5.3 where 1 mM zinc nitrate solution was unable to inhibit any bacterial growth. Similar to the AgNPs, the shape-dependent activity was explained in terms of the percent of active facets in the NPs. Rod-shaped ZnONPs have (111) and (100) facets, whereas spherical nanostructures mainly have (100) facets. High-atom-density facets with (111) facets exhibit higher antibacterial activity (Sirelkhatim et al., 2015). Rods and wires penetrate into cell walls of bacteria more easily than the spherical ZnONPs that were obtained in this work.

CHAPTER 6

SUMMARY AND FINDINGS

6.1 Summary

This study focused on isolating secondary metabolites from two medicinal plants species which are indigenous to KwaZulu-Natal, South Africa, namely, *Chrysanthemodis monilifera* and *Harpephyllum caffrum*. Both of these plants are commonly used in South African traditional medicine to treat, manage or control a variety of human ailments. Quercetin was isolated from the extract of *C. monilifera* and catechin from that of *H. caffrum*. The crude extracts and the isolated compounds were used for the synthesis of end-capped silver, selenium and zinc oxide nanoparticles. The biosynthesised nanoparticles were compared with chemically synthesised freestanding nanoparticles. Optimisation studies using quercetin at various concentrations showed that growth was concentration dependant and occurred with agglomeration and subsequent re-orientation of the nanoparticles. The optimum concentration for nanoparticle growth was found to be 2 mM quercetin and 1 mM metal ion solution.

The reaction for the chemical synthesis of freestanding nanoparticles proceeded much faster than those using the biomolecules. The order of formation of NPs was: AgNPs (formed immediately), ZnONPs (hours) and SeNPs (days). The silver ions had a +1 oxidation state which made them easier (and quicker) to reduce to Ag⁰ compared to the Zn ions which had an oxidation state of +2 and Se ions with an oxidation state of +4. The sizes and shapes of the NPs varied with reducing agent, with quercetin producing the highest variation of AgNP shapes (mixture of spheres, hexagons, triangles and rods). The shapes of NPs produced by the extracts were similar. AgNPs synthesised with quercetin and catechin were capped with the biomolecules. Although capping was not observed under HRTEM analysis for SeNPs and ZnONPs, FTIR analysis indicated that biomolecules adsorbed to the surface of the NPs. Particles were often polycrystalline, face centred cubic structures for all AgNPs, trigonal phase for all SeNPs and hexagonal (wurzite) structures for ZnONPs. With regards to size of nanoparticles produced, the following trend was observed for the various metals:

AgNPs: catechin > quercetin > freestanding > *C. monilifera* extract > *H. caffrum* extract

SeNPs particles: *H. caffrum* extract > *C. monilifera* extract > freestanding > quercetin

SeNPs rods: quercetin > freestanding > *C. monilifera* extract > *H. caffrum* extract

ZnONPs: catechin > quercetin > freestanding > *C. monilifera* extract > *H. caffrum* extract

The antioxidant activity of NPs was dependent on the capping of the active biomolecule. Nanoparticles capped with quercetin and catechin and compounds from the extracts showed improved activity indicating a synergistic relationship between NPs and the reducing and/or capping agent.

The antibacterial potential of AgNPs increased with a reduction in particle size; this effect was more pronounced for AgNPs at 10 nm. The capping of the NPs may have a passivating effect or could provide a slow ion release mechanism to NPs thereby affecting their activity as antibacterial agents.

6.2 Conclusion

This study demonstrated a greener and more cost-effective method for the synthesis of silver, selenium and zinc oxide nanoparticles using extracts from the plant species, *Chrysanthemodis monilifera* and *Harpephyllum caffrum* and their isolates, quercetin and catechin, respectively. Freestanding nanoparticles were synthesised for comparison. The results showed biomolecules to act as both reducing and end-capping agents in the synthesis of nanoparticles. The use of plant material avoids the usage of harmful and toxic reducing and stabilising agents. The results showed the structure and morphology of nanoparticles to depend on the metal ion and type of biomolecule used in the synthesis. However, the different extracts and compounds were not found to affect the phase of the nanoparticles produced. The nanoparticles produced showed antioxidant and antibacterial promise.

6.3 Recommendation for further work

The synthesis of nanoparticles is a rapidly growing field/discipline and more research needs to be done on the mechanisms of nanoparticle formation which may lead to fine tuning of the process, ultimately leading to the synthesis of nanoparticles with a strict control over the size and shape parameters. There is still a challenge with the antioxidant assays (DPPH, FRAP and H₂O₂) since the nanoparticles do not dissolved in MeOH and most other solvents that can be used for these tests. Longer incubation times for anti-oxidant activity testes with the insoluble nanoparticles should be considered. The amount/quantity of catechin and quercetin capped around the nanoparticles is also unknown. This makes it difficult to compare the antioxidant activity of pure compounds with known concentration to end-capped nanoparticles with unknown concentrations of capping agents. Future work could include elemental analysis to determine the metal content of the nanoparticles and TGA-DSC can also be used to find the decomposition of the organic capping agent which should be significantly lower than that of the metal nanoparticle. This would bring us closer to determining the concentration of the organic layer capped on the metal nanoparticles thus allowing more comparable results for the antioxidant assays. To further this project, the nanoparticles could be tested for other biological activity (i.e. anti-cancer). This could possibly lead to new applications for nanoparticles.

REFERENCES

- Acharya, P., Gnawali, G.R. and Rajbhandari, M. 2013. Isolation of catechin from *Acacia catechu* Willdenow estimation of total flavonoid content in *Camellia sinensis Kuntze* and *Camellia sinensis Kuntze var. assamica* collected from different geographical region and their antioxidant activities. *Scientific World*, 11: 32-36.
- Agnihotri, S., Mukherji, S. and Mukherji, S. 2014. Size-controlled silver nanoparticles synthesized over the range 5-100 nm using the same protocol and their antibacterial efficacy, *RSC Advances*, 4: 3974-3983.
- Ågren, M.S. 1990. Percutaneous absorption of zinc from zinc oxide applied topically to intact skin in man, *Dermatology*, 180: 36-39.
- Ahmad, A., Senapati, S., Khan, M.I., Kumar, R. and Sastry, M. 2005. Extra-/intracellular biosynthesis of gold nanoparticles by an alkalotolerant fungus, *Trichothecium sp*, *Journal of Biomedical Nanotechnology*, 1: 47-53.
- Ahmad, N., Sharma, S., Alam, Md.K., Singh, V.N., Shamsi, S.F., Mehta, B.R. and Fatma, A. 2010. Rapid synthesis of silver nanoparticles using dried medicinal plant of basil, *Colloids and Surfaces B: Biointerfaces*, 81: 81-86.
- Ahmed, S., Saifullah, S.M, Ahmad, Swami, B.L and Ikram, S. 2016. Green synthesis of silver nanoparticles using *Azadirachta indica* aqueous leaf extract, *Journal of Radiation Research and Applied Sciences*, 9: 1-7.
- Akhtar, M.S., Panwar, J. and Yun, Y-S. 2013. Biogenic synthesis of metallic nanoparticles by plant extracts, *ACS Sustainable Chemistry and Engineering*, 1 : 591-602.
- Ali, H., Khan, E. and Sajad, M.E. 2013. Phytoremediation of heavy metals--concepts and applications, *Chemosphere*, 91: 869-81.
- Ali, N., Al-Fatimi, M., Crouch, R.A., Denkert, A., Setzer, W. and Wessjohann, L. 2013. antimicrobial, antioxidant, and cytotoxic activities of the essential oil of *Tarhonanthus camphoratus*. *Natural Products Communications*, 8 : 683-686.
- Amic, A., Lucic, B., Stepanic, V., Markovic, Z., Markovic, S., Dimitric Markovic, J. M. and Amic, D. 2017. Free radical scavenging potency of quercetin catecholic colonic metabolites: Thermodynamics of 2H(+)/2e(-) processes, *Food Chemistry*, 218: 144-1451.
- Amic, D., Stepanić, V., Lucic, B., Marković, Z. and Dimitrić-Marković, J.M. 2013. PM6 study of free radical scavenging mechanisms of flavonoids: Why does O-H bond dissociation

enthalpy effectively represent free radical scavenging activity?, *Journal of Molecular Modelling*, 19 : 2593-2603.

- A. Ashrafia) and C. Jagadish. 2007. Review of zincblende ZnO: Stability of metastable ZnO phases, *Journal of Applied Physics*, 102: 1-12
- AshaRani, P.V., Mun, L.K.G., Hande, M.P. and Valiyaveetil, S. 2009. cytotoxicity and genotoxicity of silver nanoparticles in human cells, *ACS Nano*, 3: 279-90.
- Auer, G., Woditsch, P., Westerhaus, A., Kischkewitz, J., Griebler O.D. and Liedekerke, M. 2006. Pigments, Inorganic, 2. White Pigments. *Ullmanns Encyclopedia of Industrial Chemistry*. Wiley, Weinheim.p. 257.
- Avendaño, R., Chaves, N., Fuentes, P., Sánchez, E., Jiménez, J.I. and Chavarría, M. 2016. Production of selenium nanoparticles in *Pseudomonas putida* KT2440, *Scientific Reports*, 6: 1-9.
- Awwad, A.M., Salem, N.M. and Abdeen, A.O. 2012. biosynthesis of silver nanoparticles using *Olea europaea* leaves extract and its antibacterial activity, *Nanoscience and Nanotechnology*, 2 : 164-170.
- Beattie, M. and Taylor, J. 2011. Silver alloy vs. uncoated urinary catheters: a systematic review of the literature, *Journal of Clinical Nursing*, 20: 2098-108.
- Bhainsa, K.C. and D'Souza, S.F. 2006. Extracellular biosynthesis of silver nanoparticles using the fungus *Aspergillus fumigatus*, *Colloids and Surface B: Biointerfaces*, 47: 160-4.
- Bindhu, M.R. and Umadevi, M. 2013. Synthesis of monodispersed silver nanoparticles using *Hibiscus cannabinus* leaf extract and its antimicrobial activity, *Spectrochimica Acta Part A: Molecular and Biomolecular Spectroscopy*, 101: 184-90.
- Bohm, B.A., and Stuessy, T.F. 2001. *Flavonoids of the Sunflower Family (Asteraceae)*.Springer. Wien-New York, 182-193.
- Bors, W., Heller, W., Michel, C. and Saran, M. 1990. Flavonoids as antioxidants: determination of radical-scavenging efficiencies, *Methods in Enzymology*, 186: 343-55.
- Brand-Williams W, Cuvelier M.E, Berset C. 1995. Use of a free radical method to evaluate antioxidant activity. *Lebenson Wiss Technology*. 28: 25-30.
- Bundschuh, M., Filser, J., Lüderwald, S., McKee, M. S., Metreveli, G., Schaumann, G. E., Schulz, R and Wagner, S. 2018. Nanoparticles in the environment: where do we come from, where do we go to? *Environmental Sciences Europe*, 30: 1-17.

- Bukhari, S.B., Memon, S., Mahroof-Tahir, M. and Bhanger, M.I. 2009. Synthesis, characterization and antioxidant activity copper-quercetin complex, *Spectrochimica Acta Part A: Molecular and Biomolecular Spectroscopy*, 71: 1901-6.
- Burk, R.F. 1983. Biological activity of selenium, *Annual Review of Nutrition*, 3: 53-70.
- Calderón, L., Han, T.T., McGilvery, C.M., Yang, L., Subramaniam, P., Lee, K-B., Schwander, S., Tetley, T.D., Georgopoulos, P.G., Ryan, M., Porter, A.E., Smith, R., Chung, K.F., Liou, P.J., Zhang, J. and Mainelis, G. 2017. Release of airborne particles and Ag and Zn compounds from nanotechnology-enabled consumer sprays: Implications for inhalation exposure, *Atmospheric Environment*, 155: 85-96.
- Catarino, D., Silva, A.M.S., Saraiva, S.C., Sobral, A.J.F.N. and Cardoso, S.M. 2015. Characterization of phenolic constituents and evaluation of antioxidant properties of leaves and stems of *Eriocephalus africanus*, *Arabian Journal of Chemistry*, 11 : 62-69.
- Chacko, S.M, Thambi, P.T., Kuttan, R. and Nishigaki, I. 2010. Beneficial effects of green tea: A literature review, *Chinese Medicine*, 5: 13-13.
- Chang, C.J, Chang, M.C.Y., Damrauer, N.H. and Nocera, D.G. 2004. Proton-coupled electron transfer: a unifying mechanism for biological charge transport, amino acid radical initiation and propagation, and bond making/breaking reactions of water and oxygen, *Biochimica et Biophysica Acta (BBA) - Bioenergetics*, 1655: 13-28.
- Cheng, H.G. and Phillips, M.R. 2014. Secondary analysis of existing data: opportunities and implementation, *Shanghai Archives of Psychiatry*, 26: 371-5.
- Cherrak, S.A., Mokhtari-Soulimane, N., Berroukeche, F., Bensenane, B., Cherbonnel, A., Merzouk, H. and Elhabiri, M. 2016. In vitro antioxidant versus metal ion chelating properties of flavonoids: A structure-activity investigation, *PLoS ONE*, 11: 1-21.
- Chitra, K. and Annadurai, G. 2013. Antimicrobial activity of wet chemically engineered spherical shaped ZnO nanoparticles on food borne pathogen.
- Coskun, O. 2016. Separation techniques: Chromatography, *Northern Clinics of Istanbul*, 3: 156-60.
- Cowan, M.M. 1999. Plant products as antimicrobial agents, *Clinical Microbiology Reviews*, 12: 564-82.
- Craig, P.J. 2003. *Organoselenium compounds in the environment*. Craig, P.J. and Maher, W.A.(Ed). *Organometallic Compounds in the Environment (2nd edition)*. Jon Wiley & Sons. Chichester. 391-398.

- Daisy, P. and Saipriya, K. 2012. Biochemical analysis of *Cassia fistula* aqueous extract and phytochemically synthesized gold nanoparticles as hypoglycemic treatment for diabetes mellitus, *International Journal of Nanomedicine*, 7: 1189-202.
- Dallas, P., Sharma, V.K. and Zboril, R. 2011. Silver polymeric nanocomposites as advanced antimicrobial agents: Classification, synthetic paths, applications, and perspectives, *Advances in Colloid and Interface Science*, 166: 119-35.
- Daniel, M.C and Astruc, D. 2004. Gold nanoparticles: Assembly, supramolecular chemistry, quantum-size-related properties, and applications toward biology, catalysis, and nanotechnology, *Chemical Reviews*, 104: 293-346.
- Das, V.L., Thomas, R., Varghese, R.T., Soniya, E.V., Mathew, J. and Radhakrishnan, E.K. 2014. Extracellular synthesis of silver nanoparticles by the *Bacillus* strain CS 11 isolated from industrialized area, *Biotechnology*, 4: 121-26.
- Dizaj, S.M., Lotfipour, F., Barzegar-Jalali M., Zarrintan, M.H. and Adibkia, K. 2014. Antimicrobial activity of the metals and metal oxide nanoparticles, *Material Science and Engineering C: Materials for Biological Applications*, 44: 278-84.
- Dmitrienko, S.G., Kudrinskaya, V.A. and Apyari, V.V. 2012. Methods of extraction, preconcentration, and determination of quercetin, *Journal of Analytical Chemistry*, 67: 299-311.
- Droy-Lefaix., M.T. 1997. Effect of the antioxidant action of *Ginkgo biloba* extract (EGb 761) on aging and oxidative stress, *American Aging Association*, 20: 141-49.
- Dye, C. 2014. After 2015: Infectious diseases in a new era of health and development, *Philosophical Transactions of the Royal Society of London B: Biological Sciences*, 369: 1-9.
- Einbond, L.S., Reynertson, K.A., Luo, X-D Basile, M.J. and Kennelly, E.J. 2004. Anthocyanin antioxidants from edible fruits, *Food Chemistry*, 84 : 23-28.
- El Sherbeiny, A.E and El Ansari, M.A. 1976. The polyphenolics and flavonoids of *Harpephyllum caffrum*. *Planta Medica*, 29: 129-132.
- Elsaesser, A and Vyvyan, H. 2012. Toxicology of nanoparticles, *Advanced Drug Delivery Reviews*, 64: 129-137.
- Feynman, R. 1960. "Theres Plenty of Room at the Bottom." In *Engineering and Science*, 23: 22-36.
- Flora, S.J.S. 2009. Structural, chemical and biological aspects of antioxidants for strategies against metal and metalloid exposure, *Oxidative Medicine and Cellular Longevity*, 2: 191-206.

- Francisco, A. 1995. The flavonoids: Advances in research since 1986. Chapman & Hall, ed. by Harborne JB. London, U.K. *Phytochemical Analysis*, 6: 55–55
- Freyschlag, R., Cassandra, G. and Madix, J. 2011. Precious metal magic: Catalytic wizardry, *Materials Today*, 14: 134-42.
- García-Barrasa, J., López-de-Luzuriaga, J.M. and Monge, M. 2011. Silver nanoparticles: synthesis through chemical methods in solution and biomedical applications, *Central European Journal of Chemistry*, 9: 7-19.
- Gokarneshan, N., Gopalakrishnan, P.P. and Jeyanthi, B. 2012. Influence of nanofinishes on the antimicrobial properties of fabrics, *ISRN Nanomaterials*, 8 : 1-9.
- Greenwood, N.N. and Earnshaw, A. 1997. Selenium, tellurium and polonium. *Chemistry of the Elements*. Butterworth-Heinemann. pg 747–788.
- Grenni, P., Ancona, V. and Caracciolo, A.B. 2017. Ecological effects of antibiotics on natural ecosystems: A review, *Microchemical Journal*, 136: 25-39.
- Haroun, M.F. and Al-Kayali, R.S. 2016. Synergistic effect of *Thymbra spicata L.* extracts with antibiotics against multidrug- resistant *Staphylococcus aureus* and *Klebsiella pneumoniae* strains, *Iranian Journal of Basic Medical Sciences*, 19: 1193-2000.
- Heijnen, C.G., Haenen, G.R., van Acker, F.A., van der Vijgh, W.J. and Bast, A. 2001. Flavonoids as peroxy nitrite scavengers: the role of the hydroxyl groups, *Toxicology In Vitro*, 15: 3-6.
- Heiligtag, F.J and Niederberger, M .2013.The fascinating world of nanoparticle research, *Materials Today*, 16: 262-271.
- Herman, P.P.J and Condy, G. 2015. *Zoutpansbergia caerulea (Asteraceae: Inuleae)*. *Flowering Plants of Africa* 64: 162–167.
- Herman, P.P.J. and Condy, G. 2017. *Rotheca myricoides sensu lato (Lamiaceae: Ajugoideae)*. *Flowering Plants of Africa* 65: 146–152.
- Horbowicz, M. 2002. Method of quercetin extraction from dry scales of onion. *Vegatables Crops Research Bulletin*, 57 :119-124.
- Husen, A and Siddiqi, K.S. 2014. Plants and microbes assisted selenium nanoparticles: characterization and application, *Journal of Nanobiotechnology*, 12: 1-10.
- Hye, M.A., Taher, M.A., Ali, M.Y., Ali, M.U. and Zaman, S. 2009. Isolation of (+)-catechin from *Acacia Catechu* (Cutch Tree) by a convenient method. *Journal of Scientific Researsch*, 1 : 300-305.

- Intra J. and Kuo, S.M. 2007. Physiological levels of tea catechins increase cellular lipid antioxidant activity of vitamin C and vitamin E in human intestinal CaCo-2 cells, *Chemico-Biological Interactions*, 169: 91-9.
- Iravani, S., Korbekandi, H., Mirmohammadi, S.V. and Zolfaghari, B. 2014. Synthesis of silver nanoparticles: Chemical, physical and biological methods. *Research in Pharmaceutical Sciences* 9: 385–406.
- Isomura, T., Suzuki, S., Origasa, H., Hosono, A., Suzuki, M., Sawada, T., Terao, S., Muto, Y. and Koga, T. 2016. Liver-related safety assessment of green tea extracts in humans: a systematic review of randomized controlled trials, *European Journal of Clinical Nutrition*, 70: 1221-29.
- Issa, B., Obaidat, I.M., Albiss, B.A., and Haik, Y.. 2013. Magnetic nanoparticles: Surface effects and properties related to biomedicine applications, *International Journal of Molecular Science*, 14: 21266-305.
- Ivan, N. 1994. *Nordic Journal of Botany*: Bremer, K. 1994. Asteraceae: cladistics and classification, *Nordic Journal of Botany*, 14: 462-62.
- Jorgensen, J. H., and J. D. Turnidge. 2007. Susceptibility test methods: dilution and disk diffusion methods, p. 1152–1172. In P.R. Murray, E. J. Baron, J. H. Jorgensen, M. L. Landry, and M. A. Pfaller(ed.), *Manual of clinical microbiology*, 9th ed. ASM Press, Washington, D.C.
- Joy, P. P., Anjana, R., Rashida, A. and Ratheesh, A. 2016. *FRUITS AS A FUNCTIONAL FOOD*.
- Jyoti, K., Baunthiyal, M. and Singh, A. 2016. Characterization of silver nanoparticles synthesized using *Urtica dioica* Linn. leaves and their synergistic effects with antibiotics, *Journal of Radiation Research and Applied Sciences*, 9: 217-27.
- Kasthuri, J., Veerapandian S. and Rajendiran, N. 2009. Biological synthesis of silver and gold nanoparticles using apiin as reducing agent, *Colloids and Surfaces B: Biointerfaces*, 68: 55-60.
- Key, J. and Leary, J.F. 2014. Nanoparticles for multimodal in vivo imaging in nanomedicine, *International Journal of Nanomedicine*, 9: 711-26.
- Khan, I., Saeed, K. and Khan, I. 2017. Nanoparticles: Properties, applications and toxicities, *Arabian Journal of Chemistry*, 5: 1-24
- Khan, N. and Mukhtar, H. 2010. Cancer and metastasis: prevention and treatment by green tea, *Cancer Metastasis Reviews*, 29: 435-45.
- Klingshirn, C. 2007. ZnO: Material, physics and applications, *ChemPhysChem*, 8: 782-803.

- Klingshirn, C.F., Geurts, J., Meyer, B.K., Waag, A., Hoffmann, A. 2010. *Zinc oxide: From fundamental properties towards novel applications*. Springer: Springer Heidelberg-Dordrecht-London-New York. pg 7.
- Kodeš, J. 1971. Photovoltaic effect in selenium photocells, *Physica Status Solidi (a)*, 5: K87-K90.
- Korkina, L.G. and Afanas'Ev, I.B. 1996. Antioxidant and Chelating properties of flavonoids. in Helmut Sies (ed.), *Advances in Pharmacology*, 38: 151-163
- Kulkarni, N. and Muddapur, U. 2014. Biosynthesis of metal nanoparticles: A review, *Journal of Nanotechnology*, 1: 1-8.
- Kumar, S.S, Venkateswarlu, P., Rao, V.R. and Rao, G.N. 2013. Chemistry and biological activities of flavonoids: An overview, *The Scientific World Journal*, 3: 1-16.
- Kumar, S.S., Venkateswarlu, P., Rao, V.R. and Rao G.N. 2013. Synthesis, characterization and optical properties of zinc oxide nanoparticles, *International Nano Letters*, 3: 1-6.
- Kumari, S., Ahsan S.M., Kumar, J.M., Kondapi, A.K. and Rao N.M. 2017. Overcoming blood brain barrier with a dual purpose temozolomide loaded lactoferrin nanoparticles for combating glioma (SERP-17-12433), *Scientific Reports*, 7:1-13.
- Kuok, C., Hoi, S., Hoi, C.F., Chan, C.H., Fong, I.H., Ngok, C.K., Meng, L.R. and Fong, P. 2017. Synergistic antibacterial effects of herbal extracts and antibiotics on methicillin-resistant *Staphylococcus aureus*: A computational and experimental study, *Experimental Biology and Medicine (Maywood)*, 242: 731-43.
- Kuppusamy, P., Ichwan, S.J., Al-Zikri, P.N., Suriyah, W.H., Soundharrajan, I., Govindan, N., Maniam G. P. and Yusoff M. M. 2016. In vitro anticancer activity of Au, Ag nanoparticles synthesized using *Commelina nudiflora L.* aqueous extract against HCT-116 colon cancer cells, *Biological Trace Element Research*, 173: 297-305.
- Kurek, A., Grudniak A.M., Kraczkiewicz-Dowjat, A. and Wolska, K.I. 2011. New antibacterial therapeutics and strategies, *Polish Journal of Microbiology*, 60: 3-12.
- Lahkar, S. and Das, M.K. 2013. Surface modified polymeric nanoparticles for brain targeted drug delivery. *Current Trends in Biotechnology and Pharmacy*, 7: 914-931.
- Lampis, S., Zonaro E., Bertolini C., Bernardi P., Butler C.S, and Vallini, G. 2014. Delayed formation of zero-valent selenium nanoparticles by *Bacillus mycoides* SeITE01 as a consequence of selenite reduction under aerobic conditions, *Microbial Cell Factories*, 13: 35.

- Lopez-Romero, S. 2009. Growth and characterization of ZnO cross-like structures by hydrothermal method. *Matéria (Rio de Janeiro)*, 14: 977-982.
- Maillard, J.Y. and Hartemann, P.. 2013. Silver as an antimicrobial: Facts and gaps in knowledge, *Critical Reviews in Microbiology*, 39: 373-83.
- Majouli, K., Hamdi, A. and Hlila, M.B. 2017. Phytochemical analysis and biological activities of *Hertia cheirifolia* L. roots extracts, *Asian Pacific Journal of Tropical Medicine*, 10: 1134-39.
- Makarov, V.V., Love, A.J., Sinitsyna, O.V., Makarova, S.S., Yaminsky, I.V., Taliansky, M.E, and Kalinina, N.O. 2014. "Green" Nanotechnologies: Synthesis of metal nanoparticles using plants, *Acta Naturae*, 6: 35-44.
- Malik, P., Shankar, R., Malik, V., Sharma, N. and Mukherjee, T.K. 2014. Green chemistry based benign routes for nanoparticle synthesis, *Journal of Nanoparticles*, 3: 1-14.
- Mallick, K., Witcomb, M.J, and Scurrrell, M.S. 2004. Polymer stabilized silver nanoparticles: A photochemical synthesis route, *Journal of Materials Science*, 39: 4459-63.
- Mandal, S.K., Roy, R.K., and Pal, A.K. 2003. Effect of particle shape distribution on the surface plasmon resonance of Ag-SiO₂ nanocomposite thin films, *Journal of Physics D: Applied Physics*, 36: 261-265.
- Mandel, S., Weinreb, O., Reznichenko, L., Kalfon, L. and Amit, T. 2006. Green tea catechins as brain-permeable, non toxic iron chelators to "iron out iron" from the brain, *Journal of Neural Transmission. Supplementa*, 71: 249-57.
- Manzetti, S. and Ghisi, R. 2014. The environmental release and fate of antibiotics, *Marine Pollution Bulletin*, 79: 7-15.
- Maoela, M.S., Arotiba, O.A., Baker, P.G.L., Mabusela, W.T., Jahed, N., Songa, E.A and Iwuoha, E.I. 2009. Electroanalytical determination of catechin flavonoid in ethyl acetate extracts of medicinal plants. *International Journal of Electrochemical Science*, 4: 1497 - 1510.
- Masallat, D.T., Omar, N.S., Khalifa, A.K. and Emara, R.M.K. 2016. Microbicidal power of silver nano particles and its benefit in soft liner obturator prosthesis. *The Egyptian Journal of Medical Microbiology*, 25: 33-37.
- McDonald, R.S. 1986. Review: infrared spectrometry, *Analytical Chemistry*, 58: 1906-1925.
- Mitchnick, M.A., Fairhurst, D. and Pinnell, S. R. 1999. Microfine zinc oxide (Z-cote) as a photostable UVA/UVB sunblock agent, *Journal of the American Academy of Dermatology*, 40: 85-90.

- Mittal, A.K., Bhaumik, J., Kumar S. and Banerjee, U.C. 2014. Biosynthesis of silver nanoparticles: Elucidation of prospective mechanism and therapeutic potential, *Journal of Colloid and Interface Science*, 415: 39-47.
- Mohamed, M. 2015. One-step functionalization of silver nanoparticles using the orsellinic acid compound isolated from the endophytic fungus *Epicoccum nigrum*: Characterization and antifungal activity, *International Journal of Nanomaterials and Chemistry*, 1: 103-110.
- Moodley, R., Koorbanally, N. and Jonnalagadda, S.B. 2013. Elemental composition and nutritional value of the edible fruits of *Harpephyllum caffrum* and impact of soil quality on their chemical characteristics, *Journal of Environmental Science and Health, Part B*, 48: 539-47.
- MubarakAli, D., Thajuddin, N., Jeganathan K. and Gunasekaran, M. 2011. Plant extract mediated synthesis of silver and gold nanoparticles and its antibacterial activity against clinically isolated pathogens, *Colloids and Surfaces B: Biointerfaces*, 85: 360-365.
- Murkovic, M. 2003. PHENOLIC COMPOUNDS A2 - (Ed) Caballero, Benjamin. in, *Encyclopedia of Food Sciences and Nutrition (Second Edition)*. Academic Press: Oxford.
- Murthy, S.K. 2007. Nanoparticles in modern medicine: State of the art and future challenges, *International Journal of Nanomedicine*, 2: 129-41.
- Nadeem, A., Khanna, T. and Vohora, S.B. 1999. Silver preparations used in Indian systems of medicine: Neuropsychobehavioural effects. *Indian Journal of Pharmacology*, 31. 214-221.
- Nagarajan, S. and Kuppusamy, K.A. 2013. Extracellular synthesis of zinc oxide nanoparticle using seaweeds of gulf of Mannar, India, *Journal of Nanobiotechnology*, 11:1-11
- Nguyen, T.H.D., Vardhanabhuti, B., Lin, M. and Mustapha, A. 2017. Antibacterial properties of selenium nanoparticles and their toxicity to caco-2 cells. *Food Control*, 77: 17-24
- Njagi, E.C., Huang, H., Stafford, L., Genuino, H., Galindo, H.M., Collins, J.B., Hoag, G.E. and Suib, S L. 2011. Biosynthesis of iron and silver nanoparticles at room temperature using aqueous sorghum bran extracts, *Langmuir*, 27: 264-71.
- Noguez, C. 2007. Surface Plasmons on metal nanoparticles: The influence of shape and physical environment, *The Journal of Physical Chemistry C*, 111: 3806-19.
- Ojewole, J. 2006. Hypoglycaemic and hypotensive effects of *Harpephyllum caffrum* Bernh ex CF Krauss (Anacardiaceae) stem-bark aqueous extract in rats. *Cardiovascular Journal of South Africa*, 17: 67-72.
- Omid, A. and Ghaderi, E. 2009. Enhancement of antibacterial properties of Ag nanorods by electric field, *Science and Technology of Advanced Materials*, 10: 1-6.

- Otari, S.V., Patil, R.M., Ghosh, S.J., Thorat, N.D. and Pawar S.H. 2015. Intracellular synthesis of silver nanoparticle by actinobacteria and its antimicrobial activity, *Spectrochimica Acta Part A: Molecular and Biomolecular Spectroscopy*, 136 : 1175-80.
- Pal, S., Tak, Y.K., and Song, J.M. 2007. Does the antibacterial activity of silver nanoparticles depend on the shape of the nanoparticle? A study of the gram-negative bacterium *Escherichia coli*, *Applied and Environmental Microbiology*, 73: 1712-20.
- Panche, A.N., Diwan, A.D. and Chandra, S. R. 2016. Flavonoids: an overview, *Journal of Nutritional Science*, 5: 1-15.
- Pantidos, N, Edmundson, M.C. and Horsfall, L. 2018. Room temperature bioproduction, isolation and anti-microbial properties of stable elemental copper nanoparticles, *New Biotechnology*, 40: 275-81.
- Park, H.H., Lee, S., Son, H.Y., Park, S.B., Kim, M.S., Choi, E.J., Singh T.S., Ha, J.H., Lee, M.G., Kim, J.E, Hyun, M.C, Kwon, T.K, Kim, Y.H. and Kim, S.H. 2008. Flavonoids inhibit histamine release and expression of proinflammatory cytokines in mast cells, *Archives of Pharmacal Research*, 31: 1303-11.
- Pell, S.K, Mitchell J.D., Miller, A.J. and Lobova, T.A. 2011. *The families and genera of vascular plants* .Springer- Verlag, Berlin.
- Perez-Tijerina, E., Gracia, M.P., Mejia-Rosales, S., Ortiz-Mendez, U., Torres, A., and Jose-Yacaman, M. 2008. Highly size-controlled synthesis of Au/Pd nanoparticles by inert-gas condensation, *Faraday Discussions*, 138: 353-62.
- Petrucci, O.D., Buck, D.C., Farrer, J.K and Watt ,R.K. 2014. A ferritin mediated photochemical method to synthesize biocompatible catalytically active gold nanoparticles: size control synthesis for small (~2 nm), medium (~7 nm) or large (~17 nm) nanoparticles, *RSC Advances*, 4: 3472-81.
- Ponomareva, K.Yu., Kosobudsky, I.D., Tretyachenko, E.V. and Yurkov, G. Yu. 2007. Synthesis and properties of CdS nanoparticles in a polyethylene matrix, *Inorganic Materials*, 43: 1160-66.
- Priya S., Murugan, K., Priya, A., Dinesh, D., Panneerselvam, C., Devi,D.G., Chandramohan, B., Kumar, P.M., Barnard, B.R, Xue, R-D., Hwang, J.S., Nicoletti M., Chandrasekar R., Amsath A., Bhagooli R., Hui Wei. 2014. Green synthesis of silver nanoparticles using *Calotropis gigantea* and their potential mosquito larvicidal property. *International Journal of Pure and Applied Zoology*, 6 : 128-137.
- Pujol, J. 1990. *Nature Africa, The Herbalist Handbook* (Natural Healers Foundation: Durban).

- Rabe, T. and van Staden, J. 1997. Antibacterial activity of South African plants used for medicinal purposes, *Journal of Ethnopharmacology*, 56: 81-7.
- Rahman, K. 2007. Studies on free radicals, antioxidants, and co-factors, *Clinical Interventions in Aging*, 2: 219-36.
- Rajalakshmi, A., Jayachitra, A., Gopal, P. and Krithiga, N. 2014. Pharmacology and toxicology research toxicity analysis of different medicinal plant extracts in Swiss Albino Mice, *Pharmacology and Toxicology Research*, 1: 1-6
- Rajiv, P., Rajeshwari, S. and Venckatesh, R. 2013. Bio-fabrication of zinc oxide nanoparticles using leaf extract of *Parthenium hysterophorus L.* and its size-dependent antifungal activity against plant fungal pathogens, *Spectrochimica Acta Part A: Molecular and Biomolecular Spectroscopy*, 112: 384-7.
- Rajput, N. 2015. Methods of preparation of nanoparticles-A review, *International Journal of Advances in Engineering and Technology*, 7: 1-6.
- Ramamurthy, C.H., Sampath K.S., Arunkumar, P., Kumar M.S., Sujatha V., Premkumar, K. and Thirunavukkarasu, C. 2013. Green synthesis and characterization of selenium nanoparticles and its augmented cytotoxicity with doxorubicin on cancer cells, *Bioprocess and Biosystems Engineering*, 36: 1131-9.
- Rasmussen, J.W., Martinez, E., Louka P. and Wingett, D.G. 2010. Zinc oxide nanoparticles for selective destruction of tumor cells and potential for drug delivery applications, *Expert Opinion Drug Delivery*, 7: 1063-1077.
- Rayman, M.P. 2000. The importance of selenium to human health, *Lancet*, 356: 233-241.
- Rice-Evans, C.A., Miller, N.J. and Paganga, G. 1996. Structure-antioxidant activity relationships of flavonoids and phenolic acids, *Free Radical Biology and Medicine*, 20: 933-956.
- Sanghavi, N., Srivastava, R. and Malode, Y. 2014. Isolation and identification of the flavonoid "Quercetin" from *Tridax procumbens linn*, *International Journal Of Pharmaceutical Sciences and Research*, 5: 1454-1459.
- Santhoshkumar, T., Rahuman A.A., Rajakumar, G., Marimuthu, S., Bagavan, A., Jayaseelan, C., Zahir, A.A., Elango, G. and Kamaraj C. 2011. Synthesis of silver nanoparticles using *Nelumbo nucifera* leaf extract and its larvicidal activity against malaria and filariasis vectors, *Parasitology Research*, 108: 693-702.
- Saraiva, C., Praça, C., Ferreira, R., Santos, T., Ferreira, L. and Bernardino, L. 2016. Nanoparticle-mediated brain drug delivery: Overcoming blood–brain barrier to treat neurodegenerative diseases, *Journal of Controlled Release*, 235: 34-47.

- Scott, J. 1996 Population ecology of *Chrysanthemoides monilifera* in South Africa: implications for its control in Australia, *Journal of Applied Ecology*, 33: 1496-1508.
- Seil, J.T. and Webster, T.J. 2012. Antimicrobial applications of nanotechnology: Methods and literature, *International Journal of Nanomedicine*, 7: 2767-2781.
- Seng, H-L., and Tiekink, E.R.T. 2012. Anti-cancer potential of selenium- and tellurium-containing species: Opportunities abound!. *Applied Organometallic Chemistry*, 26: 655-662.
- Seyoum, A., Asres, K., and El-Fiky, F.K. 2006. Structure-radical scavenging activity relationships of flavonoids, *Phytochemistry*, 67: 2058-2070.
- Shin, W-K., Cho, J., Kannan, A.G., Lee, Y-S. and Kim, D-W. 2016. Cross-linked composite gel polymer electrolyte using mesoporous methacrylate-functionalized SiO₂ nanoparticles for lithium-ion polymer batteries, *Scientific Reports*, 6: 1-9.
- Silva, N.C.C., and Fernandes Júnior, A. 2010. Biological properties of medicinal plants: a review of their antimicrobial activity, *Journal of Venomous Animals and Toxins including Tropical Diseases*, 16: 402-413.
- Sim, G-W., Lee B-C., Cho, H.S., Lee, J.W., Kim, J-H., Lee, D.H., Kim, J-H., Pyo, H-B., Moon, D.C., Oh, K-W., Yun, Y.P. and Hong, J.T. 2007. Structure activity relationship of antioxidative property of flavonoids and inhibitory effect on matrix metalloproteinase activity in UVA-irradiated human dermal fibroblast, *Archives of Pharmacal Research*, 30: 290-298.
- Singh, R., and Lillard, J.W. Jr. 2009. Nanoparticle-based targeted drug delivery, *Experimental and Molecular Pathology*, 86: 215-223.
- Singh, T., Sinha N., and Singh, A. 2013. Biochemical and histopathological effects on liver due to acute oral toxicity of aqueous leaf extract of *Ecliptaalba* on female Swiss albino mice, *Indian Journal of Pharmacology*, 45: 61-65.
- Sirelkhatim, A., Mahmud, S., Seeni, A., Haida, N., Kaus, M., Ann, L.C., Bakhori, S.K.M., Hasan, H. and Mohamad, D. 2015. Review on zinc oxide nanoparticles: Antibacterial activity and toxicity mechanism, *Nano-Micro Letters*, 7: 219-242.
- Slawson, R., Trevors, J.T. and Lee, H. 1992. Silver accumulation and resistance in *Pseudomonas stutzeri*. *Archives of Microbiology*, 158: 398-404.
- Solowey, E., Lichtenstein, M., Sallon, S., Paavilainen, H., Solowey, E. and Lorberboum-Galski, H. 2014. Evaluating medicinal plants for anticancer activity, *The Scientific World Journal*, 14: 1-12.

- Sondi, I. and Salopek-Sondi, B. 2004. Silver nanoparticles as antimicrobial agent: a case study on *E. coli* as a model for Gram-negative bacteria, *Journal of Colloid and Interface Science*, 275: 177-82.
- Song, J.Y., Jang, H.K. and Kim, B.S. 2009. Biological synthesis of gold nanoparticles using *Magnolia kobus* and *Diopyros kaki* leaf extracts, *Process Biochemistry*, 44: 1133-1138.
- Stolzoff, M., Wang, S.Q. and Webster, T.J. Efficacy and mechanism of selenium nanoparticles as antibacterial agents, *Frontiers in Bioengineering and Biotechnology*. (Conference Abstract: 10th World Biomaterials Congress)
- Storhoff, J.J., Lazarides, A.A., Mucic, R.C., Mirkin, C.A., Letsinger, R.L. and Schatz, G.C. 2000. What controls the optical properties of DNA-linked gold nanoparticle assemblies?, *Journal of the American Chemical Society*, 122: 4640-50.
- Suárez-Cerda, J., Nuñez, G.A., Espinoza-Gómez, H. and Flores-López, L.Z. 2014. A comparative study of the effect of α -, β -, and γ -cyclodextrins as stabilizing agents in the synthesis of silver nanoparticles using a green chemistry method, *Materials Science and Engineering: C*, 43: 21-26.
- Subhankari, I. and Nayak, P.L. 2013. Antimicrobial Activity of Copper Nanoparticles Synthesised by Ginger (*Zingiber officinale*) Extract. *World Journal of Nano Science and Technology* 2: 10-13.
- Sudarshan, J-H. and Park, T.S. 2000. *Surface Engineering Series Volume 2: Chemical Vapor Deposition* (Ed) Jong-Hee Park. ASM International: Scarborough, Toronto.
- Sun, Q., Cai, X., Li, J., Zheng, M., Chen, Z. and Yu, C-P. 2014. Green synthesis of silver nanoparticles using tea leaf extract and evaluation of their stability and antibacterial activity, *Colloids and Surfaces A: Physicochemical and Engineering Aspects*, 444: 226-31.
- Symonowicz, M. and Kolanek, M. 2012. Flavonoids and their properties to form chelate complexes. *Biotechnology and Food Science*, 76: 35-41.
- Tavakoli, A., Sohrabi, M. and Kargari, A. 2007. A review of methods for synthesis of nanostructured metals with emphasis on iron compounds, *Chemical Papers*, 61: 151-70.
- Tippayawat, P., Phromviyo, N., Boueroy, P and Chompoosor, A. 2016. Green synthesis of silver nanoparticles in *Aloe vera* plant extract prepared by a hydrothermal method and their synergistic antibacterial activity, *PeerJ*, 4: 1-15.
- Tiwari, P.M., Vig, K., Dennis, V.A. and Singh, S.R. 2011. Functionalized gold nanoparticles and their biomedical applications., *Nanomaterials*, 1: 31-63.

- Tran, Q.H., Nguyen, V.Q. and Le, A-T. 2013. Silver nanoparticles: Synthesis, properties, toxicology, applications and perspectives. *Advances in Natural Sciences: Nanoscience and Nanotechnology*, 4: 1-20.
- Touloukian, Y.S., (1977). Thermophysical Properties of Matter, Vol 13, Thermal Expansion of Nonmetallic Solids.
- Van Wyk, B-E., Van Oudtshoorn, B. and Gericke, N. 1997. *Medicinal Plants of South Africa*. Briza Publications: Pretoria.
- Velan. R., Ayyasamy, P.P., Raju, K. and Bhoopathy, S. 2015. Rapid decolorization of synthetic melanoidin by bacterial extract and their mediated silver nanoparticles as support. *Journal of Applied Biology and Biotechnology*, 3 : 6-11.
- Velayutham, P., Babu, A. and Liu, D. 2008. Green tea catechins and cardiovascular health: An update, *Current Medicinal Chemistry*, 15: 1840-50.
- Venkatasubbu, G., Devanand, R., Baskar, T., Anusuya, C., Seshan, A. and Chelliah, R. 2016. Toxicity mechanism of titanium dioxide and zinc oxide nanoparticles against food pathogens, *Colloids and Surfaces B: Biointerfaces*, 148: 600-06.
- Verma, A. and Mehata, M.S. 2016. Controllable synthesis of silver nanoparticles using Neem leaves and their antimicrobial activity, *Journal of Radiation Research and Applied Sciences*, 9: 109-15.
- Vidya C, Hiremath, S., Chandraprabha, M.N., Lourdu Antonyraj, M.A., Gopal, I.V., Jain, A. and Bansal, K. 2013. Green synthesis of ZnO nanoparticles by *Calotropis gigantea* , *International Journal of Current Engineering and Technology, Special Issue*: 1-3.
- Vijayaraghavan, K. and Ashokkumar, T. 2017. Plant-mediated biosynthesis of metallic nanoparticles: A review of literature, factors affecting synthesis, characterization techniques and applications. *Journal of Environmental Chemical Engineering*, 5: 4866-4883
- Vuong, Q.V., Golding, J.B., Nguyen, M. and Roach, P.D. 2010. Extraction and isolation of catechins from tea, *Journal of Separation Science*, 33: 3415-28.
- Wadhvani, S. A., Gorain, M., Banerjee, P., Shedbalkar, U.U., Singh, R., Kundu, G.C. and Chopade, B.A. 2017. Green synthesis of selenium nanoparticles using *Acinetobacter sp.* SW30: Optimization, characterization and its anticancer activity in breast cancer cells, *International Journal of Nanomedicine*, 12: 6841–6855.
- Waitkins, G.R., Bearse, A.E. and Shutt, R.. 1942. Industrial utilization of selenium and tellurium, *Industrial and Engineering Chemistry*, 34: 899-910.

- Wang, L., Hu, C. and Shao, L. 2017. The antimicrobial activity of nanoparticles: present situation and prospects for the future, *International Journal of Nanomedicine*, 12: 1227-49.
- Wang, Q., Yu, H., Zhang, J-S. and Yang, X-B. 2014. Synthesis, characterization, DNA interaction, and antitumor activities of Ia (iii) complex with schiff base ligand derived from kaempferol and diethylenetriamine, *Bioinorganic Chemistry and Applications*, 20: 1-9.
- Weerawatanakorn, M., Hung, W-L., Pan, M-H., Li, S., Li, D., Wan, X. and Ho C-H. 2015. Chemistry and health beneficial effects of oolong tea and theasinensins, *Food Science and Human Wellness*, 4: 133-46.
- Wong, K.C. 2014. Review of NMR Spectroscopy: Basic principles, concepts and applications in chemistry, *Journal of Chemical Education*, 91: 1103-04.
- Xie, J, Lee, Y.J., and Ting, Y.P. 2007. High-yield synthesis of complex gold nanostructures in a fungal system, *The Journal of Physical Chemistry C*, 111: 16858-65.
- Yah, C.S., Simate, G.S. and. Iyuke, S.E. 2012. Nanoparticles toxicity and their routes of exposures, *Pakistan Journal of Pharmaceutical Sciences*, 25: 477-91.
- Yazeji, T., Moulari B., Beduneau A., Stein V., Dietrich D., Pellequer Y., and Lamprecht, A.. 2017. Nanoparticle-based delivery enhances anti-inflammatory effect of low molecular weight heparin in experimental ulcerative colitis, *Drug Delivery*, 24: 811-17.
- Krutyakov, Y.A., Kudrinskiy, A.A, Olenin A.Yu. and Lisichkin, G.V. 2008. Synthesis and properties of silver nanoparticles: Advances and prospects, *Russian Chemical Reviews*, 77: 233-257.
- Yu, J., Wang, H., Zhan, J., and Huang, W. 2018. Review of recent UV–Vis and infrared spectroscopy researches on wine detection and discrimination, *Applied Spectroscopy Reviews*, 53: 65-86.
- Yuan, J-M. 2013. Cancer prevention by green tea: evidence from epidemiologic studies, *The American Journal of Clinical Nutrition*, 98: 1676S–1681S.
- Yuan, J-M., Sun, C. and Butler, L.M. 2011. Chapter 8. Tea and Cancer Prevention: Epidemiological Studies, *Pharmacological Research : The Official Journal of the Italian Pharmacological Society*, 64: 123-35.
- Zavada, M. and de Villiers, S. 2000. Pollen of the Asteraceae from the Paleocene-Eocene of South Africa, *Grana*, 39: 39-45.
- Zhang, X-Q., Xu, X., Bertrand, N., Pridgen, E., Swami, A. and Farokhzad, O.C. 2012. Interactions of nanomaterials and biological systems: Implications to personalized nanomedicine, *Advanced Drug Delivery Reviews*, 64: 1363-84.

Zielonka, A. and Klimek-Ochab, M. 2017. Fungal synthesis of size-defined nanoparticles, *Advances in Natural Sciences: Nanoscience and Nanotechnology*, 8: 1-10.